



Energetic Macroscopic Representation Modeling and Control of a Low Temperature Fuel Cell System Fed by Hydrocarbons

Daniela Chrenko

► To cite this version:

Daniela Chrenko. Energetic Macroscopic Representation Modeling and Control of a Low Temperature Fuel Cell System Fed by Hydrocarbons. Electric power. Université de Franche-Comté, 2008. English. NNT: . tel-00358312v1

HAL Id: tel-00358312

<https://theses.hal.science/tel-00358312v1>

Submitted on 3 Feb 2009 (v1), last revised 22 Feb 2009 (v3)

HAL is a multi-disciplinary open access archive for the deposit and dissemination of scientific research documents, whether they are published or not. The documents may come from teaching and research institutions in France or abroad, or from public or private research centers.

L'archive ouverte pluridisciplinaire **HAL**, est destinée au dépôt et à la diffusion de documents scientifiques de niveau recherche, publiés ou non, émanant des établissements d'enseignement et de recherche français ou étrangers, des laboratoires publics ou privés.

N° d'ordre : 107

Année 2008

THÈSE

présentée pour obtenir le grade de

Docteur de l'Université de Franche-Comté

Ecole Doctorale : Sciences pour l'Ingénieur et Microtechniques

Spécialité : Sciences pour l'Ingénieur

par

Daniela CHRENKO

Physical Engineer (Diploma), University of Applied Sciences Wedel, Germany

Master of Science in Process Engineering, University of Applied Sciences

Hamburg, Germany

Energetic Macroscopic Representation Modeling and Control of a Low Temperature Fuel Cell System Fed by Hydrocarbons

Soutenue le 25 novembre 2008 devant le jury composé de :

Yann BULTEL

Rapporteur

Maurice FADEL

Rapporteur

Sylvain ALLANO

Examineur

Alain BOUSCAYROL

Examineur

Ludmila GAUTHIER

Examineur

Stephan KABELAC

Examineur

Daniel HISSEL

Co-Directeur de thèse

Marie-Cécile PÉRA

Directeur de thèse

Thèse préparée à FEMTO-ST - Département ENISYS UMR CNRS 6174 dans le
cadre de l'Institut FCLAB

Contents

Contents	i
List of Figures	v
List of Tables	ix
Acknowledgments	xi
Abstract	xv
Nomenclature	xxi
General Introduction	1
1 Fuel Cell Systems	7
1.1 Introduction to Fuel Cells	7
1.1.1 Discovery of the Fuel Cell Effect	7
1.1.2 Working Principle	7
1.1.3 Different Kinds of Fuel Cells	9
1.1.4 Current and Voltage Supplied	11
1.1.5 Fuel Cell Modeling	12
1.2 Fuel Cell Systems	14
1.3 Fuel Processing	15
1.3.1 Diesel Fuel	16
1.3.2 Reformer	18
1.3.3 Heat Exchanger	20
1.3.4 Desulfurization	22
1.3.5 Water Gas Shift Reaction	22
1.3.6 Preferential Oxidation	22
1.3.7 Condenser	23

1.3.8	Fuel Processing unit for PEFC and HTPEMFC	24
1.4	System Dynamics	24
1.5	Diesel Driven Fuel Cell System	25
2	Modeling Methodology	27
2.1	Purpose of the Modeling	27
2.2	Modeling Approaches	27
2.2.1	Basic Ideas on Modeling	28
2.2.2	Electric Equivalent Model	30
2.2.3	Bond Graph	31
2.2.4	Causal Ordering Graph	32
2.2.5	Energetic Macroscopic Representation	35
2.3	Choice of Modeling Methodology	36
2.4	Basic elements of EMR	37
2.5	Inversion Based Control with EMR	41
2.6	Adaption of EMR to Diesel Fed FCS	43
2.6.1	Utilization of Energy Balance	43
2.6.2	Choice of Variables	44
2.6.3	Representation of Gas Mixtures	46
2.7	Conclusion of Methodology Choice	47
3	Fuel Processor Modeling	51
3.1	Introduction to Reformer Model	51
3.2	Hypotheses made for the Fuel Processor Model	51
3.3	Fuel Processor Model	53
3.3.1	Reformer	54
3.3.2	Heat Exchanger	58
3.3.3	Desulfurization 1	61
3.3.4	Water Gas Shift	63
3.3.5	Preferential Oxidation	64
3.3.6	Desulfurization 2	67
3.3.7	Condenser	67
3.4	Dynamic Fuel Processor Model	69
3.4.1	Temperature	70
3.4.2	Pressure	72
3.5	Fuel Processor Validation	73
3.5.1	Identification of Parameters	73
3.5.2	Introduction to Fuel Processor Validation	74
3.5.3	Stationary Fuel Processor	76
3.5.4	Dynamic Fuel Processor	78
3.6	Adaption of Fuel Processor to use in combination with HTPEMFC	79

3.7	Conclusion of Reformer Model	81
4	Fuel Cell Stack Model	85
4.1	Introduction to Fuel Cell Stack Modeling	85
4.2	Basic Ideas toward Fuel Cell Modeling	86
4.3	Hypotheses of Fuel Cell Model	88
4.4	Modeling of the PEFC	91
4.4.1	Description of Fuel Cell Inlet	91
4.4.2	Description of Fuel Cell Catalyst	94
4.4.3	Description of Gas Diffusion Layer	97
4.4.4	Description of Membrane	102
4.4.5	Combination of Sub models	106
4.5	Validation of Fuel Cell Model	106
4.5.1	Validation of Fuel Cell fed with Hydrogen	109
4.5.2	Validation Fuel Cell fed with reformat	114
4.6	Adaption toward a HTPEMFC	115
4.6.1	Adaption of the model	115
4.6.2	Validation of the HTPEM	120
4.7	Conclusion of Fuel Cell Modeling	123
5	Control Structure	125
5.1	Introduction to Control Structure Development	125
5.2	Fuel Cell System Model	126
5.3	Control Structure Design	132
5.3.1	Introduction	132
5.3.2	Mass Flow Control	134
5.3.3	Temperature Control	143
5.3.4	Overall System	144
5.4	Application of Control	144
5.5	Control Development Conclusion	151
6	Conclusion and Perspectives	153
	Bibliography	158
A	Parameters and Input Values	175

List of Figures

1.1	Basic working principle of a fuel cell.	8
1.2	SOFC Auxiliary Power Unit by Delphi (www.delphi.com)	10
1.3	Fuel Cell Systems used in space applications	11
1.4	Different losses inside fuel cell forming the polarization curve	13
1.5	Fuel cell system: multi-domain aspects	15
1.6	Fuel Processor for PEFC and HTPEM	16
1.7	Crude Oil Refining (www.howstuffworks.com)	17
1.8	Counter current heat exchanger.	21
2.1	Representation of an open system.	29
2.2	Systems with first order time dependency in different physical domains	31
2.3	COG representation of a permanent magnet dc machine.	34
2.4	System control development using block wise inversion.	35
2.5	Direct connection of subsystems	39
2.6	Subsystem connection using concatenation	40
2.7	Subsystem connection using permutation and concatenation	40
2.8	Example of a RL-load. Electric Scheme, EMR and MCS	41
2.9	Representation of an EMR element using three variables.	45
2.10	Representation of an EMR element with coupling and accumulation. .	48
3.1	EMR of a reformer	54
3.2	EMR of a heat exchanger	58
3.3	Evaluation of the molar flow vector and temperature after the mixing unit	60
3.4	EMR of the first desulfurization unit	62
3.5	EMR of a water gas shift reaction unit	63
3.6	Evaluation of the molar flow vector and temperature after the WGS unit	65

3.7	EMR of a preferential oxidation unit	65
3.8	EMR of the second desulfurization unit	68
3.9	EMR of a water gas condensation unit	68
3.10	EMR representation of the temperature dynamic.	72
3.11	EMR representation of a pressure drop element	73
3.12	Heat exchanger - reformer unit designed by N-GHY.	75
3.13	EMR representation of the fuel processor unit for the supply of a PEFC	77
3.14	Stationary mass flows inside the fuel processor (to be connected to a PEFC)	78
3.15	Stationary temperatures of the fuel processor (to be connected to a PEFC)	79
3.16	Temperature development for the reformer - heat exchanger unit.	80
3.17	Pressure development for a PEFC	80
3.18	EMR representation of the fuel processor unit for the supply of a HTPEM	82
3.19	Stationary mass flows of a HTPEM	83
3.20	Stationary temperatures of a HTPEM	83
3.21	Pressure development for a HTPEM	84
4.1	Different layers inside the fuel cell and their contribution to cell voltage.	87
4.2	Cathode inlet - EMR and schematic representation	92
4.3	Anode inlet - EMR and schematic representation	94
4.4	Cathode catalyst - EMR and schematic representation	95
4.5	Anode catalyst - EMR and schematic representation	96
4.6	Cathode gas diffusion layer - EMR and schematic representation	100
4.7	Anode gas diffusion layer - EMR and schematic representation	101
4.8	Membrane - EMR and Schematic Representation	103
4.9	EMR and schematic representation of the fuel cell stack.	107
4.10	The Ballard Nexa™ system.	108
4.11	Validation strategy	108
4.12	Load profile demanded from the hydrogen fueled system.	110
4.13	Fuel cell stack voltage development for hydrogen fueled system.	110
4.14	Fuel cell stack voltage development divided into contributors.	112
4.15	Anodic and cathodic humidity.	112
4.16	Contribution of different layers of the fuel cell stack to the voltage.	113
4.17	Current profile applied for the reformat driven fuel cell system.	115
4.18	Measured and simulated voltage development for the reformat driven fuel cell system.	116
4.19	Serenergy HTPEM Stack (picture provided by N-GHY).	120

4.20	Modeling and measurement results of a single HTPEMFC	121
4.21	Modeling and measurement results of a single HTPEMFC	122
5.1	EMR of Fuel Cell System containing Diesel, Water and Air Supply, Fuel Processor and Fuel Cell Stack.	127
5.2	EMR of the Battery.	128
5.3	EMR of the DC/DC Power Converter	128
5.4	EMR of the electric accumulation	129
5.5	EMR of the electro-mechanic conversion.	129
5.6	EMR of the mechanic accumulation	130
5.7	EMR of the pump	131
5.8	EMR of a supply system.	131
5.9	Estimation block representing the fuel cell for mass flow control. .	134
5.10	EMR and control structure of the system between heat exchanger entrance and fuel cell entrance.	135
5.11	EMR and control structure of Desulfurization 2	137
5.12	EMR and control structure of Water Gas Shift Reaction	138
5.13	EMR and control structure of Reformer	140
5.14	EMR and MCS of Heat Exchanger/Gas Mixing unit	141
5.15	EMR and MCS of the water supply system.	141
5.16	EMR and temperature MCS of the water gas shift unit.	144
5.17	EMR and MCS of a diesel supplied HTPEMFC system	145
5.18	Current profile submitted to the mass flow control.	146
5.19	Hydrogen molar flow evolution	147
5.20	Water molar flow evolution	148
5.21	Carbon monoxide molar flow development	148
5.22	Current profile submitted to the temperature control.	149
5.23	Temperature evolution of the gases	150
5.24	Temperature evolution of the surrounding boxes.	151
6.1	Objectives, major work and perspectives	157

List of Tables

2.1	Quantity pairs used to describe energy flows [1]	30
2.2	Basic Elements of Bond Graph	33
2.3	Compliance of different modeling approaches to the needs	36
2.4	Overview of basic elements of EMR and MCS	38
2.5	Molar masses of species - maybe put in Annex	47
4.1	Critical temperatures, pressures and molar masses of different systems [116]	98
4.2	Molar fractions in reformat equivalent gas mixture.	114
4.3	Parameters for cathodic voltage share of a HTPEM [95]	117
4.4	Parameters for the reaction kinetics of adsorption/desorption reaction on anode [95]	118
A.1	Input parameters of the fuel processor unit	175
A.2	Parameters to calculate the stationary behavior of the fuel processor unit	175
A.3	Parameters to evaluate the dynamic behavior of the fuel processor unit	176
A.4	Parameters to evaluate the thermal behavior of the fuel processor unit	177
A.5	Parameters of Fuel Cell	178
A.6	Parameters of Diesel, Water and Air Supply	178
A.7	Parameters of Diesel, Water and Air Supply	179

Acknowledgments

With doing a PhD thesis a dream came true for me. Even though or especially because my way towards this PhD thesis was not always linear, I am happy to have accepted this challenge. An enriching aspect of my work was the fact that I was faced with two foreign languages, writing the PhD thesis in France and being a process engineer in an electromechanics laboratory.

A PhD thesis is not a straight-line work. One has to learn to cope with drawbacks, frustrations and changes in direction, but also with moments of amazement and happiness. Even though one is *the man in charge* for ones work it is necessary to have an exchange and I would like to thank some people that have all supported to my PhD thesis.

The PhD thesis was possible because of a EGIDE scholarship for foreign students that work in France and because of the fact that I was able to participate in the project GAPPAC that was supported by the French National Agency for research (ANR) through its PAN-H program.

I would like to thank all members of the jury. First, I would like to thank the examiners, for examining my work in detail.

- Yann BULTEL from the LEPMI at the INP Grenoble for regarding my work from the electrochemical and process engineering point of view.
- Maurice FADEL from the LEEI at the INP Toulouse for his interest toward the methodology used and for the fruitful discussion.

Also, I would like to thank the other members of the jury, namely:

- Sylvain ALLANO of the SATIE at the ENS Cachan for his detailed questions and his deep interest in the methodology and the possibility of applying it to different systems.

- Alain BOUSCAYROL of the L2ET at the UTS Lille for his guidance throughout the thesis, his constant interest in my work and the fact that he recalled the basic ideas of the methodology while giving me the freedom to advance. I would like to acknowledge the detailed comments on my PhD documents which have been taken into account and which helped to further improve the manuscript.
- Ludmilla GAUTHIER of the EIFER at Karlsruhe, Germany for her interest in my work and for the questions.
- Stephan KABELAC of the Institut für Thermodynamic at the HSU Hamburg, Germany for his constant support throughout the thesis and for being a support in thermodynamic questions, also I would like to acknowledge the long and uncomfortable journey he accepted to assist at the presentation.

I was lucky to be coached throughout my PhD thesis by my PhD supervisor Marie-Cécile PÉRA of Femto-ST, Enisys at the University of Franche-Comté. I would like to thank her for her availability and her openness towards new ideas on the organizational and the technological point of view. The fact that she helped by overcoming problems with patience and with the intend rather helping me to learn and to improve myself than to give only solutions, which helped me to develop independence. I would also like to thank her for being able to detect moments of blockage and for her capability to find intelligent and pragmatic loop holes in such situations.

I would also like to thank my PhD co-supervisor Daniel HISSEL of Femto-ST, Enisys at the University of Franche-Comté of encouraging me to present my work in form of articles and conference papers and of giving me the possibility to participate at an international conference. This was a very enriching experience to come in contact with other scientists from the same domain.

Thanks go to my colleagues at work, to Laurence MARY and Isabelle CHRISTEN for their efficiency in all administrative aspects. Xavier FRANCOIS and Fabien HAREL for helping me to realize the tests and for finding simple and pragmatic solutions while having short delay. In particular I would like to thank the colleagues of my office with whom I spend so much hours for always finding the right attitude; if it was calm and concentrated or a relief and relaxation and for answering all my questions. Thank you Elie, Andres, Samir, Pierre and Charly and all other colleagues.

Thanks go also to John Scott from the NASA Lyndon B. Johnson Space Center, Houston, Texax, USA for improving the manuscript, by adjusting my

words in a way that they stayed my words and gained professionalism.

Accomplishing a PhD inside a research project was very enriching for me. The fact of having deadlines to respects helped me to organize my work. The fact of working with different partners with different interests, broadened my horizon and focused my work. The fact of having industrial partners helped to base the work on real life needs. Especially I would like to thank Elodie HERAIL, Samuel LECOQ and Julien COLIÉ from N-GHY for the time they spend and for their patience in exchanging knowledge on fuel processor as well as all the results provided that were needed to validate the model.

I would also like to acknowledge all people in my surrounding who trusted in me and who supported me with their encouragements, their patience and there trust.

And finally I want to thank a special person, Benjamin BLUNIER, for being at my side and for never stop motivating me to give my very best and to stay myself.

Abstract

Fuel cell systems (FCS) are considered to be upcoming technology for electrical power generation. They can be used for portable, stationary and transportation applications. Fuel cells are run on hydrogen. Hydrogen can be produced either by electrolysis using electricity from renewable energy or by converting conventional hydrocarbons into a hydrogen rich gas. Among others, a FCS incorporates two main components, the fuel processing unit and the fuel cell stack. The use of hydrocarbon fueled FCS as auxiliary power units (APU) in transportation applications is a possible entry market for this technology that utilizes the existing infrastructure of fuel supply.

Hydrocarbon fueled FCSs are complex multi-domain systems combining aspects from various energetic regimes, like electro-chemical, electrical, pneumatical and thermal. These systems work only in a narrow and well defined range of operation. Therefore, this application requires a well adapted system control to respect these constraints. Classical control structure development often requires the transfer function of the system. This can be difficult or even impossible to derive for complex systems. Therefore, control structure development for complex multi-domain systems is often based on empirical observation and experience. It is desirable to find an approach that allows the development of a control structure based on system description. Such an approach will simplify control structure development and ensure that the control structure is adapted to the system needs. Model based control structure design is an approach that can meet these demands.

This thesis presents a complete model of a low temperature FCS fueled by commercial diesel, and is well adapted for model based control development. The studied FCS provides 25 kW electric power, and at the same time the system waste heat is used for climatization. In chapter (2) several modeling methodologies are introduced. Each is evaluated

to see if it can be used to model a complex multi-domain system and if it can be used for model based control structure development. Energetic Macroscopic Representation (EMR) is identified as the best adapted methodology and is applied to chemical reactions and mass transfer.

In chapter (3) a model of the fuel processor is presented and implemented in Matlab/SimulinkTM. To obtain a hydrogen rich gas, the supplied hydrocarbon has to be broken up. Subsequently, the gas has to be purified in order to avoid contamination of the fuel cell with sulfur and carbon monoxide.

In chapter (4) a model of the fuel cell stack is presented. It takes into account the gas flows in the different layers, describing membrane humidification as well as the voltage supplied by the fuel cell. The model also takes into account the influence of the membrane humidity on the stack voltage.

Among low temperature fuel cells, two technologies are available. The model is developed for the more common (Polymer Electrolyte Fuel Cell - PEFC), but the emerging technology (High Temperature Proton Exchange Membrane Fuel Cell - HTPEMFC) shows advantages with regard to system volume and heat use. Therefore, the models of the fuel processor and the fuel cell stack have been adapted to this emerging technology. The demonstrated adaptability underlines the advantage of using a modular modeling approach.

The models are validated successfully against measurements, literature values and values supplied by system manufacturer.

To confirm that the model can be used for model based control development, the control structure with regard to the temperature and the mass flow control for the FCS is developed in chapter (5). It is shown that the control structure of the system can be obtained by block wise inversion of the model. This approach gives the control structure; the choice of the controllers and their parameterization is up to the developer. The application of control proves that, using EMR, it is possible to derive a control structure from the model of a complex multi domain system without the need to derive its transfer function.

The presented work is accomplished in cooperation with the French national project *GAPPAC* from the PAN-H program of the French National Agency for Research (ANR). It gathers N-GHY, Airbus and Nexter as industrial partners and LMFA, Armines, IFFI, INRETS LTN and FCLAB Institute¹ as research institutes.

¹FCLAB is a joint research institute of CEA, CNRS, INPL, INRETS, UFC, UHP, UTBM

Résumé

Les systèmes pile à combustible (SPAC) sont prometteurs pour la production d'énergie électrique. Les applications potentielles concernent les secteurs portable, stationnaire ou transport. La pile à combustible (PAC) est alimentée en hydrogène ; l'hydrogène peut être produit à partir d'un procédé d'électrolyse en utilisant des énergies renouvelables ou à partir d'hydrocarbures transformés en un gaz riche en hydrogène. Un SPAC contient, parmi d'autres éléments, deux composants clés : l'unité de production de combustible et l'empilement de cellules (stack). L'utilisation d'un SPAC alimenté en hydrocarbure comme unité de puissance auxiliaire dans le transport peut être un point de départ intéressant pour cette technologie dans la mesure où elle utilise l'infrastructure de distribution existante.

Les SPAC alimentés en hydrocarbure sont des systèmes complexes, multi physiques qui combinent différents domaines énergétiques c'est à dire électrochimique, électrique, pneumatique et thermique. Un tel système fonctionne seulement dans des conditions opérationnelles bien définies. La mise en oeuvre d'un SPAC demande donc un système de contrôle bien adapté. L'approche classique du développement d'une commande suppose souvent de définir la fonction de transfert du système complet ce qui est difficile, voire impossible, compte tenu de la complexité du système considéré. En conséquence, la structure de commande des systèmes complexes multi-domaines se base souvent sur des observations empiriques ou sur l'expertise. Il s'agit ici de trouver une approche systématique qui permet de déduire la structure de la commande à partir de la description du système. Une telle approche vise à simplifier le développement de la structure de commande pour des systèmes complexes multi domaines et à assurer que la structure de la commande est adaptée aux besoins du système.

Dans ce travail, un modèle complet d'un SPAC basse température alimenté en diesel commercial est présenté. Il est adapté au développement de la structure

de commande. Le SPAC étudié est destiné à fournir d'une part une puissance électrique de 25 kW, d'autre part de la chaleur valorisée sous cette forme ou utilisée pour la climatisation.

Dans le chapitre (2), différentes méthodologies de modélisation sont présentées. Leur degré de pertinence est évalué pour modéliser des systèmes complexes multi domaines et pour être utilisé pour le développement de la structure de la commande. La Représentation Énergétique Macroscopique (REM) est identifiée comme la méthodologie la mieux adaptée. Dans le chapitre (3) un modèle de dispositif de transformation du combustible est présenté et implanté dans Matlab/SimulinkTM. Pour obtenir un mélange riche en hydrogène, l'hydrocarbure doit être fractionné. Par la suite, le mélange de gaz doit être purifié afin d'éviter la contamination de la pile à combustible par des dérivés soufrés et/ou par du monoxyde de carbone. Dans le chapitre (4), un modèle de stack est présenté. Il prend en compte les débits gazeux dans les différentes couches, l'humidification de la membrane et la tension de pile.

Il existe deux technologies de piles à combustibles basse température. Le modèle est développé pour la technologie la plus connue (Polymer Electrolyte Fuel Cell - PEFC), mais la technologie émergente (High Temperature Proton Exchange Membrane Fuel Cell - HTPMEMFC) montre des avantages concernant le volume du système et l'utilisation de la chaleur. Ainsi, les modèles du fuel processeur et du stack pile à combustible ont été adaptés à la technologie émergente. La simplicité de l'adaptation souligne l'avantage de l'utilisation d'une approche modulaire pour la modélisation. Le modèle est validé à partir de valeurs mesurées, de valeurs de la littérature et de valeurs fournies par le constructeur du système. Pour confirmer que le modèle peut être utilisé pour le développement de la structure de commande, celle concernant la température et les débits de gaz pour le SPAC est développée au chapitre (5). La structure de commande peut être obtenue par une inversion bloc par bloc du modèle. L'approche donne une structure de commande mais le choix des régulateurs et leur paramétrage est du ressort du développeur. L'application de la commande montre qu'en utilisant la REM, il est possible de dériver la structure de la commande à partir du modèle d'un système complexe multi domaine, sans avoir besoin de la fonction de transfert du système entier.

Le travail est accompli dans le cadre du projet national française *GAPPAC* composante du programme PAN-H de l'Agence National de la Recherche (ANR). Il regroupe des partenaires industriels (N-GHY, Airbus et Nexter) et universitaires (LMFA, Armines, IFFI, INRETS LTN et l'institut FCLAB ¹).

¹FCLAB est un institut de recherche commun du CEA, du CNRS, de l'INPL, de l'INRETS, de l'UFC, de l'UHP, de l'UTBM

Zusammenfassung

Brennstoffzellensysteme (BZS) sind eine Zukunftstechnologie zur elektrischen Energieerzeugung. Sie können im portablen, stationären und Transportbereich eingesetzt werden. Brennstoffzellen werden mit Wasserstoff betrieben. Der benötigte Wasserstoff kann sowohl mit Hilfe der Elektrolyse aus erneuerbaren Energien erzeugt werden, als auch aus der Umwandlung konventioneller Treibstoffe in ein wasserstoffreiches Gas. Ein BZS besteht unter anderem aus zwei Hauptkomponenten; der Brennstofferzeugungseinheit und dem Brennstoffzellenstapel. Ein möglicher Einstiegsmarkt für diese Technologie ist die Anwendung kohlenwasserstoffbetriebener BZS zur Hilfsenergieerzeugung im Transportbereich.

Kohlenwasserstoffbetriebene BZS sind komplexe Systeme, die Fachkompetenz aus verschiedenen Arbeitsbereichen verbinden: Energietechnik, Elektrochemie, Elektrik, Pneumatik und Thermik. Ein solches System arbeitet nur in einem eng definierten Arbeitsbereich, daher ist ein gut angepasstes Steuersystem wichtig. Der klassische Ansatz zur Entwicklung einer Steuerung erfordert die Kenntnis der Übertragungsfunktion des Gesamtsystems. Die Ableitung dieser Übertragungsfunktion für solch ein komplexes System kann schwierig oder unmöglich sein. Daher basieren die angewandten Steuerungssysteme oft auf Erfahrung. Es ist wünschenswert einen Ansatz zu entwickeln, der die Entwicklung einer Systemsteuerung ermöglicht, die auf einer Systembeschreibung basiert. Ein solcher Ansatz wird die Entwicklung der Kontrollstruktur vereinfachen und sicherstellen, dass die Systemsteuerung den Systemansprüchen gerecht wird. Eine modelbasierte Systemsteuerungsentwicklung kann diese Ansprüche erfüllen.

In dieser Arbeit wird das Model eines kohlenwasserstoffbetriebenen Niedertemperatur-Brennstoffzellensystems vorgestellt, dass für die modelbasierte Steuerstrukturentwicklung angepasst ist. Das untersuchte BZS liefert eine elektrische Leistung von 25 kW und kann gleichzeitig zur Klimatisierung verwendet werden. In Kapitel (2) werden verschiedene Methoden der Modellierung vorgestellt. Es

wird erörtert, ob diese Methoden für die Beschreibung komplexer Systeme verwendet werden können und ob eine modellbasierte Steuerungsentwicklung mit ihnen möglich ist. Die Energetisch Makroskopische Representation (EMR) ist gut für die modellbasierte Steuerungsentwicklung geeignet und wird für die Beschreibung chemischer Reaktionen angepasst. In Kapitel (3) wird das Model einer Brennstoffaufbereitung präsentiert und in Matlab/SimulinkTM umgesetzt. Um ein wasserstoffreiches Gasgemisch zu erzeugen muss der langkettige Kohlenwasserstoff aufgespalten werden. Dieses Gas muss aufbereitet werden um Verunreinigungen mit Schwefel und Kohlenmonoxide zu verhindern. In Kapitel (4) wird das Model eines Brennstoffzellenstapels präsentiert. Das Model beschreibt die Stoffströme in den verschiedenen Schichten einer Brennstoffzelle und berücksichtigt daher sowohl die Befeuchtung der Membran als auch die Spannung, die von der Brennstoffzelle erzeugt wird. Dabei wird der Einfluss der Membranfeuchte auf die Spannung berücksichtigt. In der Klasse der Niedertemperaturbrennstoffzellen gibt es zwei unterschiedliche Technologien. Das Model ist für die am weitesten verbreitete Technologie (Polymer Electrolyte Fuel Cell - PEFC) erstellt. Da die aufkommende Technologie (High Temperature Proton Exchange Membrane Fuel Cell - HTPEMFC) Vorteile bezüglich des Systemvolumens und der Wärmenutzung zeigt, wurde das Model der Brennstoffaufbereitung und der Brennstoffzelle für diese Technologie angepasst. Die Möglichkeit einer schnellen Anpassung des Models bestätigt den Vorteil der Nutzung eines modularen Modelansatzes. Das Model ist mit Hilfe von Messungen, Literaturwerten und Werten des Systemherstellers validiert.

Um sicherzustellen, dass das erstellte Model für die Steuerungsentwicklung genutzt werden kann, wurde die Steuerungsstruktur des BZS für die Stoffströme und die Systemtemperatur entwickelt, siehe Kapitel (5). Es wird gezeigt, dass die Steuerungsstruktur durch eine blockweise Umkehrung des Models entwickelt werden kann. Dieser Ansatz erzeugt die Steuerungsstruktur, die Auswahl der Regler und ihre Parametrisierung bleibt dem Entwickler überlassen. Die Anwendung der Steuerung zeigt, dass es mit Hilfe von EMR möglich ist, die Steuerungsstruktur eines komplexen Systems abzuleiten ohne die Übertragungsfunktion des Gesamtsystems zu kennen.

Die vorgestellte Arbeit wurde in Zusammenarbeit mit dem französischen Projekt *GAPPAC* erstellt. Dieses Projekt ist ein Teil des PAN-H Programms der nationalen französischen Forschungsanstalt (ANR). Projektpartner seitens der Industrie sind N-GHY, Airbus und Nexter, seitens anderer Forschungsinstitute LMFA, Armines, IFFI, INRETS LTN und das FCLAB Institut¹.

¹Das Institut FCLAB ist ein Zusammenschluss aus CEA, CNRS, INPL, INRETS, UFC, UHP und UTBM

Nomenclature

Roman Symbols

a_i	Activity of species i	
b_{drag}	Electro-osmotic Drag Coefficient	
C	Integration Constant	
c	Concentration	$[\text{kg m}^{-3}]$
$C_{\text{a,c}}$	Tuning Parameter of the Cathodic Concentration Overpotential at Anode/Cathode	$[\text{V}]$
c_{H}	Factors between Hydrogen and other Species in the Fuel Vector Normalized to the Hydrogen content.	
C_i	Proportion of Heat Capacity Flow at i	
c_p	Heat Capacity	$[\text{kJ kg}^{-1} \text{K}^{-1}]$
$D_{i,j}$	Diffusion Coefficient of species i and j	$[\text{cm}^2 \text{s}^{-1}]$
E	Thermodynamic Potential	$[\text{V}]$
e	Electromotive Force	$[\text{V}]$
E_i	Energy of species i	$[\text{J}]$
\dot{E}_i	Energy Flow of species i	$[\text{W}]$
F	Faraday Constant ($96\,485,3415 \pm 0,0039$)	$[\text{C K}^{-1}]$
f	Friction	$[\text{N m s}^{-1}]$

f_a	Air Factor	
f_e	Water factor	
f_o	Oxygen Factor for Preferential Oxidation	
f_{xy}	Fraction between species x and y	
G	Gibbs Energy	[J]
g	Gravitational Acceleration (9.81)	[m s ⁻²]
H	Enthalpy	[J]
h_i	Specific Enthalpy of species i	[J mol ⁻¹]
\dot{H}	Enthalpy Flow	[W]
\mathbf{h}_i	Specific Enthalpy Vector at position i	[J mol ⁻¹]
I	Current	[A]
j	Current Density	[A cm ⁻²]
j_0	Exchange Current Density	[A cm ⁻²]
J_i	Molar Flux of species i	[mol cm ⁻² s ⁻¹]
Jm	Mechanical Inertia	[kg m ²]
k	Ideal Throttle Constant	[mol s ⁻¹ Pa ⁻¹]
kA	Heat Transfert Coefficient multiplied with the Heat Exchange Area	[W K ⁻¹]
K_e	Electro-mechanical Conversion Coefficient	[Nm A ⁻¹]
K_p	Equilibrium Constant	
\mathbf{k}	Conversion Constant between pump/compressor and molar flow	[mol rad ⁻¹]
L	Inductivity	[H]
m	Conversion Constant	
M_i	Molar Mass of species i	[kg mol ⁻¹]
\dot{m}_i	Mass Flow of species i	[kg s ⁻¹]

$\dot{\mathbf{m}}_i$	Mass Flow Vector at position i	$[\text{kg s}^{-1}]$
m_i	Mass of species i	$[\text{kg}]$
m_x	Chopper Conversion Constant for the supply of species x	
n	Number of Cells in the Stack	
N_i	Number of Transfer-Units for heat flow i	
ni	Number of Moles of species i	
\dot{n}_i	Molar Flow of species i	$[\text{mol s}^{-1}]$
$\dot{\mathbf{n}}_i$	Molar Flow Vector at position i	$[\text{mol s}^{-1}]$
P	External Energy	$[\text{W}]$
p_{ci}	Critical Pressure of Species i	$[\text{Pa}]$
p_i	Total Pressure at position i also Partial Pressure of species i	$[\text{Pa}]$
\mathbf{p}_i	Partial Pressure Vector at position i	$[\text{Pa}]$
Q	Heat	$[\text{J}]$
\dot{Q}	Heat Flow	$[\text{W}]$
R	Ideal Gas Constant ($8,314\,472 \pm 0,000\,015$)	$[\text{J mol}^{-1} \text{K}^{-1}]$
R_i	Resistance at element i	$[\Omega]$
r^M	Membrane Specific Resistance	$[\Omega \text{ cm}^2]$
S	Surface	$[\text{m}^2]$
sel	Selectivity of a reaction	
\dot{S}_i	Entropy Flow at position i	$[\text{W K}^{-1}]$
\bar{T}_i	Logarithmic Mean Temperature at position i	$[\text{K}]$
T_{ci}	Critical Temperature of species i	$[\text{K}]$
T_i	Temperature of species i	$[\text{K}]$
U	Internal Energy	$[\text{J}]$

U_i	Battery Voltage of element i	[V]
V	Volume	[m ³]
v	Velocity	[m s ⁻¹]
V_i	Voltage at element i	[V]
\dot{V}_i	Volume Flow of species i	[m ³ s ⁻¹]
W	Mechanical Work	[J]
\dot{W}	Mechanical Work Flow	[W]
\dot{W}_i	Heat Capacity Flow at point i	[W K ⁻¹]
x_i	Molar Fraction of species i	
\mathbf{x}	Molar Fraction Vector	
z	Height	[m]

Greek Symbols

α	Molecules Transported through Membrane, for each Proton transported	
α_a	Dimensionless Tuning Parameter of the Cathodic Activation Overpotential	
δ	Thickness	[m]
ϵ	Porosity	
ε	Dimensionless Temperature Change	
η_i	Overpotential caused by i	[V]
$\eta_{\text{pump},i}$	Efficiency of electro-mechanical conversion in pump for species i	
Γ	Torque	[N m]
γ	Cathode Stoichiometric Ratio for HTPEMFC	
ξ	Reaction Advancement	
λ	Water content in the membrane	
λ_H	Hydrogen stoichiometry	

λ_O	Oxygen stoichiometry	
Ω	Turning speed	$[\text{s}^{-1}]$
ρ	Density	$[\text{kg m}^{-3}]$
σ^M	Nafion conductivity	$[\text{S m}^{-2}]$
τ_{cond}	Selectivity of Liquid Flow Removal	
τ	Torosity	
θ	Surface coverage	

Superscripts

a	Anode
c	Cathode
eff	Effective
m	Membrane

Subscripts

0	Standard conditions
a	Air
act	Activation
$anode$	Anodic
B	Box
$back - diff$	Back diffusion
$cell$	One cell
$comb$	Combustion
$conc$	Concentration
$Cond$	Condensation
d	Diesel
$diff$	Diffusion

<i>drag</i>	Electro-osmotic drag
<i>env</i>	Environment
<i>f</i>	Formation
<i>H</i>	Hydrogen Production
<i>i</i>	Name of the species
<i>load</i>	Load
<i>mid</i>	Intermediate value
<i>mo</i>	Motor
<i>ohm</i>	Ohmic
<i>p</i>	Pump
<i>ref</i>	Reforming
<i>sat</i>	Saturation
<i>stack</i>	Stack
<i>Su</i>	Supply
<i>vir</i>	Virtual
<i>w</i>	Water

Acronyms

ACS	Applicable Control Structure
APU	Auxiliary Power Unit
COG	Causal Ordering Graph
Des	Desulfurization
EMR	Energetic Macroscopic Representation
FC	Fuel Cell
GDL	Gas Diffusion Layer
HTPEMFC	High Temperature Proton Exchange Membrane Fuel Cell

MCS Maximum Control Structure

PBI Poly Benzo Imidazole

PEFC Polymer Electrolyte Fuel Cell

PrOx Preferential Oxidation

RHex Reformer-Heat Exchanger

WGS Water Gas Shift

General Introduction

There are manifold signs today, telling us that our lifestyle with respect to energy consumption has to change. Our excessive use of fossil fuels is changing our climate, causing extreme weather phenomena to be more frequent and heavier [85]. At the same time, we experience a shortage in fossil fuel supply accompanied by a considerable rise in price [8]. Those problems exist in every aspect of life, such as industry, housing and transport. For stationary power supply there already exist approaches that are not based on fossil fuels, like hydro power, wind power and solar power and, in some cases, nuclear energy. For mobile applications in buses, cars, trains and aircraft these approaches are not so obvious.

There are different solutions foreseeable for the transportation sector. As resources are limited and as we are trying to extend their availability, improvement of conversion efficiency is part of the solution. Efficiency can be increased using two approaches: first, optimizing the propulsion motors. This has been done for combustion engines during the past hundred years, and no major advancements are still to be expected in this field. Otherwise, the overall system can be optimized, taking into account the interactions between the different subsystems, as well as their individual characteristics. In fact, most of the time there is only one person inside a car, and the average weight of cars has increased [23]. A change in overall system design is needed, accompanied by a change in attitude of the customers, away from big heavy cars toward small efficient cars [3].

Cars and buses can run on natural gas instead of gasoline or diesel. This option has already been applied for some cars; either a natural gas combustion engine applied in series (Volkswagen Touran EcoFuel) or complete retrofitting is possible. A natural gas fuelling network has also to be installed [4]. For buses changeover of a complete fleet can be done. The establishment of an infrastructure is easier, because they are often fuelled at a few central points. However, natural gas remains a fossil fuel, and its supply is limited even if a longer duration

is expected before this limit is reached [66].

Also the use of biofuels might be an alternative. Biofuels are liquid or gaseous fuels made from agricultural products. Bioethanol is widely used as fuel for transportation applications in Brazil. The use of biofuels has already led to an increase in corn price [129]. For the moment, biofuels are mainly produced from the food crops. Therefore, biofuels are in direct conflict with nutrition. Nutrition is still a problem in the world, and a foreseen rise in population [7] is exacerbating the problem of *eat or drive*. A second generation of biofuels using non-food crop material is under development [14, 67].

Another possibility is the use of electricity for transportation applications. Electricity is an energy vector and has to be produced from another energy source. Electricity can be produced either from fossil energy sources like coal, or from renewable energy sources like wind, water or solar energy, or from nuclear energy. The conversion from all energy sources is under constant development. Already for stationary applications the need of electric energy is increasing [86]. If not only the stationary, but also the portable market will be supplied with electricity, a considerable effort has to be done to meet the increase in demand.

The electric car is a straight forward possibility for transportation. In 1900 nearly 14 000 automobiles were on the road in the USA. A total of 40 % were steam powered, 38 % were electric and only 22 % were powered by gasoline burned in an internal combustion engine [128]. Ultimately the combustion engine cars have survived because the price of fossil fuel decreased dramatically and the batteries inside the electric cars did not show sufficient life time and autonomy. Since that day combustion engines have greatly improved. There were also improvements concerning electric motors and batteries. The lithium ion based batteries show, for example, good storage qualities. Still, they have to be improved with regard to thermal stability [159]. With those technologies and the current rise in fossil fuel price, electric cars might return.

Energy storage is the weak point of electric cars. Therefore, electric cars using other technologies along with batteries for energy storage are under consideration. Vehicles using two or more distinct power sources to move the vehicle are called *hybrid vehicles*. Secondary power sources are for example super capacitors that are used to store energy recuperated during braking and back up steep accelerations [25, 39, 40, 80]. Also, combinations with combustion engines and batteries are under consideration to increase the autonomy in cars [37].

Moreover, hydrogen is a promising energy vector to drive cars. Hydrogen can

be produced from several energy sources. Either from water split by electricity, the so called electrolysis, or directly from fossil fuels or biofuels via fuel processing. Also thermal cracking and biologic production of hydrogen from anaerobic bacteria are foreseeable. Hydrogen can be transformed into electricity directly using fuel cells. This conversion is thermodynamically more efficient than the electricity production via a heat engine using combustion spinning a turbine-generator.

Proton Exchange Membrane Fuel Cells (PEMFCs) convert hydrogen into electricity using membranes that are at the same time proton conductors and gas isolators (1.1.3). The principle is simple, but it is not autonomous. A fuel cell has to be fed with the supply streams and temperature inside the system has to be controlled. Fuel cells with their electro-chemical reaction are a good example of a multi domain system combining electrical, chemical, pneumatic and thermal aspects. The overall system efficiency depends more and more on the improved interaction between different domains, which are monitored by the system control. If a methodology proves the capabilities for developing a control for such a complex system, it can also be used for other applications.

Step changes in technology are always difficult to implement. Hence, it is unlikely to be able to change at the same time the fuel for transportation applications and the energy conversion approach. While hydrogen can be produced from different energy sources, it can also be produced from conventional fuels like gasoline and diesel by fuel processing. During fuel processing the long chain hydrocarbons forming conventional fuel are broken into hydrogen and carbon oxides. Water and/or air are added to support this process. The fuel processing unit might be incorporated inside a vehicle.

As today's vehicles do not use energy for propulsion only, but also for auxiliary power loads like air-conditioning, a combination of a conventional drive train and a fuel cell for auxiliary power supply can form an interesting entry area for fuel cell application. To rely on one fuel source only it is advantageous to feed the fuel cell system with the same fuel as the conventional drive by means of a fuel processing unit.

The presented work has been accomplished in cooperation with the French national project *GAPPAC* from the PAN-H program of the French National Agency for Research (ANR) and supported by MEGEVH. The aim of this project is to develop a fuel cell based Auxiliary Power Unit (APU) capable of trigeneration (electricity, heat and refrigeration). Different areas of transportation applications are addressed, such as land, air, salt and fresh waters. The power generation unit

considered with, 25 kW electric and 30 kW thermal power, will run on commercial fuels such as diesel. The project GAPPAC consists of the following industrial partners: Nexter Systems does the project management, the land transportation systems and vehicle integration; N-GHY supplies the fuel processing unit, does the system dimensionment and a the tests and Airbus who give constraints for the aeronautic application. Furthermore, the GAPPAC project has the following research partners: Armines-EMSE does the identification and development of sensors for hydrogen sulfide and carbon monoxide; IFFI (Paris) designs the heat management and cooling; INRETS LTN does the integration of transportation needs; LMFA (Lyon) developps the air management system and FCLAB Institute¹ which does the system modeling for model based control structure design.

Hydrocarbon fed FCSs are complex multi-domain systems combining aspects from various energetic domains, like electro-chemical, electrical, pneumatical and thermal. Those systems work only in a narrow and well defined environment. Therefore, this application requires a well adapted system control. The classical control structure development requires the transfer function of the system. This can be difficult/impossible to derive for complex systems. Therefore, the control structure development of complex multi-domain systems is often based on empirical observation and experience. In this work an approach is evaluated that allows the development of a control structure based on a system description. This approach simplifies the control structure development and ensures that the control structure is adapted to the system needs. A model based control structure design is used to meet these demands. This methodology is successfully applied to model and control a diesel supplied low temperature fuel cell system and shows that its likely that it can be adapted to other complex multi domain systems as well.

An introduction of the working principles of the considered fuel cell system is given in chapter (1). It contains the working principle of the fuel cell, an overview about the different fuel cell technologies available. It is introduced how the fuel cell current is derived form the basic chemical equation and the factors that influence the fuel cell voltage. An overview of different goals of modeling and their application is given. It is pointed out that a fuel cell system contains all elements that are needed to operate the fuel cell, for example the fuel processor. The different elements of the fuel processor are presented. In chapter (2) several modeling methodologies are introduced. It is evaluated if they are adapted to be used to model a complex multi-domain system and if they can be used for model based control structure development. The modeling

¹FCLAB is a joint research institute of CEA, CNRS, INPL, INRETS, UFC, UHP, UTBM

methodologies evaluated are: Electric Equivalent Model, Bond Graph, Causal Ordering Graph and Energetic Macroscopic Representation. The Energetic Macroscopic Representation (EMR) is identified as the most adapted methodology. An energetic graphic causal modeling approach seems well adapted for such a system. The energetic aspect affords the possibility to connect different energetic domains. The graphic aspect helps to provide an overview of a complex structure. The causal structure provides the potential to develop an inversion based control. The EMR is introduced in detail and is adapted to chemical conversion and mass transfer for the use in fuel cell systems.

In chapter (3) a model of the fuel processor is presented and implemented in Matlab/SimulinkTM. To obtain a hydrogen rich gas, the supplied hydrocarbon has to be broken up. Subsequently, the gas has to be purified in order to avoid contamination of the fuel cell with sulfur and carbon monoxide. The fuel processor unit incorporates several modules, namely: reformer, heat exchanger, desulfurization, water gas shift, preferential oxidation and condensation.

In chapter (4) a model of the fuel cell stack is presented. For the modeling in EMR the different layers inside the fuel cell regarded separately with regard to gas flow and electric potential. The model takes into account the gas flows in the different layers, describing membrane humidification as well as the voltage supplied by the fuel cell. The model takes into account the influence of the membrane humidity on the stack voltage.

Among the low temperature fuel cell, two technologies are available. The model is developed for the more common (Polymer Electrolyte Fuel Cell - PEFC), but the emerging technology (High Temperature Proton Exchange Membrane Fuel Cell - HTPPEMFC) shows advantages with regard to system volume and heat use. Therefore, the models of the fuel processor and the fuel cell stack have been adapted to the emerging technology. The demonstrated adaptability underlines the advantage of using a modular modeling approach.

The models are validated successfully against measurements, literature values and values supplied by the system provider.

To confirm that the model can be used for model based control development, the control structure with regard to the temperature and the mass flow control for the FCS is developed in chapter (5). It is shown that the control structure of the system can be obtained by the block wise inversion of the model. This approach gives the control structure, the choice of the controllers and their parameterization is up to the developer. The application of the control proofs that using EMR it is possible to derive a control structure from the model of a complex multi domain system without the need to work out its transfer function. The work ends with conclusions and perspectives presented in chapter 6.

Chapter 1

Working Principles of Fuel Cell Systems

1.1 Introduction to Fuel Cells

1.1.1 Discovery of the Fuel Cell Effect

The discovery of the fuel cell principle is generally credited to Sir William Robert Grove. In fact Friedrich Wilhelm Schoenbein (Professor of Chemistry and Physics at the University of Basel, Switzerland) described the fuel cell effect prior to Grove in the January 1839 edition of the Philosophical Magazine. Grove had similar results, but his work was only published in the February 1839 edition of the Philosophical Magazine. Because of the facts that Schoenbein also discussed other aspects in his publication and that he doubted his results, the discovery of the fuel cell effect is nowadays credited to Sir William Robert Grove. The both scientists met in 1839 and established a lifelong friendship [128].

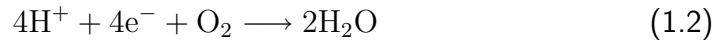
1.1.2 Working Principle

The fuel cell effect in low temperature fuel cells can be described by the observation that a current circulates in a wire connected to an oxygen source and a hydrogen source if both are connected by an ionic conductor material. It is the reverse of the electrolysis process. A fuel cell produces electricity from hydrogen and oxygen, (*Fig. 1.1*). Fuel cells can produce electricity as long as they are supplied with hydrogen and air. Therefore, fuel cells cover the advantages of batteries performing a direct electrochemical conversion and of engines which supply energy as long as they are fed with fuel.

The fuel cell can also be described by its chemical reaction. The working principle of low temperature fuel cells is described below. High temperature fuel cells exhibit slight differences in working principle [42, 41, 150]. At the anode the fuel cell is supplied with hydrogen through a flow channel. The hydrogen splits up into protons and electrons in a catalytic reaction, *Eq. 1.1*.



The protons flow through the electrolyte. Oxygen is supplied to the fuel cell cathode through a flow channel. To produce water, the oxygen has to combine with the protons flowing through the electrolyte and with electrons, *Eq. 1.2*.



As the electrons cannot traverse the electrolyte they have to flow through an external wire, thus conducting electrical work [98]. As oxygen reduction is exothermic, the fuel cell also produces heat, *Eq. 1.3*.

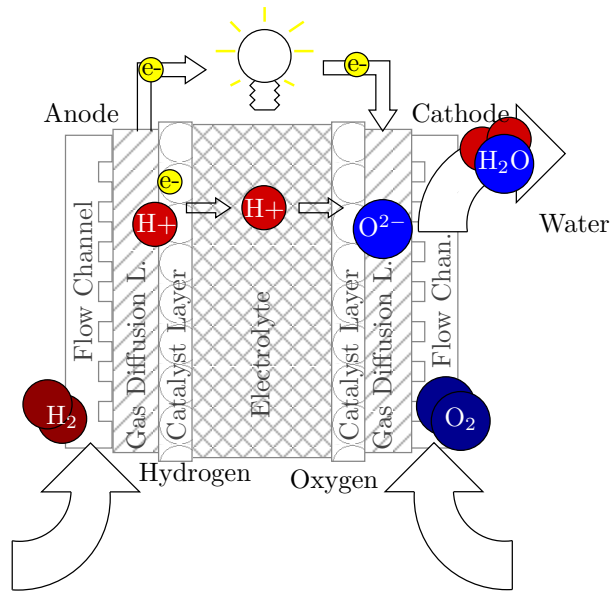
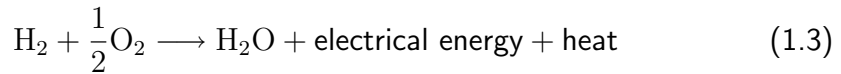


Figure 1.1: Basic working principle of a fuel cell.

1.1.3 Different Kinds of Fuel Cells

The electrolyte consists of a special material which is at the same time a conductor for protons and an isolator for electrons. Different materials show this behavior at different temperatures, building a whole family of fuel cells. The names of the different fuel cells are mainly acronyms of the electrolyte material. They differ not only in temperature, but also with regard to proton transport and physical condition of the electrolyte. The most common classification by temperature are listed below [150]:

- High Temperature Fuel Cells

SOFC: The solid oxide fuel cell works at temperatures between 800°C and 1000°C. It has been found that this working temperature has some thermodynamic advantages. At the same time such high temperatures cause long heat up times and material problems. This is why there is currently work done to decrease the working temperatures below 700°C. This working temperature would also be advantageous for cogeneration [125, 126]. The SOFC is under development for stationary [5] and automotive applications, (*Fig. 1.2*).

MCFC: The molten carbonate fuel cell has working temperatures around 650°C. This working temperature is well adapted to the use of common material such as steel and at the same time to use waste heat for cogeneration. The molten carbon is corrosive and liquid and is therefore mostly adapted for stationary power supply [2].

- Low Temperature Fuel Cells

AFC: The alkaline fuel cell was the fuel cell system the NASA used for their Apollo missions. This fuel cell operates at temperatures of around 80°C and has very high demands on the purity of fuel. Fed with pure hydrogen and pure oxygen, it was not only capable of supplying the NASA Apollo missions with electric energy, the produced water has also been used, (*Fig. 1.3(b)*).

PAFC: The Phosphoric Acid Fuel Cell is the only commercialized fuel cell system. Around 200 systems are constructed and in use for stationary power [91]. The PAFC works at temperatures around 200°C. The phosphoric acid is a liquid. The system is therefore sensitive to vibration and pressure differences and can be used for stationary applications mainly.

PEFC: The Polymer Electrolyte Fuel Cell is probably the most developed fuel cell. Nowadays, the denomination PEMFC, standing for proton

exchange membrane fuel cell, is generally used. Nearly all automotive, a big part of portable applications, as well as a big part of small and medium sized stationary applications of fuel cells use PEFCs. Their cell materials are sulphonated fluoro-polymers, commercialized, for example, under the name NafionTM by Dupont. The PEFC is working on nominal temperatures between 50 °C and 80 °C and is able to be started at lower temperatures. This low temperature makes it difficult to reject heat. Moreover, the water is partly produced in liquid form, complicating its evacuation. It has relatively high demands on the purity of the fuel. For example sulfur and carbon monoxide cause degradations in net efficiency.

HTPEMFC: The HTPEMFC is an emerging technology. As it works at nominal temperatures around 180 °C the name High Temperature Proton Exchange Membrane Fuel Cell (HTPEMFC) is used. Due to the higher working temperature the HTPEMFC has some advantages over the PEMFC, namely: simplified cooling, simplified water management, greater tolerance against pollution, however they cannot be operated at temperatures below 100 °C. The name HTPEMFC is misleading. More precisely it should be called Poly Benzo Imidazole (PBI) Fuel Cell [48, 104]. This material is comparable to that of a PAFC. The electrolyte is the same [130]. It is liquid and has to be captured inside a matrix to be stabilized, only the matrix material between PAFC and HTPEMFC are different, leading to the fact that the HTPEMFC is much more stable as well with regard to vibration and with regard to pressure difference. The HTPEMFC development is recent.



Figure 1.2: SOFC Auxiliary Power Unit by Delphi (www.delphi.com)

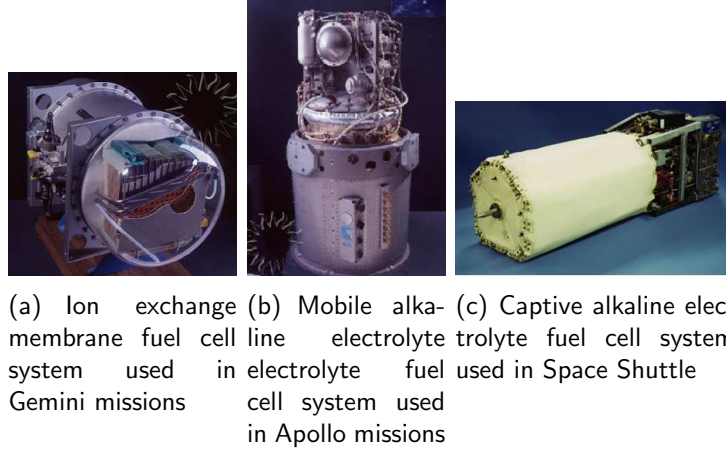


Figure 1.3: Fuel Cell Systems used in space applications

1.1.4 Current and Voltage Supplied

A fuel cell is defined by current and voltage. There is a direct connection between the hydrogen consumption and the current supplied by the fuel cell I , as every reacting hydrogen molecule causes two electrons to perform work. This effect is known as Faraday's Law using the Faraday Constant F , Eq. 1.4 [84].

$$I = \dot{n}_{\text{H}_2} \cdot 2 \cdot F \quad (1.4)$$

This equation imposes that the hydrogen molar flow needed \dot{n}_{H_2} to create the current is always available, but there are limitations. On the one hand, the hydrogen molar flow can be limited by the external system supply. On the other hand, the hydrogen supply might be limited inside the fuel cell as the hydrogen reaches the catalyst layer by diffusion and the diffusion has a limited rate. Similarly, oxygen has to be supplied to the cathode to form water which in turn has to be removed. As the current is a function of the cell surface area it is often advantageous to use the current density j in A cm^{-2} instead of the current. For the moment, the state of the art concerning the maximum current density j is around 1 A cm^{-2} , with standard procedures.

The maximum available voltage is defined by the thermodynamic potential E_0 . It can be calculated from the standard Gibbs energy ΔG_0 using [84], Eq. 1.5.

$$\Delta G_0 = -2 \cdot F \cdot E_0 \quad (1.5)$$

The values of ΔG and E in Eq. 1.5 have to be adjusted for different pressures

of the gases. This leads to the so called Nernst equation, Eq. 1.6:

$$E = E_0 - \frac{RT}{2F} \ln \frac{p_{H_2O}}{p_{H_2} p_{O_2}^{1/2}} \quad (1.6)$$

The thermodynamic potential E_0 of a hydrogen, pure oxygen fuel cell at 25 °C and 101 325 Pa is 1.23 V. This value cannot be reached in a real fuel cell for several reasons. One is that fuel cells do not work at standard conditions. All previously introduced fuel cells have working temperatures of 50 °C or higher. This already decreases the maximum voltage available. Furthermore, the partial pressures p_i taken into account in Eq. 1.6 are the partial pressures at the catalyst. The catalytic sites are separated from the in/outlet by a gas diffusion layer (GDL). Throughout the GDL the partial pressures change. If a species is consumed at the catalyst its partial pressure decreases throughout the GDL; if a species is produced at the catalyst its partial pressure increases throughout the GDL. Finally, in nearly all fuel cells the cathode is fed with ambient air, thus reducing the oxygen partial pressure at the inlet. Also, the anode can be fed by gas mixtures reducing the hydrogen partial pressure [137]. Using pressurized fuel cells might reduce these effects, while imposing higher parasitic loads for auxiliaries [21, 71, 72, 99].

Furthermore, the fuel cell itself imposes additional potential losses associated with the various layers of the fuel cell, (Fig. 1.1). The catalytic reaction is not reversible and imposes losses. The cathode activation losses are more significant than the anode activation losses. When the protons flow through the electrolyte they loose some energy (through friction). As this voltage drop is proportional to the current provided by the system it is called ohmic loss. The ohmic losses incorporate as well the voltage drop by the proton resistance of the membrane, but also the electric resistance of the bipolar plates and the connections. Also the transport of the molecule from the flow channel to the catalyst imposes some losses, those losses increase up to the limit of supply [84].

A combination of all those effects leads to the characteristic current-voltage curve called *polarization curve*, (Fig. 1.4). It starts at an reversible thermodynamic cell potential considerably below the value of 1.23 V and shows a rapid fall at low current densities. In the center of the polarization curve the fall is slower and the curve is almost linear dominated by ohmic losses. At high current densities the voltage curve shows a rapid fall down to the value limiting current density where no voltage can be supplied anymore [98].

1.1.5 Fuel Cell Modeling

After the discovery of the fuel cell effect, development was rather slow, even though its feasibility for transportation application was shown early [128]. Fuel

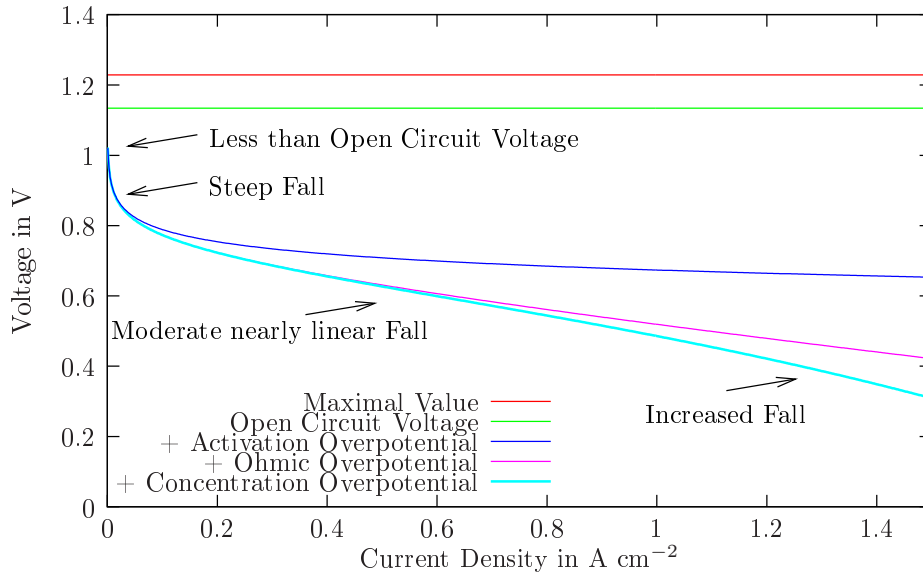


Figure 1.4: Different losses inside fuel cell forming the polarization curve

cell development gained speed as fuel cells were identified as potential energy converters for space missions. The interest in the understanding and mathematical description of fuel cells increased accordingly. Some of basic publications concerning PEMFC from this period came from Bernadi, Verbrugge [18, 19] and Springer, Zawodzinski and Gottesfeld [138].

Those mathematical approaches were soon followed by approaches with different aims. The work started with a one dimensional approach for system prediction [100], soon followed by the discussion of two and three dimensional effects using computational fluid dynamics [161]. This was needed because fuel cells are highly dependent on their working conditions, and the formation of so called hot spots or liquid water might lead to system degradation and/or damage [20, 63, 64, 89, 110, 114, 115, 139, 140]. Also gas transport is a domain in which several studies have been done [131, 154, 155].

According to the desired application, a multitude of foci for fuel cell modeling exist. In order to identify the points where system amelioration is most suitable, exergy and entropy analysis are meaningful [90, 134]. Furthermore, models can be used for diagnostic reasons, decreasing the number of sensors that have to be placed inside the fuel cell or predicting failures that would otherwise be hard to detect [17, 36, 82]. Also, however, more economic aspects can be addressed [16, 34].

In some cases it is sufficient to regard the steady state behavior of a fuel cell [100, 109]. Often, however, a steady state approach is not sufficient, because most of failures occur during operational transients. Furthermore, the interaction of dynamic aspects inside a fuel cell is interesting because several time dependencies interact, imposing different time constants [75]. Dynamic aspects are discussed by Davari et al. [61] and others [102, 123, 151, 157, 158].

As our overall system shall be fed by diesel, it is important to regard the influence of hydrogen rich gas with sulfur and carbon monoxide contamination [35, 46, 105, 137].

One of the advantages of the recent development of HTPEMFC is the improved resistance against contamination. As their development is recent, publications dealing with pure hydrogen like that of Cheddie, Munroe are rare [48]. Often the system modeling approach addresses directly the effects of contamination [11, 124]. The work of Korsgaard et al. [95, 97] on HTPEMFCs has to be emphasized as a complete modeling approach for HTPEMFCs taking into account contamination.

A good overview of existing fuel cell models has been published by Cheddie, Munroe [47]. Also the work by Haraldson et al. [77] is remarkable, because it gives a good overview of different modeling approaches.

1.2 Fuel Cell Systems

The maximum theoretical cell voltage of a fuel cell is 1.23 V [84]. Its current capability depends on the cell surface area. To obtain voltage and current levels that are well adapted for applications, several fuel cells are connected in series. This assembly is called *fuel cell stack*. A fuel cell stack is not self sufficient to run. It has to be supplied with fuel and air. In most cases the fuel cell is pressurized, so that a compressor has to be used for gaseous supplies [21]. In the case of the use of PEFC, it is advantageous to humidify the supplied gases to increase the power density. The humidification can either be done by injecting water from a separate water storage or by *recycling* a part of the water produced by the fuel cell. The diluted air and the produced water have to be removed from the stack. As a fuel cell stack produces heat, it has to be cooled, imposing a heat management system. It can be seen in (*Fig. 1.4*) that the cell voltage changes with current densities. Thus, the output electrical power might have to be transformed according to the consumer by adding a DC/DC or a DC/AC converter.

Both functions can be combined inside the power management. The combination of all these aspects shows the complexity and multi-domain involvement, (Fig. 1.5). A fuel cell, based on an electrochemical reaction, unifies a chemical reaction with electric aspects of the power conditioning, pneumatic aspects of the gas supply and thermal aspects of the heat management in a single unit. These multi-domain phenomena make fuel cell systems an interesting working field for causal, inversion based control development.

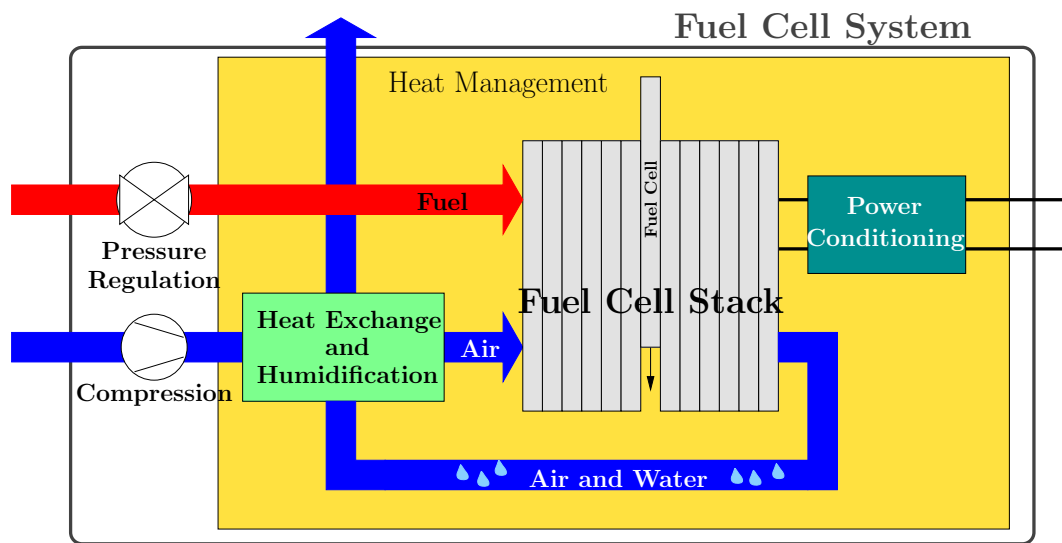


Figure 1.5: Fuel cell system: multi-domain aspects

A lot of work has been done to describe fuel cell systems; also considerable work has been done regarding the auxiliaries like power management [113] or compressors [21, 143, 144]. As systems consist of several subsystems that have to be combined, it is not sufficient to work only on the subsystems individually and then combine them afterward [21, 24, 122]. Considerable work has still to be done to find a combination that assures a well adapted mode of operation for the overall system.

1.3 Fuel Processing

The fuel processing unit converts a long chain hydrocarbon into a hydrogen rich gas mixture. Considered hydrocarbons are, for example: methane [92, 121], methanol [65, 70, 156], iso-octane [93, 94], gasoline [132], JP-8 [44] and diesel [9, 10, 135, 136, 153]. It is possible to build multi-fuel processors [33]. The fuel

processor introduced hereafter and modeled in chapter (3) is a multi-fuel processor. For this work commercial diesel is considered as fuel to produce a hydrogen rich gas mixture. Therefore, several steps have to be taken, both to convert the molecules to obtain hydrogen and to clean the gas. The transformation of long chain hydrocarbons into hydrogen rich gas is effectuated inside the reformer. The water gas shift unit, the preferential oxidation unit and the desulfurization unit carry out the gas cleaning. Other elements like the heat exchanger or the condenser adjust the thermal condition to desired values. The multitude of different elements is necessary because diesel fuel is a combination of different molecules, thus producing not only pure hydrogen, but also a multitude of byproducts. As fuel cells are sensitive to pollution namely by carbon monoxide and sulfur components, but also by other materials, the produced gas has to be cleaned. Different fuel cells have different sensitivities toward pollution. A PEFC as well as an HTPEMFC approach have been considered for the APU application in this work. The PEFC is more sensitive toward pollution, because of its lower working temperature and its different membrane material. Therefore, the fuel processing needed to supply a PEFC is introduced; later the fuel processing unit to supply a HTPEMFC can be defined as a subgroup of the original fuel processing unit. First, diesel fuel and its characteristics are introduced, followed by an introduction of the reformer unit and different clean up stages, (Fig. 1.6).

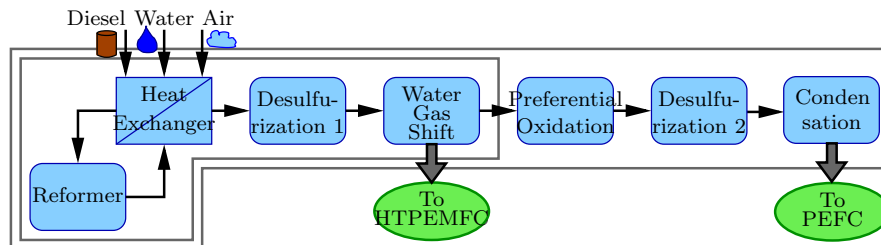


Figure 1.6: Fuel Processor for PEFC and HTPEM

1.3.1 Diesel Fuel

Diesel is a hydrocarbon mixture obtained in the fractional distillation of crude oil at temperatures between 200 °C and 350 °C at atmospheric pressure (Fig. 1.7). It is defined by its density of 850 g L⁻¹ and its lower heating value (LHV). Diesel is used for transportation applications, but also for stationary applications as in the heating and hot water supply of houses. Diesel fuel has a higher density and a higher heating value than gasoline. Due to the higher heating value, diesel fuelled cars show a better fuel economy than gasoline fuelled cars. As diesel fuel comes from a lower fraction of crude oil distillation, it contains more

byproducts and has therefore sometimes to be filtered. Recently the limits on diesel sulfur content have been strengthened to 10 mg kg^{-1} (European Directive 2003/17/CE) so that desulfurization steps have to take place. Crude oil based diesel contains a multitude of different molecules. It is namely composed of about 75% of saturated hydrocarbons and 25% aromatic hydrocarbons as well as sulfur components, silicon components and others.

For the application inside a model it is difficult to take into consideration a vast variety of different molecules. Therefore, one single, virtual molecule representing the mean composition of diesel is used. It consists of the carbon (C), hydrogen (H), oxygen (O) and sulfur (S) atoms, which shares are represented by real numbers.

$$\text{C}_n\text{H}_m\text{O}_p\text{S}_q$$

$$n = 13.4$$

$$m = 25.05$$

$$p = 0.031$$

$$q = 0.009$$

$$M_{\text{C}_n\text{H}_m\text{O}_p\text{S}_q} = 186.243 \text{ kg kmol}^{-1}$$

$$Hu_{\text{C}_n\text{H}_m\text{O}_p\text{S}_q} = 45.640 \text{ MJ kg}^{-1}$$

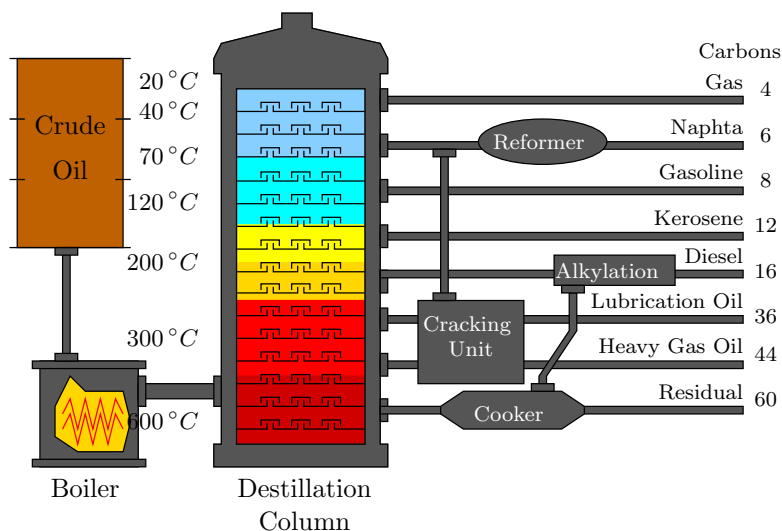


Figure 1.7: Crude Oil Refining (www.howstuffworks.com)

1.3.2 Reformer

Inside the reformer, the long chain diesel molecules are split in smaller molecules, mainly hydrogen, carbon monoxide, carbon dioxide and hydrogen sulfide, but also methane and other molecules might be formed. As the reforming process takes place at high conversion temperatures of around 1400 °C, the formation of those undesirable molecules can be inhibited [10]. Different reforming approaches exist.

Equilibrium between Carbon Monoxide, Water, Carbon Dioxide and Hydrogen

All reforming approaches are only introduced qualitatively. The partition between carbon monoxide, water, carbon dioxide and hydrogen depends largely on the temperature *Eq. 1.7*. The temperature dependent equilibrium between the species for ideal gases can be obtained by *Eq. 1.8* and *Eq. 1.9* with the equilibrium constant K_p :



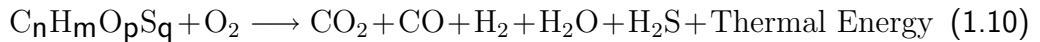
$$K_p = \exp\left(\frac{-\Delta G}{R \cdot T}\right) \quad (1.8)$$

$$K_p = \frac{(x_{\text{CO}_2} + \xi)(x_{\text{H}_2} + \xi)}{(x_{\text{CO}} - \xi)(x_{\text{H}_2\text{O}} - \xi)} \quad (1.9)$$

The application of the advancement ξ to the molar fraction gives the equilibrium between the four species for a given temperature. In the following the assumption is made that this equilibrium is obtained inside the reformer. A rough estimation of the residence time of the gas inside the reformer against the temperature dependent reaction time shows that this assumption is valid.

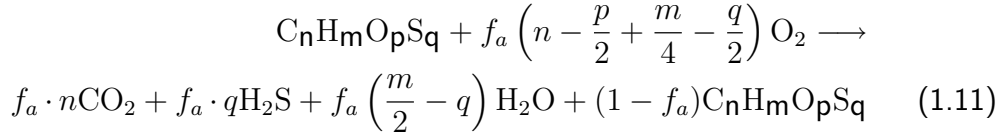
Partial Oxidation

For the partial oxidation, oxygen is added to the diesel fuel causing a catalytic oxidation toward carbon monoxide, carbon dioxide hydrogen and water *Eq. 1.10*. Partial oxidation is exothermic; it delivers more thermal energy than it consumes [153].



If enough oxygen is available, a complete oxidation takes place forming only carbon dioxide and water. Hydrogen can only be produced if the amount of oxygen available is not sufficient for a complete oxidation, *Eq. 1.11*. The availability of oxygen is described using the air factor (f_a), *Eq. 1.12*. It is defined

from the ratio of oxygen available against the ratio of oxygen needed for complete oxidation. For reasons of simplicity only combustion reactions are taken into consideration for the definition of the air factor [121, 153].



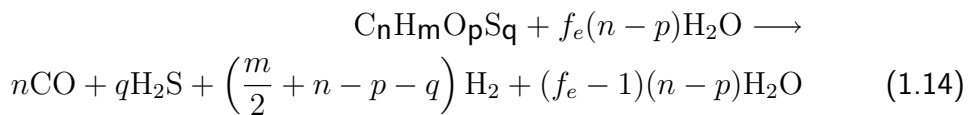
$$\text{with } f_a = \frac{\dot{n}_{\text{O}_2}}{(n - p + \frac{m}{4} - \frac{q}{2})\dot{n}_{\text{C}_n\text{H}_m\text{O}_p\text{S}_q}} \quad (1.12)$$

Steam Reforming

For the steam reforming process, water is added to the diesel fuel causing the formation of carbon monoxide and hydrogen mainly, but also the formation of carbon dioxide *Eq. 1.13*. Steam reforming is endothermic. Thermal energy has to be added to the system to maintain the reaction.



Normally, more water is provided to the system than is demanded for the reaction, *Eq. 3.5*. The availability of water is described using the water factor (f_e), *Eq. 1.15*. It is defined as the ratio of water available against the ratio of water needed for the complete reaction of the diesel. For reasons of simplicity only reactions considering the formation of hydrogen, carbon monoxide and hydrogen sulfide are taken into consideration. The final gas composition can be found using the equilibrium reaction between the species.



$$\text{with } f_e = \frac{\dot{n}_{\text{H}_2\text{O}}}{(n - p)\dot{n}_{\text{C}_n\text{H}_m\text{O}_p\text{S}_q}} \quad (1.15)$$

Steam reforming approaches have been applied in [9, 10, 65, 70, 111, 135].

Autothermal Reforming and other Reforming Approaches

Both the partial oxidation and the steam reforming show disadvantages namely with regard to heat management. During partial oxidation considerable amounts of heat have to be removed whereas during steam reforming considerable amounts of heat have to be supplied. Hence, the combination of both approaches seems

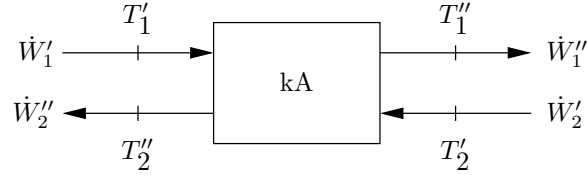
advantageous. Both approaches can be combined in a way that thermal energy has neither to be supplied nor to be removed, this approach is called *autothermal reforming* [33, 44, 93, 132, 136]. The case that neither heat has to be supplied nor removed is an ideal case. It is hard to stabilize the reaction with changing gas flows at exactly this point. Therefore, a combination of steam and autothermal reforming is sometimes applied where a reduced amount of cooling is needed with regard to the preferential oxidation. This approach is applied in the studied case.

1.3.3 Heat Exchanger

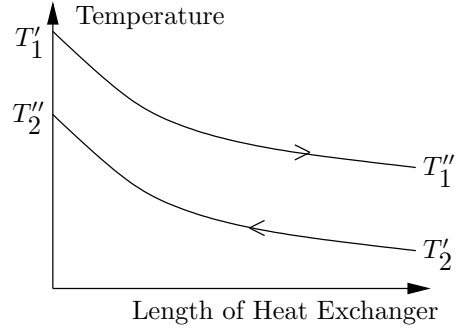
The gas mixture enters the fuel processing unit at low temperature. The reforming process is supposed to run at temperatures above 1400 °C. To heat up the incoming gas to these temperatures, significant exothermic combustion is needed, which decreases the net efficiency of the process [44]. At the same time, the gas leaves the reformer with a much higher temperature than the one the following steps require. The cooling would also be energy consuming. To mitigate those two disadvantages a heat exchanger is used to increase the temperature of the gas flow before entering the reformer and to cool it down before entering the following gas treatment units.

The heat exchanger is used to transfer thermal energy from one mass flow to another. Hence, two gas flows are entering and exiting the heat exchanger (*Fig. 1.8(a)*). The temperature profile inside a counter current heat exchanger is introduced in (*Fig. 1.8(b)*). To calculate the temperatures of the two gas flows at the exit of the heat exchanger, the approach introduced by Baehr [13] is used. This approach is only valid for ideal gas mixtures. Furthermore, the approach introduced is for stationary systems only. The calculation is based on the energy conservation *Eq. 1.16* and *Eq. 1.18*. \dot{W}_i is the heat capacity flow. It is the product of the mass flow times the heat capacity. The assumption that the heat capacity c_{pi} and the overall heat transfer coefficient multiplied by the heat exchange area kA do not change a lot over the process is made as well, *Eq. 1.17* and *Eq. 1.19*. Thereafter, the problem is translated to a dimensionless problem, with N_i the number of transfer units, C_i the proportion of heat capacity flows and ε_i the dimensionless temperature change, *Eq. 1.20*, *Eq. 1.21*, *Eq. 1.22*, *Eq. 1.23* and *Eq. 1.24*.

This system can be solved analytically once the overall heat transfer coefficient multiplied by the heat exchange area (kA) of the interface between the two gas flows is defined.



(a) Combined Heat Exchanger and Reformer



(b) Temperature development in a counter current heat exchanger.

Figure 1.8: Counter current heat exchanger.

$$\dot{Q} = \dot{m}_1(h_1' - h_1'') = \dot{m}_2(h_2'' - h_2') \quad (1.16)$$

$$\dot{W}_i = \dot{m}_i \cdot \overline{c_{pi}} \quad (1.17)$$

$$\dot{Q} = \dot{W}_1(T_1' - T_1'') = \dot{W}_2(T_2'' - T_2') \quad (1.18)$$

$$\dot{Q} = kA(T_1 - T_2) \quad (1.19)$$

$$\varepsilon_i = \frac{T_i' - T_i''}{T_1' - T_2'} \quad (1.20)$$

$$N_i = \frac{kA}{\dot{W}_i} \quad (1.21)$$

$$C_1 = \frac{\dot{W}_1}{\dot{W}_2} \quad (1.22)$$

$$C_2 = \frac{\dot{W}_2}{\dot{W}_1} \quad (1.23)$$

$$\varepsilon_i = \frac{1 - \exp[(C_i - 1)N_i]}{1 - C_i \cdot \exp[(C_i - 1)N_i]} \quad (1.24)$$

Another approach has been introduced by Korsgaard [95]. Different from the approach chosen by Baehr, the approach of Korsgaard takes into consideration the inertia of the box surrounding the heat exchanger. This implies an energy storage, which is not desired in this case. As the inertia shall be taken into consideration in a different step here (3.4.1), the approach of Baehr is preferred over the approach of Korsgaard.

1.3.4 Desulfurization

Even small amounts of sulfur, in the order of parts per million, will deactivate the catalyst in the fuel cell and reduce its durability. Sulfur has therefore to be removed from the reformat flow. Differing from Pukrushpan [121] or Virji [153] the desulfurization is not neglected in this case. Various desulfurization methodologies exist often the hydrogen sulfide is captured by an adsorbing material, for further information see [142]. In this case it is assumed that a constant fraction of the sulfur is removed. Only the selectivity (*sel*) of the desulfurization is important *Eq. 1.25* and *Eq. 1.26*.

$$\dot{n}_{\text{Sulfur-removed}} = \text{sel} \cdot \dot{n}_{\text{Sulfur-in}} \quad (1.25)$$

$$\dot{n}_{\text{Sulfur-out}} = (1 - \text{sel}) \cdot \dot{n}_{\text{Sulfur-in}} \quad (1.26)$$

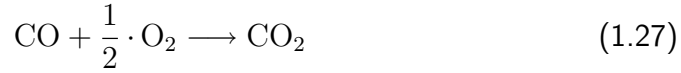
1.3.5 Water Gas Shift Reaction

The reformer produces hydrogen along with carbon monoxide. Carbon monoxide deactivates the catalyst of the PEMFC and has therefore to be removed. There is an equilibrium between hydrogen, water, carbon monoxide and carbon dioxide that depends on their molar fraction and the temperature of the system, (1.3.2). This fact can be used to reduce the carbon monoxide fraction in the gas, by decreasing the temperature and/or by introducing water. In this case the temperature has to be reduced, also because the gas leaving the heat exchanger is too hot to enter directly into the fuel cell. The water gas shift reaction (WGS) can reduce the carbon monoxide fraction down below 5 % [130].

1.3.6 Preferential Oxidation

As very low carbon monoxide fractions cannot be obtained by WGS, an additional gas cleaning step has to be made to further decrease the carbon monoxide content

of the reformed gas down to a percentage not critical for a PEFC. This is done using preferential oxidation. Therefore, a small amount of air is introduced in the gas flow; a catalyst assures that mainly carbon monoxide and not hydrogen reacts with the air *Eq. 1.27*. The preferential oxidation can reject carbon monoxide below 10 ppm [130].



1.3.7 Condenser

A non negligible amount of water is introduced into the reformer at autothermal reforming (f_e) and the reforming takes place at high temperatures of around 1400 °C. During the fuel processing the gases are cooled down to temperatures of 80 °C for PEFCs and 200 °C for HTPEMFC. This temperature difference introduces a considerable risk of having liquid water inside the gas stream. Inside a PEFC, liquid water is disadvantageous because it deactivates areas of the membrane increasing the risk of flow channel blockage or the so called flooding.

To avoid this risk the use of a condenser between the fuel processing unit and the fuel cell can be advantageous. Inside the condenser some energy might be removed from the system to further cool it down, at the same time liquid water is separated from the gas stream.

At stationary conditions liquid water is available in the gas stream if the water partial pressure is above the saturation pressure. In this case, the partial pressure of liquid water is equal to the saturation pressure and the rest of the water is available in liquid form. The saturation pressure of water depends on the temperature. Several approaches to calculate the saturation pressure can be found [148]. In this case the approach of Keenan and Keys to calculate the saturation pressure in Pa from the temperature in K is used, *Eq. 1.28*. It is valid for temperatures between 0.01 °C and 260 °C. As the saturation pressure above this temperature exceeds 50 bar which is far above the system pressure, no evaluations for liquid water are made at higher temperatures.

$$p_{\text{sat}} = R \frac{A + B T + C T^2 + D T^3 + E T^4}{F T + G T^2} \quad (1.28)$$

$$A = -27405.526; B = 97.5413; C = -0.146244; D = 0.12558 \cdot 10^{-3};$$

$$E = -0.48502 \cdot 10^7; F = 4.34903; G = -0.39381 \cdot 10^{-2}; R = 22105649.25;$$

1.3.8 Fuel Processing unit for PEFC and HTPEMFC

The fuel processing unit considered to run a PEFC consists of: Heat Exchanger, Reformer, Desulfurization 1, Water Gas Shift, Preferential Oxidation, Desulfurization 2 and Condenser (*Fig. 1.6*). The fuel processing unit to run a HTPEMFC consists of: Heat Exchanger, Reformer, Desulfurization 1, Water Gas Shift and Desulfurization 2. The fuel processing to supply a HTPEMFC with hydrogen extracted from diesel contains fewer subsystems. The reason for this is that a HTPEMFC is less sensitive to contamination by sulfur or carbon monoxide. The HTPEMFC can accept carbon monoxide content of up to 5 %, whereas the PEFC can accept carbon monoxide contents of not more than 10 ppm [95, 130]. As the technological availability for PEFCs is much higher than that of HTPEMFCs, a fuel processor model meeting the requirements of PEFCs is developed in section (3). Still, the diesel fuel processing unit adapted to the needs of a HTPEMFC can be derived thereafter by means of simplification [95].

1.4 System Dynamics

Until now the elements described for a fuel cell system have been introduced phenomenologically by their reactions. Those reactions are static. To be able to develop a model that can be used for control it is not sufficient to regard static reactions. The purpose of control is manipulating quantities in systems in a way that their behavior is at any time the closest possible to a desired behavior, therefore controllers are used. As real systems always exhibit time dependencies it is important that they are taken into consideration inside the model as well.

Fuel cell systems are complex multi domain systems. Different time dependencies from different energetic domains are expected throughout the system [75]:

- chemical time constant: ≈ 1 ms
- electrical time constant: 10 ms to 100 ms
- pneumatic time constant: ≈ 1 s
- thermal time constant: ≈ 1 min

In this approach only pneumatic and thermal time constants shall be taken into consideration, as the chemical and electrical reactions are supposed to be instantaneous.

1.5 Diesel Driven Fuel Cell System

The PEFC as the HTPEMFC technology are adapted to be fed with a commercial hydrocarbon if this hydrocarbon undergoes a fuel processing to be transformed into a hydrogen rich gas. A combination between PEFC, fuel processor for natural gas and cogeneration has demonstrated for stationary application [108, 107]. As the fuel cell system developed during the GAPPAC project shall be used as an auxiliary power source in a transportation application that is used for trigeneration, the HTPEMFC technology shows some advantages. In transportation applications the installation volume available is limited in most cases. As the HTPEMFC technology contains fewer conversion steps it is supposed to have a higher density and is therefore more adapted for transportation applications. The introduced fuel cell system shall be used for trigeneration (using the system heat for refrigeration). PEFC and HTPEMFC systems produced comparable amounts of heat, but the quality of the produced heat is superior for HTPEMFC systems, as the heat is provided at a higher temperature. This work will follow two approaches. First, a fuel processing unit for PEFC application is modeled and validated. Second, a PEFC system is modeled and validated for the use with reformat. Third, the PEFC model is changed to meet the requirements of HTPEMFC. Fourth, a model of a HTPEMFC is connected with an adapted fuel processing unit (the PEFC fuel processing unit had therefore to be simplified) for system control development.

At any rate the work is focused on two aspects. First, the development of the model intended for model based control design of a low temperature fuel cell unit driven by commercial diesel and second on the development and adaption of a methodology to obtain a causal functional model of a complex multi domain system which paves the way toward model based control development.

Chapter 2

Choice and Introduction of the Modeling Methodology

2.1 Purpose of the Modeling

A diesel driven fuel cell system for auxiliary power supply in mobile application has been identified to be a promising research topic due to two reasons: first, because it permits an introduction of the fuel cell technology while using the existing diesel infrastructure. Second, because diesel driven fuel cell systems build a complex multi domain platform. If the methodology can be supplied successfully on such a complex system it is likely that it can also be applied to other systems. Different modeling approaches are presented in (2.2), a choice of the most adapted modeling methodology is given in (2.3). The Energetic Macroscopic Representation (EMR) is introduced in detail in (2.4), followed by the control structure development using EMR in (2.5), before the adaptations of our system are given in (2.6).

2.2 Modeling Approaches

In section (1.1.5) different types of physical models used to describe fuel cells have been introduced. But they have only been introduced regarding their capability to describe physical phenomena. Here, different macroscopic modeling methodologies that have been used to describe fuel cell system are introduced. Next to the general aspects, advantages, disadvantages and examples will be given showing the capabilities for model based control development.

In general, modeling approaches can be assigned to two different categories [6]. In the *structural* approach, the object is described according to its physical sys-

tem defined by its material characteristics or its structure. With this approach systems can be visualized using images or symbols representing their physical structure. Structural approaches are often used for system conception and definition. Examples for structural software are: Saber, Spice, PSim, Dymola and Amesim and also structural applications for the functional software MatlabTM, for example SimPower, SimDriveline or SimMechanics.

In the *functional* approach, the object is described according to its function. This representation might seem more virtual, because it does not reproduce necessarily what can be seen from the system. The functionality of the system can be described using mathematical equations, transfer functions or graphic representations. Functional approaches are mainly used for analysis, abstraction or control development. As the functional approach is more general than the structural approach, different modeling softwares can be used, for example mathematical software like Modelica or MatlabTM or graphic software incorporating system effects like Simplorer or SimulinkTM.

If every structural aspect of a system incorporates a functional implication and vice versa, it is possible to describe a system at the same time functional and structural. Such a combination is most adapted to describe complex multi domain systems.

It has to be mentioned that most work with regard to fuel cell control that has been done, cannot be classified according to the modeling methodologies introduced here. Some works apply directly to fuel cell power systems like Candusso et al. [43], concerning the control of HTPEMFC only little work is known [87, 96]. With regard to the fuel processor control some work has been published [49]. More general approaches to be mentioned are [45, 61, 106, 117, 141, 147]. Some work has been done regarding model based control development [62, 73, 74, 76, 112, 119], but none is based on one of the introduced modeling methodologies.

2.2.1 Basic Ideas on Modeling

Models are intended to describe the behavior of systems [12]. An effective way to describe a system is by representing it in form of a thermodynamic system. The thermodynamic system is a well defined area that is separated from the outside by a real or imaginary boundary. A system can then be classified by its boundary and quantities which enter and exit. Work, energy, heat and enthalpy flow through the boundary. If there is no matter flow through the boundary, like in a light bulb, the system is called *closed system*. If there is matter flowing through the boundary, like in a pump, the system is called *open system*. A thermodynamic system can be described using the first law of thermodynamics, Eq. 2.1 with E

the energy of the material, Q the heat energy and W the mechanical energy:

$$dE = dE_{\text{in}} - dE_{\text{out}} + \Delta Q + \Delta W \quad (2.1)$$

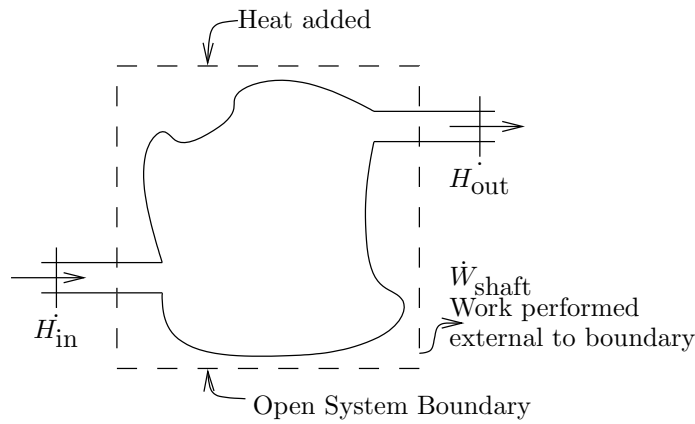


Figure 2.1: Representation of an open system.

The change of internal energy depends on the internal energy of the matter flowing into and out of the system, the heat crossing the system boarder and the work done. When an open system is regarded, the energy balance can be transformed into an energy flow balance. An energy flow is equal a to power. A large fraction of system models are based on the first law of thermodynamics for open systems. Normally, a complex system is divided in a multitude of small units, each representing a thermodynamic system. The subsystems can be divided into continuous systems which show stationary behavior over time even if mass or energy flows enter the systems and open systems that take into consideration time dependent behavior. The subsystems are connected by quantities representing an energy flow. This kind of approach is called *energetic approach*.

The causality of the system, which is the physical relation between cause and effect, is taken into consideration [?, 6]. As a subsystem represents a stationary conversion, the causality and therefore the definition of input and output is not fixed. For time dependent system this is not the case. The energy accumulated inside a system cannot change instantaneously. If the input value undergoes a step change also the output value will change, but it will take a certain time to reach the new stationary condition (transient behavior). This transient behavior is represented by an integration. Therefore, time dependent behaviors have to be represented in integral form, respecting the causality and thus defining the input and the output quantity.

Table 2.1: Quantity pairs used to describe energy flows [1]

Mechanical	Force (F)	Velocity (v)
	Torque (Γ)	Angular velocity (ω)
Electrical	Voltage (V)	Current (i)
Hydraulic	Pressure (p)	Volume flow rate (dq/dt)
Thermal	Temperature (T)	Entropy change rate (ds/dt)
	Pressure (p)	Volume change rate (dV/dt)
Chemical	Chemical potential (μ)	Mole flow rate (dN/dt)
	Enthalpy of Formation (h)	Mass flow rate (dm/dt)
Magnetic	Magneto-motive force (m_m)	Magnetic flux (Φ)

In most cases (Bond Graph, Electric Equivalent Model) models use a combination of two different variables to describe an energy flow. Those two quantities represent an extensive variable that is related to the size of the system and an intensive variable which is invariable for the size of the system. Those variables are labeled differently in different approaches, for example: action and reaction (Energetic Macroscopic Representation), flow and effort (Bond Graph) or through and across (VHDL-AMS). A multitude of systems from different domains can be described by a connection of such two variables, *Tab. 2.1*. The product of those two quantities defines the energy flow exchanged.

2.2.2 Electric Equivalent Model

The electric equivalent model is based on the idea that systems from different domains can be reduced to few basic elements. In different energetic domains there are not time depending elements representing losses due to electrical or flow resistance (friction). There are also time depending elements, representing an accumulation like in springs that store energy or in capacitors that store energy in form of charge. In the electric domain the extensive variable is the current, the intensive variable is the voltage. Different accumulation elements are used if kinetic energy is stored (inductor) or potential energy is stored (capacitor). This difference can be made also for other energetic domains. Finally, there are intersections where one stream is split into different streams like in valves or in Kirchhoff nodes. A multitude of systems can be described by a combination of those basic elements, for example electric systems but also hydraulic and pneumatic systems (*Fig. 2.2*).

Electric systems are well studied and there is a multitude of software available (e.g. PSpiceTM) for its representation, characterization and its control. If systems from other energetic domains can be described using the same approach, they

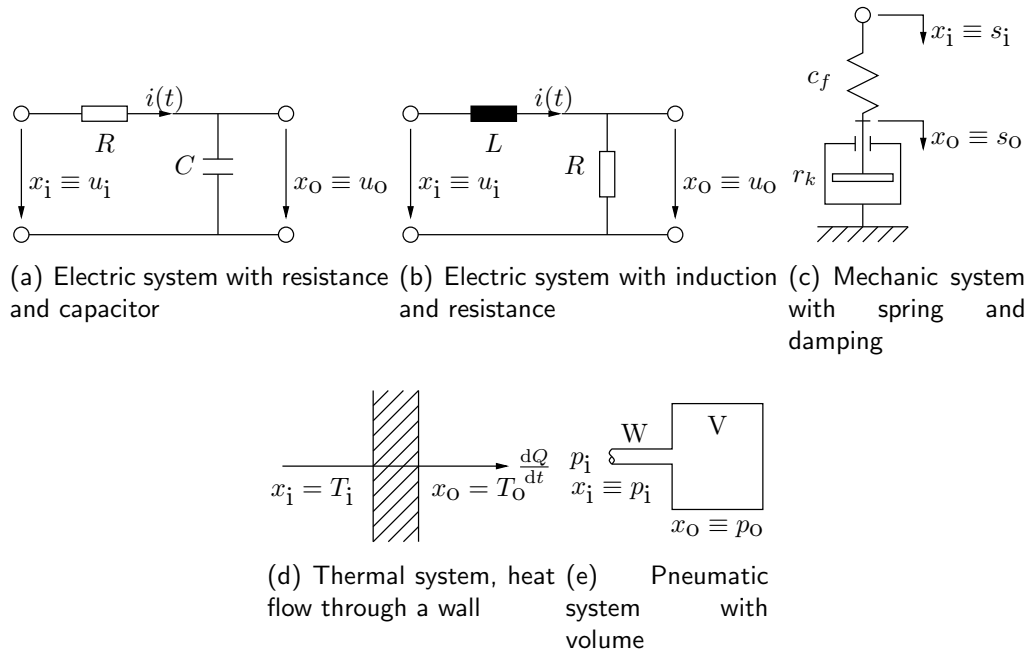


Figure 2.2: Systems with first order time dependency in different physical domains

can be implemented in the same software. This reduces software development time and cost. Furthermore, an unified approach simplifies the communication between experts from different domains. Electric equivalence can only be used if the system depends on two quantities, one intensive and one extensive quantity. The approach using electric equivalence has been applied for fuel cells and fuel cell systems by Hernandez [81], Chnani [50] and others [68, 160].

2.2.3 Bond Graph

Bond Graph [1] is an approach to describe systems graphically using a limited number of standardized blocks connected by power bonds. It is a causal explicit graphical tool. Bond graph is based on the first law of thermodynamics for open systems, but the notion of power exchanged has been favored over energy flows. Furthermore, it implies causalities to a large extent, helping to understand the systems working principle and at the same time facilitate the controllability, observability and fault diagnosis. Bond graph has been developed during the 1960s by Payner [118] with main contributions of Karnopp, Rosenberg [88] and Thoma [146].

Bond graph is based on a limited number of basic elements, *Tab. 2.2*. The basic elements include time independent changes (R-Element for losses, TF-

element for power factor transmission flow to flow, GY-element for power factor transmission effort to flow), accumulation elements (I-element for accumulation of kinetic energy, C-element accumulation of potential energy) and sources (SE for effort source and SF for flow source). The elements are connected by power bonds representing effort and flow or their time integrals.

The power bonds are half arrows with a stroke. The direction of the arrow represents the power direction. The stroke represents the direction in which the effort signal is directed and therefore the causality. Time dependencies in form of accumulations are favored [60]. Furthermore, the causality of three port junctions is fixed, because only one bond (the strong bond) can bring the information concerning the effort or flow.

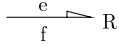
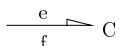
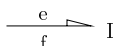
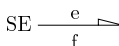
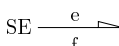
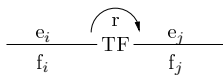
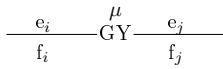
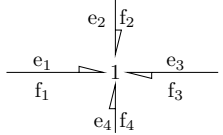
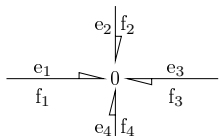
Based on those ideas a multitude of different systems can be described including complex, multi domain systems. As the basic methodology is well defined, considerable work has been done on the utilization of bond graph for control development [60]. The utilization of bond graph for system modeling demands an adapted software. Therefore, special software or additional packages to use general software have to be purchased, demanding an investment. To develop the control structure of a system its overall transfer function can be derived from the bond graph model. The derivation of the transfer function is well known, but for complex systems difficulties might occur.

Considerable work has been done to describe fuel cells and fuel cell system using bond graph [127, 131, 149], but at the moment no work is known considering the development of a control structure for fuel cells using bond graph.

2.2.4 Causal Ordering Graph

The causal ordering graph (COG) is a graphic, functional, causal approach for system description [78, 79]. It is the basis of inversion based control because the causality is exclusively represented in integral form. A system is divided in subsystems (represented by ovals) having an input and an output. The notation represents the causality. If the connection between the input and the output is static, the subsystem is labeled with a double arrow. If the system incorporates an energy storage, this has to be described in integral form (2.2.1). It cannot be inverted keeping integral causality. Therefore, such systems are labeled with a single arrow. Furthermore, there can be coupling elements connecting two inputs to an output. Based on those three basic blocks, it is possible to describe a multitude of different systems. As only one quantity is used, it cannot be an energetic representation. To introduce the energetic aspect a secondary system description has to be used, describing the reaction variable (*Fig. 2.3*), [6].

Table 2.2: Basic Elements of Bond Graph

one port elements - passive			
R-Element: 1-port resistance	static relation between flow and effort, usually dissipation of energy		$e = f \cdot R$
C-Element: 1-port capacitor	relation between effort and general displacement, energy storage without losses		$e = C^{-1} \int_{-\infty}^t f dt$
I-Element: 1-port inductance	relation between flow and general displacement		$f = L^{-1} \int_{-\infty}^t e dt$
one port elements - active			
SE: Effort source	give reaction to the source		
SF: Flow source	give reaction to the source		
two port elements			
TF-Element: Transformer	transmits factors of power with proper scaling (flow-to-flow, effort-to-effort), no change in overall energy		$e_j f_j = e_i f_i$
GY-Element: Gyrator	transmits factors of power with proper scaling (flow-to-effort), no change in overall energy		$e_j = \mu f_i;$ $e_i = \mu f_j$
three port junctions			
1-Junction	equality of flows, efforts sum up to zero, conserve power, reversible		$f_i = f_j;$ $\sum e_i = 0$
0-Junction	equality of efforts, flows sum up to zero, conserve power, reversible		$e_i = e_j;$ $\sum f_i = 0$

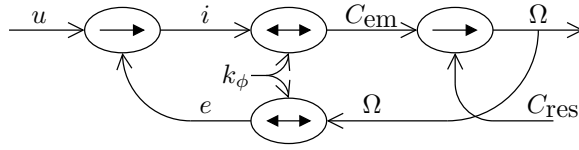


Figure 2.3: COG representation of a permanent magnet dc machine.

The basic idea of the control is to find the input variable needed to produce a desired output. A desired output can be obtained by manipulating one input variable. The input variable needed can be found by inverting the system model defining the causal chain from the output to an input.

Regarding the basic elements of COG, it can be said that static elements can be inverted directly using their mathematical inverse function. Accumulation elements with time dependency cannot be inverted keeping an integral time dependency. Hence, a controller has to be used for their inversion. Until now, it can only be said that a controller has to be used, the choice of the controller is done according to the representation of the accumulation element or the experience of the developer. For the inversion of a coupling element, two values have to be known to be able to find the missing value. Based on these reflections a strategy of system control development using COG can be developed (Fig. 2.4):

1. **System model:** To be able to describe a system, it has first to be modeled and validated.
2. **Definition of tuning path:** The tuning path is the causal connection between the output value that shall be controlled and the corresponding input value.
3. **Block wise inversion of the system:** The block wise inversion is the inversion of the system block by block using the approaches described above. This leads to the maximum control structure (MCS) of the system. The MCS is based on the assumption that every value is measurable. This might not be applicable in every case for example, because no measurement approaches are defined yet or because the measurement is time-consuming and cannot be done in real-time or because a measurement is too expensive to be applied.
4. **Strategic aspects:** In the case that the system has still more degrees of freedom than constraints, strategic aspects can be incorporated inside the system control.
5. **Simplification:** If there are values that do not change during the function

of the system or that have little influence on the system, simplifications can be applied.

6. **Estimation of non measurable values:** Estimation rules can be applied on those values that are not measurable, leading to a practical control structure (PCS).

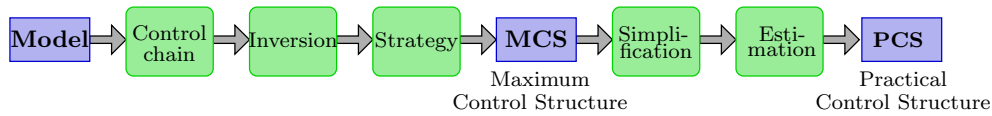


Figure 2.4: System control development using block wise inversion.

2.2.5 Energetic Macroscopic Representation

The causal ordering graph shows considerable potential for control structure development, but its application is still somewhat bulky for a complex multi physic system. Therefore, another approach has been developed at the *Electrotechnic and Power Electronic Laboratory of the University of Lille, France* since the year 2000. The Energetic Macroscopic Representation (EMR) tries to combine the needs regarding causality and energetic aspect for inversion based control development, with demands regarding adaptability [6]. The EMR combines the advantages of the control structure development for COG with an energetic approach simplifying readability, in a format that can be applied in a commercial software [26, 30].

The EMR is an easy to read graphic approach for system modeling. It incorporates the functional aspects with an integral causality and a choice of input and output keeping the energetic aspect and is thus based on the first principle of thermodynamic. As the EMR of a system is defined, the control structure can be developed using the approach introduced in (2.2.4). An application of different methodologies to describe the traction system of an automatic subway showing advantages and disadvantages is given by Bouscayrol et al. [32].

The EMR was developed to describe electro-mechanical systems [26, 27, 31], but as it is based on energy flows, it is possible to adapt it to different energetic domains. Until now it has been used for example to describe wind power [28, 29, 30], paper machines [101, 133], subway traction [152], hybrid vehicle [103], fuel cell stack [52, 53, 55, 59, 58, 83].

Table 2.3: Compliance of different modeling approaches to the needs

Approach	Electric Equivalent Model	Bond Graph	COG	EMR
Domains	all simplified to electrical model	different	different	different
Modular	yes	yes	yes	yes
Energetic	implicit	yes	no	yes
Causality	no	mostly	yes	yes
Visualization	electric representation	graphic	graphic	graphic
Software	PSpice	20-sim	Matlab Simulink	Matlab Simulink
Control	electric approach	overall transfer function needed	yes	yes

2.3 Choice of Modeling Methodology

Different modeling approaches with different characteristics have been introduced in (2.2). In this case the methodology shall be used to develop the control structure of a diesel fed fuel cell system. Therefore, it is necessary that the modeling approach meets the following demands:

- representation of different energetic domains,
- modularity,
- handling of parameters needed,
- visualization of a complex system,
- adaptability to a commercial simulation software,
- inversion based control structure development.

The compliance of the different modeling approaches to those demands is presented in *Tab. 2.3*. The EMR is the most adapted to the problem, even though the methodology is relatively recent. It comprises as well the multi domain aspect as the inversion based block wise control structure development developed

for the COG. Furthermore, it can be adapted to the use of multiple variables, see (2.6.2). Therefore, EMR has been chosen for the application on a diesel feed fuel cell system.

2.4 Basic Elements of Energetic Macroscopic Representation

The basic elements of EMR are:

Source element: The source elements indicate the interface of the system to its surrounding. Via the source, energy streams can enter and exit the system. The source element is represented by a light green oval with dark green rim.

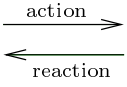


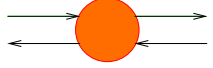
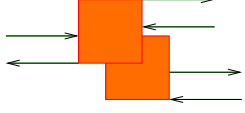
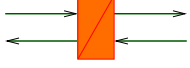
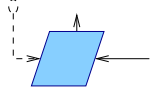
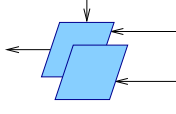
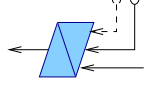


Conversion element: The conversion elements calculate conversions of any kind. They can be separated in conversions in the same domain and conversions between different domains. An electric transformer is an example for conversion in the same energetic domain. It is represented by an orange square with red rim. A heating element is an example for a conversion between different energetic domains (electricity to thermal). It is represented by an orange circle with red rim. The conversion element can incorporate a tuning parameter which defines the kind of conversion.

Coupling element: A special case of the conversion is the coupling. It is used to describe the coupling or decoupling of two or more energy streams, like Kirchhoff nodes. Coupling elements are represented by overlapping orange squares with red rim. The conversion element can incorporate a tuning parameter which defines the kind the fraction of the coupling.

Accumulation element: The accumulation element is used to represent an energy storage. It is the only element capable of representing time dependent behavior. For reasons of causality, only integral time dependencies can be represented in EMR (2.2.1). Different from other modeling approaches, no difference is made between the accumulation of kinetic energy and the accumulation of potential energy. The symbol for an accumulation is a barred orange rectangle with red rim.

The elements are connected by a quantity pair indicating action and reaction, see also *Tab. 2.1*. They are represented by two black lines with arrows, where the arrows show in different directions. Those quantity pairs reflect the causality of the system. The choice of quantities is based on the first law of thermodynamics. Therefore, the methodology is called *energetic* macroscopic representation.

Table 2.4: Overview of basic elements of EMR and MCS

Energetic Macroscopic Representation (EMR)		
Pair of action and reaction		two parallel black arrows pointing in opposite directions
Source of energy		light green oval with dark green rim
Energy conversion, same domain		orange square with red rim
Energy conversion, different domains		orange circle with red rim
Coupling device (distribution of energy)		overlapping orange squares or circles with red rim
Energy accumulation		orange rectangle with red rim and red diagonal bar
Maximum Control Structure (MCS)		
Control block without controller		light blue parallelogram with dark blue rim
Control block with coupling		overlapping light blue parallelograms with dark blue rim
Control block with controller		light blue parallelogram with dark blue rim and dark blue diagonal bar
Strategic block		cyan parallelogram with dark blue rim
Estimation block		magenta parallelogram with dark blue rim

The EMR gives only the structure of the system and the variables used, how the calculation is put into practice inside the elements is open to the user. This permits also to have different levels of detail in the same model or to detail the representation of one element without changing the overall structure.

The connection of elements can be realized as follows. Elements can be connected directly if their exchange variables are the same, if the exit of one element corresponds to the entry of the other system and if the values are equal in the moment of connection, (Fig. 2.5).

There are cases possible where elements cannot be directly connected, for

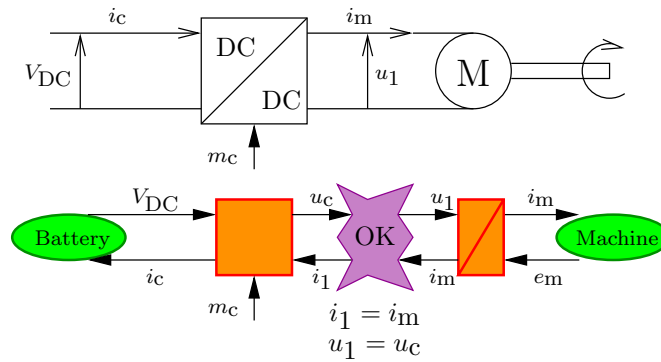


Figure 2.5: Direct connection of subsystems

example if two inductances are connected in series if a chopper with a smoothing induction is connected to an electric motor, (Fig. 2.6). In this case the inductance has the same input and output and cannot be connected. Reason for this is that the current has to be equal in both cases. To be able to apply this system in EMR, the two consecutive inductances have to be concatenated to one single accumulation element. Such a concatenation reduces the legibility of the model and should therefore only be used if necessary.

A similar problem can occur, having a conversion element between the two accumulation elements, for example if two shafts are connected by a gearbox, (Fig. 2.7). If both the conversion and the accumulation element have the same inputs and outputs, they can be permuted keeping the same functionality. Thereafter, the two accumulation elements causing causality problems might be connected. The permutation of two elements reduces the legibility of the model, as the physical structure is not longer respected. Hence, the permutation should only be applied in the case of need.

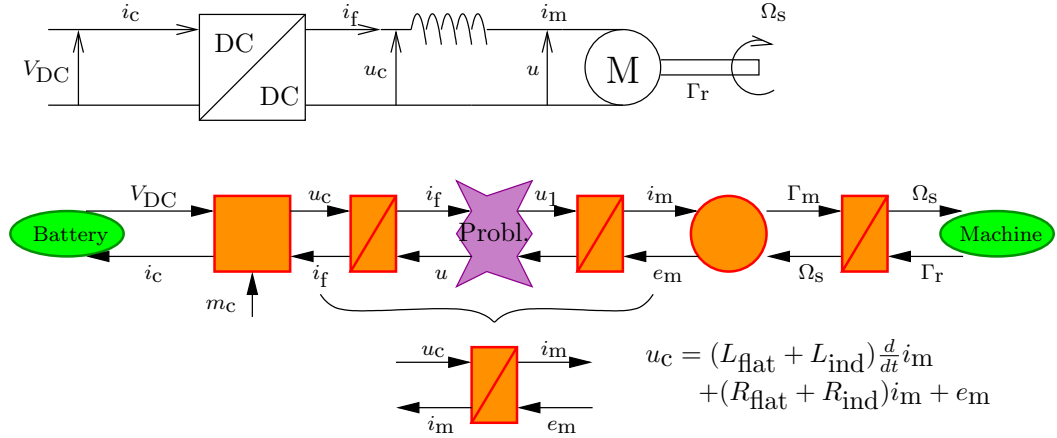


Figure 2.6: Subsystem connection using concatenation

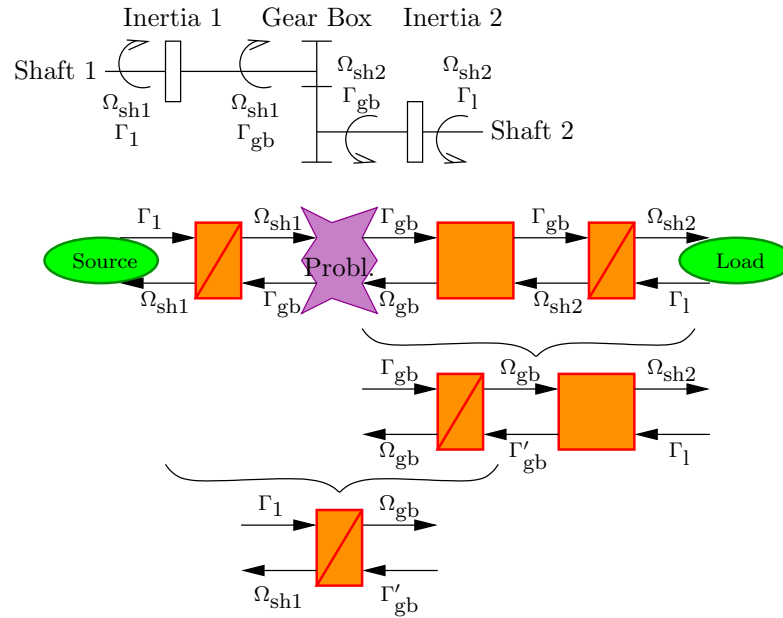


Figure 2.7: Subsystem connection using permutation and concatenation

2.5 Inversion Based Control Structure Development with EMR

When the system is modeled using EMR, the deduction of Maximum Control Structure (MCS) is possible, see also example given in (Fig. 2.8). The MCS is developed following the steps introduced in (2.2.4). After the control chain is defined (Fig. 2.8, *yellow highlights*), the MCS is obtained by a block wise inversion of the EMR along the control path (Fig. 2.8, *EMR elements indicated with single prime, MCS elements indicated with double prime*). This methodology needs only the individual representation of each block. It is not necessary to know the overall transfer function. In some cases strategic aspects can be included in the MCS.

The basic blocks are inverted as follows:

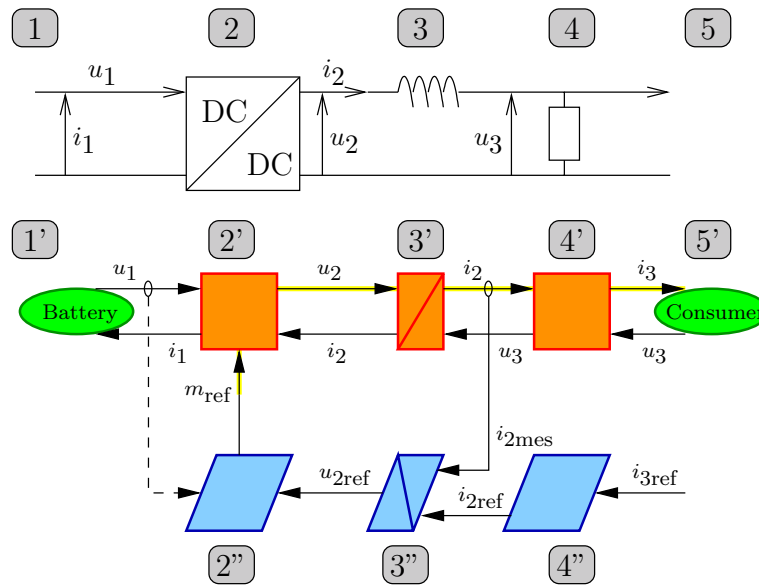


Figure 2.8: Example of a RL-load. Electric Scheme, EMR and MCS

Inversion of sources: Sinks and sources are not inverted

Inversion of conversion elements: Conversion elements can be inverted directly using the mathematical invert of the function used in the model (Fig. 2.8, $2''$ and $4''$). In some cases a conversion parameter is needed, depending on the control chain (Fig. 2.8, $2''$). The conversion parameter can be an output of the conversion or an input. Inverted conversion elements are represented by a light blue parallelogram with a dark blue rim, Tab. 2.4.

Inversion of coupling elements: Coupling elements can be inverted directly using the mathematical invert of the function used in the model. Normally, they consist of two or more inputs (reference or measured value) and one output. If a split has to be inverted the two or more inputs are added to find the output value. If a combination has to be inverted the repartition of the elements has to be known. An inverted coupling element is represented by multiple overlapping light blue parallelograms with a dark blue rim, *Tab. 2.4*.

Inversion of accumulation elements: Accumulation elements cannot be inverted keeping integral causality. Therefore, a controller has to be introduced. Only the position of the controller is defined, the choice of the controller is up to the developer. A controller has at least two inputs representing the reference value and the measured value of the same magnitude (*Fig. 2.8, 3''*). Goal is to adjust the controller parameters so as the measured value is equal to the reference value. An inverted accumulation element is represented by a light blue parallelogram with a dark blue rim and a dark blue bar, *Tab. 2.4*.

Differing from the EMR model with a pair of quantities, only the transferred reference variable is used in the MCS. Solid lines represent essential control inputs and outputs, dotted lines represent optional inputs. A measurement is represented by a small black oval on the EMR representation of the value to be measured.

The MCS contains a maximum number of control elements and measurements. Furthermore, it is based on the assumption that all elements are measurable. A practicable control structure (PCS) can be derived from the MCS in a second step with the help of simplifications and estimations or observations of non measurable values.

Strategic elements: Sometimes, it is advantageous to shortcut the control chain to obtain a desired reference value. In this case a strategic element can be used. It contains a stationary function. A strategic element is represented by a cyan parallelogram with dark blue rim, *Tab. 2.4*.

Estimation element: It is possible that values represented in the MCS are non measurable (for physical or economical reasons). In this case an estimation element can be used to derive the desired value from other, more accessible values to form an applicable control structure. An estimation element is represented by a magenta parallelogram with dark blue rim, *Tab. 2.4*.

The developed system control will be very close to the causality of the system. Still, to run the overall system, global aspects have to be taken into consideration. This can be done based on a breakdown of the degrees of freedom that

may leave the possibility to incorporate global and strategic aspects.

2.6 Adaption of EMR to a Diesel Fed Fuel Cell System

2.6.1 Utilization of Energy Balance

The EMR is based on the first law of thermodynamics (2.2.1). Conversion elements do not contain energy accumulation. Hence, the energy conversation can be used to evaluate a stationary element in certain cases. The energy conversion for continuous steady systems, says that the sum of all energy entering a control system \dot{E}_{in} is equal to the sum of all energy flowing out of the system \dot{E}_{out} .

$$\sum \dot{E}_{in} = \sum \dot{E}_{out} \quad (2.2)$$

As there is no energy storage, the first law of thermodynamics as it has been introduced in (2.2.1, p. 29), Eq. 2.3, can be applied for continuous steady systems as an energy conservation law, Eq. 2.4.

$$dE = dE_{in} - dE_{out} + \Delta Q + \Delta W \quad (2.3)$$

$$0 = d\dot{E}_{in} - d\dot{E}_{out} + \Delta\dot{Q} + \Delta P \quad (2.4)$$

The energy E transported with the mass flows consists of the internal energy U , the kinetic energy ($0.5 m \cdot v^2$) and the potential energy ($g \cdot z$). Very often the kinetic and potential energy are much smaller than the internal energy and therefore neglected. The thermal work Q can be the sum of different heat exchanges. The mechanical work W combines all works implemented to the system from the outside, among those the volume change work. Changing the first law of thermodynamics, Eq. 2.1, to an energy conservation law from continuous steady state systems without accumulation, Eq. 2.4, following changes have to be made. First, as there is no accumulation the left hand term of the equation is equal to zero. Second, the different energies have to be transformed into energy flows \dot{E} and \dot{Q} . The notation of work flow \dot{W} is not common, but it is referred to as power P .

The volume change work can be combined with the internal energy to form the enthalpy H . The specific enthalpy h is the enthalpy per mole of molecules ($H_i = h_i \cdot n_i$ or $\dot{H}_i = h_i \cdot \dot{n}_i$). It is dependent on the temperature and the pressure $h_i = h(T_i, p)$. The enthalpy gets only sense considering a change from

one state to another [12]. As the specific enthalpy depends only little of the pressure p an approach using the dependency on the temperature only developed by the NASA/Janney is applied. This approach uses a nonlinear equation with a set of nine parameters for each species. This approach explained by Burcat et al.[38] is applicable not only for the specific enthalpies, but also for the specific heat capacities and the specific Gibbs energies. The energy conservation law for stationary system is *Eq. 2.5*.

$$0 = \dot{H}_{\text{out}}(T_{\text{in}}, p_{\text{in}}) - \dot{H}_{\text{in}}(T_{\text{out}}, p_{\text{out}}) + \Delta\dot{Q} + \Delta P \quad (2.5)$$

2.6.2 Choice of Variables

As introduced in (2.2.1) the choice of variables is based on the first law of thermodynamics, thus the input and output variables have to be capable to represent the energy flow through a system boarder. Furthermore, two parameters are used to incorporate also the notion of causality. In many cases, two state variables are sufficient to represent an energetic flow and very often the multiplication of those two variables gives the energetic flow. This is right for a great number of pairs of variables from different energetic domains, see *Tab. 2.1*, but it is neither fixed that it has to be two quantities, nor that their connection has to be multiplicative.

In the case of a fuel cell with diesel reformer, a gas mixture is the principal energy transfer medium. An ideal gas can be described by the ideal gas law:

$$\frac{pV}{T} = nR \quad (2.6)$$

The ideal gas law has four variable parameters: pressure, volume, temperature and mole number. Hence, three parameters have to be given to be able to describe the system, except for the case that one of the parameter is fixed at a constant value in the model. In the case of a diesel fed fuel cell system containing a fuel processor, all described values show considerable fluctuations (temperatures between 80 °C and 1400 °C; pressure between 1 bar and 3 bar, and the volume flows and molar flows change according to the current produces). Therefore, no parameter can be fixed to be constant, they all have to be taken into consideration.

To comply to the basic idea to describe systems analog to thermodynamic systems, the used variables have to be combined to form an energy flow in the case of steady, continuous systems. Based on the state variables introduced by the

ideal gas law, the energy transported can be described using *Eq. 2.7*.

$$\dot{H} = \sum_i \dot{n}_i \cdot h_i(T_i, p_i) \quad (2.7)$$

The energy flow is a product of the molar flow times the enthalpy, which depends on the system pressure and temperature. The use of the three state variables pressure (p), temperature (T), and molar flow vector (\dot{n}) complies as well to the needs to describe gas flows, as to the demands regarding the description of energy flows. A gas flow presents at the same time a thermal energy and a pneumatic energy. A separation between the thermal and pneumatic domain cannot be done, because a change in the gas composition due to a chemical reaction changes the internal energy and this changes the temperature in turn, which influences the internal energy. The case would be different if no chemical reactions take place, in this case the thermal and the pneumatic domain could be decoupled, a change in temperature would necessarily be influenced by a entropy flow entering the system. To comply to the demands regarding causality at least one state variable has to represent an action, at least one other has to represent a reaction. The variables inside the block have to be connected in a way that all output values can be calculated from the combination of input values, with the help of constant parameters. Furthermore, all time dependencies have to be in integral form (*Fig. 2.9*).

If the choice of the variables does not comply to the general approach using



Figure 2.9: Representation of an EMR element using three variables.

two variables that multiply to a power its application on EMR might be called pseudo-EMR, in analogy to pseudo-Bond Graph [145]. It gives the possibility to handle the system parameters in some areas more freely.

When a system is cooled or heated an energy flow is supplied to or extracted from a subsystem. As introduced in *Tab. 2.1* the thermal domain can be described by the temperature and the entropy flow, in some cases it is possible to describe the cooling power with a single quantity, as it has been introduced by Oubamama in the book of Dauphin-Tanguy [60]. The same approach has been applied in this case (3.4.1).

2.6.3 Representation of Gas Mixtures

Fuel cells are rarely supplied with pure gases (*Fig. 1.3(b), hydrogen and oxygen for AFC*), but mostly with gas mixtures like air. If the system contains a fuel processor, the gas supplied to the fuel cell represents a mixture of several gases. In order to avoid to join a set of variables to each component separately, it has been preferred to connect all gas components into one single set of variables. Vectors are used for the extensive values (molar flow vector $\dot{\mathbf{n}}$) and scalars for the intensive values (temperature T). The molar flow vector has been chosen as a compromise; it is capable to apply the mass conservation law (using the molar masses *Tab. 2.5*) and the chemical reaction stoichiometry.

The pressure has to be considered more carefully. Two ways of describing the pressure are used. As gas flows with different compositions enter and exit a volume, a mixture takes place inside the volume. This gas mixture can be represented by the vector of partial pressures \mathbf{p} . Also in the case of diffusion, a change of the partial pressure of a species takes place that is best indicated with a partial pressure vector. The partial pressure vector is the most complete approach of pressure description. In some cases, for example if a throttle is used (*Eq. 3.52*), it is sufficient to know the total pressure of the system p . As the total pressure is a scalar and not depending on the gas mixture inside a volume, it is easier to handle than the partial pressure vector. The total pressure can be applied for the entire fuel processor modeling and also for the fuel cell inlets, only if the penetration to deeper layers of the fuel cell is used; the representation of pressure is switched to the partial pressure vector.

For reasons of modularity it has been chosen to use one conception of vector for the overall system. Therefore the vector has to contain all molecules that might appear throughout the course of the system.

$$\text{Gas Vector} = \begin{pmatrix} \text{Diesel} \\ \text{Hydrogen} \\ \text{Methan} \\ \text{Carbon Monoxide} \\ \text{Hydrogen sulfide} \\ \text{Carbon Dioxide} \\ \text{Nitrogen} \\ \text{Water (liquid)} \\ \text{Water (gaseous)} \\ \text{Oxygen} \end{pmatrix}$$

Table 2.5: Molar masses of species - maybe put in Annex

Species	Representation	Molar Mass g mol^{-1} .
Diesel	$\text{C}_n\text{H}_m\text{O}_p\text{S}_q$	186.246
Hydrogen	H_2	2.014
Methane	CH_4	16.038
Carbon Monoxide	CO	28.
Hydrogen Sulfide	H_2S	34.074
Carbon Dioxide	CO_2	43.99
Nitrogen	N_2	28.
Water gaseous	$\text{H}_2\text{O}(g)$	18.004
Water liquid	$\text{H}_2\text{O}(l)$	18.004
Oxygen	O_2	31.98

Blocks with coupling and accumulation

As introduced in paragraph (2.4), each element of the EMR is associated with a single modification. One strength of EMR is that complex systems are divided into a multitude of small elements, each element containing a simple conversion. During the modeling of the fuel cell, it has been identified that this decoupling is not possible in every case. The fuel cell inlet (as well at the anode as at the cathode side) is an element combining coupling and accumulation element (4.4.1). There is a gas stream entering the system, there is a gas stream leaving the system and there is a gas stream penetrating deeper layers of the fuel cell. As there are three gas flow connections to the volume it is a coupling element. As the inlet represents a volume, it is an accumulation element. Gas is stored inside the volume. The pressure inside the inlet depends on the accumulation of inflowing and outflowing gas streams. No mean could be found to divide the inlet into two independent blocks. For the moment a combination of coupling and accumulation has been used, indicated by overlapping barred rectangles (*Fig. 2.10*). The representation of the pressure can differ from one exit of the system to another.

2.7 Conclusion of Methodology Choice

The aim of this work is to develop a model of a diesel fed fuel cell system that is able to be used for model based control development. Therefore, a modeling methodology has to be chosen that suits best to the demands of the system and its application.

In chapter 2 several modeling methodologies are introduced. It is evaluated if

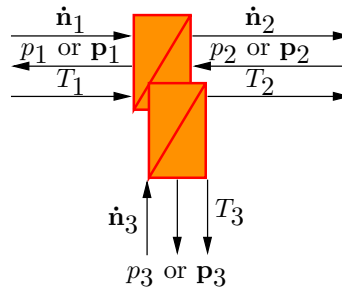


Figure 2.10: Representation of an EMR element with coupling and accumulation.

they are adapted to be used to model a complex multi-domain system and if they can be used for model based control structure development. First, an evaluation of different modeling approaches has been done (2.2). To be able to understand the basic ideas of the different approaches, the importance of the first law of thermodynamics for system modeling is introduced (2.2.1). In order that the modeling methodology is capable to model complex multi domain systems and to be used for model based control structure design it has to fulfill different criteria. To model complex multi domain systems it is advantageous if the system description is graphic to keep an overview about the system. Furthermore, it is advantageous if the system description is modular to be able to start with the modeling of a simplified system and to enlarge it subsequently. The use of an approach based on the energy conservation / first law of thermodynamics simplifies the connection between different energetic domains. At the same time the model shall be used for inversion based control structure design. Therefore, it has to be causal in order to keep the connections between cause and effect. The modularity helps to divide the complex system into a multitude of blocks that can be inverted elementwise. Different modeling methodologies are introduced and evaluated with regard to these criteria. The modeling methodologies evaluated are: Electric Equivalent Model (2.2.2), Bond Graph (2.2.3), Causal Ordering Graph (2.2.4) and Energetic Macroscopic Representation (2.2.5). The Energetic Macroscopic Representation (EMR) is identified as the most adapted methodology (2.3), because it is an energetic graphic causal modeling approach. The energetic aspect implements the possibility to connect different energetic domains. The graphic aspect helps keeping the overview over a complex structure. And the causal structure gives the possibility to develop an inversion based control. The application of EMR (2.4) and its inversion (2.5) are introduced in more detail. Still the application on a fuel cell system means an expansion of the methodology to another application. Therefore, some adaptations to chemical conversion and mass transfer for the use in fuel cell systems are made (2.6). The application of the methodology to a simplified fuel cell system model is published

in [58].

Chapter 3

Modeling of the Fuel Processor Unit

3.1 Introduction to Reformer Model

Inside the fuel processor unit, long chain hydrocarbons are converted into a hydrogen rich gas. As fuel cells are sensitive to certain contaminants of the gas, several gas cleaning steps have to be foreseen. PEFC have stricter specifications toward the gas quality than HTPEMFCs caused by their low working temperature. Hence, the fuel processing unit to supply PEFCs is more complex than this to supply HTPEMFCs, (*Fig. 1.6*), [54]. The structure and elements of a fuel processing unit have already been introduced in (1.3).

After giving the hypotheses made for the modeling (3.2), the application of each block used for fuel processing into a model is introduced (3.3). The stationary modeling of each block is introduced first; thereafter dynamic effects have to be taken into consideration. Approaches to consider pressure and temperature dynamics are introduced (3.4). The fuel processor model for a PEFC can then be obtained by a combination of the elements introduced. The fuel processor model is validated for stationary and dynamic aspects (3.5). The fuel processor for a HTPEMFC unit, obtained by the simplification of the PEFC fuel processor, is finally introduced (3.6).

3.2 Hypotheses made for the Fuel Processor Model

A model is never capable to represent all physical phenomena. This is not necessary as long as the assumptions and simplifications made still lead to results that correspond enough to the behavior observed in the real system to fulfill the aim of the model. If a model does not reproduce the real behavior correctly this

can often be explained by the fact that one or more hypotheses are too strong. The hypotheses posed for the fuel processor model are thus marked hereafter:

General Hypotheses

H 3.1 *Ideal gas law can be applied on all gases.*

Hypothesis concerning the overall system

H 3.2 *The temperature after the gas mixing unit is about 160 °C and does not decrease to levels below 100 °C until the condenser so the expected partial pressure of water rests below saturation pressure at the expected temperature. Then it can be considered that all flows are in gaseous phase between the gas mixing unit and the condenser.*

H 3.3 *Only the species defined in (2.6.3) occur in the reaction.*

H 3.4 *The formation of methane inside the reformer can be neglected [10].*

Hypotheses concerning the stationary behavior

H 3.5 *Two reactions occur inside the reformer unit, the combustion and the reforming reaction (1.3.2). In the real system, both reactions occur simultaneously. For the reformer model, first the combustion reaction is taken into consideration, than the reforming reaction. This hypothesis does not change the composition of the gas after the reformer if the temperature is known, because the composition depends on the temperature dependent equilibrium between hydrogen, water, carbon monoxide and carbon dioxide.*

H 3.6 *The hot gas mixture coming from the reformer keeps its composition while it is cooled down inside the heat exchanger.*

H 3.7 *It can be assumed that the fuel processing unit is controlled in a way that the oxygen supplied to the preferential oxidation does not exceed the amount needed to react all carbon monoxide and all hydrogen.*

H 3.8 *The condenser splits all liquid water from the remaining gaseous contents T_{cond} .*

H 3.9 *The modules of the fuel processor are placed in boxes. These are metallic surroundings. As the distinction between heat exchanger and reformer is only made for reasons of modeling and cannot be seen physically, those two modules are combined inside one box; all other modules have individual boxes.*

Hypotheses concerning the dynamic behavior

H 3.10 *For a gaseous system, a volume is an element presenting pressure dynamics. For reasons of simplicity the chemical reactions and the pressure development shall be regarded separately. Therefore, it is assumed that no volume is affected to the places where the reaction takes place. Hence, no pressure change occurs. Furthermore, the influence of condensation and evaporation on the total pressure inside a conversion block is neglected.*

H 3.11 *All chemical reactions are considered to be instantaneous (1.4).*

H 3.12 *All electrical conversions are considered to be instantaneous (1.4).*

H 3.13 *For the temperature development of the combined heat exchanger - reformer box, only the heat exchanged between the reformer gas and the box is considered. There is no heat exchange between the box and the environment.*

H 3.14 *The composition of the molar flow does not change inside a volume element. Changes in the composition of the molar flow vector occur only in conversion blocks.*

H 3.15 *The external system cooling uses the extracted heat power P as only parameter. This imposes that the cooling of the combination box/reformer gas is instantaneous.*

H 3.16 *The temperature and the pressure evolutions are decoupled due to the difference in dynamic time constant (1.4).*

H 3.17 *All surrounding boxes have a temperature of 300 K as initial condition, except the heat exchanger - reformer block being at 800 K, so the transient from the ambient is not taken into account.*

3.3 Fuel Processor Model

In the following, the implication of the respective elements of the fuel processing for the system model is introduced. This concerns the stationary behavior only. Therefore, all elements are represented by conversion elements. Thereafter, the dynamic aspects with regard to pneumatic and thermal development are taken into consideration (3.4), building a system model.

3.3.1 Reformer

Different reformer approaches have been introduced in (1.3.2). In this case an autothermal reformer developed by N-GHY is considered. The reaction inside the reformer is divided into three steps: the combustion reaction, the reforming reaction and the water gas shift reaction, (H3.5). All three reactions occur simultaneously. Those reactions follow the functions introduced in (1.3.2), only the species defined in (2.6.3) occur in the reaction, (H3.3). As introduced by Amphlett [10, 111] the formation of methane is neglected due to the high conversion temperatures of about 1400 °C (H3.4).

The reactions taking place inside the reformer are stationary and can therefore be represented by a conversion element. In a later step (3.4.1), the temperature dynamic will be added to the block. Thus, a coupling element has to be chosen for the EMR representation. As different energetic domains (gas flow and thermal domain), interact a coupling element in different energetic domains is chosen (orange circles with red rim), (Fig. 3.1, 1). The other elements (Fig. 3.1, 2 and 3) are related to pressure and temperature dynamics and will be introduced in (3.4).

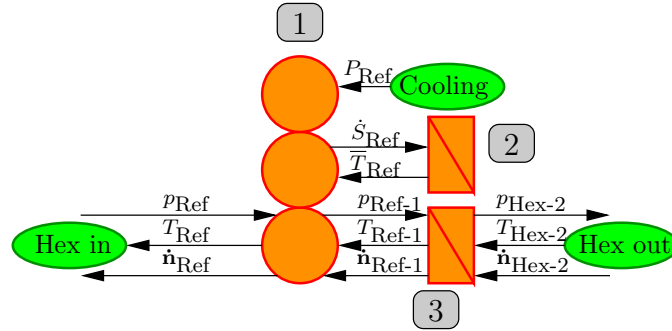


Figure 3.1: EMR of a reformer

The temperature of the preheated gas mixture $T_{\text{Ref-1}}$, the upstream molar flow vector $\dot{n}_{\text{Ref-1}}$ and the downstream pressure p_{Ref} are imposed by the heat exchanger. The upstream pressure $p_{\text{Ref-1}}$, the downstream molar flow vector \dot{n}_{Ref} and the downstream temperature T_{Ref} have to be calculated.

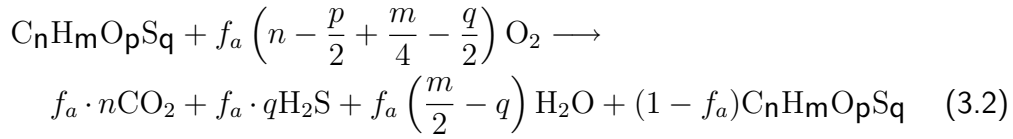
Evaluation of upstream pressure

According to (H3.10) the upstream pressure is equal to the downstream pressure, Eq. 3.1.

$$p_{\text{Ref-1}} = p_{\text{Ref}} \quad (3.1)$$

Evaluation of downstream molar flow vector

For the calculation of the downstream molar flow vector, several steps have to be done. First the air factor is calculated as introduced in (1.3.2), Eq. 3.3.

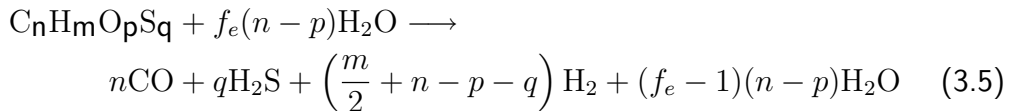


$$\text{with } f_a = \frac{\dot{n}_{\text{O}_2}}{(n - p + \frac{m}{4} - \frac{q}{2})\dot{n}_{\text{C}_n\text{H}_m\text{O}_p\text{S}_q}} \quad (3.3)$$

Afterward, the fuel composition after the combustion reaction can be evaluated transforming Eq. 1.11 into a matrix, Eq. 3.4.

$$\dot{\mathbf{n}}_{\text{comb}} = \begin{bmatrix} \dot{n}_{\text{comb-Diesel}} \\ \dot{n}_{\text{comb-H}_2} \\ \dot{n}_{\text{comb-CH}_4} \\ \dot{n}_{\text{comb-CO}} \\ \dot{n}_{\text{comb-H}_2\text{S}} \\ \dot{n}_{\text{comb-CO}_2} \\ \dot{n}_{\text{comb-N}_2} \\ \dot{n}_{\text{comb-H}_2\text{Og}} \\ \dot{n}_{\text{comb-H}_2\text{O}} \\ \dot{n}_{\text{comb-O}_2} \end{bmatrix} = \dot{\mathbf{n}}_{\text{in}} \cdot \begin{bmatrix} (1 - f_a) & 0 & 0 & 0 & 0 & 0 & 0 & 0 & 0 & 0 \\ 0 & 1 & 0 & 0 & 0 & 0 & 0 & 0 & 0 & 0 \\ 0 & 0 & 1 & 0 & 0 & 0 & 0 & 0 & 0 & 0 \\ 0 & 0 & 0 & 1 & 0 & 0 & 0 & 0 & 0 & 0 \\ f_a \cdot q & 0 & 0 & 0 & 1 & 0 & 0 & 0 & 0 & 0 \\ f_a \cdot n & 0 & 0 & 0 & 0 & 1 & 0 & 0 & 0 & 0 \\ 0 & 0 & 0 & 0 & 0 & 0 & 1 & 0 & 0 & 0 \\ f_a \cdot (m/2 - q) & 0 & 0 & 0 & 0 & 0 & 0 & 1 & 1 & 0 \\ 0 & 0 & 0 & 0 & 0 & 0 & 0 & 0 & 0 & 0 \\ 0 & 0 & 0 & 0 & 0 & 0 & 0 & 0 & 0 & 0 \end{bmatrix} \quad (3.4)$$

The gas mixture after combustion $\dot{\mathbf{n}}_{\text{comb}}$ undergoes the reformer reaction. First, the water factor f_e is calculated as introduced in (1.3.2), Eq. 3.6. Afterward, the fuel composition after the reforming reaction can be evaluated by into a matrix, Eq. 3.7.



$$\text{with } f_e = \frac{\dot{n}_{\text{H}_2\text{O}}}{(n - p)\dot{n}_{\text{C}_n\text{H}_m\text{O}_p\text{S}_q}} \quad (3.6)$$

$$\dot{\mathbf{n}}_{\text{Ref}} = \dot{\mathbf{n}}_{\text{comb}} \cdot \begin{bmatrix} 0 & 0 & 0 & 0 & 0 & 0 & 0 & 0 & 0 & 0 \\ (m/2 - q - p + n) & 1 & 0 & 0 & 0 & 0 & 0 & 0 & 0 & 0 \\ 0 & 0 & 1 & 0 & 0 & 0 & 0 & 0 & 0 & 0 \\ n & 0 & 0 & 1 & 0 & 0 & 0 & 0 & 0 & 0 \\ q & 0 & 0 & 0 & 1 & 0 & 0 & 0 & 0 & 0 \\ 0 & 0 & 0 & 0 & 0 & 1 & 0 & 0 & 0 & 0 \\ r & 0 & 0 & 0 & 0 & 0 & 1 & 0 & 0 & 0 \\ (f_e - 1) \cdot (n - p) & 0 & 0 & 0 & 0 & 0 & 0 & 0 & 1 & 0 \\ 0 & 0 & 0 & 0 & 0 & 0 & 0 & 0 & 0 & 0 \\ 0 & 0 & 0 & 0 & 0 & 0 & 0 & 0 & 0 & 1 \end{bmatrix} \quad (3.7)$$

The obtained gas mixture ($\dot{\mathbf{n}}_{\text{ref}}$) gives values for the hydrogen, water, carbon monoxide and carbon dioxide content of the system that are not balanced according to the system temperature (1.3.2). This is compensated using the water gas shift reaction, defining the equilibrium between water, carbon monoxide, hydrogen and carbon dioxide. It has been shown that for reasons of gas temperature, reaction kinetics and residence time of the gas inside the reformer, the gas composition at the exit is equal to the gas composition at 1000 °C, [111]. Thus, equations *Eq. 3.9* and *Eq. 3.10* that have been introduced in (1.3.2, p. 18), can be applied directly using 1000 °C for the temperature, leading to the equation *Eq. 3.13*



$$K_p = \exp\left(\frac{-\Delta G}{R \cdot T}\right) \quad (3.9)$$

$$K_p = \frac{(x_{\text{CO}_2} + \xi)(x_{\text{H}_2} + \xi)}{(x_{\text{CO}} - \xi)(x_{\text{H}_2\text{O}} - \xi)} \quad (3.10)$$

$$p = \frac{(-K_p x_{\text{CO}} - K_p x_{\text{H}_2\text{O}} - x_{\text{CO}_2} - x_{\text{H}_2})}{(K_p - 1)} \quad (3.11)$$

$$q = \frac{(K_p x_{\text{CO}} x_{\text{H}_2\text{O}} - x_{\text{CO}_2} x_{\text{H}_2})}{(K_p - 1)} \quad (3.12)$$

$$\xi_1 = -\frac{p}{2} + \sqrt{\frac{p^2}{4} - q} \quad (3.13)$$

$$\xi_2 = -\frac{p}{2} - \sqrt{\frac{p^2}{4} - q} \quad (3.14)$$

Evaluation of the gas temperature

Once the output molar flow vector is known, the output temperature can be calculated. Therefore, the energy balance of the system (Eq. 3.15) has to be solved. The energy balance of the system has been introduced in (2.6.1, p. 44)

$$0 = \dot{H}(T_{\text{out}}, p_{\text{out}}) - \dot{H}(T_{\text{in}}, p_{\text{in}}) + \Delta\dot{Q} + P \quad (3.15)$$

The energy balance contains the enthalpy of the input flows ($\dot{H}(T_{\text{in}}, p_{\text{in}})$) and the enthalpy of the output flows ($\dot{H}(T_{\text{out}}, p_{\text{out}})$) as well as cooling energy (P). The temperature dynamic will introduce a further thermal energy flow (\dot{Q}). As the pressure does not change inside the system, the enthalpy can be calculated using approach presented among others by Burcat [38]. It has to be taken into consideration that the molar flow is represented by a vector, hence representing all elements by an enthalpy vector (\mathbf{h}), Eq. 3.16.

$$\dot{H}(T_{\text{out}}, p_{\text{out}}) = \sum_{i=1 \dots 10} \dot{n}_i h(T_i, p_i) \quad (3.16)$$

The enthalpy is calculated by a fifth order polynomial of the temperature (Eq. 3.17) and this polynomial is applied to each species (Eq. 3.18).

$$h_i(T) = a_{i1} \cdot T + a_{i2} \cdot T^2 + a_{i3} \cdot T^3 + a_{i4} \cdot T^4 + a_{i5} \cdot T^5 + a_{i6} \quad (3.17)$$

$$\mathbf{h}_{\text{out}} = \begin{bmatrix} h_1 \\ \vdots \\ h_{10} \end{bmatrix} \quad (3.18)$$

The enthalpy vector has furthermore to be applied twice. One time for the input temperature $T_{\text{Ref-1}}$ and once for output temperature T_{Ref} . This leads to the fact that the output temperature (the value to be defined) is represented by a fifth order polynomial. As it is not possible to solve this equation analytically, a solver is used. During the solving process the value of the output temperature is changed until the energy is balanced. The value of the temperature balancing the energy conservation equation is the output temperature T_{out} . In this approach the reformer is considered as adiabatic, in a real system heat losses can be seen that shall to be taken into account in the temperature development in a future step.

3.3.2 Heat Exchanger

The stationary model of the heat exchanger consists of two blocks. First, a mixing unit where diesel, water and air are mixed. Second, the heat exchanger itself with a hot gas stream coming out of the reformer and a colder gas stream coming from the mixing unit.

Inside the mixing unit the three gas streams (diesel, water and air) are combined into one gas stream. The mixing unit is represented by a coupling block in the same domain, (Fig. 3.2, 1).

The heat exchanger is represented by a coupling block in the same domain as well. The particularity is that this block has two incoming gas streams and two outflowing gas streams, (Fig. 3.2, 2). Neither pressure nor temperature dynamics are associated to the heat exchanger.

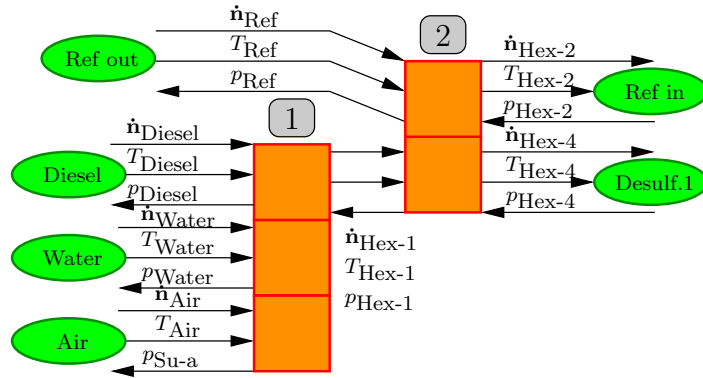


Figure 3.2: EMR of a heat exchanger

Gas Mixing Unit

For the gas mixing unit the molar flow vectors of diesel \dot{n}_{Su-d} , water \dot{n}_{Su-w} and air \dot{n}_{Su-a} as well as the corresponding temperatures T_{Su-d} , T_{Su-w} and T_{Su-a} are known input values. Also the downstream pressure p_{Hex-1} is known. The molar flow vector after mixing \dot{n}_{Hex-1} , the temperature of the gas mixture T_{Hex-1} and the upstream pressures p_{Su-d} , p_{Su-w} and p_{Su-a} have to be evaluated.

It is supposed that the pressure does not change inside the mixing unit (H3.10). Hence, the three upstream pressures are equal to the imposed downstream pressure, Eq. 3.19.

$$p_{Su-d} = p_{Su-w} = p_{Su-a} = p_{Hex-1} \quad (3.19)$$

As first approach, the downstream molar flow vector is equal to the sum of the three upstream molar flow vectors. This is right for all species but water. In the studied case the three upstream flows have different temperatures. Liquid water and diesel are supplied in liquid form with a temperature of 40 °C. Air is supplied with a temperature of 200 °C. Hence, the mixture will have an intermediate temperature. As the temperature rises, liquid water vaporises. The maximum fraction of gaseous water is defined by the saturation pressure p_{sat} . The saturation pressure depends on the temperature (Eq. 1.28). The downstream molar flow vector is therefore directly linked to the downstream temperature.

The temperature can be evaluated solving the energy balance (Eq. 2.5) as introduced in 3.3.1.

Until now the total pressure p was used inside the model. This pressure is the sum of all partial pressures $p = \sum_i p_i$. The saturation pressure p_{sat} has to be compared to the partial pressure of gaseous water $p_{\text{H}_2\text{Og}}$. Therefore, it is necessary to describe the partial pressures. For ideal gases (H3.1) the molar fraction and the pressure fraction are equal, Eq. 3.20:

$$x_i = \frac{p_i}{\sum_i p_i} = \frac{\dot{n}_i}{\sum_i \dot{n}_i} \quad (3.20)$$

All water is gaseous if the partial pressure of water (liquid and gas) is inferior to the saturation pressure at a given temperature. If the partial pressure is superior, the amount equivalent to the saturation pressure is gaseous and the rest is liquid.

Starting with the assumption that all water is gaseous the temperature is calculated as introduced in (1.3.2) using the energy balance (Eq. 2.5). Thereafter, it is verified if the partial pressure of gaseous water is superior or inferior to the saturation pressure of the temperature found. If the saturation pressure is superior, the assumption that all water is in gaseous form was correct. If not, a fraction of water is assumed to be in liquid phase and the energy balance is solved finding a new temperature. The definition of this fraction of liquid water is empiric. The value chosen has to be sufficiently big to give a difference in temperature and to lead to a result with a limited number of steps. At the same time the condensed fraction has to be sufficiently small that it does not cause important overestimations of liquid water. In our case the value of a condensation of 0.3 % of the gaseous water has been chosen. This strategy is continued until a combination of upstream temperature $T_{\text{Hex-1}}$ and upstream partial pressures is found such as the partial pressure of gaseous water is equal or inferior to the saturation pressure. Knowing the partial pressure of gaseous and liquid water, the

upstream molar flow vector $\dot{n}_{\text{Hex-1}}$ is calculated using Eq. 3.20. A schematic of the calculation of the molar flow vector and the temperature is given in (Fig. 3.3).

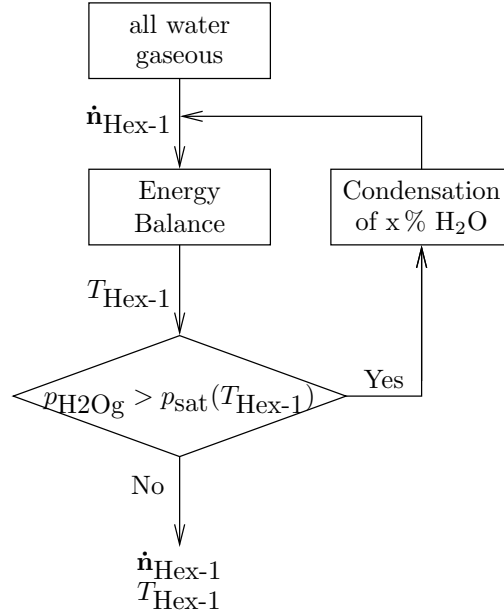


Figure 3.3: Evaluation of the molar flow vector and temperature after the mixing unit

Heat Exchange

The second block inside the heat exchanger unit (Fig. 3.2, 2) calculates the actual heat exchange between a cold gas flow coming from the mixer that is to be heated up before entering the reformer and a hot gas flow coming from the reformer that has to be cooled down before entering the first desulfurization stage. The molar flow vector coming from the gas mixing unit $\dot{n}_{\text{Hex-1}}$, its temperature $T_{\text{Hex-1}}$ and its downstream pressure $p_{\text{Hex-2}}$ as well as the molar flow vector coming from the reformer \dot{n}_{Ref} , its temperature T_{Ref} and its downstream pressure $p_{\text{Hex-4}}$ are known input parameters. The molar flow vector entering the reformer $\dot{n}_{\text{Hex-2}}$, its temperature $T_{\text{Hex-2}}$ and its upstream pressure $p_{\text{Hex-1}}$ as well as the molar flow vector entering the desulfurization unit $\dot{n}_{\text{Hex-4}}$, its temperature $T_{\text{Hex-4}}$ and its upstream pressure p_{Ref} have to be calculated.

The pressures do not change inside the block (H 3.10). The upstream pressures are therefore equal to the downstream pressures, Eq. 3.21 and Eq. 3.22.

$$p_{\text{Ref}} = p_{\text{Hex-4}} \quad (3.21)$$

$$p_{\text{Hex-1}} = p_{\text{Hex-2}} \quad (3.22)$$

The change inside the molar flow vectors is minor. The molar flow vector of the hot gas coming from the reformer is supposed not to change at all (H3.6), Eq. 3.23.

$$\dot{n}_{\text{Hex-4}} = \dot{n}_{\text{Ref}} \quad (3.23)$$

It is possible to have still some liquid water in the gas flow entering from the mixer. As the heat exchanger is set to heat up the diesel-water-air-mixture up to 800 °C, the saturation pressure after the heat exchange will be much higher than the total pressure. Therefore, the assumption that all water exits the heat exchanger in gaseous form is valid (H3.2). Furthermore, the calculation of the output temperatures of the heat exchanger is based on a single phase system. Hence, the heat exchange is calculated in two steps. First, it is assumed that all water is gaseous. Therefore, the difference in heat between the gas mixture entering the system with liquid water $\dot{n}_{\text{Hex-1}}$ and the same gas mixture at the same temperature with only gaseous water $\dot{n}_{\text{Hex-1}'}$ is evaluated, Eq. 3.24.

$$\Delta Q = \dot{n}_{\text{Hex-1}} \cdot h(T_{\text{Hex-1}}) - \dot{n}_{\text{Hex-1}'} \cdot h(T_{\text{Hex-1}}) \quad (3.24)$$

This energy is used to cool down the gas stream coming from the reformer \dot{n}_{Ref} . This gives a virtual temperature of the gas mixture $T_{\text{Ref}'}$, Eq. 3.25.

$$0 = \dot{n}_{\text{ref}} \cdot h(T_{\text{Ref}}) - \dot{n}_{\text{ref}} \cdot h(T_{\text{Ref}'}) + \Delta Q \quad (3.25)$$

The temperatures after the heat exchange $T_{\text{Hex-2}}$ and $T_{\text{Hex-4}}$ are then calculated applying the approach introduced in (1.3.3) using the all gaseous molar flow vector from the gas mixing unit $\dot{n}_{\text{Hex-1}'}$ and the virtual temperature of the gas coming from the reformer $T_{\text{Ref}'}$.

3.3.3 Desulfurization 1

For the stationary calculation, a desulfurization unit is represented by a combined coupling block with conversion into different domains (Fig. 3.4, 1). Inside the desulfurization unit, hydrogen sulfide is split from the gas and connected to a sink (Fig. 3.4, 2). Therefore, a coupling unit is used. Furthermore, the temperature dynamic will be connected to the desulfurization block and discussed in (3.4.1), (Fig. 3.4, 3). This imposes the use of a coupling block in differ-

ent energetic domains. The accumulation block upstream the conversion block (Fig. 3.4, 4) represents the pressure dynamic introduced in (3.4).

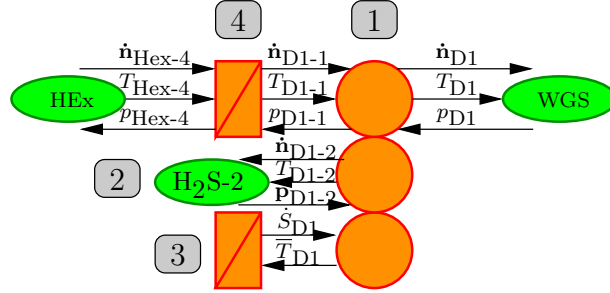


Figure 3.4: EMR of the first desulfurization unit

The upstream molar flow vector \dot{n}_{D1-1} and its temperature T_{D1-1} are input values as well as the downstream pressures p_{D1} and p_{D1-2} . The downstream molar flow vector toward the WGS \dot{n}_{D1} and the molar flow vector of the separated sulfur \dot{n}_{D1-2} with the respective temperatures T_{D1} and T_{D1-2} have to be evaluated as well as the upstream p_{D1-1} .

As the pressure does not change inside the conversion element (H3.10) the upstream pressure is equal to the downstream pressure, Eq. 3.26.

$$p_{D1-1} = p_{D1} \quad (3.26)$$

Inside the molar flow vector only the element representing the hydrogen sulfide is changing, all other elements stay unchanged. The reduction of the hydrogen sulfide is due to a selectivity factor (sel) as introduced in (1.3.4, p. 22) and can be calculated following Eq. 3.27. The hydrogen sulfide flow stored \dot{n}_{D1-2} is calculated from Eq. 3.28 accordingly.

$$\dot{n}_{\text{Sulfur-removed}} = sel \cdot \dot{n}_{\text{Sulfur-in}} \quad (3.27)$$

$$\dot{n}_{\text{Sulfur-out}} = (1 - sel) \cdot \dot{n}_{\text{Sulfur-in}} \quad (3.28)$$

The temperature of the leaving gas stream is calculated according to the energy balance Eq. 2.5. As the desulfurization is basically a split of gas stream, the upstream and downstream molar flow vectors are supposed to be the same. The temperature is only influenced by heat flows ΔQ and P introduced in (3.4.1). The temperature of the stored sulfur is the same as the downstream temperature $T_{D1-2} = T_{D1}$. The upstream temperature T_{D1} is evaluated solving Eq. 2.5

according to the approach introduced in (3.4.1), see Eq. 3.29.

$$0 = \dot{H}(T_{D1-1}) - \dot{H}(T_{D1}) + \Delta Q + P \quad (3.29)$$

3.3.4 Water Gas Shift

The stationary reaction of the WGS block is represented in EMR using a coupling block in different energetic domains (Fig. 3.5, 1). The WGS reaction itself is a conversion inside the same energetic domain. In (3.4.1) the temperature dynamic of the system will be described (Fig. 3.5, 2), demanding the use of a coupling element in different energetic domains (Fig. 3.5, 1). Furthermore, the pressure dynamic (Fig. 3.5, 3) will be introduced in (3.4.2) as well.

The upstream molar flow vector \dot{n}_{WGS-1} , its temperature T_{WGS-1} and the downstream pressure p_{WGS} are known input parameters. The downstream molar flow vector \dot{n}_{WGS} , its temperature T_{WGS} and the upstream pressure p_{WGS-1} have to be evaluated.

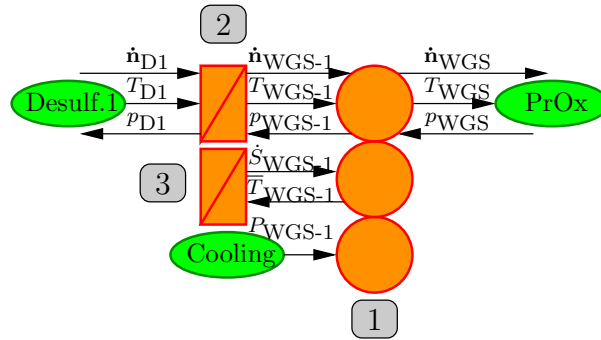


Figure 3.5: EMR of a water gas shift reaction unit

As stated in (H3.10) the pressure inside the block does not change. Therefore, the upstream pressure is equal to the downstream pressure, Eq. 3.30.

$$p_{WGS-1} = p_{WGS} \quad (3.30)$$

Inside the water gas shift reactor, the fact that the equilibrium between water, carbon monoxide, carbon dioxide and hydrogen depends on the temperature is used. The water gas shift block is cooled by P_{WGS-1} . The cooling of the gas stream leads to a decrease in temperature. A temperature decrease is necessary to be able to supply the gas to the fuel cell. The change in temperature decreases at the same time the molar fraction of the harmful carbon monoxide. The equilibrium reaction is introduced in (1.3.2, p. 18).



$$K_p = \exp\left(\frac{-\Delta G}{R \cdot T}\right) \quad (3.32)$$

$$K_p = \frac{(x_{\text{CO}_2} + \xi)(x_{\text{H}_2} + \xi)}{(x_{\text{CO}} - \xi)(x_{\text{H}_2\text{O}} - \xi)} \quad (3.33)$$

$$p = \frac{(-K_p x_{\text{CO}} - K_p x_{\text{H}_2\text{O}} - x_{\text{CO}_2} - x_{\text{H}_2})}{(K_p - 1)} \quad (3.34)$$

$$q = \frac{(K_p x_{\text{CO}} x_{\text{H}_2\text{O}} - x_{\text{CO}_2} x_{\text{H}_2})}{(K_p - 1)} \quad (3.35)$$

$$\xi_1 = -\frac{p}{2} + \sqrt{\frac{p^2}{4} - q} \quad (3.36)$$

The downstream molar flow vector and the downstream temperature are closely related. Two equations have to be solved in a form that both are satisfied. On the one hand the energy flow balance *Eq. 2.5* has to be equal to zero. On the other hand the advance of the reaction ξ has to be equal to zero *Eq. 3.36*. The temperature occurs in the calculation of the advancement in a non linear form. Therefore, the system of two equations with two unknowns (the temperature and the molar flow vector) cannot be solved analytically, but only numerically. In our case a loop is used to solve the system. At first the energy balance is used to find a first temperature guess, this guess is used to refine the conception of the molar flow vector, which is in turn used to calculate the temperature balance and so forth until the change of temperature between two calculations is inferior a certain value. The result gives the downstream temperature and is used to define the downstream molar flow vector, (*Fig. 3.6*).

3.3.5 Preferential Oxidation

The stationary reaction of the preferential oxidation block is represented by a coupling block in different domains, (*Fig. 3.7, 1*). The reason for using a different domain approach is the connection to the temperature dynamic (3.4.1), (*Fig. 3.7, 2*). The accumulation element in front of the coupling elements represents the pressure dynamic introduced in (3.4.2), (*Fig. 3.7, 3*).

For the preferential oxidation, an air stream is supplied to the system. With the help of a catalyst, the supplied oxygen is considered to react with the carbon monoxide mainly. The preferential oxidation has been introduced in detail

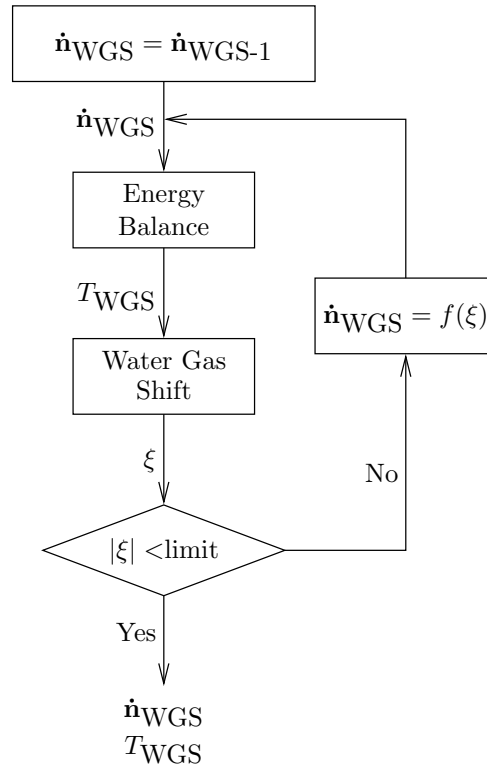


Figure 3.6: Evaluation of the molar flow vector and temperature after the WGS unit

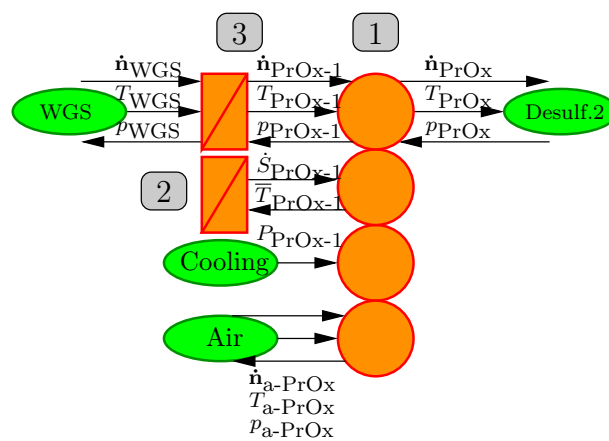


Figure 3.7: EMR of a preferential oxidation unit

in (1.3.2). When the preferential oxidation is applied for carbon monoxide reduction, two chemic reactions are possible *Eq. 3.37* and *Eq. 3.38*. Due the the use of a catalyst the carbon monoxide oxidation *Eq. 3.37* is largely privileged over the hydrogen oxidation.



The upstream molar flow vector $\dot{\mathbf{n}}_{\text{PrOx-1}}$, its temperature $T_{\text{PrOx-1}}$ and the downstream pressure p_{PrOx} are known input values. The downstream molar flow vector $\dot{\mathbf{n}}_{\text{PrOx}}$, its temperature T_{PrOx} and the upstream pressure $p_{\text{PrOx-1}}$ have to be evaluated.

As the pressure does not change inside the conversion element (*H3.10*) the upstream pressure is equal to the downstream pressure, *Eq. 3.39*.

$$p_{\text{PrOx-1}} = p_{\text{PrOx}} \quad (3.39)$$

The reaction occurring inside the preferential oxidation unit can be described in matrix form. A maximum percentage of carbon monoxide can react with the supplied oxygen, before the oxidation of hydrogen starts (*sel*) *Eq. 1.27*. As a maximum, the totality of the carbon monoxide can be burned (*H3.10*). In the first step only the carbon monoxide oxidation is regarded *Eq. 3.40*. The intermediate mass flow vector is named $\dot{\mathbf{n}}_{\text{PrOx}'}$.

$$\dot{\mathbf{n}}_{\text{PrOx}'} = \begin{bmatrix} \dot{n}_{\text{PrOx}'\text{-Diesel}} \\ \dot{n}_{\text{PrOx}'\text{-H}_2} \\ \dot{n}_{\text{PrOx}'\text{-CH}_4} \\ \dot{n}_{\text{PrOx}'\text{-CO}} \\ \dot{n}_{\text{PrOx}'\text{-H}_2\text{S}} \\ \dot{n}_{\text{PrOx}'\text{-CO}_2} \\ \dot{n}_{\text{PrOx}'\text{-N}_2} \\ \dot{n}_{\text{PrOx}'\text{-H}_2\text{Og}} \\ \dot{n}_{\text{PrOx}'\text{-H}_2\text{OI}} \\ \dot{n}_{\text{PrOx}'\text{-O}_2} \end{bmatrix} = \begin{bmatrix} 1 & 0 & 0 & 0 & 0 & 0 & 0 & 0 & 0 & 0 \\ 0 & 1 & 0 & 0 & 0 & 0 & 0 & 0 & 0 & 0 \\ 0 & 0 & 1 & 0 & 0 & 0 & 0 & 0 & 0 & 0 \\ 0 & 0 & 0 & 1 & 0 & 0 & 0 & 0 & 0 & -2\text{ sel} \\ 0 & 0 & 0 & 0 & 1 & 0 & 0 & 0 & 0 & 0 \\ 0 & 0 & 0 & 0 & 0 & 1 & 0 & 0 & 0 & 2\text{ sel} \\ 0 & 0 & 0 & 0 & 0 & 0 & 1 & 0 & 0 & 0 \\ 0 & 0 & 0 & 0 & 0 & 0 & 0 & 1 & 1 & 0 \\ 0 & 0 & 0 & 0 & 0 & 0 & 0 & 0 & 0 & 0 \\ 0 & 0 & 0 & 0 & 0 & 0 & 0 & 0 & 0 & (1 - \text{ sel}) \end{bmatrix} \cdot \dot{\mathbf{n}}_{\text{PrOx-1}} \quad (3.40)$$

In a second step the remaining oxygen is used to oxidize water *Eq. 3.41*.

$$\dot{n}_{\text{PrOx}} = \begin{bmatrix} 1 & 0 & 0 & 0 & 0 & 0 & 0 & 0 & 0 & 0 \\ 0 & 1 & 0 & 0 & 0 & 0 & 0 & 0 & 0 & -2 \\ 0 & 0 & 1 & 0 & 0 & 0 & 0 & 0 & 0 & 0 \\ 0 & 0 & 0 & 1 & 0 & 0 & 0 & 0 & 0 & 0 \\ 0 & 0 & 0 & 0 & 1 & 0 & 0 & 0 & 0 & 0 \\ 0 & 0 & 0 & 0 & 0 & 1 & 0 & 0 & 0 & 0 \\ 0 & 0 & 0 & 0 & 0 & 0 & 1 & 0 & 0 & 0 \\ 0 & 0 & 0 & 0 & 0 & 0 & 0 & 1 & 1 & 2 \\ 0 & 0 & 0 & 0 & 0 & 0 & 0 & 0 & 0 & 0 \\ 0 & 0 & 0 & 0 & 0 & 0 & 0 & 0 & 0 & 0 \end{bmatrix} \cdot \dot{n}_{\text{PrOx}}' \quad (3.41)$$

It is not supposed that the oxygen supplied during preferential oxidation exceeds the amount of hydrogen present (*H 3.7*).

The downstream temperature is calculated using the energy balance. The expected temperature of the gas mixture is about 120 °C. At this temperature the reaction velocities are much lower than inside the reformer for example. The gas has left the block before the equilibrium reaction can occur. Therefore, the equilibrium between water, carbon monoxide, carbon dioxide and hydrogen is not longer considered. There is the chance that condensation occurs. The approach of the energy balance taking into consideration condensation has been introduced for the mixing unit of the heat exchanger (3.3.2). It is applied in the same form here.

3.3.6 Desulfurization 2

The second desulfurization unit is completely analogue to the first desulfurization unit introduced in 3.3.3. The EMR representation can be seen in (*Fig. 3.8*).

3.3.7 Condenser

Inside the condensation element the gas mixture is cooled down and the liquid water is split from the gas stream. The condensation element is described by a coupling element. A coupling element is necessary because the stream is split into liquid water and gaseous components. As cooling is involved in the stationary process a representation in different energetic domains is required, (*Fig. 3.9, 1*). Furthermore, the temperature dynamics (*Fig. 3.9, 2*) will be introduced in section (3.4.1). The accumulation element in front of the coupling elements represents the pressure dynamic introduced in (3.4.2), (*Fig. 3.9, 3*).

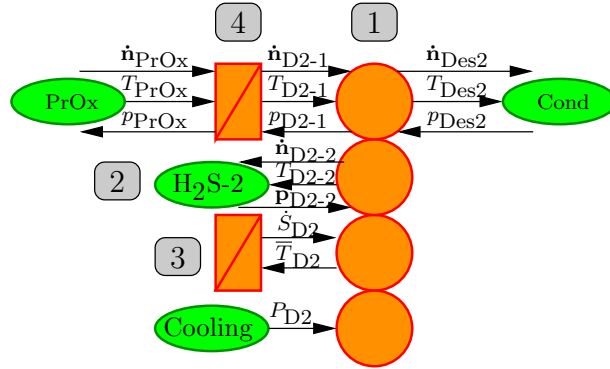


Figure 3.8: EMR of the second desulfurization unit

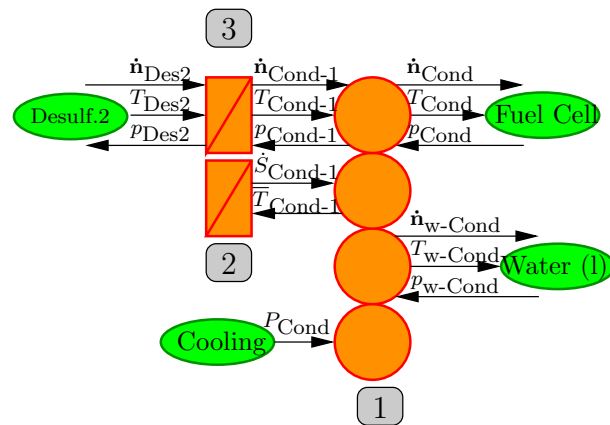


Figure 3.9: EMR of a water gas condensation unit

The upstream molar flow vector $\dot{\mathbf{n}}_{\text{Cond-1}}$, its temperature $T_{\text{Cond-1}}$ and the downstream pressure p_{Cond} as well as the pressure of the liquid water storage $p_{\text{Cond-H2O}}$ are known input values. The downstream molar flow vector $\dot{\mathbf{n}}_{\text{Cond}}$, its temperature T_{Cond} , the downstream molar flow vector of liquid water $\dot{\mathbf{n}}_{\text{Cond-H2O}}$, its temperature $T_{\text{Cond-H2O}}$, as well as the upstream pressure $p_{\text{Cond-1}}$ have to be evaluated.

The pressure does not change inside the conversion element (H3.10), the upstream pressure is equal to the downstream pressure Eq. 3.42.

$$p_{\text{Cond-1}} = p_{\text{Cond}} \quad (3.42)$$

$$T_{\text{Cond-H2O}} = T_{\text{Cond}} \quad (3.43)$$

A large percentage of the liquid water is extracted inside the condenser (H3.8). The both downstream temperatures are the same, Eq. 3.43. The evaluation of the both downstream molar flow vectors $\dot{\mathbf{n}}_{\text{Cond}}$ and $\dot{\mathbf{n}}_{\text{Cond-H2O}}$ and the downstream temperatures can be done as follows: first, the energy balance including condensation is applied as it has been introduced in (3.3.2). This procedure defines the downstream temperature T_{Cond} and a molar flow vector $\dot{\mathbf{n}}_{\text{Cond}}'$ including liquid and gaseous water. Second, the fraction of liquid water defined by the split constant $\tau_{\text{cond}} = 1$ is split from the molar flow vector (H3.8), forming the liquid water output $\dot{\mathbf{n}}_{\text{Cond-H2O}}$, Eq. 3.44. The remaining molar flow vector forms the gaseous output of the system $\dot{\mathbf{n}}_{\text{Cond}}$, Eq. 3.45.

$$\dot{\mathbf{n}}_{\text{w-Cond}} = \dot{\mathbf{n}}_{\text{Cond}}' \cdot [0 \ 0 \ 0 \ 0 \ 0 \ 0 \ 0 \ 0 \ \tau_{\text{cond}} \ 0]' \quad (3.44)$$

$$\dot{\mathbf{n}}_{\text{Cond}} = \dot{\mathbf{n}}_{\text{Cond}}' \cdot [1 \ 1 \ 1 \ 1 \ 1 \ 1 \ 1 \ 1 \ (1 - \tau_{\text{cond}}) \ 1]' \quad (3.45)$$

All stationary elements of the fuel processing unit to convert diesel into hydrogen rich gas with an adequate purity to supply a PEFC system have been introduced. The dynamic aspects are presented in the following section.

3.4 Dynamic aspects inside the Fuel Processor Model

The modeling of the stationary behavior of a fuel processing unit is already non obvious. The goal of this approach is to obtain a model based control structure, thus it is indispensable to go further and to take into consideration time dependent effects. As introduced in (1.4) only thermal and pneumatic time

dependent effects are considered, the chemical reactions (*H3.11*) and electrical conversions (*H3.12*) are considered to be instantaneous. How the thermal and pneumatic time dependency can be incorporated inside the fuel processor model is introduced hereafter.

The EMR representations of the respective element incorporated already the thermal and pneumatic time dependent blocks. As the general structure of thermal and pneumatic time dependency is equal for the different blocks, they are only introduced once.

The temperature and the pressure development are decoupled (*H3.16*). They are represented by two different EMR blocks. The thermal development is associated to the block where the reaction takes place, explaining the use of coupling blocks in different energetic domains. This block has no volume (*H3.10*). The volume has been lumped into one single element accumulation element which is placed before the block where the reaction takes place (for example (*Fig. 3.9, 3*)). This element considers the pneumatic time dependency.

3.4.1 Temperature

As the chemical reactions are considered to be instantaneous (*H3.11*), the gas flows can change their temperature immediately. Still, inside the real system it can be observed that the temperatures do not undergo step changes. Reason for this is that not every reaction takes place instantaneously, because there are heat exchanges between the gas and because there are energy exchanges of the gas flows with their surrounding. In this case only the heat exchange between the gas and the surrounding is taken into consideration, therefore some hypotheses have been made.

The different modules of the fuel processor are placed in so called boxes. This is the metallic surrounding of the respective module (*H3.9*). There is a heat exchange between the gas flow and the box. The only possible heat exchange of the box is toward the gas flowing through it, (*H3.13*). There is no heat exchange between the box and the environment. In section (2.6.2) it was introduced that entropy flow \dot{S} and the temperature T build a well adapted parameter pair to describe heat exchange. The entropy flow between the gas and the box is defined by the temperature of the box T_B and the temperature of the gas mix \bar{T} as well as a constant parameter representing the heat exchange coefficient times the connection surface kA , *Eq. 3.46* [12].

$$\dot{S} = kA \frac{(\bar{T} - T_B)^2}{\bar{T} \cdot T_B} \quad (3.46)$$

The temperature of the gas mix \bar{T} can be defined as the logarithmic mean temperature of the incoming and outflowing gas, Eq. 3.47 [12, 95].

$$\bar{T} = \frac{T_{\text{out}} - T_{\text{in}}}{\log\left(\frac{T_{\text{out}}}{T_{\text{in}}}\right)} \quad (3.47)$$

Inside the box, heat energy Q is stored. The only way energy can enter the box is via the heat exchange with the gas (H3.13). Hence, the thermal energy inside the block can be calculated using two approaches. Firstly, the integration of the heat flow exchanged with the gas Eq. 3.48 and secondly, the heat capacity of the box, taking into considerations its mass m and its heat capacity c_p , Eq. 3.49. In this case the environmental temperature T_{env} is used as reference value. If the box has the same temperature as the environment $T_{\text{B}} = T_{\text{env}}$, no heat is stored. The combination of those two equations allows to evaluate the temperature of the box T_{B} .

$$Q = \int (\dot{S} \cdot T_{\text{B}}) dt \quad (3.48)$$

$$Q = m \cdot c_p (T_{\text{B}} - T_{\text{env}}) \quad (3.49)$$

Furthermore, the module can be cooled by a secondary cooling system. The energy flow withdrawn by the cooling is indicated as P (Fig. 3.10). For the cooling, only one parameter, the power, is used. This imposes that the cooling is instantaneous. This assumption (H3.15) has been made because otherwise another heat exchanger like the one introduced in section (1.3.3) had to be considered for each module, which would have complicate the system considerably.

The consideration of the temperature dynamic defines the exchanged heat flow $\Delta\dot{Q}$ in the energy balance, Eq. 3.50 as it has been introduced in (2.6.1, p. 43). Next to the enthalpies \dot{H}_{in} and \dot{H}_{out} , the energy balance contains two other terms, the energy exchanged with the box $\Delta\dot{Q} = \dot{S} \cdot T_{\text{B}}$ and the cooling power P .

$$0 = \dot{H}_{\text{out}}(T_{\text{in}}, p_{\text{in}}) - \dot{H}_{\text{in}}(T_{\text{out}}, p_{\text{out}}) + \Delta\dot{Q} + \Delta P \quad (3.50)$$

The stationary behavior represented by the chemical reaction and introduced for the different models in (3.3) interacts with the temperature development via the application of the energy balance Eq. 2.5. With the help of the energy balance the upstream temperature T_{out} is evaluated. Once the input and the output temperatures are known the logarithmic mean temperature of the gas \bar{T}

can be evaluated, which is applied to find the entropy flow \dot{S} in Eq. 3.46. As the entropy flow is known, the temperature of the box T_B can be evaluated according to Eq. 3.48 and Eq. 3.49. With the knowledge of the temperature of the box the heat flow $\Delta\dot{Q}$ can be evaluated, which in turn influences the upstream temperature.

The thermal dynamic is represented in EMR with the help of two blocks, (Fig. 3.10). The conversion block where the reaction takes place is expanded to a coupling block connecting different energetic domains, (Fig. 3.10, 1). The different energetic domains have been chosen to represent that here an interaction between the chemical and the thermal domain takes place. The box is represented by an accumulation block, (Fig. 3.10, 2). The coupling block and the accumulation block are connected by the parameter pair of the temperature of the box T_B and the entropy flow \dot{S} . The entropy flow is calculated inside the coupling block using Eq. 3.46. The temperature inside the box is calculated using Eq. 3.48 and Eq. 3.49. The cooling, represented by the cooling power P is represented by a source block, (Fig. 3.10, 3).

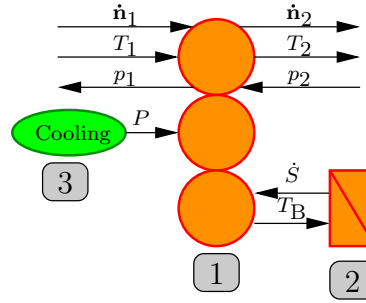


Figure 3.10: EMR representation of the temperature dynamic.

3.4.2 Pressure

The pneumatic time dependency is decoupled from the reaction (H3.16). The volume of the block is affected to the pressure development element. The pressure inside the block is defined by the flows entering and exiting the volume Eq. 3.51, due to the fact that all gases can be supposed to be ideal (H3.1).

$$p_1 = \frac{R \cdot T}{V} \int (\sum \dot{n}_1 - \sum \dot{n}_2) dt \quad (3.51)$$

In most cases the downstream molar flow vector (\dot{n}_2) is not known. It can be calculated by the linear throttle equation using the downstream pressure, which

is normally given, Eq. 3.52. At the same time, the throttle constant k imposes the static pressure drop due to friction.

$$\dot{n}_2 = k \cdot (p_1 - p_2) \quad (3.52)$$

Equation 3.52 only gives the total molar flow \dot{n}_2 , not the needed molar flow vector $\dot{\mathbf{n}}_2$. It is assumed that the composition of the gas leaving the elements is equal to the composition inside the element. Changes in composition of the molar flow vector only occur in conversion blocks (H3.14).

$$x_i = \frac{\int (\dot{n}_{1,i} - \dot{n}_{2,i} - \dot{n}_{3,i}) dt}{\sum (\int (\dot{\mathbf{n}}_1 - \dot{\mathbf{n}}_2 - \dot{\mathbf{n}}_3) dt)} \quad (3.53)$$

$$\dot{\mathbf{n}}_2 = \mathbf{x} \cdot \dot{n}_2 \quad (3.54)$$

The accumulation element used to represent the pressure drop element has three input parameters (Fig. 3.11), the upstream molar flow vector $\dot{\mathbf{n}}_1$, the upstream temperature T_1 and the downstream pressure p_2 and three output elements, the downstream molar flow vector $\dot{\mathbf{n}}_2$, the downstream temperature T_2 and the upstream pressure p_1 .

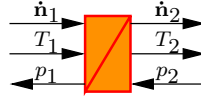


Figure 3.11: EMR representation of a pressure drop element

3.5 Fuel Processor Validation

3.5.1 Identification of Parameters

A number of parameters is needed to model the fuel processor model. The parameters are either physical values defined by the system, or empiric parameters that can be used to fit the model to measured results. For reasons of clarity the parameters needed are introduced blockwise: first for stationary behavior, then for pressure development, finally for temperature development.

The system works at a pressure of $3 \cdot 10^5$ Pa. Water and diesel are supplied at 40°C , air is supplied at 180°C . The input parameters are given in Tab. A.1.

For the stationary model some parameters of the heat exchanger have to be known, namely the heat transfer coefficient times the overall heat transfer area

kA . Even if this value is physical, it is sometimes difficult to determine, especially in this case, where the heat exchanger is not physically decoupled from the reformer. Therefore, the heat transfer coefficient times the heat transfer area kA is used as tuning parameter. Furthermore, the heat capacity of each species of the gas have to be known at 700 °C and 1200 °C. The selectivity of the two desulfurization units and the preferential oxidation sel_{D1} , sel_{D2} and sel_{PrOx} as well as the splitting factor of liquid water inside the condensation unit τ_{cond} have to be known. Those are parameters given by the constructors. All parameters of the stationary fuel processor model are given in *Tab. A.2*.

For the evaluation of the pressure dynamic, two parameters have to be known for each block: the free volume V and the throttle constant k . The free volume of the block is a physical parameter. The throttle constant is more difficult to evaluate, as it represents the pressure losses due to friction, the throttle parameter is tuned to reproduce the evaluated pressure losses. The parameters of the pressure development for all blocks of the model are given in *Tab. A.3*.

For the evaluation of the temperature development for each block, three parameters have to be known. The heat transfer coefficient times the surface between the gas flow and the block kA , the mass of the block m and its heat capacity c_p . The mass and the heat capacity are physical values. Even if the heat transfer coefficient times the surface between the gas flow and the block is a physical value, it is often difficult to determine. Furthermore, additional heat losses might be taken into consideration by changing this value. Therefore, the heat transfer coefficient times the surface between the gas flow and the block kA is used as tuning parameter. All parameters of the temperature dynamic of the fuel processor model are given in *Tab. A.4*.

3.5.2 Introduction to Fuel Processor Validation

The introduced fuel processor is capable to transform commercial diesel into hydrogen rich gas with an appropriate purity to supply a PEFC system delivering an electric power of 25 kW. The model has to be validated. As the considered fuel processing unit is still in the phase of development and the work contributes to its development, not all measurement data needed for the validation are yet available. Fortunately, the system developer N-GHY provided the data they predict for this fuel processing unit based on their own confidential models. N-GHY has sized and build several fuel processors for other applications where their dimensioning models could be validated. Such a dimensioning model is used to validate the results of the presented model. The dynamic behavior of the combined heat exchanger - reformer unit with regard to the temperature is validated versus measurement data from the N-GHY reformer presented in (*Fig. 3.12*).

A representation of the overall system including the thermal and pneumatic



Figure 3.12: Heat exchanger - reformer unit designed by N-GHY.

time dependencies can be seen in (Fig. 3.13).

3.5.3 Validation of the Stationary Fuel Processor Behavior

The models of the elements introduced in (3.3 and 3.4) are implemented one by one in Matlab/SimulinkTM to build a system model. The system is parametrized with the data given in *Tab. A.2*, *Tab. A.3* and *Tab. A.4*. At first the steady state behavior is validated at the design point. To produce a hydrogen rich gas flow at the fuel cell that is capable to be transformed into 25 kW_e, 0.0109 mol s⁻¹ of diesel, 0.2253 mol s⁻¹ of water and 0.3025 mol s⁻¹ of air (0.2253 mol s⁻¹ of nitrogen 0.0772 mol s⁻¹ of oxygen) have to be supplied to the system.

Figure 3.14 shows the gas composition after the respective blocks for stationary behavior. The results obtained by the dynamic, control oriented EMR model introduced here are labeled *FCLAB*. Results obtained by a confidential, stationary dimensioning model delivered by the company and project partner N-GHY are labeled *N-GHY*.

The first results are at the heat exchanger output (Ref-Hex). The mass flows of the different components after reforming and heat exchange are in good agreement. Thereafter, the first desulfurization process removes a large fraction of the hydrogen sulfide. As even the initial fraction of hydrogen sulfide is small in comparison to other fractions, its decrease from $2.24 \cdot 10^{-5}$ mol s⁻¹ to $5.66 \cdot 10^{-7}$ mol s⁻¹, is difficult to identify in (Fig. 3.14). In the following water gas shift reaction, the fraction of carbon monoxide is decreased. The carbon dioxide fraction is increased. At the same time the hydrogen fraction decreased slightly and the water fraction is increased due to the equilibrium reaction. Still, the simulation data are in good accordance with dimensioning data. In the preferential oxidation module, the remaining fraction of carbon monoxide is decreased below detection limit. Finally, the remaining fraction of hydrogen sulfide is decreased to $4.8 \cdot 10^{-8}$ mol s⁻¹ a fraction that is well below the fuel cell limit of $10 \cdot 10^{-6}$ mol s⁻¹.

Figure 3.15 shows the temperatures after the respective blocks for a stationary system, with *FCLAB* the results of the described model and *N-GHY* the results given by the system supplier. The temperature rises to over 450 °C/723 K after the heat exchanger and the first desulfurization. In the water gas shift the temperature is reduced to 280 °C/553 K, favoring an equilibrium containing less carbon monoxide. During the preferential oxidation the temperature reduces again. It might be strange that after an oxidation process the temperature is lower than before, because oxidation processes are exothermic, but in this case the thermal losses by cooling are much higher than the energy gained by oxidation. Finally, levels of 80 °C/353 K are reached after the condensation.

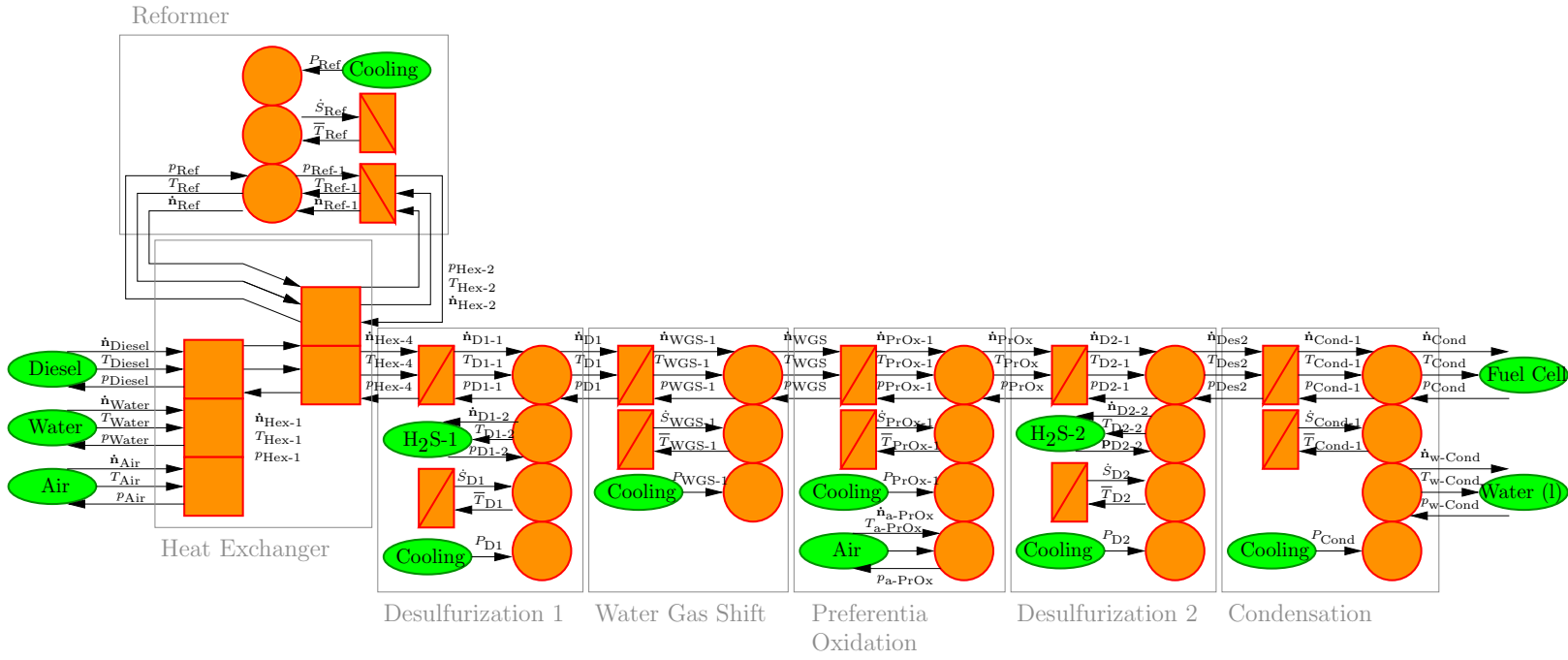


Figure 3.13: EMR representation of the fuel processor unit for the supply of a PEFC

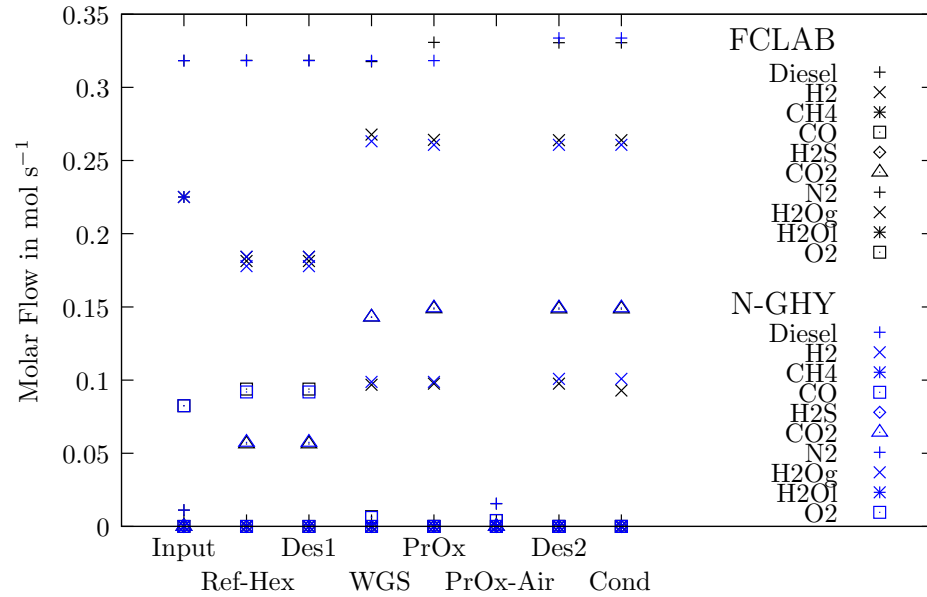


Figure 3.14: Stationary mass flows inside the fuel processor (to be connected to a PEFC)

The simulation results are in good agreement with the value of dimensioning throughout the entire fuel processing (*Fig. 3.14*) and (*Fig. 3.15*). Only the temperatures after the heat exchanger differ. The heat exchanger and the reformer are modeled as separate blocks, in the real system they are combined to one single block (*Fig. 3.12*). This connection might cause interactions that have not been regarded in the model. After the WGS the results show good agreement.

3.5.4 Validation of Dynamic Fuel Processor Behavior

Temperature

Figure 3.16 shows the temperature development for the heat exchanger-reformer unit for a step change between no fuel stream supplied and the design point. The calculated values of the temperature development are compared to measurement data from a reformer installed at N-GHY that can be seen in (*Fig. 3.12*). The simulation is started with a system temperature of about $727^\circ\text{C}/1000\text{ K}$, below this temperature heat up phenomena occur that are not covered by the model. Thereafter, the system heat up takes more than 2000 s before the final temperature of over $1427^\circ\text{C}/1700\text{ K}$ is reached. It is considered that all blocks have a temperature of $25^\circ\text{C}/298\text{ K}$ as initial condition (*H3.17*). Even though the

3.6. ADAPTION OF FUEL PROCESSOR TO USE IN COMBINATION WITH HTPEMFC79

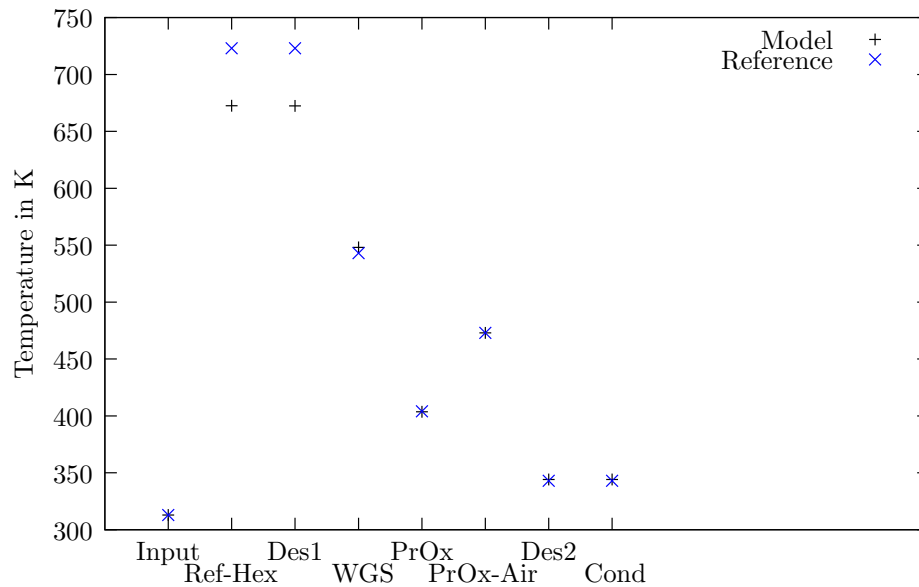


Figure 3.15: Stationary temperatures of the fuel processor (to be connected to a PEFC)

system heat up inside the model is based on the assumption that the only heat transfer occurs between to the block and the surrounding the gas flow (*H 3.13*), the measured and calculated values show good agreement.

Pressure

Figure 3.17 shows one simulated pressure evolution of the fuel processing unit over a time period of 0.2 s. The pressure development is based on the free volume inside the respective modules. It can be seen that after a change in pressure a stationary behavior is reached after less than 0.1 s. There are no measurement data yet available for comparison.

3.6 Adaption of Fuel Processor to use in combination with HTPEMFC

As introduced in 1.5 not only a PEFC system, but also a HTPEMFC systems are used for a diesel driven fuel cell system. In this case, the fuel processing unit has to be adapted to be connected to a HTPEMFC. As introduced in section (1.1.3) the HTPEMFC is less sensitive for contamination than the PEFC. The reduction of carbon monoxide in the water gas shift reaction leads to values sufficient for

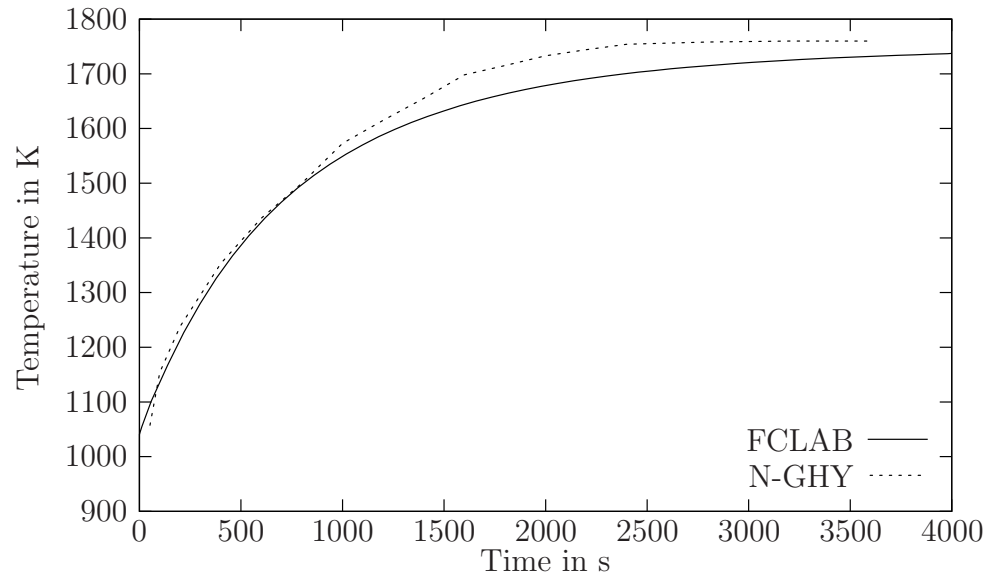


Figure 3.16: Temperature development for the reformer - heat exchanger unit.

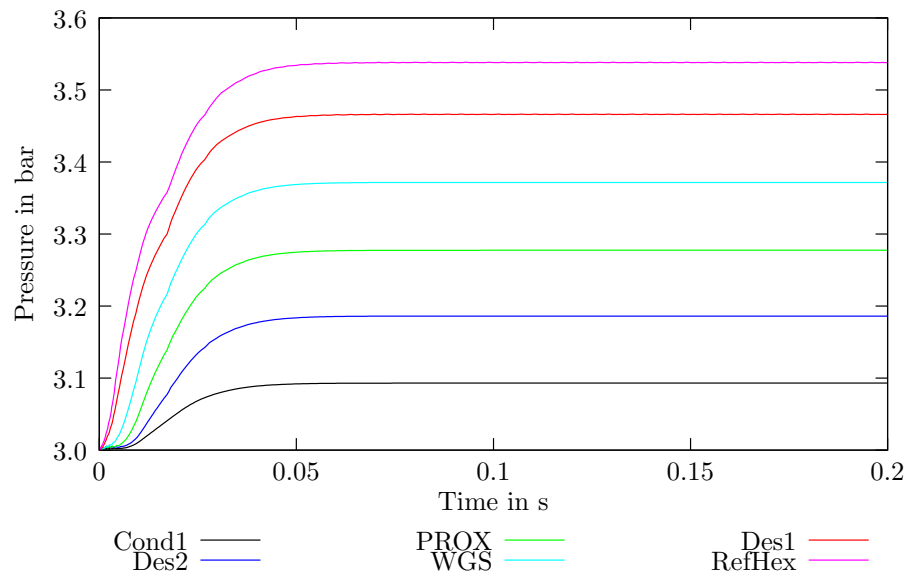


Figure 3.17: Pressure development for a PEFC

a HTPEMFC. It is possible to pass on the preferential oxidation unit. Furthermore, no condensation unit is needed. Even one desulfurization unit is sufficient to reduce the sulfur contents in the gas mixture entering the fuel cell, but for reasons of redundancy two desulfurization units are kept for the moment.

The architecture of the fuel processor model has to be adapted due to the changed demands. The advantages of the modular approach provided by EMR modeling can be seen. The fuel processing unit adapted for the supply of a HT-PEMFC can be obtained by removing the preferential oxidation and condensation block. Due to the fact that the causality stays unchanged, the WGS block and the second desulfurization block can be connected directly. As also in reality the same modules are used, the same parameters as identified for the fuel processor in (3.5.2) can be used. A representation of the fuel processor unit adapted for a combination with a HTPEMFC system can be seen in (*Fig. 3.18*).

As for the model, the real system uses exactly the same subunits for the PEFC fuel processing and the HTPEM fuel processing. The model has been validated accordingly. The stationary massflows are shown in (*Fig. 3.19*). The stationary temperatures are shown in (*Fig. 3.20*) and the pressure development is shown in (*Fig. 3.21*).

3.7 Conclusion of Reformer Model

This chapter introduces the fuel processor modeling. After basic aspects of the architecture and the governing reactions inside the fuel processor have already been introduced in (1.3), this chapter focuses on the application and validation. The hypotheses on which the model is based are introduced one by one (3.2). With the help of those hypotheses, each block inside the fuel processor unit is introduced. First, the stationary behavior is introduced separately for each module (3.3), giving the EMR representation. Then, the application of the thermal time dependency is explained (3.4.1). Some of the modules are cooled externally. The cooling is considered to be instantaneous. As the same concept is applied to each module it only has to be introduced once. Likewise, the pneumatic time dependency is introduced in (3.4.2). As all elements are introduced the overall system model is the aggregation of all subsystems (*Fig. 3.13*).

The validation of the system is done with the help of data provided by the system constructor N-GHY. After the parameters are introduced in (3.5.1), the stationary behavior is modeled in (3.5.3). The stationary mass flows and temperatures at each module are compared to reference values (*Fig. 3.14*) and (*Fig. 3.15*). The thermal time dependent behavior is validated using measurement data of

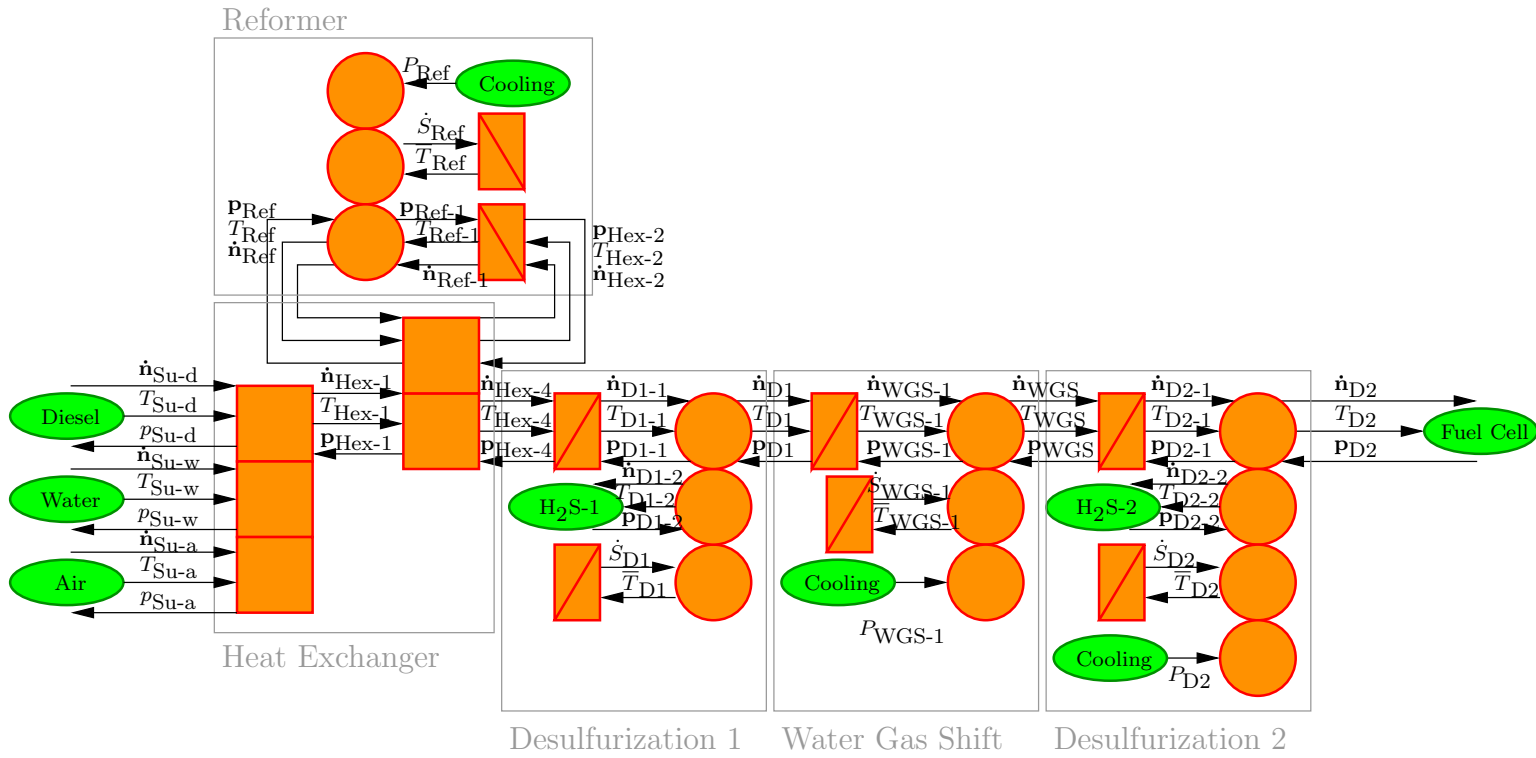


Figure 3.18: EMR representation of the fuel processor unit for the supply of a HTPEM

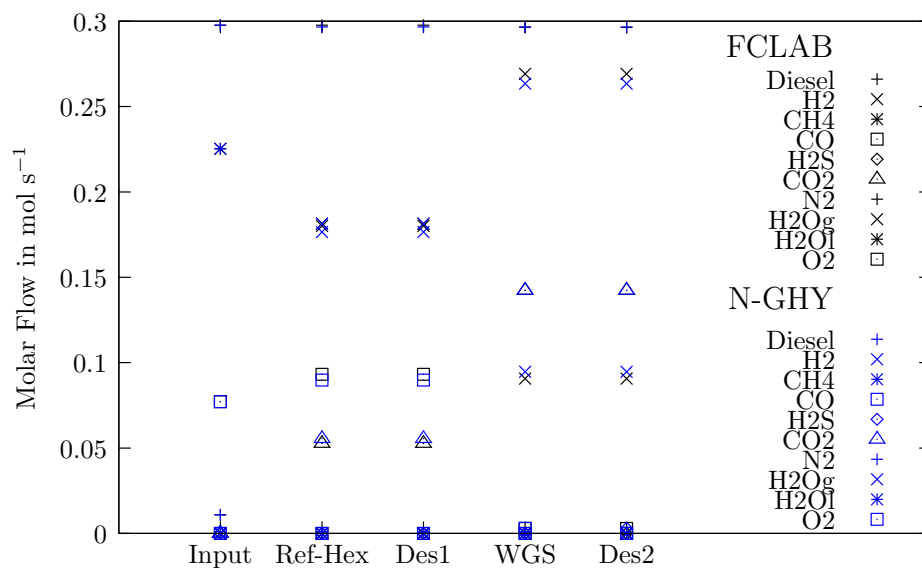


Figure 3.19: Stationary mass flows of a HTPEM

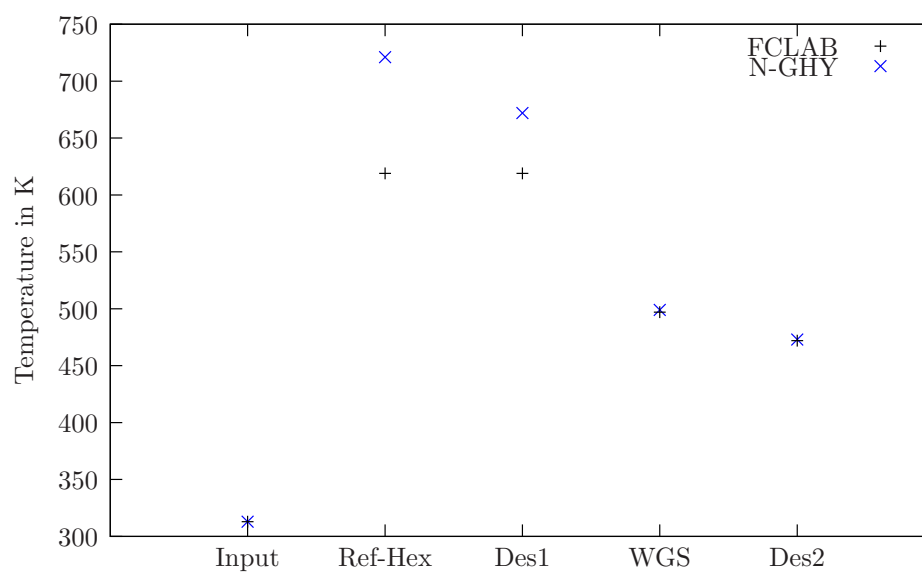


Figure 3.20: Stationary temperatures of a HTPEM

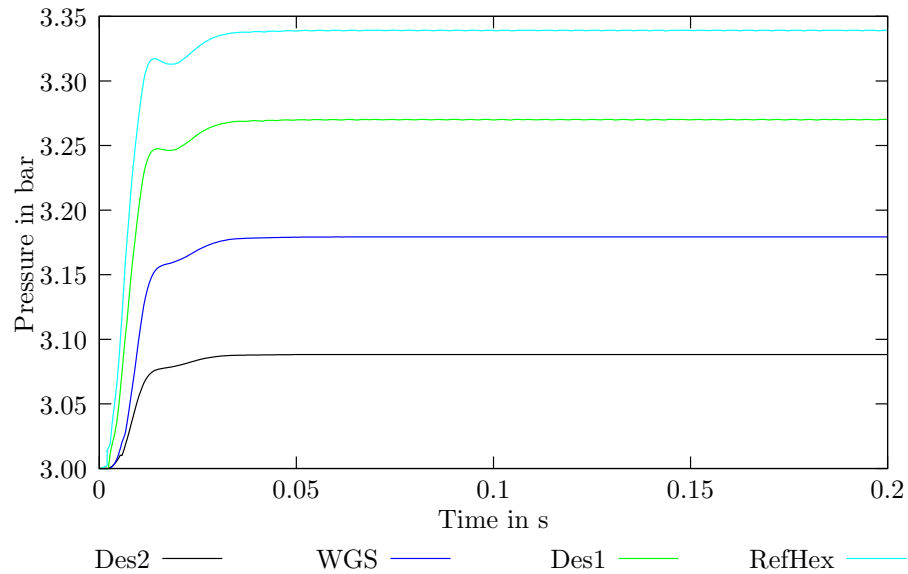


Figure 3.21: Pressure development for a HTPEM

a reformer (*Fig. 3.12*) and (*Fig. 3.16*). The pneumatic time dependent behavior could not be validated with measurement data, but is presented in (*Fig. 3.17*). Finally, the adaption of the fuel processor unit to the use of a HTPEMFC system is introduced (3.6).

The fuel processor modeling shows that EMR is a well adapted tool to model macroscopic systems of gas flows undergoing chemical reactions. The approach, using a limited number of simple elements, helps to divide a complex system in a multitude of small systems that are relatively easy to describe. Even with the considerable number of hypotheses made, the model shows good agreement with observations for stationary as well as for dynamic behavior, as far as data of the system supplier are available.

After the fuel processor model has been introduced successfully, a fuel cell stack model will be presented in chapter 4.

Chapter 4

Fuel Cell Stack Model

4.1 Introduction to Fuel Cell Stack Modeling

A model based control shall be developed for a diesel fed fuel cell system. The energetic macroscopic representation (EMR) has been chosen to be a well adapted tool to obtain a model, which can give a base for a model based control development. A diesel fed fuel cell system consists of the fuel processing unit as introduced in (3), the fuel cell stack and auxiliaries like air compressors, pumps and heat exchangers (1.2). In this chapter, the fuel cell stack modeling is introduced [56, 58]. Differing from a previous fuel cell model in EMR [83], this model emphasizes the multi-dimensional character of the fuel cell, the different energetic domains like the fluidic and electrochemic domain are connected directly and their integration, for exemple the humidity dependant membrane resistance, is taken into account.

The PEFC is the most studied low temperature fuel cell. It is considered for multiple applications including stationary, mobile and portable application. Hydrogen is the most considered fuel, but the supply of a PEFC with other fuels in combination with a fuel processing unit has been shown successfully [122]. Therefore, the PEFC technology has been addressed for stack modeling. The GAPPAC project aims to use a diesel fed low temperature fuel cell system for auxiliary power supply in transportation application. The power output will be up to 25 kW and the system shall be used for trigeneration at the same time (use of the system electricity, heat and heat for cooling applications). Due to the application in a mobile system the installation volume is limited. A HT-PEMFC system is supposed to use less volume than a PEFC system. At the same time, the higher working temperature of a HTPEMFC is advantageous for trigeneration. Furthermore, diesel fuel contains sulfur components and during

the reforming process carbon monoxide is formed. Both elements lead to a fuel cell poisoning. Even if the elimination of those elements is possible in clean up steps during the fuel processing it is necessary to constantly monitor its levels. No standardized sensors for the online measurement of hydrogen sulfide and carbon monoxide with an accuracy sufficient for the levels bearable by a PEFC are known. The use of a HTPEMFC allows elevated levels of hydrogen sulfide and carbon monoxide, their measurement is simpler in this case. That is why a PEFC stack model is presented as well as a HTPEMFC stack model.

Some basic ideas toward the fuel cell modeling are introduced in (4.2). The hypotheses of the model are given in (4.3). Afterward, the PEFC fuel cell is modeled (4.4). The introduced model is validated in (4.5) for the use of hydrogen and hydrogen rich gas with a composition comparable to the gas composition provided by the fuel processor unit. The basic structure established for the PEFC model is applied to the HTPEMFC model. Hence, the HTPEMFC model can be obtained by a modification of the PEFC model (4.6). The chapter ends with a conclusion related to the fuel cell stack modeling (4.7).

4.2 Basic Ideas toward Fuel Cell Modeling

As the voltage provided by a single fuel cell is limited (1.1.4), several single fuel cells are connected in parallel from the pneumatic point of view and in series from the electric point of view to supply an adequate voltage and current. Such an assembly is called *fuel cell stack*. There are slight differences between the individual cells of a real stack [11]. The differences of the voltages of the individual cells, depend on production differences of the fuel cells and the gas supplies. For a correct representation it has also to be taken into consideration that the gas flows arriving at the fuel cell differ depending on the positioning of the cell inside the stack. Also the temperature level of the cell depends on the cooling and the position of the cell inside the stack. Still, as the differences in voltage over the stack are below $\pm 2.5\%$ [11], it is assumed that all single fuel cells behave in exactly the same way. Hence, the fuel cell stack can be described by a single fuel cell, multiplied by the number of cells inside the stack (H4.2).

Moreover, a fuel cell is composed of different layers. Each layer is associated with a different material and has a different contribution to the functionality of the fuel cell. To describe the working principle of the fuel cell correctly, each layer is described individually. Due to the different functionality of each layer, a contribution toward species transport and cell voltage can be assigned to each layer [21, 149].

A fuel cell consists of the following elements (*Fig. 4.1*):

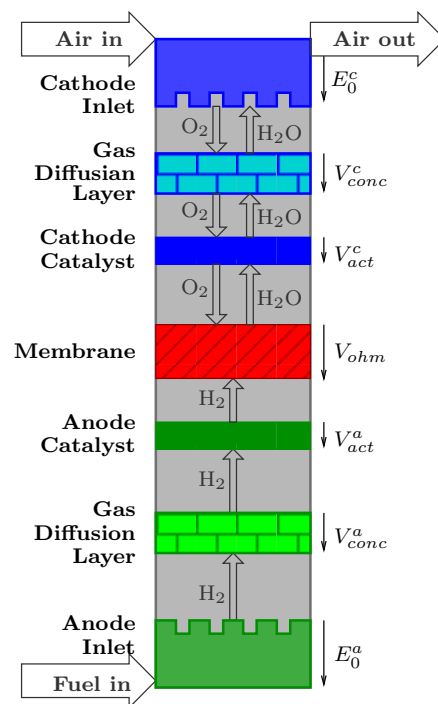


Figure 4.1: Different layers inside the fuel cell and their contribution to cell voltage.

- **Anode Inlet:** Hydrogen rich gas is supplied to the stack by the anode inlet. If only hydrogen is supplied, the system might work in dead end mode. In this case no gas stream is leaving at the anode. In many cases of hydrogen use [162] and if hydrogen rich gas is used, a diluted gas stream leaves the anode.
- **Cathode Inlet:** Oxygen, mostly in form of air, is supplied to the fuel cell by the cathode inlet. The diluted air leaves the cathode inlet. At the same time, water is removed from the fuel cell on the same path.
- **Anode GDL:** Hydrogen is supplied to the catalyst by the gas diffusion layer (GDL). The concentrations of hydrogen change over the GDL thickness according to their consumption at the anode catalyst.
- **Cathode GDL:** Oxygen is supplied to and water is removed from the cathode gas catalyst via the cathodic gas diffusion layer (GDL). The concentration of water and oxygen changes over the GDL thickness according to its production/consumption inside the cathode catalyst.
- **Anode Catalyst:** Hydrogen is consumed at the anode catalyst.
- **Cathode Catalyst:** Oxygen is consumed and water is produced at the cathode catalyst.
- **Membrane:** Protons and water are transported through the membrane. At the same time the membrane is an isolator for electrons, thus forcing the electrons to pass from the anode to the cathode by an external wire doing electrical work before completing the electro-chemical reaction.

The stack voltage V_{stack} is calculated from the reversible stack voltage, reduced by the different overpotentials multiplied by the number of cells in the stack n Eq. 4.1.

$$V_{stack} = n (E_0^a - V_{conc}^a - V_{act}^a - V_{ohm} - V_{act}^c - V_{conc}^c + E_0^c) \quad (4.1)$$

The formation of the stack voltage is represented in the EMR model by a coupling element in the same energetic domain, as can be seen in (Fig. 4.9).

4.3 Hypotheses of Fuel Cell Model

The hypotheses posed for the fuel cell model are marked hereafter:

General Hypotheses

H 4.1 *All gases are considered to be ideal. The gas temperatures are around 60 °C, the system pressures are around 1.2 bar. In this working window gases behave ideal.*

Hypotheses concerning the fuel cell stack

H 4.2 *Measurement of real systems show that there are differences in the voltages of the individual cells inside a fuel cell stack [11]. Those differences are imposed by production differences and by phenomena that are connected to the fuel cell, flow channel and cooling geometry that are not considered in this case. As the fluctuation of the individual cell voltages are below $\pm 2.5\%$ [11], it is assumed that all fuel cells inside the stack show the same characteristics and that they can be considered as a multitude of n times the same fuel cell.*

H 4.3 *Pressure drops caused by friction are neglected.*

H 4.4 *Each element of the cell voltage description Eq. 4.1 is assigned to one layer of the fuel cell. All overvoltages can be attributed directly to a layer due to the physical effects leading to them. The reversible cell voltage depends as well on the anode as on the cathode inlet. Physically it can only occur in combination of the two. For the modeling the reversible cell voltage is split to an anodic part E_0^a and a cathodic part E_0^c . This split is only made for reasons of modeling simplicity [22, 127].*

- *The anode inlet contributes to the reversible thermodynamic cell potential of the anode E_0^a .*
- *The cathode inlet contributes to the reversible thermodynamic cell potential of the cathode E_0^c .*
- *The anode GDL supplies the concentration overpotential anode share V_{conc}^a to the fuel cell voltage.*
- *The cathode GDL supplies the concentration overpotential cathode share V_{conc}^c to the fuel cell voltage.*
- *The activation overpotential anode share V_{act}^a is provided by the anode catalyst.*
- *The activation overpotential cathode share V_{act}^c is provided by the cathode catalyst.*
- *The membrane provides ohmic overpotential V_{ohm} .*

H 4.5 *All elements occurring inside the stack are gaseous, also the water. It is not probable to have liquid water formation inside the fuel cell stack, due to the fact that the gases entering the system are not humidified. It is possible to reach partial pressures of water that exceed the saturation pressure, still no condensation is considered in this case.*

H 4.6 *The temperature is controlled and considered homogeneous over the entire fuel cell stack. This hypothesis can be made, as the gases enter the fuel cell preheated at the fuel cell temperature. If there are temperature differences it can be assumed that the gases heat up instantaneously. Furthermore, it can be assumed that a heat management system exists inside the fuel cell stack, controlling the temperature perfectly.*

H 4.7 *The HTPEMFC has the same general structure as the PEFC [130].*

H 4.8 *The reactions inside the fuel cell layers are supposed to be instantaneous.*

Hypotheses concerning the inlet

H 4.9 *The inlet air contains two components, oxygen and nitrogen, the molar fraction of oxygen is 21 %.*

H 4.10 *The gas leaving the cathode/anode has the same composition as the gas stored inside the respective volume.*

Hypotheses concerning the gas diffusion layer

H 4.11 *The total pressure rests constant throughout the GDL.*

H 4.12 *Diffusion is always in steady state.*

H 4.13 *It is assumed that the change in concentration throughout the gas diffusion layer follows a linear description.*

H 4.14 *The following species are considered for diffusion:*

Hypotheses concerning the catalyst

H 4.15 *There is no volume connected to the catalyst layers.*

H 4.16 *The anodic activity is considered to be so high that the anodic overpotential can be neglected compared to the cathodic activation losses. $V_{act}^a = 0$.*

Binary Diffusion	Cathode	Oxygen, Water (gas)
	Anode	Hydrogen, Water (gas)
Multi Species Diffusion	Cathode	Oxygen, Water (gas), Nitrogen
	Anode	Hydrogen, Water, Carbon Monoxide, Carbon Dioxide, Nitrogen

H 4.17 *The levels of hydrogen sulfide of the gas entering the fuel cell stack is so low that the influence of sulfur on the fuel cell voltage is neglected.*

H 4.18 *The influence of carbon monoxide on the cell voltage is not taken into consideration for the PEFC.*

Hypotheses concerning the membrane

H 4.19 *The membrane is supposed to be in stationary condition [116]. Water is only passing through the membrane, the amount of water stored in the membrane is not regarded from the mass flow point of view.*

H 4.20 *The water diffusion coefficient does not change by large quantities over the membrane [116].*

4.4 Modeling of the PEFC

4.4.1 Description of Fuel Cell Inlet

The anode and cathode inlet are the points where gas flows are supplied to and removed from the fuel cell. The inlet is an element which is flown through by three molar flow vectors: the supply molar flow vector, the removed molar flow vector and the molar flow vector penetrating deeper into the fuel cell layers. Furthermore, there is the contribution of the inlet to the reversible thermodynamic cell voltage, represented by a parameter pair from the electric domain. At the same time the inlet is an accumulation element, incorporating the pressure dynamic as it is introduced in (3.4). Therefore, the inlet is described as a combined coupling and accumulation element. In EMR an element combining coupling and accumulation is not foreseen. As no alternative has been found, in this case a triangle is to describe the inlet 2.6.3, (Fig. 4.2) and (Fig. 4.3).

Cathode

The input parameters to the cathode inlet as can be seen in (Fig. 4.2) are the upstream molar flow vector \dot{n}_1 (H4.9), the upstream temperature T_1 , the downstream pressure p_2 , the molar flow coming from inside the fuel cell \dot{n}_3 and the fuel cell current I_{FC} . The output temperature T_2 , the temperature of the gas penetrating deeper into the fuel cell T_3 as well as the molar flow vector leaving the fuel cell have to be evaluated. The outside pressure is given in form of a scalar p_2 , this value is necessary to evaluate the molar flow out of the system \dot{n}_2 , in this case the absolute pressure is sufficient. For the fuel processor unit upstream the fuel cell the absolute pressure is sufficient. Therefore, the pressure p_1 is a scalar as well. As deeper layers of the fuel cell are discussed, the total pressure inside the block does not give enough information. The actual partial pressures of the species have to be known. Therefore, the partial pressures vector p_3 has to be evaluated. Furthermore, the cathodic fraction of the reversible thermodynamic cell potential E_0^c has to be calculated.

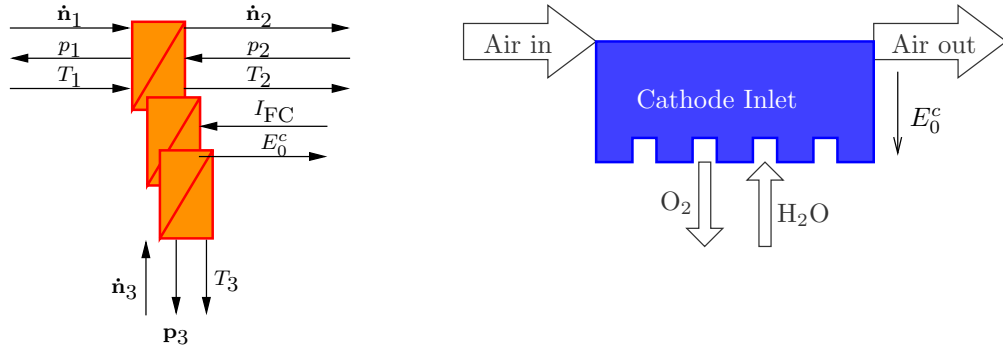


Figure 4.2: Cathode inlet - EMR and schematic representation

The upstream pressure p_1 can be calculated as result of the accumulation Eq. 4.2 for ideal gases (H4.1). The signs take the flow directions into consideration. Pressure drops due to friction are neglected (H4.3).

$$p_1 = \frac{R \cdot T}{V} \int \left(\sum_i (\dot{n}_1 - \dot{n}_2 - \dot{n}_3) \right) dt \quad (4.2)$$

The downstream molar flow vector \dot{n}_2 , can be calculated as for the pressure drop element introduced in 3.4.2. The valve is considered to have a constant opening in this case. There are other approaches existing, where the exit valve opening is used as control parameter [45]. Eq. 3.52 gives only the total molar flow in scalar form \dot{n}_2 . The transmission to the molar flow vector can be done as

follows, (H4.10): the molar fraction of the gas species stored inside the cathode inlet can be calculated following Eq. 4.3. Once this is done for all elements, this builds the molar fraction vector \mathbf{x} . The molar flow vector is the product of the molar fraction vector \mathbf{x} and the molar flow \dot{n}_2 , Eq. 4.4. This approach has already been introduced in (3.4.2, p. 72).

$$x_i = \frac{\int (\dot{n}_{1,i} - \dot{n}_{2,i} - \dot{n}_{3,i}) dt}{\sum (\int (\dot{n}_1 - \dot{n}_2 - \dot{n}_3) dt)} \quad (4.3)$$

$$\dot{n}_2 = \mathbf{x} \cdot \dot{n}_2 \quad (4.4)$$

The partial pressure vector of the cathode inlet \mathbf{p}_3 is a parameter handed over toward the deeper layers of the fuel cell. It is based on the molar fractions of the cathode \mathbf{x} and can therefore be calculated as shown in Eq. 4.5:

$$\mathbf{p}_3 = \mathbf{x} \cdot p_1 \quad (4.5)$$

Based on (H4.6) the temperature does not change inside the cathode inlet. Hence, the temperatures T_2 and T_3 are equal to the upstream temperature T_1 , Eq. 4.6.

$$T_1 = T_2 = T_3 \quad (4.6)$$

The cathodic fraction of reversible thermodynamic cell potential can be calculated by first calculating the time and pressure dependent Gibbs energy G_{fi} of the species used inside the reaction Eq. 1.2 using Eq. 4.7. Afterward, the Gibbs energy of the cathodic part of the reaction can be calculated using Eq. 4.8. Finally, as introduced in Eq. 1.5 the cathodic contribution to the reversible thermodynamic cell potential can be calculated using Eq. 4.9.

$$G_{fi}(T_i, p_i) = G_0^i(T_i) + R T_i \ln(p_i) \quad (4.7)$$

$$G_0^c = G_{fH_2O}(T, p_{H_2O}) - \frac{1}{2} G_{fO_2}(T, p_{O_2}) \quad (4.8)$$

$$E_0^c = \frac{G_0^c}{2F} \quad (4.9)$$

The fuel cell current I_{FC} is given as parameter, even though it is not used for the calculation.

Anode

The anode inlet can be seen in (Fig. 4.3) with the input parameters: the upstream fuel molar flow vector \dot{n}_1 , the upstream molar flow temperature T_1 , the downstream pressure p_2 , the molar flow vector coming from inside the fuel cell

\dot{n}_3 and the current demanded from the fuel cell I_{FC} . The values to be calculated are the upstream pressure p_1 , the downstream molar flow vector \dot{n}_2 , the downstream temperature T_2 , the partial pressure vector to the fuel cell p_3 , the temperature of the molar flow to the fuel cell T_3 and the anodic contribution to the reversible thermodynamic cell potential E_0^a .

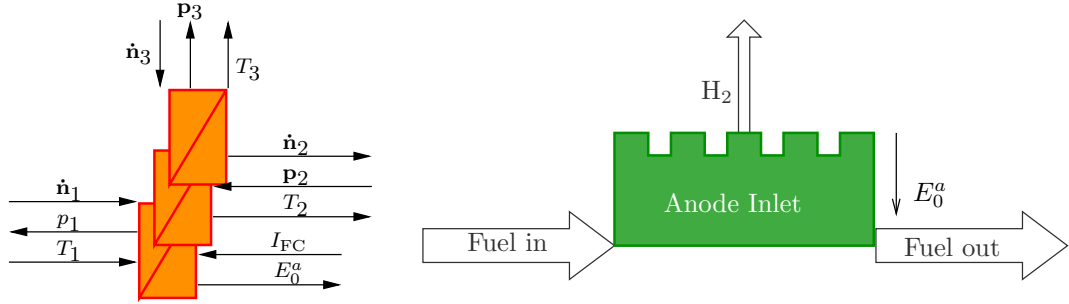


Figure 4.3: Anode inlet - EMR and schematic representation

The calculation approach is exactly the same as introduced for the cathode in (4.4.1). The upstream pressure p_1 is calculated using Eq. 4.2. The downstream molar flow vector \dot{n}_2 is calculated using Eq. 3.54. The downstream temperature T_2 and the temperature of the molar flow to the fuel cell T_3 are equal to the upstream temperature T_1 , Eq. 4.6. Only the part of the chemical reaction taking place in the anode changes, Eq. 1.2, and the share of the reversible thermodynamic cell potential has to be calculated accordingly, Eq. 4.7, Eq. 4.10 and Eq. 4.11.

$$G_0^a = -G_{f,O_2}(T, p_{O_2}) \quad (4.10)$$

$$E_0^a = \frac{G_0^a}{2F} \quad (4.11)$$

4.4.2 Description of Fuel Cell Catalyst

At the catalyst layer an electrochemical reaction takes place, and a catalyst is needed to split the molecules. The most used catalyst material is platinum or a platinum alloy. As there are activation losses occurring during catalytic reaction, the catalyst imposes an activation overpotential V_{act} . There might also be losses due to contamination with sulfur. Those losses are neglected here (H4.17). Two gas flows are interacting with the catalyst. The gas flow from anode or cathode \dot{n}_1 and the gas flow to the membrane \dot{n}_2 . There is also the electric implication of the catalyst represented by the activation overpotential V_{act} . Hence, the catalyst is described by a coupling element in different domains (Fig. 4.4) and

(Fig. 4.5). According to (H4.15) no volume is related to the catalyst. Therefore, the temperature and the pressure do not change inside the catalyst Eq. 4.12 and Eq. 4.13.

$$p_1 = p_2 \quad (4.12)$$

$$T_1 = T_2 \quad (4.13)$$

Cathode

The cathodic catalyst (Fig. 4.4) has the flowing inputs: the molar flow vector from the membrane \dot{n}_2 , the upstream partial pressure vector p_1 , the upstream temperature T_1 and the fuel cell current I_{FC} . The parameters to be calculated are the gas flow toward the cathode inlet \dot{n}_1 , the temperature of the water flowing through the membrane T_2 , the partial pressure vector at the membrane p_2 and the cathodic activation overpotential V_{act}^c .

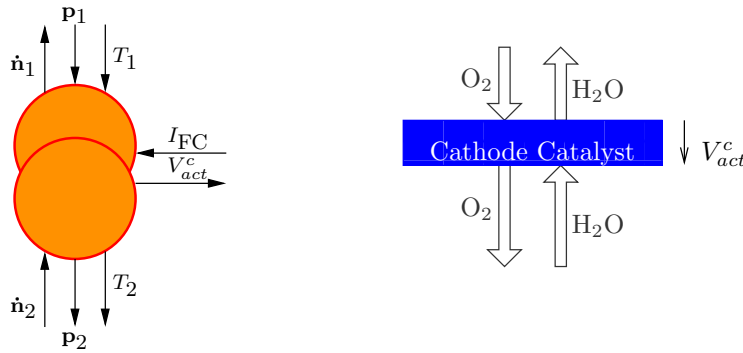


Figure 4.4: Cathode catalyst - EMR and schematic representation

In the cathodic catalyst, oxygen is consumed and water is produced. The difference between consumption and production is expressed using different signs. The oxygen consumption and the water production can be explained using the Faraday law Eq. 1.4. Furthermore, there might be an exchange of molar flow with the membrane. The molar flow vector toward the cathode inlet \dot{n}_1 can therefore be described using Eq. 4.14.

The signs for the molar flow vectors have to be considered carefully. The direction of the arrow indicates the causality. It does only indicate if the parameter describes an input or an output of the calculation, the flow directions have to be defined separately. A positive sign indicates a production or a flow in the same direction as the arrow, a negative sign indicates a consumption or a flow in the opposite direction. As there is consumption and production occurring in parallel,

positive and negative signs occur in Eq. 4.14.

$$\dot{\mathbf{n}}_1 = \frac{n \cdot I}{4 \cdot F} [0 \ 0 \ 0 \ 0 \ 0 \ 0 \ 0 \ 2 \ 0 \ -1]' + \dot{\mathbf{n}}_2 \quad (4.14)$$

The partial pressure vector at the membrane \mathbf{p}_2 is equal to the partial pressure vector at the inlet \mathbf{p}_1 , Eq. 4.12. The water temperature T_2 is the same as the temperature of the incoming gas stream T_1 , Eq. 4.13.

The cathodic share of the activation overpotential V_{act}^c is calculated according to the approach presented by Barbir [15] using Eq. 4.15

$$V_{act}^c = \frac{RT}{\alpha_a F} \log \left(\frac{j}{j_0} \right) \quad (4.15)$$

with j the current density $j = I/S_{cell}$ and S_{cell} the surface of a single cell in cm^2 . The exchange current density j_0 and the dimensionless factor α_a have to be tuned.

Anode

The anodic catalyst (Fig. 4.5) has the following inputs: the molar flow vector from the membrane $\dot{\mathbf{n}}_2$, the upstream partial pressure vector \mathbf{p}_1 , the upstream temperature T_1 and the fuel cell current I_{FC} . The parameters to be calculated are the gas flow toward the anode inlet $\dot{\mathbf{n}}_1$, the temperature of the water flowing through the membrane T_2 , the partial pressure vector at the membrane \mathbf{p}_2 and the anodic activation overpotential V_{act}^a .

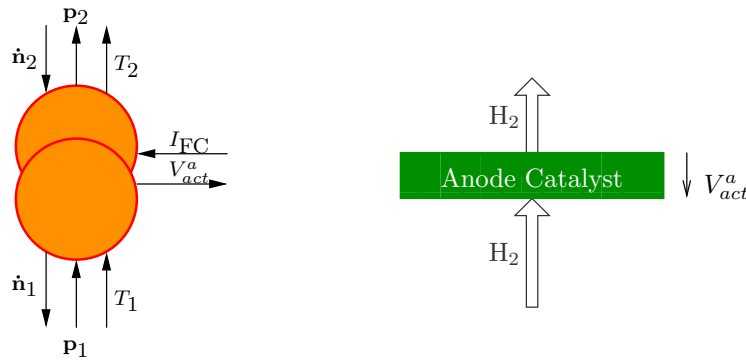


Figure 4.5: Anode catalyst - EMR and schematic representation

In the anodic catalyst, hydrogen is consumed. The hydrogen consumption can be expressed using the Faraday law Eq. 1.4. Furthermore, there might be

an exchange of molar flow of water with the membrane. The output molar flow vector $\dot{\mathbf{n}}_1$ can therefore be described as using Eq. 4.16

$$\dot{\mathbf{n}}_1 = \frac{n \cdot I}{2 \cdot F} [0 \ -1 \ 0 \ 0 \ 0 \ 0 \ 0 \ 0 \ 0 \ 0] + \dot{\mathbf{n}}_2 \quad (4.16)$$

The exit pressure vector \mathbf{p}_2 is equal to the input pressure vector \mathbf{p}_1 , Eq. 4.12. The exit temperature T_2 is equal to the entry temperature T_1 , Eq. 4.13. The anodic share of the activation overpotential can be neglected as the anodic activity is considered high with regard to the cathodic activity, (H4.16), Eq. 4.17.

$$V_{act}^a = 0 \quad (4.17)$$

4.4.3 Description of Gas Diffusion Layer

Between the input and the catalyst is the gas diffusion layer (GDL). This is a porous medium allowing the species to migrate between the inlet and the catalyst [15]. Inside the GDL the concentrations of the gas species are evaluated. The concentrations of the gases species are influenced by their consumption or production.

Some of fuel cell models [116, 122] are limited the Fick Diffusion which is valid if only two species are involved. This is valid if pure hydrogen is used as fuel. In the discussed case reformat is foreseen to be used as fuel. Therefore, the Stefan-Maxwell-Diffusion for multi species is used [138, 69]. Still, the Fick diffusion is introduced first as a baseline. Then, the adaption toward Stefan-Maxwell-Diffusion is made. As well the approach of the Fick diffusion as the approach for the Stefan-Maxwell-Diffusion hold only for ideal gases. After introducing the diffusion principle the model of the cathode and anode GDL is applied in EMR.

Fick Diffusion

The Fick's law is used to describe the diffusion of binary gases. It calculates the molar flux J and can be explained as a function of the diffusion coefficient D and the derivative of the concentration over the GDL thickness dc/dx as can be seen in Eq. 4.18. The molar flux J is a function of the molar flow (\dot{n}) divided by the cell surface area (S_{cell}): $J = \dot{n}/S_{cell}$.

$$J = -D \frac{dc}{dx} \quad (4.18)$$

According to hypothesis (H4.12), (H4.13) the Fick's Law is applied in its

linear form *Eq. 4.19*.

$$J = -D \frac{c_i(\delta) - c_i(0)}{\delta} \quad (4.19)$$

with δ the diffusion layer thickness in m. In this case the diffusion layer thickness is $350 \mu\text{m}$ [116].

As the partial pressure is a quantity that is already used inside the model, it would be advantageous to adapt the Fick's Law in a way that the concentration is replaced by the partial pressure. Fortunately, there is a connection between the concentration and the partial pressure for ideal gases, *Eq. 4.20*.

$$c_i(x) = \frac{1}{RT} p_i(x) \quad (4.20)$$

The calculation of the diffusion coefficient D , *Eq. 4.21*, has been among others introduced by O'Hayre [116]:

$$p D_{ij} = a \left(\frac{T}{\sqrt{T_{ci} T_{cj}}} \right)^b (p_{ci} p_{cj})^{\frac{1}{3}} (T_{ci} T_{cj})^{\frac{5}{12}} \left(\frac{1}{M_i} + \frac{1}{M_j} \right)^{\frac{1}{2}} \quad (4.21)$$

with $a = 3.640 \cdot 10^{-4}$ and $b = 2.334$ for diffusion pairs containing a polar gas as for example water and $a = 2.745 \cdot 10^{-4}$ and $b = 1.823$ for diffusion pairs without polar component. The values of the critical temperatures T_c , critical pressures p_c and molar masses M can be seen in table 4.1.

Table 4.1: Critical temperatures, pressures and molar masses of different systems [116]

Substance	M (kg kmol ⁻¹)	T_c (K)	p_c (bar)
H ₂	2.016	33.3	12.8
O ₂	31.999	154.4	49.7
H ₂ O	18.015	647.3	217.5
CO ₂	44.010	304.2	72.8
CO	28.010	132.9	34.5
N ₂	28.013	126.2	33.5

The diffusion coefficient calculated in *Eq. 4.21* is valid for the diffusion in free space. For porous structures like they can be found inside the GDL, the Bruggemann correction is used *Eq. 4.22*.

$$D_{ij}^{eff} = \epsilon^\tau \cdot D_{ij} \quad (4.22)$$

with ϵ the porosity that is around 0.4 for fuel cells and τ_i the tortuosity, which is usually between 1.5 and 10 [116]; here a value of 5 is applied.

Multi Element Diffusion

The Fick diffusion is limited to binary gases. For hydrogen driven fuel cells, the Fick diffusion might be a valid simplification. In the considered application the fuel cell shall be fed with reformat. For the PEFC, the carbon monoxide influence is not taken into consideration (H4.18). The same model shall be used to model a HTPMFC as well. As the carbon monoxide fractions for the HTPMFC are much higher than for the PEFC it is not possible to neglect its influence on the cell voltage. As the carbon monoxide influence occurs at the anodic catalyst, the partial pressure of carbon monoxide at the membrane has to be known. Therefore, it has to be taken into consideration in the gas diffusion layer. The assumption of a binary gas can no longer be applied. The diffusion of multi component gas is described by the Stefan-Maxwell-Diffusion. As introduced by Springer [138], the diffusion can be explained by a combination taking into account the molar fractions and molar fluxes of two species at a time, summed over all species, Eq. 4.23. The diffusion coefficients D_{ij} and D_{ij}^{eff} are the same as introduced in Eq. 4.21 and Eq. 4.22.

$$\frac{dx_i}{dz} = RT \sum_j \frac{x_i J_j - x_j J_i}{p D_{ij}} \quad (4.23)$$

Still, the diffusion is considered stationary and a linear change of concentration throughout the GDL is assumed (H4.13) and (H4.12). The equation can be linearized accordingly, giving Eq. 4.24.

$$\frac{x_i(\delta) - x_i(0)}{\delta} = RT \sum_j \frac{x_i(\delta) J_j - x_j(0) J_i}{p D_{ij}} \quad (4.24)$$

Furthermore, we are working with molar flows (\dot{n}) instead of molar fluxes (J). As the both are connected by the cell surface area S_{cell} , the Stefan-Maxwell Diffusion can be written as function of molar flows. Also, the signs have to be considered carefully, taking into consideration the flow directions as well as the fact if production or consumption occurs. Finally, as the partial pressure is a parameter of the model, it would be advantageous to calculate the partial pressures before and after the gas diffusion layer instead of the molar fraction. This can be done applying (H4.11), using Eq. 3.20. The linear Stefan-Maxwell Diffusion adapted to our system is given in Eq. 4.25. The species taken into

account are given in (H4.14).

$$p_i(\delta) = \frac{RT}{S} \sum_j \frac{x_i \dot{n}_j - x_j \dot{n}_i}{p D_{ij}} + p_i(0) \quad (4.25)$$

Cathode

The cathodic GDL (Fig. 4.6) is represented by a conversion block in different energetic domains. Its inputs are, the upstream partial pressure vector \mathbf{p}_1 , the upstream temperature T_1 , the downstream molar flow vector $\dot{\mathbf{n}}_2$ and the fuel cell current I_{FC} . The values to be calculated are the upstream molar flow vector $\dot{\mathbf{n}}_1$, the downstream partial pressure vector \mathbf{p}_2 , the downstream temperature T_2 and cathodic fraction of the concentration overpotential V_{conc}^c .

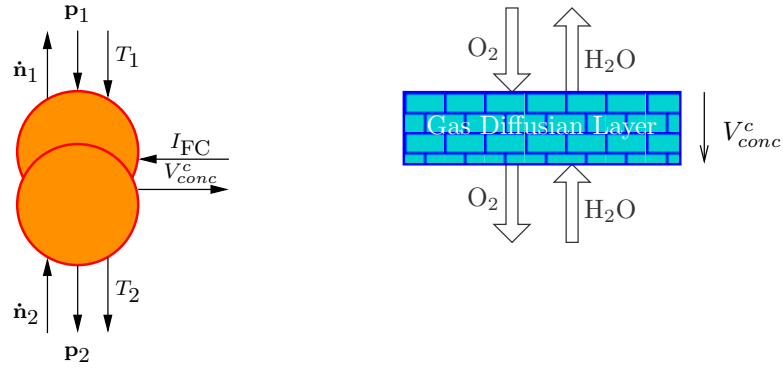


Figure 4.6: Cathode gas diffusion layer - EMR and schematic representation

As no consumption or production occurs inside the gas diffusion layer, the upstream molar flow vector is equal to the downstream molar flow vector Eq. 4.26.

$$\dot{\mathbf{n}}_1 = \dot{\mathbf{n}}_2 \quad (4.26)$$

The downstream partial pressure vector changes due to diffusion applying Eq. 4.20 in the case of binary diffusion and Eq. 4.25 in the case of multi element diffusion. Oxygen and water are taken into consideration in the case of binary diffusion (H4.14). In the case of multi species diffusion also nitrogen is taken into consideration. According to (H4.6) the temperature is homogeneous throughout the fuel cell and does not change upstream and downstream of the gas diffusion layer, Eq. 4.27.

$$T_1 = T_2 \quad (4.27)$$

In this case the concentration overpotential is indicated as to be found at

across the gas diffusion layer. This approach is valid for modeling, as our approach is based on the change of the partial pressure of the oxygen due to diffusion. In reality the potential cannot be gripped over the gas diffusion layer. The concentration overpotential is proportional to the logarithm between the change of partial pressure of the species needed for the reaction over the GDL thickness [116]. It can be written using Eq. 4.28. From the species inside the cathode, only oxygen is needed for the reaction.

$$V_{conc}^c = n C_c \ln \left(\frac{p_{O_2}(0)}{p_{O_2}(\delta)} \right) \quad (4.28)$$

with the parameter C_c that has to be tuned. C_c has been initialized to the value $7.17 \cdot 10^{-3} \text{ V}$ [116].

Anode

The anodic GDL (Fig. 4.7) is represented by a coupling block in different energetic domains. Its inputs are, the upstream partial pressure vector \mathbf{p}_1 , the upstream temperature T_1 , the downstream molar flow vector $\dot{\mathbf{n}}_2$ and the fuel cell current I_{FC} . The values to be calculated are the upstream molar flow vector $\dot{\mathbf{n}}_1$, the downstream partial pressure vector \mathbf{p}_2 , the downstream temperature T_2 and cathodic fraction of the concentration overpotential V_{conc}^a .

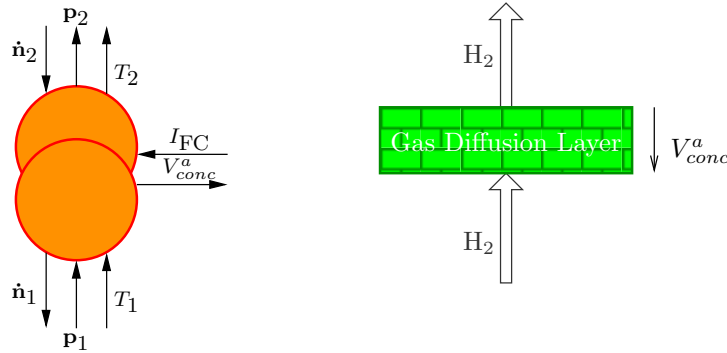


Figure 4.7: Anode gas diffusion layer - EMR and schematic representation

No consumption or production occurs inside the GDL. Hence, the upstream and the downstream molar flow vectors are equal, Eq. 4.29.

$$\dot{\mathbf{n}}_1 = \dot{\mathbf{n}}_2 \quad (4.29)$$

The downstream partial pressures can be calculated due to diffusion. In the case that hydrogen is used as fuel, the binary diffusion introduced in Eq. 4.20

can be used. If gas coming from the reformer is used, the multi species diffusion introduced in Eq. 4.25, taking into consideration hydrogen, water, carbon monoxide, carbon dioxide and nitrogen, is used.

According to (H4.6), the temperature does not change throughout the GDL, Eq. 4.30

$$T_1 = T_2 \quad (4.30)$$

The anodic share of the concentration overpotential can be calculated using Eq. 4.31, taking into consideration the partial pressure of hydrogen. Here, the concentration overpotential is also indicated over the gas diffusion layer, knowing that the tension cannot be found in this place in reality.

$$V_{conc}^a = n C_a \ln \left(\frac{p_{H2}(0)}{p_{H2}(\delta)} \right) \quad (4.31)$$

with the parameter C_a that has to be tuned. C_a has been initialized to the value $7.17 \cdot 10^{-3} \text{ V}$ [116].

4.4.4 Description of Membrane

The fuel cell membrane separates the cathode from the anode. It will be transferred through by protons and water and is at the same time an isolator for water. Ohmic losses take place inside the membrane when protons flow through it. The membrane is represented by a coupling block in different domains (Fig. 4.8). The input values are the cathodic partial pressure vector \mathbf{p}_1 , the anodic partial pressure vector \mathbf{p}_2 , the cathodic temperature T_1 , the anodic temperature T_2 and the fuel cell current I_{FC} . The output values are the cathodic $\dot{\mathbf{n}}_1$ and anodic molar flow vector $\dot{\mathbf{n}}_2$ and the ohmic overpotential V_{ohm} . Only water flows through the membrane. Hence, the molar flow vector has only one non zero element. The anode and cathode molar flow vectors are represented by the same water flow (H4.19). Due to their causality they have opposite signs $\dot{\mathbf{n}}_1 = -\dot{\mathbf{n}}_2$.

Water flow through the membrane

There are two phenomena considered for the water transport inside the membrane:

- **electro-osmotic drag:** Every time protons flow through the membrane they pull some water molecules with them.
- **back diffusion:** If the water activity on one side of the membrane differs from the other side of the membrane, a diffusive water flow tries to reduce this difference.

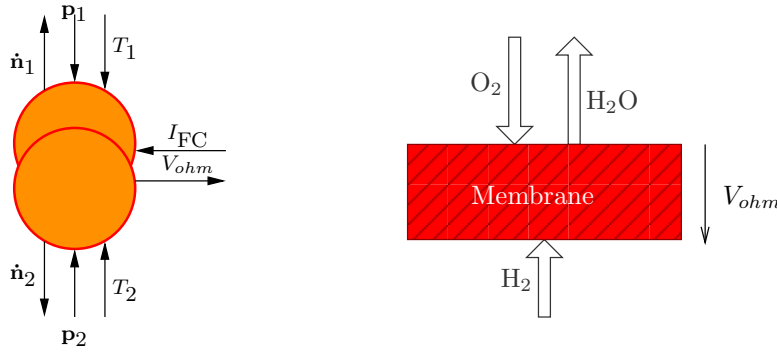


Figure 4.8: Membrane - EMR and Schematic Representation

The calculation and parameters introduced hereafter are for Nafion membrane material. As membrane material of the Ballard NexaTM fuel cell system is not known and the Nafion behavior is the best studied membrane material, it is used for the validation in this case.

The activity is used to calculate the back diffusion. It is calculated as the fraction of the partial pressure over the saturation pressure: $a_{\text{H}_2\text{O}} = p_{\text{H}_2\text{O}}/p_{\text{sat}}(T)$. Springer [138] introduced the water content of the membrane λ , the number of water molecules per Nafion molecule in the membrane, as function of the activity using Eq. 4.32.

$$\lambda = \begin{cases} 0.43 + 17.81 a_{\text{H}_2\text{O}} - 39.85 a_{\text{H}_2\text{O}}^2 + 36.0 a_{\text{H}_2\text{O}}^3 & \text{if } 0 < a_{\text{H}_2\text{O}} \leq 1 \\ 14 + 1.4 (a_{\text{H}_2\text{O}} - 1) & \text{if } 1 < a_{\text{H}_2\text{O}} \leq 3 \end{cases} \quad (4.32)$$

Those values have been evaluated for 30 °C, but it is assumed that they are also valid for 80 °C [138]. For $0 < \lambda \leq 14$ the water is considered to be gaseous, for $14 < \lambda \leq 22$ the water is assumed to be liquid. As introduced in (H4.5) all water is considered to be gaseous from the pneumatic point of view, even if $\lambda > 14$.

The molar flux due to electro-osmotic drag $J_{\text{H}_2\text{O},\text{drag}}$ can be calculated depending on the current density j following Eq. 4.34 [116, 138].

$$b_{\text{drag}} = b_{\text{drag}}^{\text{Sat}} \frac{\lambda}{22} \quad (4.33)$$

$$J_{\text{H}_2\text{O},\text{drag}} = 2 \cdot b_{\text{drag}} \frac{j}{2F} \quad (4.34)$$

The saturation drag coefficient is $b_{\text{drag}}^{\text{Sat}} = 2.5$.

The molar flux due to back diffusion $J_{\text{H}_2\text{O}, \text{ back-diff}}$ can be calculated using Eq. 4.35 following [116].

$$J_{\text{H}_2\text{O}, \text{ back-diff}} = -\frac{\rho_{\text{dry}}}{M_{\text{m}}} D_{\lambda} \frac{d\lambda}{dy} \quad (4.35)$$

The dry density of the Nafion membrane is $\rho_{\text{dry}} = 1970 \text{ kg m}^{-3}$ and its molar mass is $M_{\text{m}} = 1.0 \text{ kg mol}^{-1}$. The directions of the mass flows have to be considered carefully. In this case the water flow from the anode to the cathode is considered to be positive. The evolution of the water content $d\lambda/dx$ is unknown. According to O'Hayre [116] this problem can be solved by calculating the total water flux $J_{\text{H}_2\text{O}} = J_{\text{H}_2\text{O}, \text{ drag}} + J_{\text{H}_2\text{O}, \text{ back-diff}}$, Eq. 4.36, and by substituting it with a simplified equation using the coefficient α , Eq. 4.37, representing how many water molecule are transported along with each proton. The two equations can be equaled to give the derivative of the water content over the membrane thickness, Eq. 4.38.

$$J_{\text{H}_2\text{O}} = 2 \cdot b_{\text{drag}} \frac{i}{2F} - \frac{\rho_{\text{dry}}}{M_{\text{m}}} D_{\lambda} \frac{d\lambda}{dz} \quad (4.36)$$

$$J_{\text{H}_2\text{O}} = \frac{\alpha I}{2 F S_{\text{cell}}} \quad (4.37)$$

$$\frac{d\lambda}{dy} = \left(2 b_{\text{drag}}^{\text{Sat}} \frac{\lambda}{22} - \alpha \right) \frac{I \cdot M_{\text{m}}}{2 F \rho_{\text{dry}} D_{\lambda} S_{\text{cell}}} \quad (4.38)$$

All parameters but the diffusion coefficient over the membrane D_{λ} are known. The assumption that the diffusion coefficient does not change by large quantities can be made (H4.20). The diffusion coefficient for the mean content $\langle \lambda \rangle$ Eq. 4.39 and Eq. 4.40 can be used [116].

$$\langle \lambda \rangle = \frac{\lambda_{\text{a}} + \lambda_{\text{c}}}{2} \quad (4.39)$$

$$D_{\langle \lambda \rangle} = D(\langle \lambda \rangle) \quad (4.40)$$

This leads to a development of the water content over the membrane thickness Eq. 4.41.

$$\lambda(x) = \frac{11\alpha}{b_{\text{drag}}^{\text{Sat}}} + C \exp \left(\frac{I M_{\text{m}} b_{\text{drag}}^{\text{Sat}}}{22 F S_{\text{cell}} \rho_{\text{dry}} D_{\langle \lambda \rangle}} \right) \quad (4.41)$$

The two unknowns α and C can be calculated as the boundary conditions are known. The interface between the anode GDL and the membrane is defined

as: $\lambda(0) = \lambda_a$ and the interface between the cathode GDL and the membrane is defined as: $\lambda(\delta) = \lambda_c$.

Finally the molar flow through the membrane can be written as in Eq. 4.42.

$$\dot{n}_1 = -\dot{n}_2 = \begin{bmatrix} 0 & 0 & 0 & 0 & 0 & 0 & 0 & \frac{n \alpha I}{2 F} & 0 & 0 \end{bmatrix} \quad (4.42)$$

Ohmic losses

The ohmic overpotential V_{ohm} can be calculated using Eq. 4.43. It depends on the the membrane specific resistance r^M .

$$V_{ohm} = n r^M \frac{I}{S_{cell}} \quad (4.43)$$

The membrane specific resistance r^M can be obtained by the integration of the inverse of the membrane conductivity σ^M over the membrane thickness Eq. 4.44.

$$r^M = \int_0^\delta \frac{dx}{\sigma^M(T, \lambda(x))} \quad (4.44)$$

The membrane conductivity σ^M can be calculated using Eq. 4.45.

$$\sigma^M(T, \lambda(x)) = \sigma_{303K}^M(\lambda) \exp \left[1268 \left(\frac{1}{303} - \frac{1}{T} \right) \right] \quad (4.45)$$

$$\sigma_{303K}^M(\lambda) = \sigma_1 \lambda - \sigma_2 \quad (4.46)$$

with $\sigma_1 = 0.005193 \Omega^{-1} \text{m}^{-1}$ and $\sigma_2 = 0.00326 \Omega^{-1} \text{m}^{-1}$.

As has been shown by Blunier [21] Eq. 4.44 can be integrated using Eq. 4.41, giving Eq. 4.47, [56].

$$r^M = \frac{2 n S_{cell} \exp [1268 ((1/T) - (1/303))]}{I M_m (22 \sigma_1 \alpha - 2 \sigma_2 b_{drag}^{Sat})} \left[-22 F \rho_{dry} D_{\langle \lambda \rangle} \ln \cdot \right. \quad (4.47)$$

$$\left(22 \sigma_1 \alpha + 2 \sigma_1 C b_{drag}^{Sat} \cdot \exp \left(\frac{\delta^M I M_m b_{drag}^{Sat}}{22 n S_{cell} F \rho_{dry} D_{\langle \lambda \rangle}} \right) - 2 \sigma_2 d_{drag}^{Sat} \right)$$

$$\left. + \frac{\delta^M I b_{drag}^{Sat}}{n S_{cell}} + 22 F \rho_{dry} D_{\langle \lambda \rangle} \ln (22 \sigma_1 \alpha + 2 \sigma_1 C b_{drag}^{Sat} - 2 \sigma_2 b_{drag}^{Sat}) \right]$$

4.4.5 Combination of Sub models

In section (4.2), the EMR modeling of the fuel cell is presented with its different layers that have different tasks for the operation of the fuel cell. In section (4.4) the individual layers are introduced one by one, showing the input and output variables and their connection. A combination of those different layers forms the fuel cell system model, (H4.4) (Fig. 4.9). The model has been implemented in Matlab/Simulink™.

4.5 Validation of Fuel Cell Model

The fuel cell stack model introduced in (4.4) has been parametrized according to the values given in Tab. A.5. It is validated with the help of a Ballard Nexa™ fuel cell system (Fig. 4.10), [51, 59]. The Nexa™ system is a commercially available fuel cell system with a maximum electrical power output of 1.2 kW. The system has to be supplied with hydrogen. It is equipped with two fans ensuring the oxygen supply to the cathode and the cooling. The output voltage varies between 30 V and 45 V depending on the demanded current. The stack temperature is not regulated but limited to a maximum value of 65 °C, leading to the fact that the stack temperature varies with the power drawn from the system between 35 °C and 65 °C. The Nexa™ system is encapsulated and controlled. At the same time, it is equipped with an integrated data acquisition system providing essential values of the stack operation like the stack voltage, the current drawn from the stack, the stack temperature and the quantity of air supplied to the system. Values about the actual hydrogen consumption and the characteristics of the individual cells are not provided. The number of cells inside the Nexa™ system is not given, but can be evaluated to be 46 [120]. Furthermore, the active cell surface area is not known, this value could only be assumed. It has been fixed to a value of 54 cm². As can be seen in [21] the cell surface area has only little influence on the accuracy of the results.

The introduced fuel cell model needs the air and fuel mass flows as well as the stack temperature as input values (H4.6). When the Ballard Nexa™ fuel cell system runs, the integrated data acquisition system is able to acquire these needed values. Those values have been used for the initialization of the fuel cell model. The fuel cell model evaluates the expected output voltage. The modeled and measured system voltages can be compared, (Fig. 4.11).

Having measured values of the stack voltage and all input parameters needed, the missing system parameters can be evaluated. Therefore, the Matlab™ optimization toolbox has been used. The system model is extended by a comparison between simulated and calculated stack voltage giving the voltage error. The

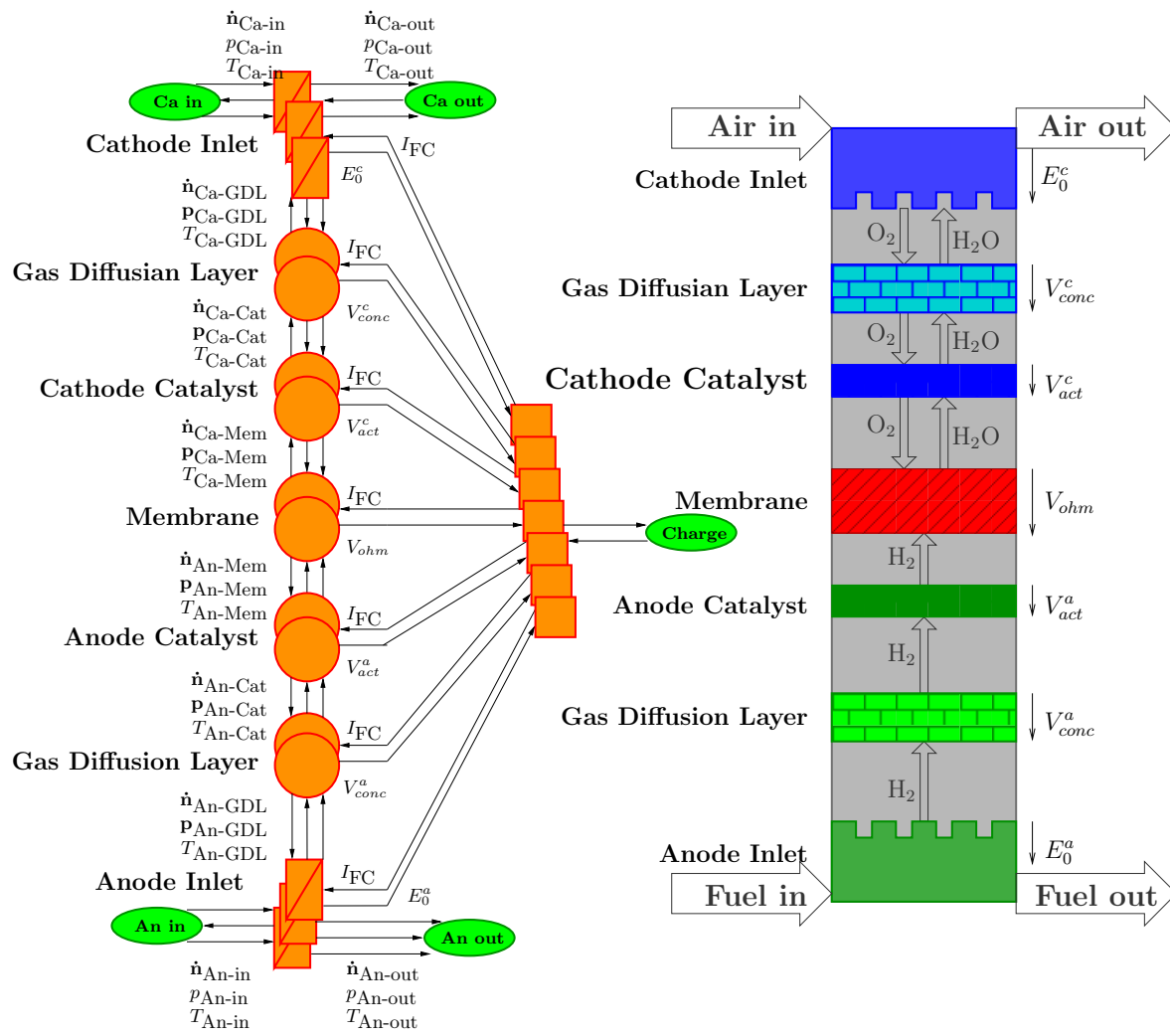


Figure 4.9: EMR and schematic representation of the fuel cell stack.

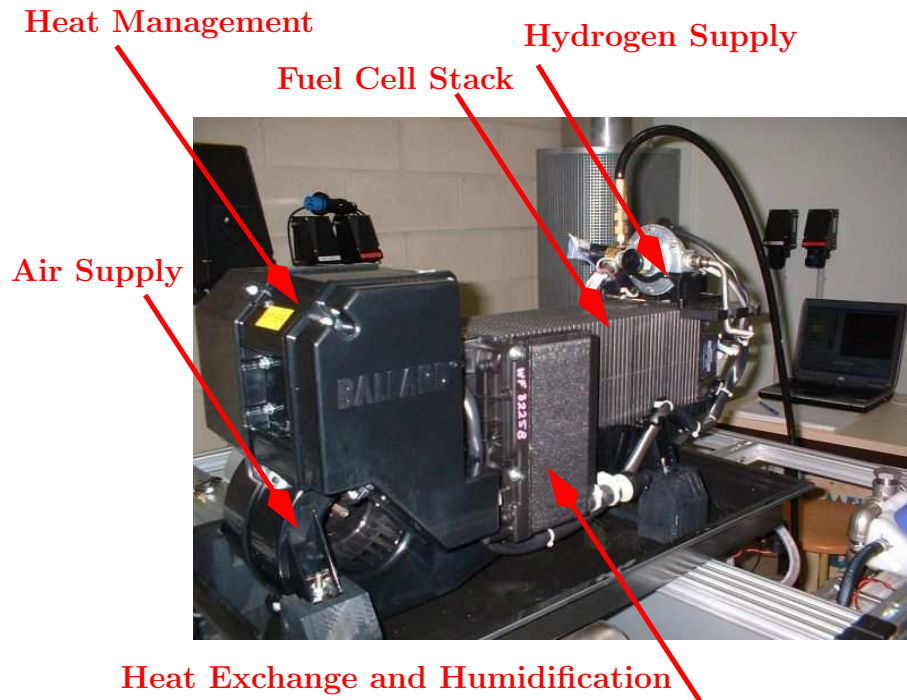


Figure 4.10: The Ballard Nexa™ system.

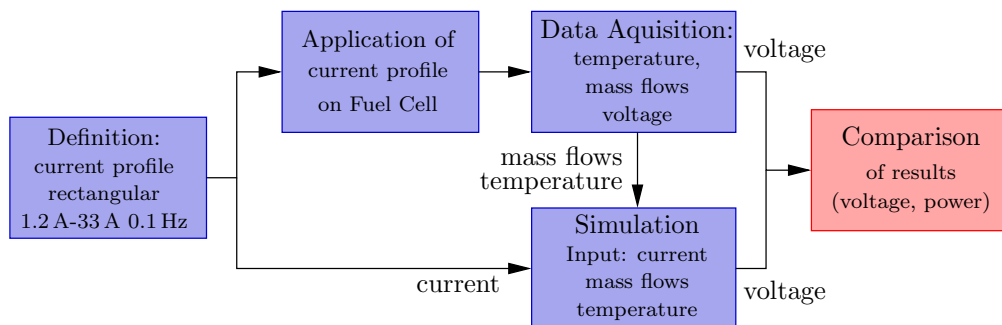


Figure 4.11: Validation strategy

absolute difference between them is integrated over a certain period. This *voltage error* was minimized adapting the parameters to be tuned. The unknown system parameters are the single cell active surface S_{cell} , the charge transfer coefficient α_a , the exchange current density j_0 and the concentration overpotential parameters C_c and C_a . The optimization was done by the function *fmincon* (non linear least squares Gauß-Newton method) where the stack model was handled like a non linear function with the fuel cell current I_{FC} , the cell temperature T , the input air mass flow vector \dot{n}_{in} and the tuning parameters as input and the voltage error as output. As has been shown by Blunier [21], the parameter of the cell surface area S_{cell} as well as concentration overpotential parameters C_c and C_a have little influence on the simulation results and have therefore not been regarded for parameter fitting. The order of magnitude of the system parameters α_a and j_0 are known as literature values exist [116]. To simplify the optimization process, constraints were associated to the parameters: $10^{-6} < \alpha_a < 0.1$; $10^{-6} \text{ A cm}^{-2} < j_0 < 0.1 \text{ A cm}^{-2}$. Furthermore, initial values were provided for the parameters: $\alpha_a = 0.064$; $j_0 = 2 \times 10^{-3} \text{ A cm}^{-2}$. The values obtained by optimization were in the same order of magnitude as the initial values.

4.5.1 Validation of Fuel Cell fed with Hydrogen

First, the model is validated for the use of hydrogen. In the case of hydrogen use, the binary diffusion is applied as well to the anode as to the cathode GDL (H4.14).

A load profile with step currents between 0 A and 45 A has been demanded from the system (Fig. 4.12). This load profile is derived from the needs toward the system for a specific transportation application.

Figure 4.13 shows the measured and simulated voltage development. The achieved voltage values are in the same order. Good agreement between measurement and simulation can be obtained at the beginning of the simulation (until 580 s) where the current levels are comparably low (below 45 A). Afterward, when high current levels above 45 A are demanded from system, the simulation predicts lower voltages than can be found in the measurement. This difference is most important for currents above 45 A (up to 2 V) and decreases for lower currents, but the initial good agreement is not reproduced. In (Fig. 4.14) the measured and simulated voltage as well as the contributions to the voltage is shown for the time between 500 s and 800 s. The only value changing significantly for changing currents is the ohmic loss over the membrane V_{ohm} . The membrane humidity depends on the anodic and cathodic humidity level. The anodic humidity level inside the model is considered to be below 14 and has been fixed at 6. It is shown in (Fig. 4.15) that the cathode humidity level drops for

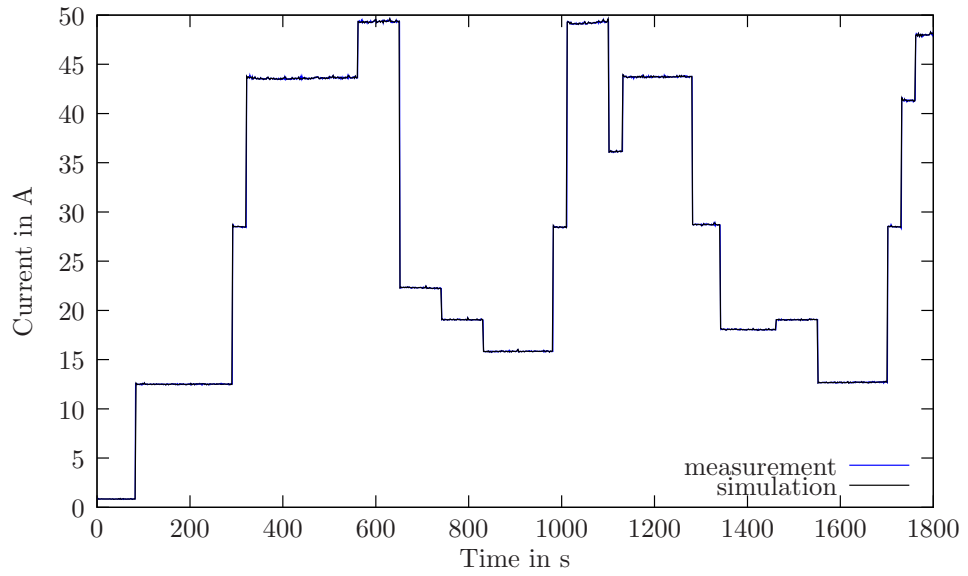


Figure 4.12: Load profile demanded from the hydrogen fueled system.

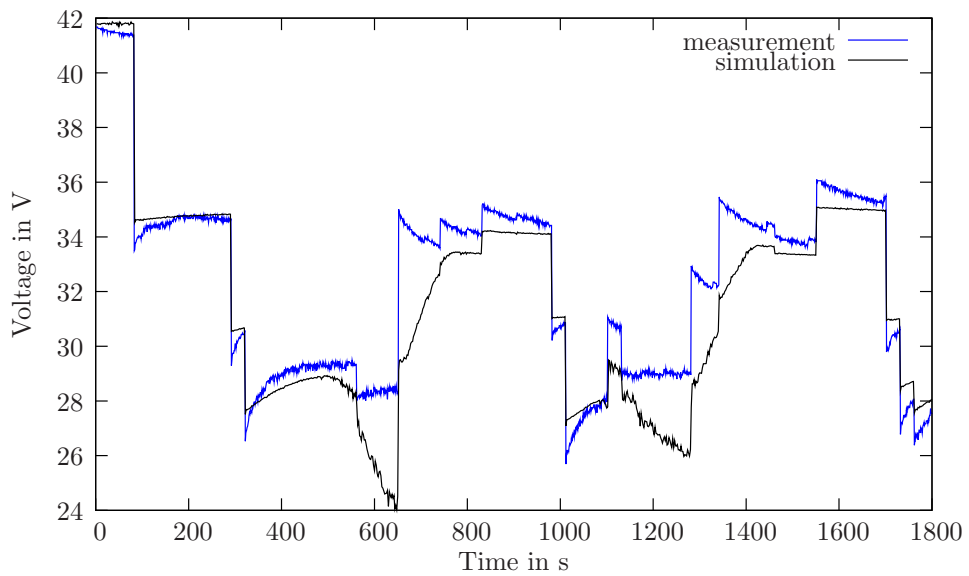


Figure 4.13: Fuel cell stack voltage development for hydrogen fueled system.

high current levels for example around 600 s. Inside the real system there is a cathodic humidity exchanger, which recaptures humidity exiting the cathode and reintroduces it into the cathode inlet. At high current levels, where a large air flow passes through the cathode, this humidity exchange might lead to higher humidity levels in the cathode than foreseen in the simulation, thus decreasing the ohmic losses.

The measured voltage levels do not reach their stationary level directly after a step change in current. Up to 100 s are needed to reach the next stationary level. This behavior cannot be explained by the change in temperature, because the temperature is an input parameter of the model that is taken from system measurement, (Fig. 4.11). Therefore, the model and measurement temperature equal at any time. As introduced in 4.4.4, the ohmic losses depend on the humidity of the membrane. Just after a step increase in current, the measured voltages are lower than the simulated voltages (Fig. 4.13, at 300 s). For a step decrease in current the measured voltages are higher than the simulated voltages (Fig. 4.13, at 700 s). This fact can also be explained by the cathodic humidity. As the fuel cell is not temperature controlled, higher currents mean higher fuel cell temperature. At higher temperatures, the saturation pressure increases and the cathodic humidity exchanger may introduce higher humidity partial pressures in the cathode, which have positive influence on the membrane humidification and thus the stack voltage. Therefore, after a step increase in current an initial drop of measured values with regard to simulation values takes place followed by an adjustment of the measured voltage. Likewise, a step reduction in current, decreases the stack temperature and the cathodic humidity level. Directly after the step change, a high humidity level is available, leading to measured voltage values that are superior to the simulation results. The measured values decrease in the following.

The realization of the anode outlet differs between the model and the real system. In the hydrogen Ballard NexaTM fuel cell system a purge valve is installed at the anode outlet. Only pure hydrogen is supplied to the anode, but there is also some nitrogen and water diffusion through the membrane. This nitrogen and water accumulates at the anode, causing a drop in cell voltage. Therefore, the purge cell voltage is recorded continuously. The purge cells are the two cells inside the stack that are most affected by this voltage drop. Once the purge cell voltage drops below 80 % of the reference value the purge valve is opened for two seconds. It has been shown in [51, 58] the time between purges decreases hyperbolically over the current.

Inside the model more hydrogen is supplied than consumed by reaction, a constant purge with a molar flow proportional to the current is foreseen. This purge does not lead to a complete evacuation of accumulated water.

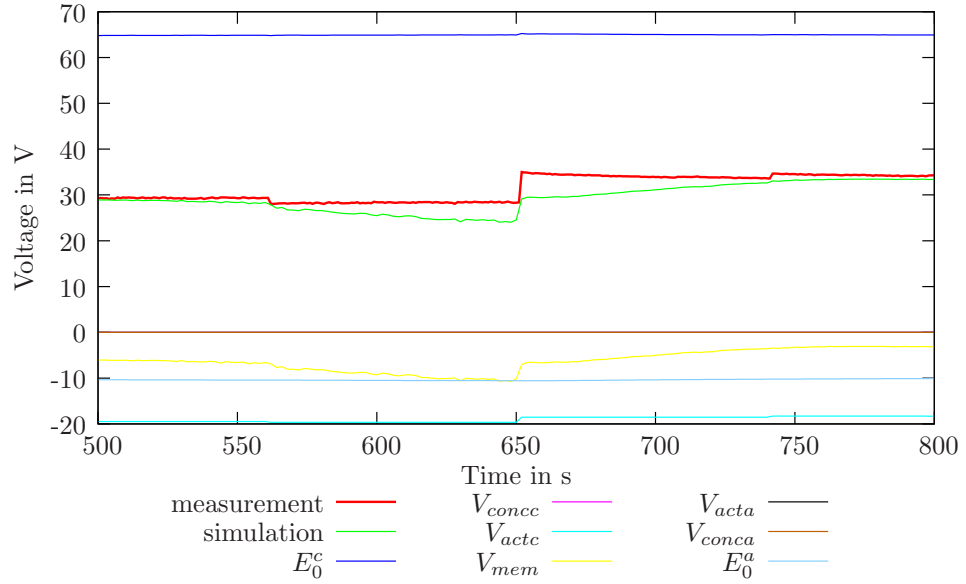


Figure 4.14: Fuel cell stack voltage development divided into contributors.

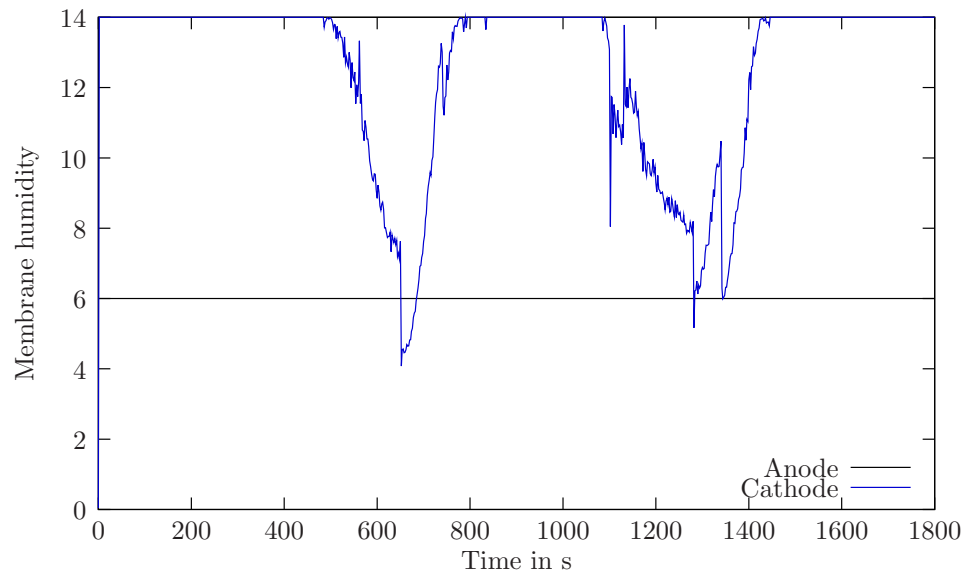


Figure 4.15: Anodic and cathodic humidity.

The modeling approach gives the possibility to split the stack voltage according to the contribution of the different layers of the fuel cell stack. It can be seen for only a small time window (Fig. 4.16) that the cathode inlet E_0^c is the only point with positive voltage contribution. It stays relatively constant even if the change in current presented, which is bigger than 30 A. Also the cathodic concentration overpotential V_{conc}^c does not change considerably. Only at the cathode activation overpotential V_{act}^c the influence of the current step can be seen. The ohmic overpotential V_{ohm} is big for large currents and small for small currents this is in accordance to the observation. The electro-osmotic drag has a considerable share of the membrane humidity and therefore the ohmic losses are humidity dependent as well. The anode activation overpotential V_{act}^a is zero according to (H4.16). The anode concentration overpotential V_{conc}^a and the anodic contribution of the reversible cell voltage E_0^a do not depend on the current. For this description it has to be taken into account that the reversible thermodynamic cell potential calculation has been divided in two parts. This is not justified chemically, because a reaction can only take place when all contributors are available and in contact. Still, for the application in EMR this is meaningful because it simplifies the description of the conversions.

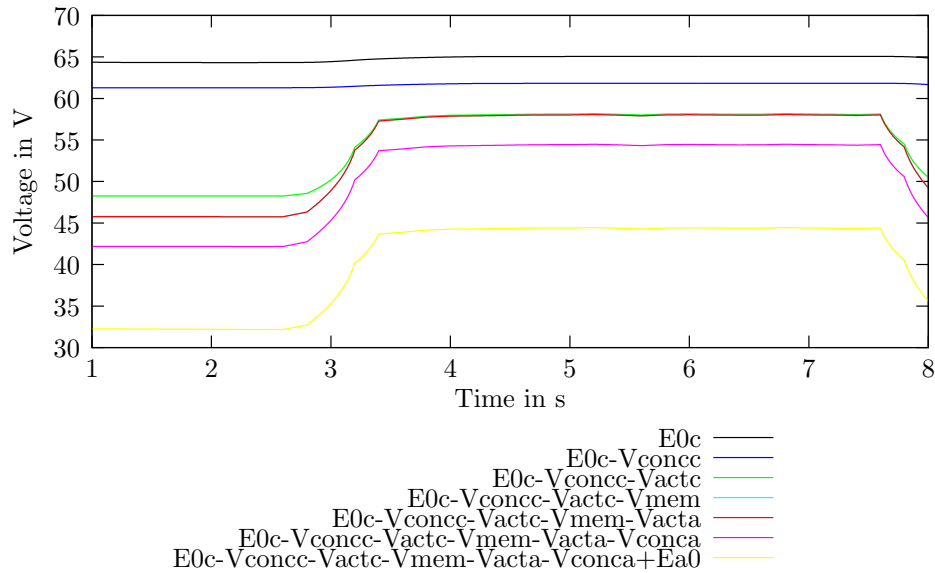


Figure 4.16: Contribution of different layers of the fuel cell stack to the voltage.

4.5.2 Validation Fuel Cell fed with reformat

The Ballard Nexa™ fuel cell system is intended to be used with pure hydrogen only, but for some projects Ballard Nexa™ fuel cell systems were adapted for the use with reformat. Reformat is the hydrogen rich gas mixture produced by the fuel processor. One of those Ballard Nexa™ fuel cell systems was available for testing. The main modification has been made concerning the anode outlet. A purge valve that is just opened occasionally is installed at the anode outlet of the hydrogen fed Ballard Nexa™ fuel cell system. This is removed for the use of reformat. The Nexa™ fuel cell system has no upstream anodic volume flow regulation. Therefore, a mass flow regulator has been installed at the anode outlet. The outlet volume flow is controlled to be proportional to the current demanded from the fuel cell *Eq. 4.48*.

$$\dot{V}_{\text{anode-out}} = A + b \cdot I_{\text{FC}} \quad (4.48)$$

with the parameters $A = 1.08 \text{ L s}^{-1}$ and $b = 0.78 \text{ L s}^{-1} \text{ A}^{-1}$.

Furthermore, the maximum anodic flow through the fuel cell has been adapted for the reformat driven fuel cell. For the hydrogen supplied system, the mass flow was limited to 2 L min^{-1} , for the reformat driven Nexa™ system this value was augmented to 20 L min^{-1} .

The fuel cell system was fed with a gas mixture that was close to the composition expected from the fuel processing unit at nominal conditions. For reasons of simplicity only hydrogen, nitrogen and carbon dioxide were used for the gas mixture. The fractions are given in *Tab. 4.2*.

Table 4.2: Molar fractions in reformat equivalent gas mixture.

Substance	Molar Fraction
H ₂	35 %
CO ₂	20 %
N ₂	45 %

The load profile is introduced in (*Fig. 4.17*). The load profile is the same as presented in (*Fig. 4.12*) with the difference that due to the reduced partial pressure of hydrogen the available currents are limited. Therefore, the maximum current for the system validation against reformat is at 15 A instead of 50 A.

It can be seen in (*Fig. 4.18*) that the measured and modeled voltage responses are generally in good agreement. The simulation values of the voltage are in good agreements for currents below 10 A. For higher values, the simulation

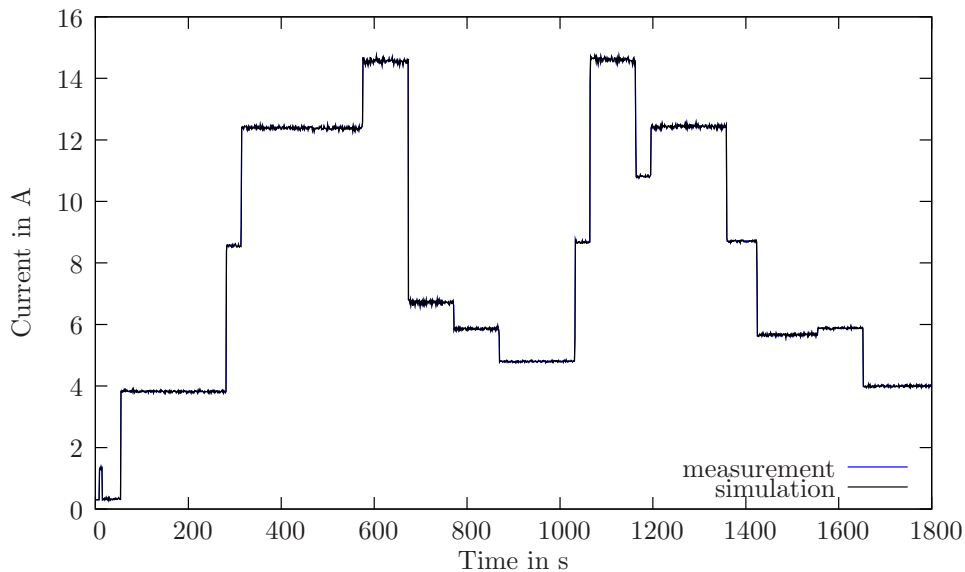


Figure 4.17: Current profile applied for the reformate driven fuel cell system.

overestimates the voltage. The same effect concerning humidification of the cathode can be seen as for the hydrogen fed fuel cell.

4.6 Adaption toward a HTPEMFC

The fuel cell system developed during the GAPPAC project shall be used for transportation auxiliary power supply. At the same time the system heat shall be used for trigeneration. A HTPEMFC system promises a higher volumetric density and their higher working temperatures around 180 °C are more adapted for trigeneration application (using heat for refrigeration) than PEFC systems. Furthermore, the higher working temperature decreases the sensitivity of the fuel cell with regard to catalyst contamination (1.1.5). Therefore, HTPEMFC architecture has been chosen for GAPPAC. Promising results for HTPEMFC systems were presented [11, 87, 97]. Hence, a the modeling of a HTPEMFC stack is developed here.

4.6.1 Adaption of the model

It can be supposed that the HTPEMFC has the same general structure as the PEFC, (Fig. 4.9), (H 4.7). Therefore, the main structure of the fuel cell can be kept. The modeling has two main aspects. The modeling supplies the gas flows through the individual layers of the fuel cell and the evaluation of the voltage.

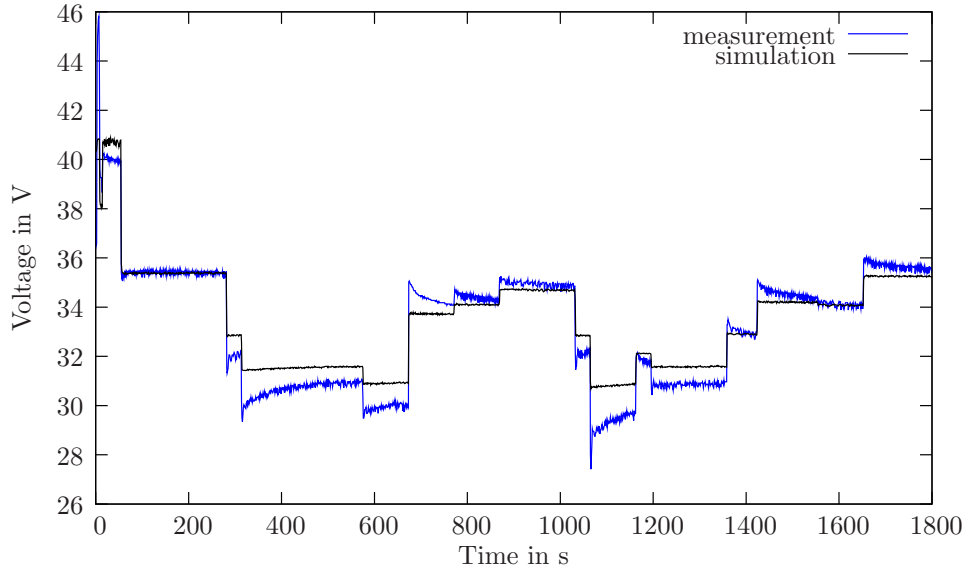


Figure 4.18: Measured and simulated voltage development for the reformat driven fuel cell system.

For the gas inlet and gas diffusion layer, the same characteristics can be supposed as a first guess. Even the functionality of the catalysts does not change dramatically, however the membrane material changes. Still, the working principle stays the same, and even if the material is different, there is a water transport through the membrane, governed by electro-osmotic drag and back diffusion. As, for the moment, the characteristics of the HTPFC membrane with regard to water content are not known, the parameters for the PEFC Nafion membrane are retained. This leaves the possibility to adapt the model by changing the parameter in the initialization file later on, [104].

The approach toward cell voltage evaluation given in *Eq. 4.49* and *Eq. 4.50* proposed by Korsgaard [95] is used. The model and its parametrization are used here. The model is developed for a single fuel cell.

$$V_{\text{cell}} = V_0 - \eta_{\text{act}} - \eta_{\text{ohmic}} - \eta_{\text{diff}} - \eta_{\text{anode}} \quad (4.49)$$

$$V_{\text{cell}} = V_0 - \frac{RT}{4\alpha_1 F} \ln \left(\frac{j + j_0}{j_0} \right) - R_{\text{ohm}} j - \frac{R_{\text{conc}} j}{\gamma - 1} - \eta_{\text{anode}} \quad (4.50)$$

where V_0 is the open circuit voltage, γ is the cathode stoichiometric ratio and the four variables α_1 , j_0 , R_{ohmic} and R_{conc} are obtained from *Eq. 4.51*, *Eq. 4.52*,

Eq. 4.53 and Eq. 4.54.

$$\alpha_1 = a_0 T + b_0 \quad (4.51)$$

$$j_0 = a_3 \exp(-b_3 T) \quad (4.52)$$

$$R_{\text{ohm}} = a_1 T + b_1 \quad (4.53)$$

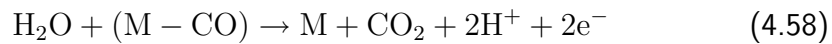
$$R_{\text{conc}} = a_2 T + b_2 \quad (4.54)$$

The empiric parameters (a_i, b_i) are given in Tab. 4.3.

Table 4.3: Parameters for cathodic voltage share of a HTPEM [95]

Parameter	Notation	Value	Unit
Charge transfer constant	a_0	$2.761 \cdot 10^{-3}$	K^{-1}
Charge transfer constant	b_0	-0.9453	
Ohmic loss constant	a_1	$-1.667 \cdot 10^{-4}$	$\Omega \text{ K}^{-1}$
Ohmic loss constant	b_1	0.2289	Ω
Diffusion limitation constant	a_2	$-8.203 \cdot 10^{-4}$	$\Omega \text{ K}^{-1}$
Diffusion limitation constant	b_b	0.4306	Ω
Limiting current constant	a_3	$33.3 \cdot 10^3$	A
Limiting current constant	b_3	0.04368	

Equation 4.50 gives only the open circuit voltage and the cathodic participation to the fuel cell voltage, but there is also an influence of carbon monoxide on the cell voltage caused by the coverage of a fraction of the catalyst surface needed for hydrogen reaction with carbon monoxide. This aspect has also been studied by Korsgaard [95]. Four different mechanisms with regard to CO adsorption/desorption are considered in the anode catalyst layer Eq. 4.55, Eq. 4.56, Eq. 4.57 and Eq. 4.58.



Equations 4.55 and 4.56 represent the general adsorption/desorption process. Equation 4.57 describes the electrochemical oxidation of hydrogen, Eq. 4.58 describes the oxidation of carbon monoxide to carbon dioxide, which only occurs at high current densities.

Based on the four reactions, a set on the kinetic equations can be defined *Eq. 4.59* and *Eq. 4.60*.

$$\rho \frac{d\theta_{H_2}}{dt} = 0 = k_{fh} x_{H_2} p (1 - \theta_{H_2} - \theta_{CO})^l - b_{fh} k_{fh} \theta_{H_2}^l - j \quad (4.59)$$

$$\rho \frac{d\theta_{CO}}{dt} = 0 = k_{fc} x_{CO} p (1 - \theta_{H_2} - \theta_{CO}) - \frac{j k_{ec} \theta_{CO}}{2 k_{eh} \theta_{H_2}} \quad (4.60)$$

The surface coverage of hydrogen θ_{H_2} shall be calculated. The anode density ρ is a known parameter. The parameter l is set to 2, indicating that the intermediate hydrogen step is second order in catalyst sites. k_{fh} , k_{fc} , k_{eh} , k_{ec} , b_{fh} and b_{fc} are temperature dependent parameters of reaction kinetics that have to be calculated according to the Arrhenius equation, *Eq. 4.61*. The coefficients are given in *Tab. 4.4*.

$$k_x = A_x \exp \left(\frac{-E_{Ax}}{R \cdot T} \right) \quad (4.61)$$

Table 4.4: Parameters for the reaction kinetics of adsorption/desorption reaction on anode [95]

Parameter	Notation	Value	Unit
Pre-exponential factors used for anode model			
CO desorption rate	b_{fc}	$8.817 \cdot 10^{12}$	bar
H ₂ desorption rate	b_{fh}	$2.038 \cdot 10^6$	bar
CO electrooxidation rate	k_{ec}	$3.267 \cdot 10^{18}$	A cm ⁻²
H ₂ electrooxidation rate	k_{eh}	25 607	A cm ⁻²
CO adsorption rate	k_{fc}	94.08	A cm ⁻² bar ⁻¹
H ₂ adsorption rate	k_{fh}	$2.743 \cdot 10^{24}$	A cm ⁻² bar ⁻¹
Activation energy values			
CO desorption rate	E_{bfc}	127 513	J mol ⁻¹
H ₂ desorption rate	E_{bfh}	47 904	J mol ⁻¹
CO electrooxidation rate	E_{kec}	196 829	J mol ⁻¹
H ₂ electrooxidation rate	E_{keh}	34 777	J mol ⁻¹
CO adsorption rate	E_{efc}	19 045	J mol ⁻¹
H ₂ adsorption rate	E_{efh}	$1.899 \cdot 10^5$	J mol ⁻¹

As stationary behavior is assumed for the anodic reaction (*H4.8*), those equations lead to a system of two equations with the surface coverage of hydrogen and carbon monoxide as two unknowns θ_{H_2} and θ_{CO} . The hydrogen surface coverage θ_{H_2} is used to evaluate the anodic overpotential, *Eq. 4.62*. As it decreases, the

anodic overpotential increases. Furthermore, the anodic overpotential is based on the temperature dependent reaction kinetic term k_{eh} that has already been introduced. Also the charge transfer constant α_1 is taken into consideration. Even if considerable work has been effectuated with regard to carbon monoxide poisoning, this work is mainly limited to PEFCs [35, 46, 105, 137]. Korsgaard [95] unified this approaches for the description of the anodic overpotential of a HT-PEMFC.

$$\eta_{anode} = \frac{RT_{cell}}{\alpha_1 F} \operatorname{arcsinh} \left(\frac{j}{2 k_{eh} \theta_{H_2}} \right) \quad (4.62)$$

The approach to evaluate the cell voltage using Eq. 4.50 and Eq. 4.62, can be adapted to a HTPEMFC stack. Based on (H4.2), the stack voltage is equal to the number of cells n times the cell voltage, Eq. 4.63.

$$V_{stack} = n \cdot V_{cell} \quad (4.63)$$

It is furthermore possible to associate each term of the cell voltage evaluation to one layer of the fuel cell.

- The open circuit voltage V_0 can be associated to the cathode inlet, the anode inlet voltage can be assumed to be zero $E_0^a = 0$.
- The activation overpotential η_{act} (Eq. 4.49 and Eq. 4.50) can be associated to the cathodic catalyst.
- The diffusive overpotential η_{diff} (Eq. 4.49 and Eq. 4.50) can be associated to the cathodic GDL.
- The ohmic overpotential η_{ohmic} (Eq. 4.49 and Eq. 4.50) can be associated to the membrane.
- The anodic overpotential η_a (Eq. 4.62) can be associated to the anodic catalyst.
- For the HTPEMFC as well as for the PEFC the anode kinetics are much faster than the cathode kinetics, therefore only the cathodic concentration overpotentials are taken into consideration.

Using this approach it is possible to model a HTPeMFC stack. The EMR representation of the HTPeMFC stack is the same as the presentation of the PEFC stack (4.4). Only the description of the voltages inside the blocks is changed. This proves one advantage of EMR. As the general function stays unchanged the structure can be kept. As the approach is modular, the description inside the blocks can be changed without changing the entire model.

4.6.2 Validation of the HTPeM

The HTPeMFC model was validated against a HTPeMFC (*Fig. 4.19*). Each fuel cell has a surface of 45 cm^2 . The fuel cell is supplied with fuel and air. The air is at the same time used to supply the fuel cell with oxygen and for its cooling. The working temperatures are around 180°C . Evaluations have been made with using single cells [97] with a power of some W and using stacks of up to 65 cells with a power of around 1 kW [11]. The Serenergy HTPeMFC stack does not have an integrated heat management system. It is heated up by a heating resistance which is installed close to the stack. The absence of a heat management system leads to the fact that the temperature is not homogeneous throughout the fuel cell stack.

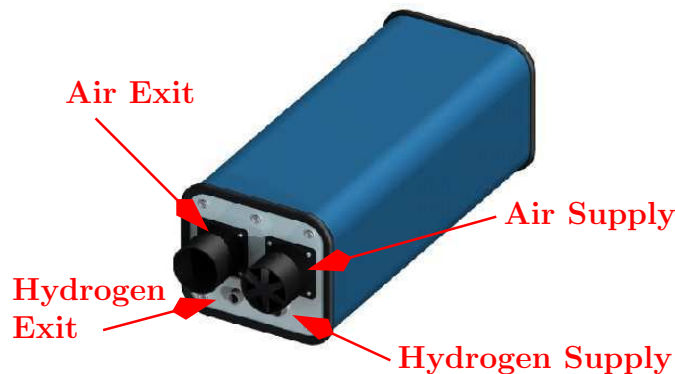
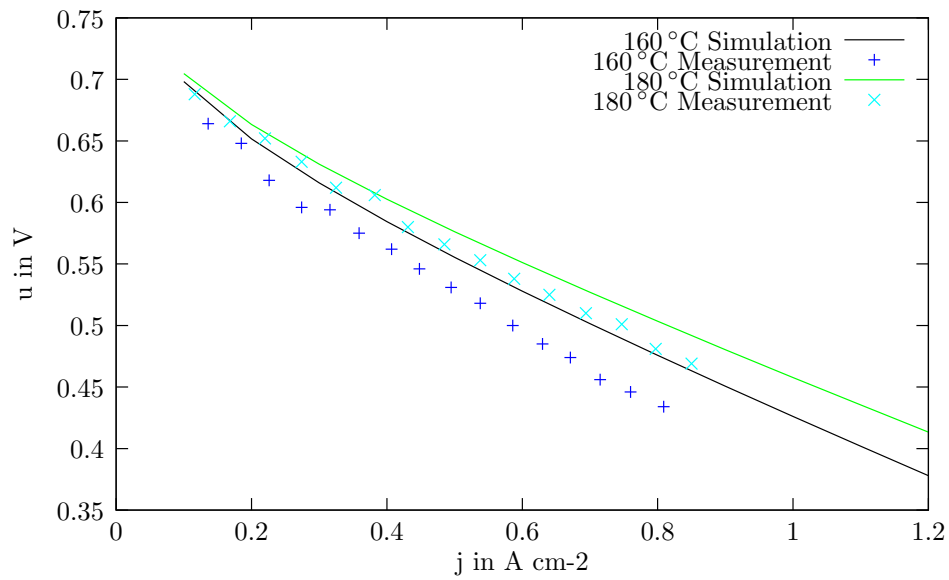


Figure 4.19: Serenergy HTPeM Stack (picture provided by N-GHY).

A validation has been made for two different temperatures 160°C and 180°C and for four different gas compositions:

- pure hydrogen (*Fig. 4.20(a)*),
- 75 % hydrogen 25 % carbon dioxide (*Fig. 4.20(b)*),



(a) pure hydrogen [97]

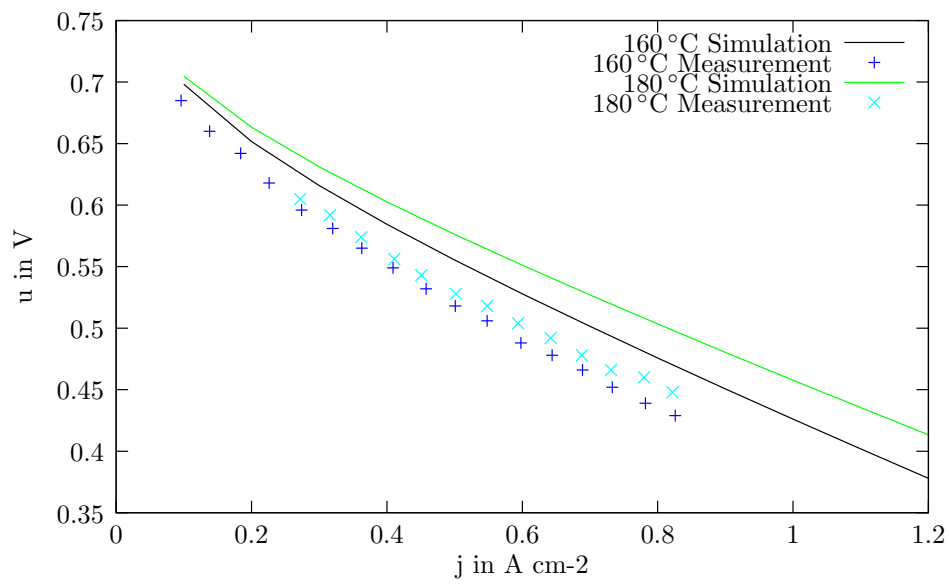
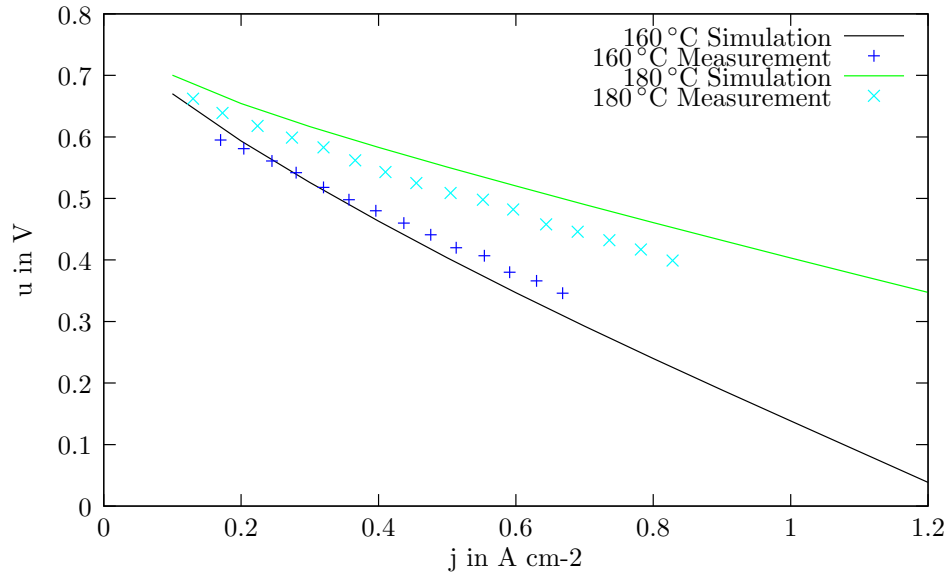
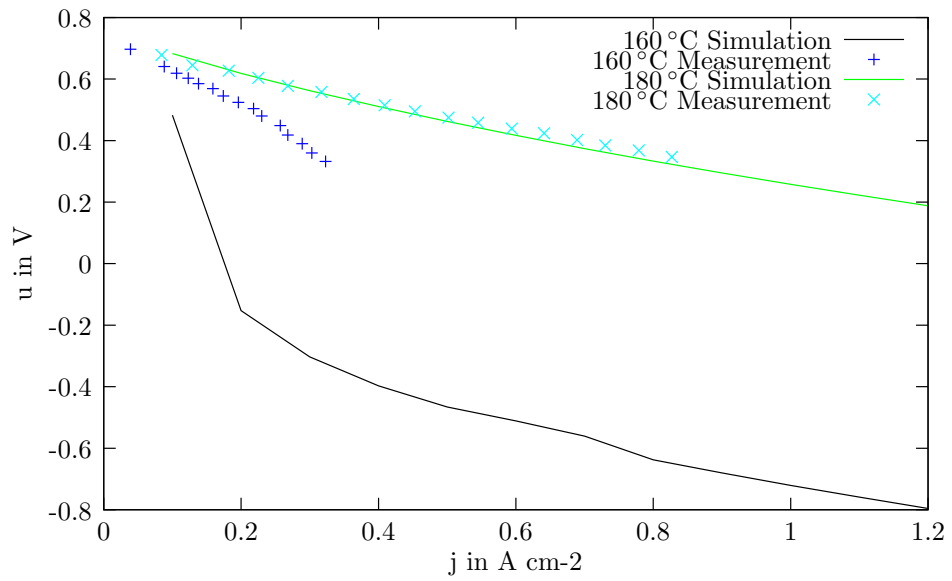
(b) 25 % CO₂ [97]

Figure 4.20: Modeling and measurement results of a single HTPEMFC



(a) 1% CO [97]



(b) 5% CO [97]

Figure 4.21: Modeling and measurement results of a single HTPEMFC

- 75 % hydrogen 24 % carbon dioxide 1 % carbon monoxide (*Fig. 4.21(a)*),
- 75 % hydrogen 20 % carbon dioxide 5 % carbon monoxide (*Fig. 4.21(b)*).

The modeling and measurement results for pure hydrogen are generally in good agreement (*Fig. 4.20(a)*). The model predicts slightly higher voltages, than found during measurement. As the measurement results were extracted from literature data, their precision is not very high.

In the case of the use of diluted hydrogen (*Fig. 4.20(b)*), the predicted voltages are higher than the measured voltages. As diluted hydrogen is used instead of pure hydrogen, lower voltage levels are expected, because the hydrogen partial pressures are lower for the diluted hydrogen. As *Eq. 4.50* does not depend on the hydrogen partial pressure, no change in voltage can be seen from the model. Measurement results show a decrease in voltage using diluted hydrogen instead of pure hydrogen.

The effect of a small contamination with carbon monoxide (*Fig. 4.21(a)*) is represented correctly. For 160 °C the results of the simulation are in good agreement, with the measurement. For 180 °C the simulation results are a little bit more optimistic than the measurement results.

In the case of strong carbon monoxide contamination (*Fig. 4.21(b)*), the model predicts the behavior of the system at 180 °C correctly. The results for 160 °C do not reproduce the voltage development correctly. The voltage drop evaluated by the model is so important that it leads to negative cell voltages. In this case the model leaves its application window. In the case of strong carbon monoxide contamination the fuel cell might be damaged irreversibly. The fuel cell damage depends also on the temperature.

As the system is foreseen to run at temperatures of 180 °C and maximum carbon monoxide contamination well below 5 %, the model introduced by is a valid approach for the modeling of the studied system.

4.7 Conclusion of Fuel Cell Modeling

In this chapter a fuel cell stack model is presented. After giving some basic ideas (4.2), the hypotheses which are assumed are introduced in section (4.3). The interest of this fuel cell model is its application in EMR. Therefore, the fuel cell is described respecting the functionality of the different layers of the fuel cell. This allows taking into consideration at the same time the gas flows in the individual layers and the share of each layer on the overall voltage. The layers of the fuel cell, their modeling and their representation are given one by one in (4.4) before they are connected to the stack model. It is considered that the fuel cell temperature is fixed. This can be achieved by an external cooling system.

The PEFC model was validated against measurements of a Ballard NexaTM fuel cell system (4.5). This validation has been done running a Ballard NexaTM fuel cell system on hydrogen (4.5.1) and on reformat (4.5.2) showing promising results. The fact that the cathodic humidification has not been modeled, leads to differences in the measured and modeled values. This phenomenon can be seen especially at high currents. The model incorporates a permanent anodic purge, whereas the real systems anodic purges occur batch-wise.

As a HTPeMFC architecture was chosen for the fuel cell system realized inside the GAPPAC project, the fuel cell model was adapted to describe the behavior of a HTPeMFC. The basic working principles and the tasks of the layers of the fuel cell do not change between a HTPeMFC and a PEFC. The water transport mechanism is not known for HTPeMFCs; therefore the model for the PEFC is kept for the moment, leaving the possibility of parameter adaptation. The calculation of the HTPeMFC voltage, is based on the work of Korsgaard [95]. His approach is introduced and it is shown that it can be easily adapted to the model structure (4.6.1). With the adaption of the model to the HTPeMFC technology it is shown that the functional, modular approach of EMR is well adapted for model evaluation. The HTPeMFC model is validated against single cell results extracted from literature, using diluted hydrogen as well as carbon monoxide contaminated hydrogen as fuel, section (4.6.2). The results show good agreement for pure hydrogen, the model shows weaknesses at high CO fractions of 5 %. As the fractions causing difficulties are larger than the expected carbon monoxide fractions of our system, the model is well adapted for the system under consideration.

After the introduction of the modeling of the main elements of the fuel cell system, they can thereafter be combined and extended to a system model, which builds the baseline of the control design.

Chapter 5

Fuel Cell System Modeling and Control Structure Design

5.1 Introduction to Control Structure Development

The work has been accomplished in the frame of the project GAPPAC. As well the PEFC as the HTPEMFC showed feasibility to be fed by hydrogen rich gas produced from commercial diesel. The PEFC and the HTPEMFC produce approximatively the same amount of heat that has to be removed from the system. As the HTPEMFC operates on higher temperatures than the PEFC (180 °C instead of 60 °C), the withdrawal of heat is simplified for the HTPEMFC and the heat exchange surface is reduced. Therefore, the HTPEMFC system is likely to need less volume and the utilization of heat for trigeneration purposes is simplified. Furthermore, the demands on fuel purity are less strict for HTPEMFC. All three aspects (volume, trigeneration and fuel composition) show advantages of the HTPEMFC over the PEFC for the application in as diesel supplied auxiliary power unit for transportation applications as it is envisaged inside the GAPPAC project. A HTPEMFC system architecture is therefore used as baseline for the control structure development. The modeling of the two main elements of the fuel cell system has already been introduced. The fuel processor model is introduced in (3), the fuel cell stack model is introduced in (4). To design the control structure, a fuel cell system model has to be available. The introduced elements of the fuel cell system presented before are connected and extended to a fuel cell system model in (5.2). Based on this model the control structure can be designed (5.3). The application of the control including the definition of control parameter is introduced in (5.4). The chapter ends with conclusions and

perspectives (5.5).

5.2 Fuel Cell System Model for Control Structure Design

The fuel cell system for which the control structure shall be developed is the diesel driven HTPEMFC system, defined for the project GAPPAC. The model based control structure will be designed using an overall system model. The evaluated model consist of the supply of the species to the system, the fuel processor unit and the fuel cell stack. The model of the fuel processor unit has already been introduced in (3.6). The model of the HTPEMFC stack has already been introduced in (4.6). Both models can be connected directly, as the molar flow of hydrogen rich gas exiting the fuel processor is at the same time the hydrogen rich gas entering the fuel cell (*Fig. 5.1*).

Until now the mass flows of diesel, water and air supplied to the system have been represented as source blocks (3.3.2). Their supply is not instantaneous and has to be taken into consideration for the control structure development [57].

Diesel and water can be supplied to the system using an electrical driven pump. Air is supplied by an electric driven compressor. The modeling of the diesel supply is introduced. A similar approach is introduced by Boulon [24]. The diesel supply consists of the following elements (*Fig. 5.7*):

Battery

The battery supplies the energy to the system. It is a source of electrical energy. The battery is represented in EMR using a source block (*Fig. 5.2*).

DC/DC Converter:

The rotational speed of the motor is controlled by the voltage supplied to it. Therefore, the voltage supplied by the battery has to be adapted to the desired voltage level. In this case an ideal DC/DC converter is used. It is supposed that it has no losses and the entire power is transferred *Eq. 5.1*. The voltage after DC/DC conversion has to be adapted to the needs of the system. Therefore, the conversion coefficient m_d is used *Eq. 5.2* and *Eq. 5.3*. A DC/DC converter is represented in EMR by a conversion in the same energetic domain, represented

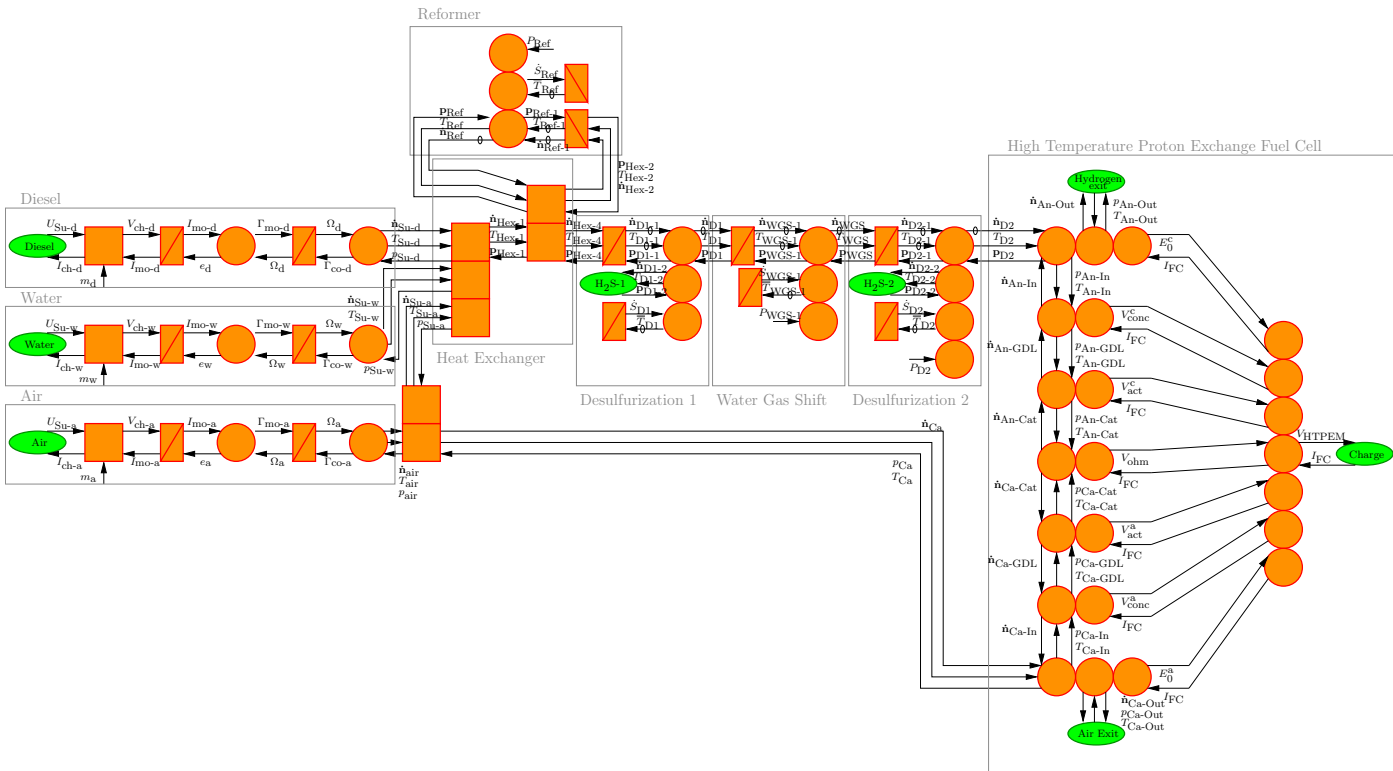


Figure 5.1: EMR of Fuel Cell System containing Diesel, Water and Air Supply, Fuel Processor and Fuel Cell Stack.

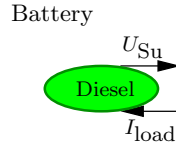


Figure 5.2: EMR of the Battery.

by an orange square (Fig. 5.3).

$$I_{load} \cdot V_{load} = I_{Su} \cdot U_{Su} \quad (5.1)$$

$$V_{load} = m_d \cdot U_{Su} \quad (5.2)$$

$$I_{load} = m_d \cdot I_{mo} \quad (5.3)$$

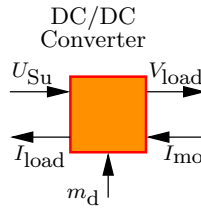


Figure 5.3: EMR of the DC/DC Power Converter

The pump is driven by an electric motor. The motor contains three elements:

- The electric accumulation. Due to the use of winded wires imposes an electric inductance.
- The conversion of electrical energy into mechanical energy, thus representing a conversion between different energetic domains.
- And the shaft that is turning. It represents a mechanic accumulation [31]. The mechanic accumulation might combine the inertia of the motor and the inertia of the pump.

For the EMR representation, the three elements can be introduced individually, starting with the electric accumulation.

Electric Accumulation:

The connection between the motor current (I_{mo}), the supply voltage (V_{load}) and the electromotive force (e) is given in Eq. 5.4. This equation is time dependent

with a derivative term. For the application in EMR this equation has to be written in integral form *Eq. 5.5*. The electric accumulation is represented in EMR using an accumulation block (orange rectangle with bar), (*Fig. 5.4*).

$$V_{ch} - e = L \frac{dI_{mo}}{dt} + R \cdot I_{mo} \quad (5.4)$$

$$\int (V_{ch} - e) dt = L \cdot I_{mo} + R \int I_{mo} dt \quad (5.5)$$

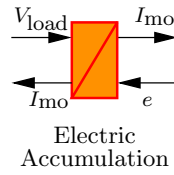


Figure 5.4: EMR of the electric accumulation

Electro-mechanical Conversion:

The electro-mechanical conversion between the motor current I_{mo} and the motor torque Γ_{mo} depends on the electro-mechanical conversion constant (K_e), *Eq. 5.6*. The electromotive force e is calculated by *Eq. 5.7*. The electro-mechanical conversion is represented in EMR using a conversion element for a conversion in different domains, represented by a orange circle, (*Fig. 5.5*).

$$\Gamma_{mo} = K_e \cdot I_{mo} \quad (5.6)$$

$$e = K_e \cdot \Omega_d \quad (5.7)$$

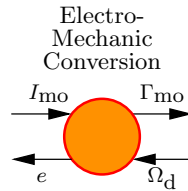


Figure 5.5: EMR of the electro-mechanic conversion.

Mechanic Accumulation:

The rotational speed of the electric motor Ω_d is calculated using the motor inertia Γ_{mo} and the pump inertia Γ_p Eq. 5.10. The calculation takes into account the the system inertia Jm and friction f . This equation is time dependent with a derivative term. For the application in EMR it has to be written in integral form Eq. 5.9. The mechanic accumulation is represented in EMR using an accumulation block (orange rectangle with bar), (Fig. 5.6). The system inertia Jm and friction f contain, in this case, as well the contribution of the motor as the contribution of the pump. It is therefore a concatenation of the motor inertia and the pump inertia (Fig. 2.6).

$$\Gamma_{mo} - \Gamma_p = Jm \frac{d\Omega_d}{dt} + f \cdot \Omega_d \quad (5.8)$$

$$\int (\Gamma_{mo} - \Gamma_p) dt = Jm \cdot \Omega_d + f \int \Omega_d dt \quad (5.9)$$

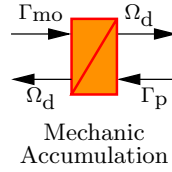


Figure 5.6: EMR of the mechanic accumulation

Pump:

The diesel pump converts the rotational speed of the motor into a diesel molar flow. In the most simplified case it can be assumed that for every turn of the motor a certain molar flow is transported. This can be represented using Eq. 5.10. The mechanic accumulation is represented in EMR using a conversion block (orange circle with red rim), (Fig. 5.7). The torque of the pump Γ_p is calculated by the energy conservation.

$$\dot{n} = \eta_{Pump-d} \cdot k \cdot \Omega \quad (5.10)$$

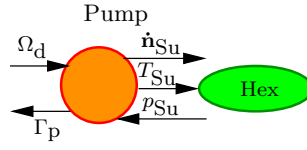


Figure 5.7: EMR of the pump

Diesel, Water and Air Supply

A representation of the diesel supply system is given in (Fig. 5.8).

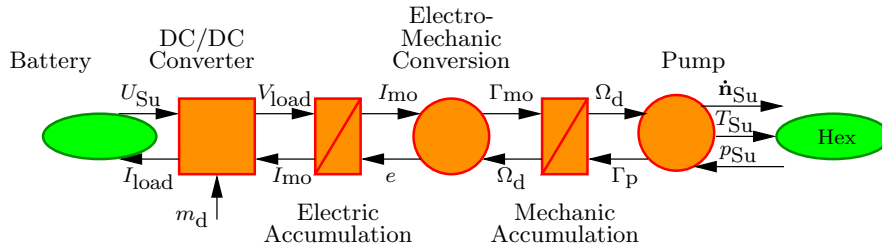


Figure 5.8: EMR of a supply system.

As water is a liquid such as diesel, the water supply can be described in the same way than the diesel supply. Only the parameters might change due to the use of a different motor and/or pump.

The air supply differs from the diesel and water supply. As the air is gaseous and the fuel cell system is pressurized, the air has to be supplied with the help of a compressor. As for the use of a pump an electric motor is used to run the compressor, therefore the elements: battery, chopper, electrical accumulation, electro-mechanical conversion and mechanical accumulation are equivalent, only the parameters differ [24]. The EMR representation of the compressor system is identical to the one of a pump system, (Fig. 5.8). Furthermore, the compressor supplies not only the air needed for the fuel processing, but also the air needed to supply the fuel cell. As the fraction between the both air streams is kept constant in the first approach (H5.2), a coupling element in the same domain, (orange overlapping rectangles) is used to split the air stream, (Fig. 5.1).

5.3 Inversion based Control Structure Design for a Fuel Cell System using EMR

5.3.1 Introduction

The basic approach toward model based control structure development is introduced in (2.2.4). Several steps have to be followed to reach a practical control structure. One important intermediary step on this way is the maximal control structure (MCS). The MCS is the block wise inversion of the model. It is based on the assumption that all values are measurable. The MCS is rarely applicable on a real system, because not all values are measurable with a reasonable effort in time and costs. Furthermore, sometimes it is advantageous to apply simplification steps. In this case the control structure is developed based on the MCS, but there are some spots identified where simplifications are applied to lead to a practical control structure.

H 5.1 *It can be assumed that the mass flow development and the temperature development are decoupled, because their time constants differ in several orders of magnitude (3.5.4). Therefore, the temperature can be assumed to be constant for the mass flow development and the mass flow changes can be assumed to be instantaneous for the temperature development.*

H 5.2 *The fuel cell can only work in a small, well defined working window that is defined by the temperature [96] and the working temperature inside the fuel processor is largely influenced by the fraction between diesel, water and air supplied to the system. Therefore, it can be assumed that the fractions between diesel, water and air supplied to the fuel processor stay constant over the entire working range. Furthermore, both the air demand of the fuel cell stack and the air demand of the fuel processor are proportional to the current drawn from the system (1.1.4). Hence, it can be stated that the fraction between the air supplied to the fuel processor and the air supplied to the fuel cell stack stay constant.*

In order to be able to run a fuel cell sufficient amounts of oxygen and hydrogen have to be supplied at any time. Hence, the species flow control is an important aspect of the system control. In the described system hydrogen rich gas is produced by a fuel processor unit. Diesel, water and air have to be supplied to the fuel processor in order to produce hydrogen rich gas. This is why the control of the diesel, water and air supply is developed as one basic aspect of the control of the system.

The fuel processor unit consists of multiple well defined conversion steps. For the

conversion of diesel into hydrogen rich gas not only the gas fractions, but also the temperatures of the gases in the respective units have to stay in a small well defined working window. This is why the temperature control of the fuel processor units is another basic aspect of the system control. As the time constants attended from the mass flow development and the temperature development are different in several orders of magnitude - around 1 s for the mass flow and around 100 s for the temperature - they can be regarded as decoupled (H5.1).

If, as in this case, the anode has an exit and the diluted hydrogen is consumed elsewhere, for example in a burner, it is common to supply more hydrogen to the anode than needed for the reaction. This tactic inhibits low hydrogen pressures. Low hydrogen pressures can impose voltage drops that can lead to the extinction of the fuel cell. In the worst case irreversible damages might occur. The fraction of hydrogen supplied to the hydrogen needed is called hydrogen stoichiometry $\lambda_H = \dot{n}_{H2 \text{ supplied}} / \dot{n}_{H2 \text{ needed}}$. It can be assumed that the fuel cell shall work with a constant hydrogen stoichiometry λ_H . Hence, the fuel cell itself does not have to be inverted. The reference hydrogen flow $\dot{n}_{H2\text{-in}}$ can be calculated from the reference current $I_{FC\text{-ref}}$, that is the current desired from the system. This conversion is represented by an estimation block (Fig. 5.9) (Tab. 2.4) using the inverse of the Faraday law Eq. 5.11. The use of an estimation block marks the passage from the MCS to the PCS. The ratios between hydrogen and the other species inside the fuel mixture are equally fixed (H5.2). The molar flow vector expected $\dot{n}_{FC\text{-in}}$ can hence be calculated from the reference hydrogen flow $\dot{n}_{H2\text{-in}}$ times a vector representing the expected ratios x_H , Eq. 5.12. One estimation block is sufficient to calculate the reference fuel vector of the anode $\dot{n}_{FC\text{-ref}}$.

$$\dot{n}_{H2\text{-in}} = \frac{\lambda_H n I_{FC\text{-ref}}}{2 F} \quad (5.11)$$

$$\dot{n}_{FC\text{-ref}} = \dot{n}_{H2\text{-in}} \cdot x_H \quad (5.12)$$

Likewise, the cathodic part of the fuel cell is described using an estimation block containing the Faraday law extended by the oxygen stoichiometry λ_O , Eq. 5.13. The oxygen stoichiometry is the ratio between the oxygen supplied to the fuel cell stack against the oxygen needed for the reaction, it shall not be mistaken with the air fraction which is the fraction between the amounts of gas supplied to the fuel processor and the to fuel cell. The amount of oxygen supplied to the fuel cell is extended by a vector representing the expected ratio of nitrogen x_H , Eq. 5.14 to build the air vector required by the fuel cell cathode $\dot{n}_{Ca\text{-ref}}$.

$$\dot{n}_{\text{O2-in}} = \frac{\lambda_{\text{O}} n I}{4 F} \quad (5.13)$$

$$\dot{n}_{\text{Ca-ref}} = \dot{n}_{\text{O2-in}} \cdot x_{\text{O}} \quad (5.14)$$

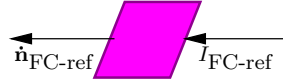


Figure 5.9: Estimation block representing the fuel cell for mass flow control.

5.3.2 Mass Flow Control

The control structure of the mass flow control is obtained by inversion of the control chain between the fuel cell entrance and the mass flow supply. The amount of hydrogen rich gas at the fuel processor outlet shall be controlled. As the entire system is complex, first the inversion from the fuel cell entrance to the fuel processor unit entrance and afterward the inversion for the three supply flows will be described. It is intended to find out by means of which parameter the quantities of the gas flows can be described.

The control chain between the fuel cell entrance and the fuel processor entrance is highlighted in (Fig. 5.10, yellow highlights). It consists of:

- the molar flow vector coming out of the second desulfurization unit, \dot{n}_{D2} ;
- the molar flow vector coming out of the pressure drop of the second desulfurization unit, $\dot{n}_{\text{D2-1}}$;
- the molar flow vector coming out of the water gas shift unit, \dot{n}_{WGS} ;
- the molar flow vector coming out of the pressure drop of the water gas shift unit, $\dot{n}_{\text{WGS-1}}$;
- the molar flow vector coming out of the first desulfurization unit, \dot{n}_{D1} ;
- the molar flow vector coming out of the pressure drop of the first desulfurization unit, $\dot{n}_{\text{D1-1}}$;
- the molar flow vector between the heat exchanger and the first desulfurization unit, $\dot{n}_{\text{Hex-4}}$;

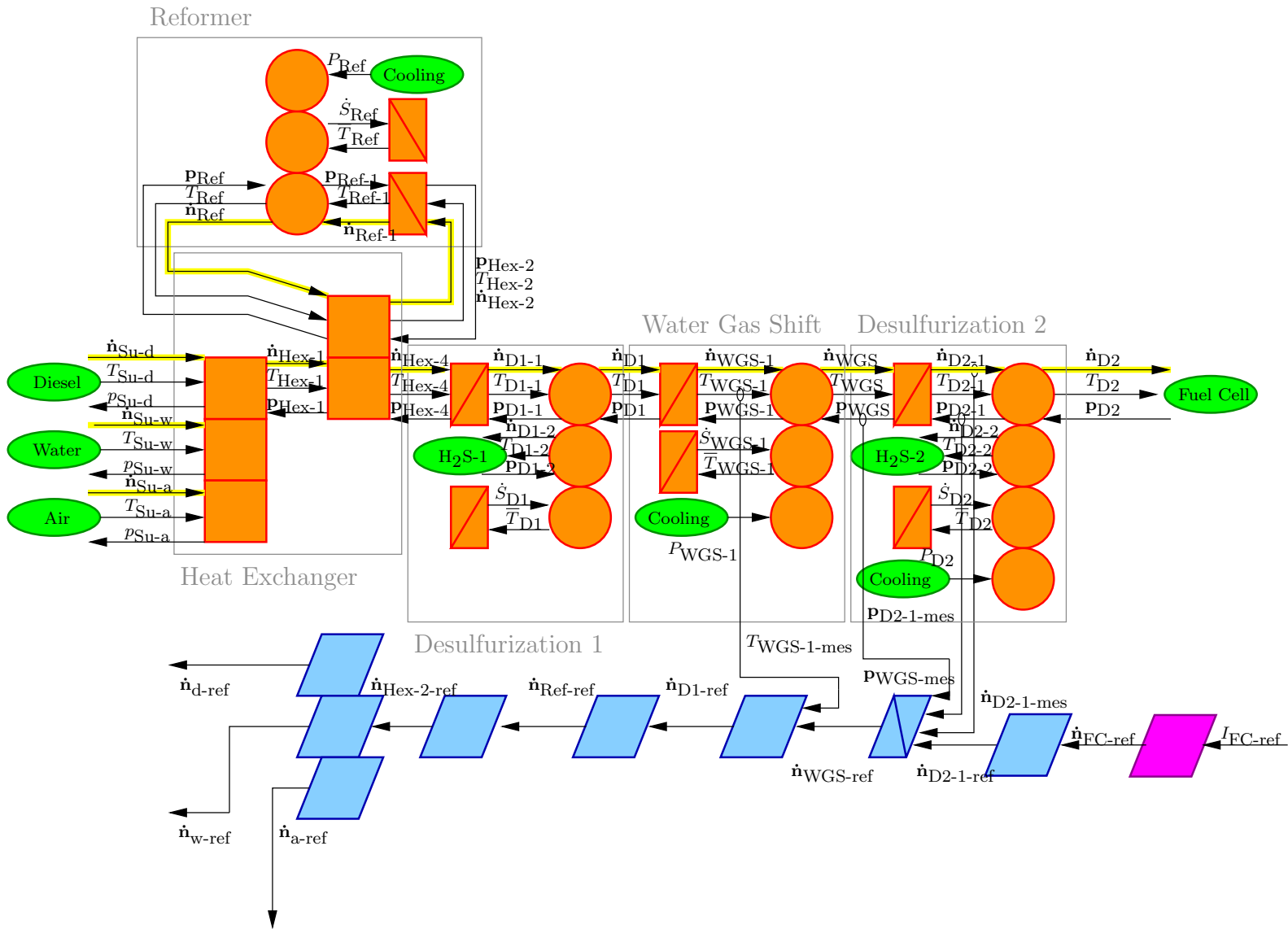


Figure 5.10: EMR and control structure of the system between heat exchanger entrance and fuel cell entrance.

- the molar flow vector coming out of the reformer, \dot{n}_{Ref} ;
- the molar flow vector coming out of the pressure drop of the reformer, $\dot{n}_{\text{Ref-1}}$;
- the molar flow vector between the heat exchanger and the reformer, $\dot{n}_{\text{Hex-2}}$;
- the molar flow vector coming out of the element mixing the diesel, water and air molar flow, $\dot{n}_{\text{Hex-1}}$
- the three molar flow vectors entering the fuel processor unit, $\dot{n}_{\text{Su-d}}$, $\dot{n}_{\text{Su-w}}$ and $\dot{n}_{\text{Su-a}}$.

Once the control chain is defined the elements along the control chain can be inverted one by one.

Desulfurization 2

To invert the desulfurization units the proportional connection between the final and the initial sulfur content via the known system selectivity as introduced in *Eq. 1.25* is used. All elements but the sulfur content stay unchanged *Eq. 5.15*, *Eq. 5.16*. (The numbers 1 – 10 refer to lines of the vector containing all elements introduced in (2.6.3).) The inversion of the desulfurization block is represented by a control block *Tab. 2.4*, (*Fig. 5.11*).

$$\text{for } i = 1 - 4; 6 - 10 \quad \dot{n}_{\text{D2-1-ref}}^{(i)} = \dot{n}_{\text{FC-ref}} \quad (5.15)$$

$$\text{for } i = 5 \quad \dot{n}_{\text{Sulfur-D2-1-ref}}^{(i)} = \frac{\dot{n}_{\text{Sulfur-FC-ref}}}{1 - sel} \quad (5.16)$$

The pressure development block contains a time dependency, *Eq. 3.51* and *Eq. 3.52*. Hence, its inversion requests the use of a controller. As it is a first order time dependency a PI controller has been chosen represented by a control block with controller, *Tab. 2.4*, (*Fig. 5.11*). For reasons of simplicity only one controller is used to respond to the four pressure drop blocks inside the system. (The control of several first order time dependancies in the same order of magnitude is not evident.) The use of only one controller means a simplification of the control toward the PCS.

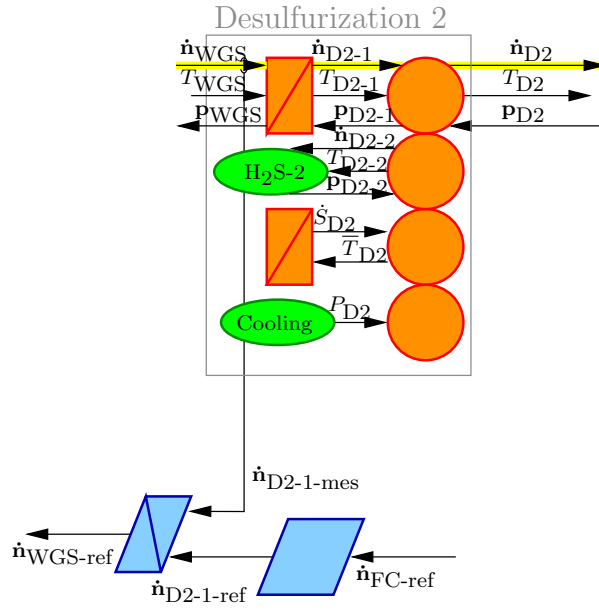


Figure 5.11: EMR and control structure of Desulfurization 2

Water Gas Shift

The water gas shift reaction is a conversion reaction that is not time dependent. Its inversion can thus be represented by a control block without controller, *Tab. 2.4*, (*Fig. 5.12*). The water gas shift reaction uses the fact that the equilibrium between hydrogen, carbon dioxide, carbon monoxide and water depends on the temperature (1.3.2). This connection can also be used for the inversion of the block. The reference value of the gas composition downstream of the water gas shift reaction block is known $\dot{n}_{\text{WGS-ref}}$. The temperature upstream of the water gas shift reaction block $T_{\text{WGS-1-mes}}$ can be measured. Hence, the gas composition at the upstream temperature $\dot{n}_{\text{D1-ref}}$ can be evaluated by applying the reaction advancement ξ to the reference gas flow vector $\dot{n}_{\text{WGS-ref}}$. The reaction advancement ξ for the measured temperature $T_{\text{WGS-1-mes}}$ and the reference gas flow vector $\dot{n}_{\text{WGS-ref}}$ can be calculated using *Eq. 1.8* and *Eq. 1.9*. The representation of the Water Gas Shift modeling and control in EMR is given in (*Fig. 5.12*).

Desulfurization 1

The inversion of the first desulfurization is equivalent to the inversion of the second desulfurization unit that has already been introduced.

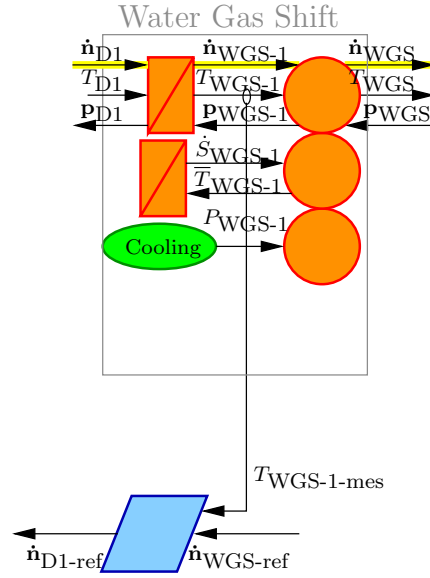


Figure 5.12: EMR and control structure of Water Gas Shift Reaction

Heat Exchanger

Inside the heat exchanger block it can be assumed that no change of the gas composition occurs, (*H3.6*). As the gas composition stays unchanged, no control block is needed for the massflow control, *Eq. 5.17*. The fact that a coupling block that is not changing the molar flow vector is not represented in the control structure, means a simplification of the system toward the PCS.

$$\dot{n}_{\text{Hex-1-ref}} = \dot{n}_{\text{Hex-2-ref}} \quad (5.17)$$

Reformer

The reaction taking place inside the reformer is a conversion reaction that is not time dependent. Its inversion can thus be represented by a control block without controller *Tab. 2.4*, (*Fig. 5.13*). To invert the reformer block, the assumption is made that the reformer has to run in a limited working window, defined by constant fractions between diesel, water and air input *Eq. 5.24*, *Eq. 5.25* and *Eq. 5.26*. Those constant fractions are supplied as system parameters by N-GHY and are used to find the mass flows of diesel, water and air corresponding to a certain, imposed hydrogen flow. Furthermore, the element balance of each element can be introduced. For the element balance the conception of diesel $C_nH_mO_pS_q$

has to be known. Hence, the coefficients n, m, p, q are used. Furthermore, every element in the gas mixture has to be addressed individually. The sulfur content is neglected for the control, because it represents only a very small fraction of the gas flows. The hydrogen balance is given in Eq. 5.18 and Eq. 5.19. The oxygen balance is given in Eq. 5.20, Eq. 5.21 and Eq. 5.22. The nitrogen balance is given in Eq. 5.23. The reformer is inverted using the inversion of a conversion element (Fig. 5.13).

Hydrogen-balance:

$$f_{WD} = \frac{\dot{n}_{\text{Hex-2-ref}}(H_2Og)}{\dot{n}_{\text{Hex-2-ref}}(Diesel)} \quad (5.18)$$

$$m \cdot \dot{n}_{\text{Hex-2-ref}}(Diesel) + 2 \cdot \dot{n}_{\text{Hex-2-ref}}(H_2Og) = 2 \cdot \dot{n}_{\text{Ref-ref}}(H_2) + 2 \cdot \dot{n}_{\text{Ref-ref}}(H_2Og) \quad (5.19)$$

Oxygen-balance:

$$f_{WD} = \frac{\dot{n}_{\text{Hex-2-ref}}(H_2Og)}{\dot{n}_{\text{Hex-2-ref}}(Diesel)} \quad (5.20)$$

$$f_{OD} = \frac{\dot{n}_{\text{Hex-2-ref}}(O_2)}{\dot{n}_{\text{Hex-2-ref}}(Diesel)} \quad (5.21)$$

$$p \cdot \dot{n}_{\text{Hex-2-ref}}(Diesel) + 2 \cdot \dot{n}_{\text{Hex-2-ref}}(H_2Og) + 2 \cdot \dot{n}_{\text{Hex-2-ref}}(O_2) = \dot{n}_{\text{Ref-ref}}(CO) + 2 \cdot \dot{n}_{\text{Ref-ref}}(CO_2) + \dot{n}_{\text{Ref-ref}}(H_2Og) \quad (5.22)$$

Nitrogen-balance:

$$f_{NO} = \frac{\dot{n}_{\text{Hex-2-ref}}(N_2)}{\dot{n}_{\text{Hex-2-ref}}(O_2)} \quad (5.23)$$

Factors:

$$f_{WD} = 20.1 \quad (5.24)$$

$$f_{OD} = 7.37 \quad (5.25)$$

$$f_{NO} = 3.87 \quad (5.26)$$

Mixing Unit

In the mixing unit a non time dependent coupling occurs. The inversion of such an element can be done using a control block with coupling, Tab. 2.4. The inverse of the mixing is a split. The molar flow vector representing the mixture is split in three molar flow vectors: one representing the diesel flow ($\dot{n}_{d\text{-ref}}$), one representing the water flow ($\dot{n}_{w\text{-ref}}$) and one representing the air flow (containing

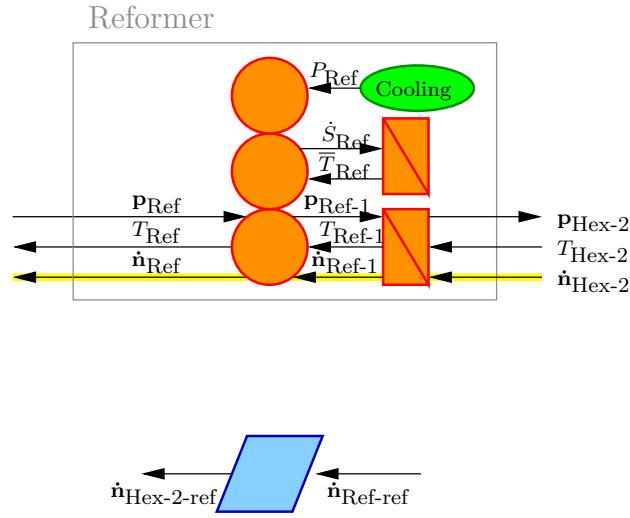


Figure 5.13: EMR and control structure of Reformer

oxygen and nitrogen) (\dot{n}_{a-ref}). Finally, the molar flow vector can be split inverting the mixing element, as each element of the vector can be attributed to one of the three supply flows, (Fig. 5.14).

Mass Flow Supply

The three supply mass flows (diesel, water and air) have to be controlled. They are controlled in the same way that is why the strategy is introduced only once for the water supply.

In the first step the control chain is defined from the reformer inlet to the mass flow supply. The control chain contains the speed of the motor Ω , the motor torque Γ , the motor current I_{mo} and the chopper voltage V_{ch} , see yellow highlights in (Fig. 5.15).

The molar flow vector \dot{n}_{Su} has to be controlled. Therefore, the pump is inverted in (Fig. 5.15, 5 and 5'). It can be inverted using Eq. 5.10. The reference turning speed Ω_{Ref-w} can be calculated using Eq. 5.27.

$$\Omega_{Ref-w} = \frac{\dot{n}}{\eta_{Pump-w} \cdot k} \quad (5.27)$$

The mechanic accumulation (Fig. 5.15, 4) has to be inverted to find the reference torque $\Gamma_{mo-w-ref}$. As it contains a time dependent element, a controller

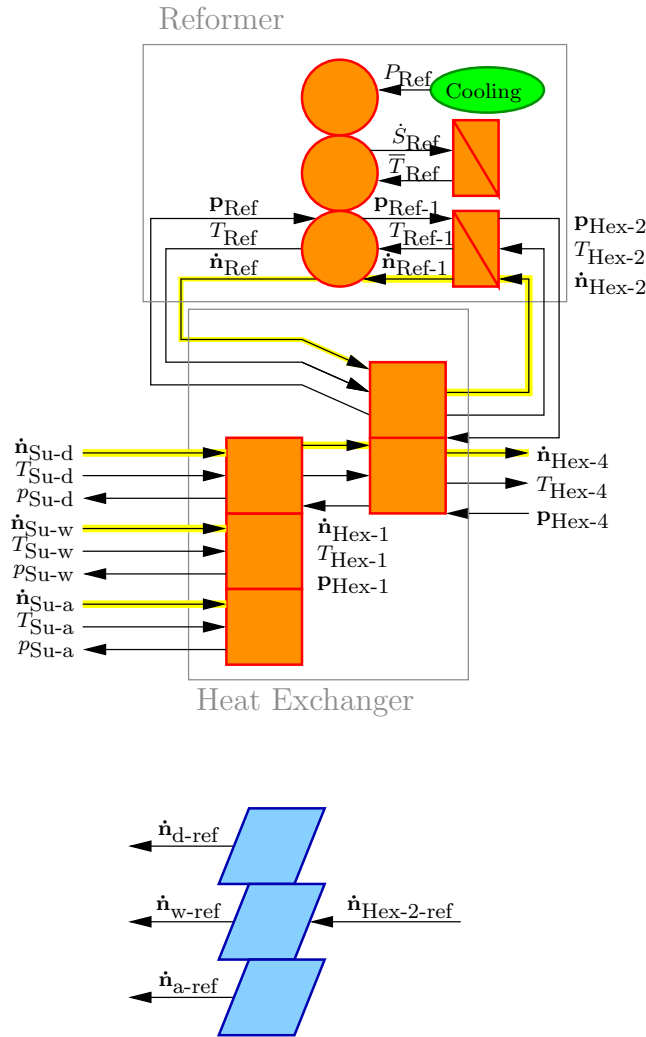


Figure 5.14: EMR and MCS of Heat Exchanger/Gas Mixing unit

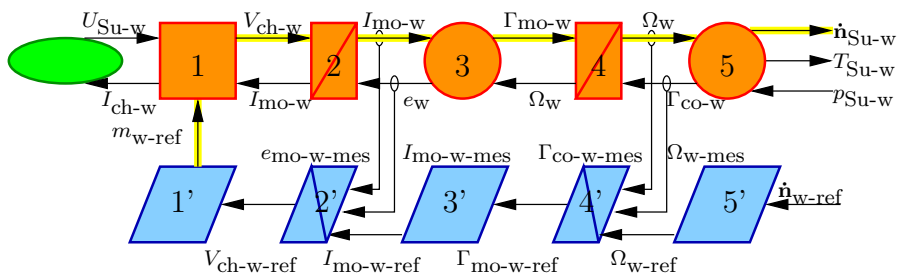


Figure 5.15: EMR and MCS of the water supply system.

has to be used to invert the accumulation element. A PI controller is used and parametrized (Eq. 5.28) by pole placement. For the control, the turning speed of the motor has to be measured Ω_{w-mes} in order to level it with the reference value. Furthermore, the torque $\Gamma_{co-w-mes}$ has to be measured to be able to find the reference value of the motor torque $\Gamma_{mo-w-ref}$.

$$\Gamma_{mo-w-ref} = \Gamma_{co-w-mes} + (\Omega_{w-ref} - \Omega_{w-mes}) \cdot K_p \left(1 + \frac{1}{T_n \cdot s} \right) \quad (5.28)$$

The electro-mechanic conversion (Fig. 5.15, 3) can be described using the proportional connection between the motor torque Γ_{mo} and the motor current I_{mo-w} as introduced in Eq. 5.5. The inversion of the electro-mechanical conversion is represented by the conversion block (Fig. 5.15, 3').

The electric inductance (Fig. 5.15, 2) has to be inverted. As this element is time dependent, a controller has to be used to invert it. A PI controller is used and parametrized by pole placement. A control block is used for its representation (Fig. 5.15, 2'). The reference supply voltage $V_{ch-w-ref}$ has to be evaluated. Therefore, the electromagnetic force e_{w-mes} and the motor current $I_{mo-w-mes}$ have to be measured. The control is effectuated using Eq. 5.29.

$$V_{ch-w-ref} = e_{w-mes} + (I_{mo-w-ref} - I_{mo-w-mes}) \cdot K_p \left(1 + \frac{1}{T_n \cdot s} \right) \quad (5.29)$$

The conversion of the DC/DC converter (Fig. 5.15, 1) can be done using Eq. 5.2. As the supply voltage of the battery U_{Su-w} is constant, the conversion constant m_{w-ref} can be calculated using Eq. 5.30. The inversion is presented by a control element (Fig. 5.15, 1').

$$m_{w-ref} = \frac{V_{ch-w-ref}}{U_{Su-w}} \quad (5.30)$$

The control structure of the fuel cell system model shows that the hydrogen rich gas production depends on the supply of diesel, water and air to the fuel processor. It is shown that the supply of water can be controlled via the conversion constant for DC/DC conversion m_{w-ref} . The control of the diesel and air can be done analogue via the conversion constant of the DC/DC conversion m_{d-ref} and m_{a-ref} . The control of these values allows to assure an appropriate flow of hydrogen rich gas at the fuel cell entrance, taking into consideration different current demands.

5.3.3 Temperature Control

For the temperature control inside the fuel processor unit it is considered that the fuel processing unit works only inside a small and well defined working window. The expected temperature of the gas after each block T_{ref} is well known. If this temperature is not obtained, it is not possible to achieve the desired fuel conception. Furthermore, the model might leave its limits of validity. Hence, to control the gas temperature every unit of the fuel processor is considered separately. Here, the temperature control for the water gas shift reaction is introduced, the temperature control for the other modules is developed analogue.

The control chain starts at the gas temperature at the outlet of the water gas shift reaction T_{WGS} . The gas temperature can only be influenced via the cooling power P . The gas temperature at the outlet of the water gas shift reaction and the cooling power are connected by a coupling block containing the chemical reaction. The coupling element does not have a time dependent term. Therefore, the temperature control can be realized using a conversion block. The example of the water gas shift unit is given in (Fig. 5.16).

Inside the coupling block the water gas shift reaction takes place, at the same time it is the place where a heat exchange with the box and the cooling of the module takes place. All reactions are connected by the energy flow balance Eq. 5.31, as introduced in (2.6.1, p. 43). It has been shown in (3.3.4, p. 63) that the molar flow vector \dot{n}_{WGS} and downstream temperature T_{WGS} can only be evaluated by an iterative process. As the system is inverted the heat flow to the box is neglected and it can be assumed that all other values are measurable. Hence, the only unknown in the energy flow balance is the cooling power P . The upstream temperature $T_{\text{WGS-1}}$ and the upstream molar flow vector $\dot{n}_{\text{WGS-1}}$ are measured as well as the downstream molar flow vector \dot{n}_{WGS} .

$$0 = \dot{H}_{\text{out}}(T_{\text{in}}, p_{\text{in}}) - \dot{H}_{\text{in}}(T_{\text{out}}, p_{\text{out}}) + \Delta\dot{Q} + \Delta P \quad (5.31)$$

$$0 = \dot{n}_{\text{WGS}} \cdot \mathbf{h}(T_{\text{WGS}}, p_{\text{WGS}}) - \dot{n}_{\text{WGS-1-mes}} \cdot \mathbf{h}(T_{\text{WGS-1-mes}}, p_{\text{WGS-1-mes}}) + P \quad (5.32)$$

It has been assumed in (H3.15) that the cooling is not time dependent. Therefore, the temperature control can be realized without the need to use a specified controller, which is equal to the use of a proportional controller. The hypothesis to neglect the time dependency of the cooling is strong. It has to be considered carefully if the application of the temperature control with a proportional controller can lead to promising results or if the hypothesis neglecting the time dependency has to be rejected and the model has to be enhanced accord-

ingly.

The same procedure to develop the temperature control as presented for the water gas shift reaction has to be applied for each element inside the fuel processing unit which is actively cooled. Those elements are: the reformer, the water gas shift reaction and the second desulfurization unit.

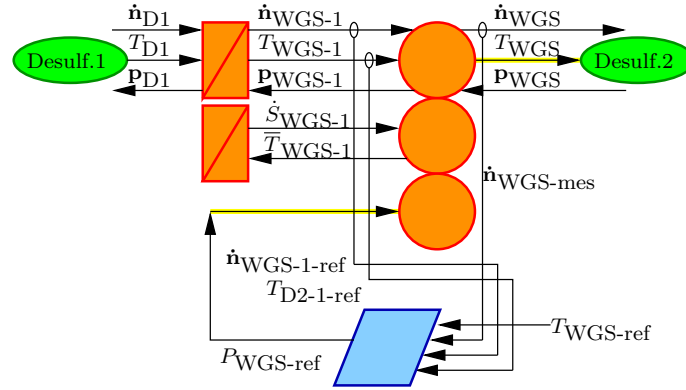


Figure 5.16: EMR and temperature MCS of the water gas shift unit.

5.3.4 Overall System

In subsection (5.3.2) the mass flow control for the mass flow supplies of the fuel processor and fuel cell system are introduced. Subsection (5.3.3) introduces the approach of the temperature control of one block inside the system, using the water gas shift reaction as example. The introduced molar flow control structure has to be applied on all flow supplies. The introduced temperature control structure has to be applied on all blocks with temperature development, leading to an overall system control with respect to mass flow and temperature. As the real system is not available, the control structure will first be evaluated by simulation. An overall picture of the fuel cell model and the mass flow and temperature control structure can be seen in (Fig. 5.17).

5.4 Application of Control

The control structure has been developed for a diesel supplied HTPMFC system as it is proposed by GAPPAC including the temperature and the molar flow evolution controls (Fig. 5.17). A current profile changing in steps is applied to the system. The current profile for the study of the molar flow development is

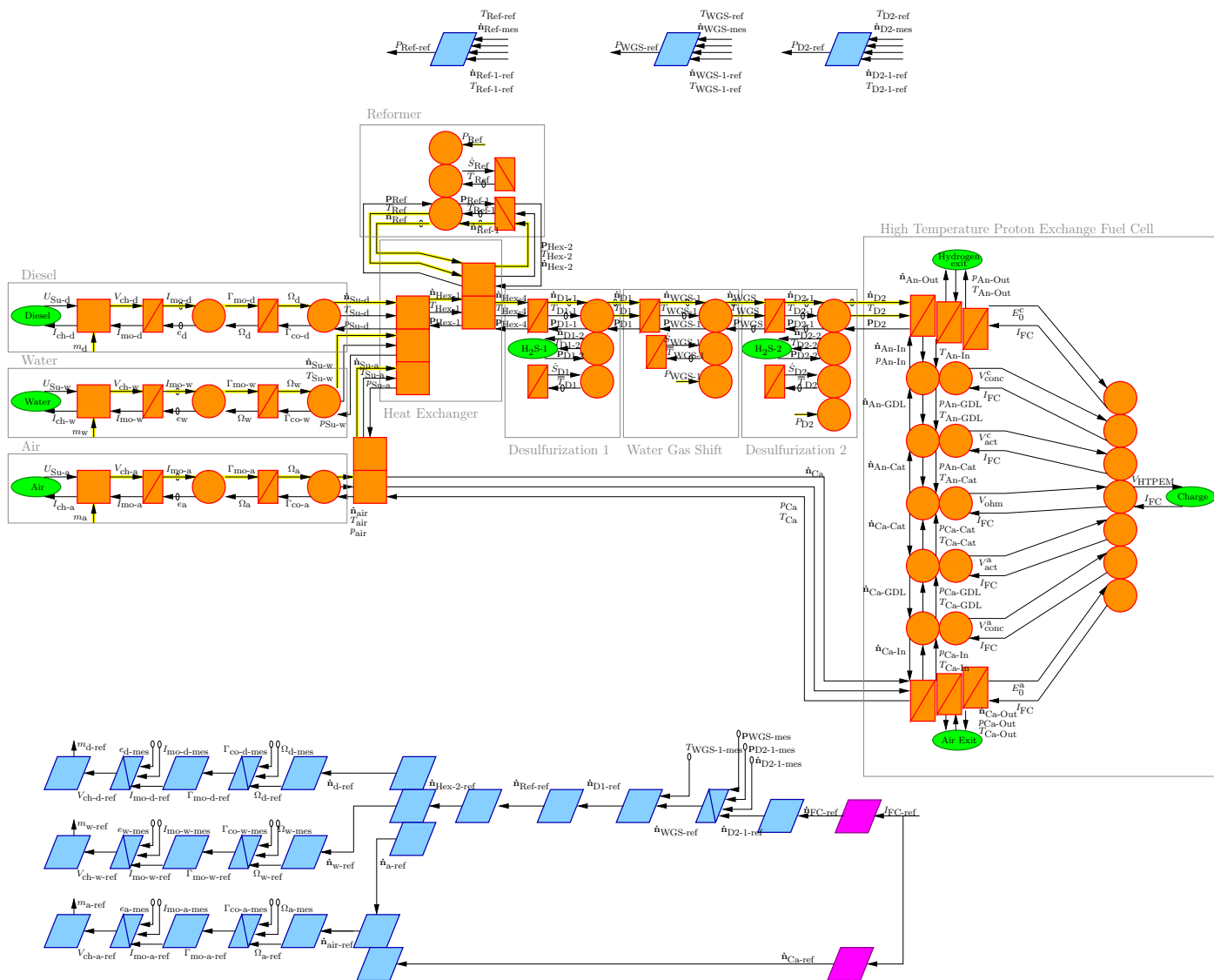


Figure 5.17: EMR and MCS of a diesel supplied HTPEMFC system

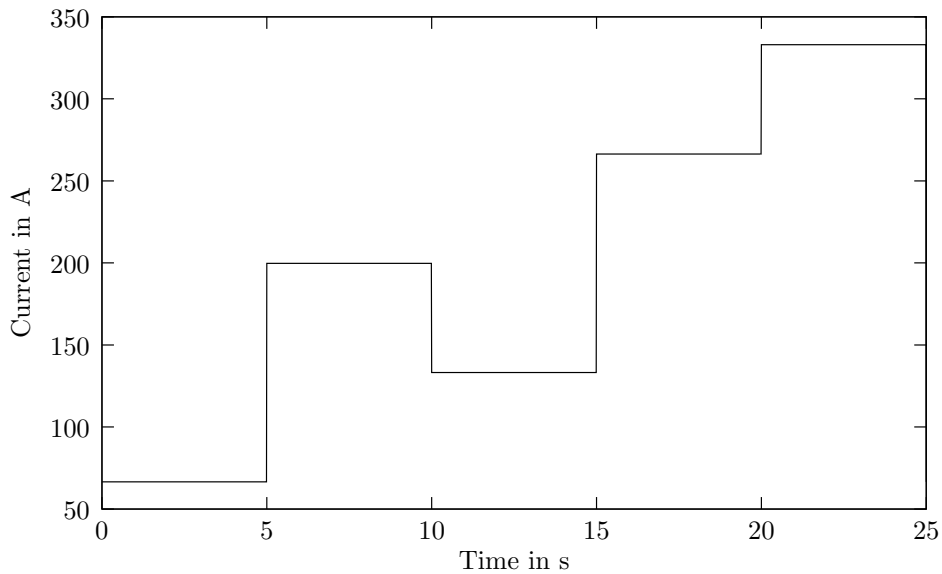


Figure 5.18: Current profile submitted to the mass flow control.

given in (Fig. 5.18).

For the molar flow evolution, the changes of the fractions of hydrogen, oxygen, water and carbon monoxide have been calculated.

The molar flow evolution of hydrogen is given in (Fig. 5.19). The system is supplied with diesel, which has to be transformed into hydrogen. The molar fraction of diesel is small compared to the fraction of hydrogen. This can be explained by the fact that diesel is a long chain molecule containing several hydrogen atoms. The fact that no hydrogen molar flow difference can be seen between the heat exchanger and the first desulfurization unit is explained by the fact that no change in the hydrogen molar flow is imposed by the desulfurization unit. The hydrogen molar flow fraction after the water gas shift and the second desulfurization are the same because the desulfurization does not impose a change in hydrogen molar flow. The hydrogen molar flow after the water gas shift and the second desulfurization unit is higher than the hydrogen molar flow before the water gas shift. It can be concluded that the water gas shift increases the hydrogen fraction. The molar flows follow the changes in current. After a period of 2 s, the pumps and compressors followed the load step. There are overshoots at the moment where the step change occurs. The parameters to describe the pumps and the compressors are preliminary. Once final values can be derived from the real system an optimization of the control parameters has to be done.

The oxygen supplied to the fuel processor is consumed entirely inside the re-

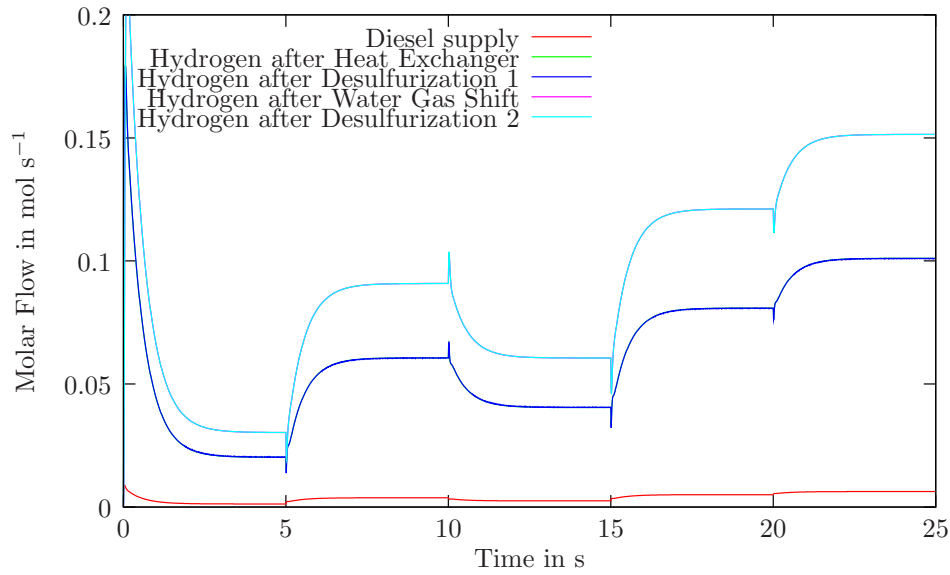


Figure 5.19: Hydrogen molar flow evolution

former. Its supply follows the demand in a way equivalent of the hydrogen molar flow. Therefore, the oxygen supply has not been demonstrated in a figure.

The water molar flow evolution is presented in (Fig. 5.20). Water is supplied to the fuel processor in form of liquid water. The liquid water is evaporated inside the heat exchanger and it can be considered as gaseous throughout the rest of the fuel processor, (H 3.2). It is shown in (Fig. 5.20) that not the entire water supplied to the system is transformed in the reaction. A certain quantity of water is available at every step of the fuel processing as well as the fuel cell entrance (after Desulfurization 2). The water at the exit of the water gas shift unit stabilizes more rapidly than the water fractions further upstream. Reason for this is that the temperature after the water gas shift unit is imposed. Inside the water gas shift unit an equilibrium reaction takes place. As the fraction of water downstream the water gas shift reaction is temperature dependent, it stabilizes quickly.

The development of the carbon monoxide molar fraction is introduced in (Fig. 5.21). As carbon monoxide poisons the fuel cell, its content has to be reduced before the gas enters the fuel cell. It is shown in (Fig. 5.21) that the carbon monoxide ratio is reduced largely after the water gas shift reaction.

For the temperature evolution a current profile equivalent to the one used before is applied. Only difference is that the time steps occur every 500 s, (Fig. 5.22).

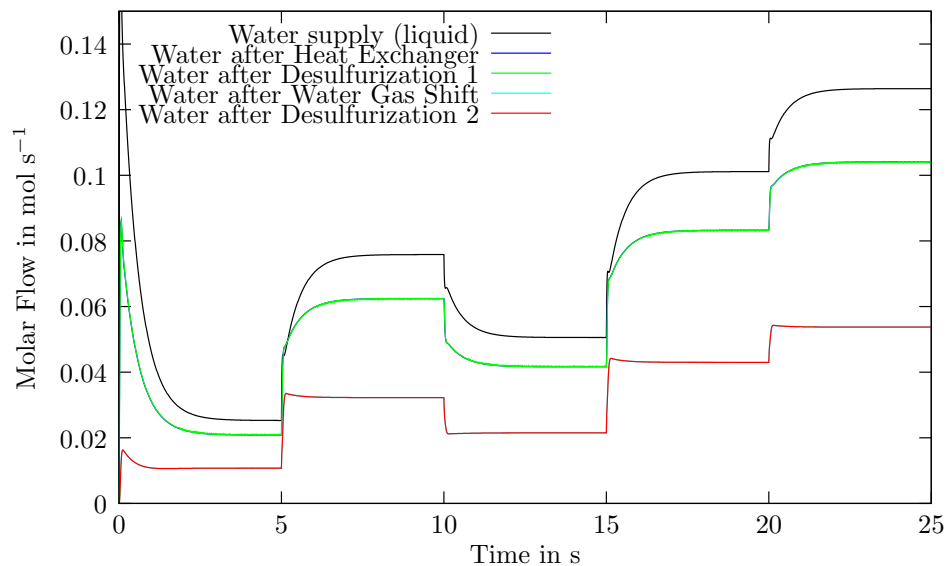


Figure 5.20: Water molar flow evolution

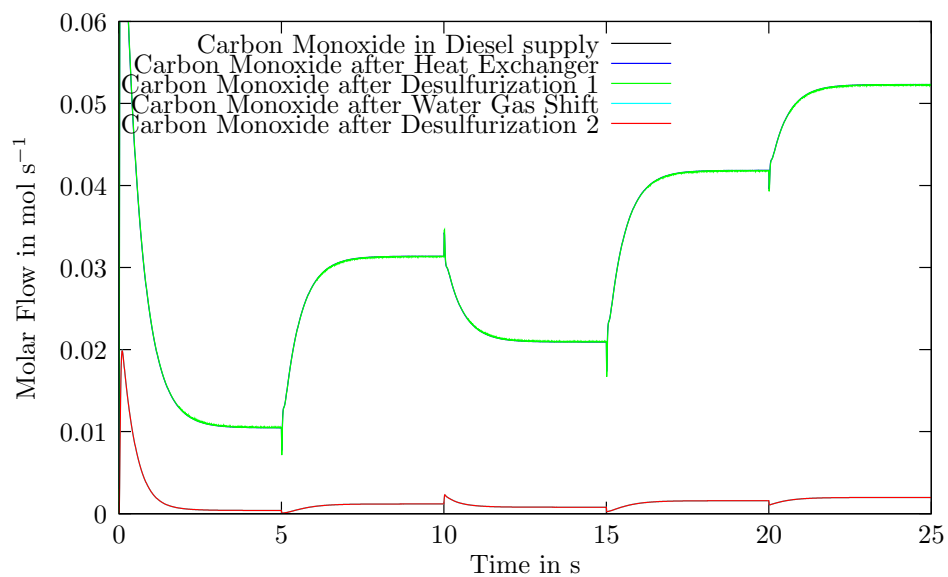


Figure 5.21: Carbon monoxide molar flow development

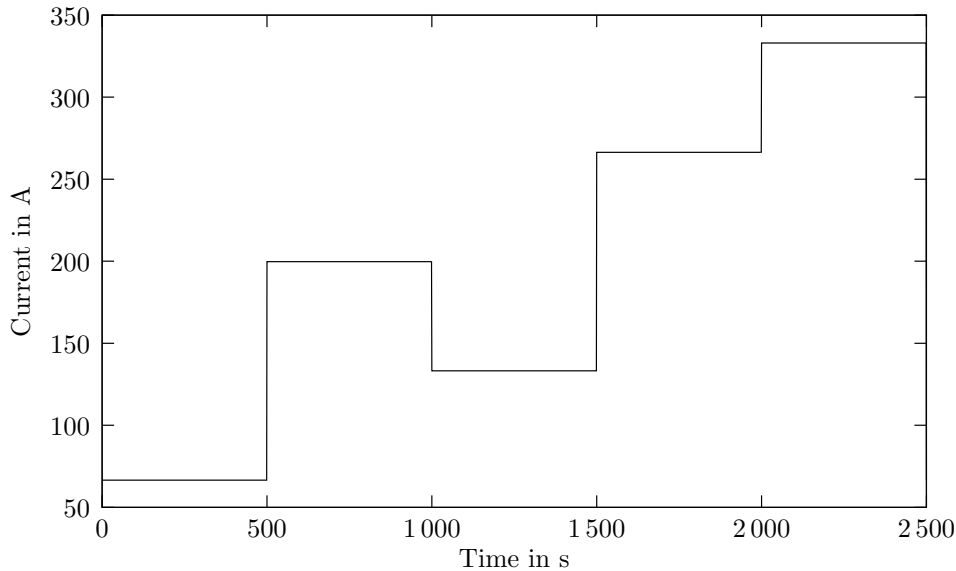


Figure 5.22: Current profile submitted to the temperature control.

The temperatures of the surrounding modules have been initialized as ambient temperature, only the combined heat exchanger reformer unit is considered to be at 650°C . The temperature limits for the gases provided for the system are:

- 1400°C for the reformer outlet,
- 222°C at the outlet of the water gas shift
- and 200°C at the outlet of the second desulfurization unit.

The model leads to the results regarding temperature evolution presented in (Fig. 5.23) for the gas stream leaving the modules and in (Fig. 5.24) for the surrounding boxes of the respective modules.

The temperature at the reformer does not reach the limit value during the course of the simulation. Inside the real system, the heat exchanger and the reformer are directly coupled. The system supplier N-GHY has measured a gas temperature after the reformer and a gas temperature after the heat exchanger. It was not possible to find a set of parameter providing both temperatures correctly. A parameter set giving the desired temperature of the heat exchanger output was chosen. This leads to a lower reformer temperature, leading to the fact that the reformer cooling limit is not reached.

The temperature of the first desulfurization unit is not controlled. It reflects the temperature at the heat exchanger, which is cross-linked with the reformer

showing complex interactions. That is why a current increase might lead to the drop in gas temperature (at 600 s). The temperatures arrive rapidly at constant values. Slight overshoots can be seen for the gas temperature after the first desulfurization unit, but they are reduced during the following blocks. The overshoots can be explained by numerical problems. Due to the fact that there is no accumulation inside the cooling system there is an algebraic loop between the system model and the control. Once the time delay of the cooling is taken into consideration, those overshoots will disappear.

The current of 60 A demanded as first value during the simulation is not sufficient to heat up the gas streams. Only cooling has been taken into account in this case. The model showed that normal working conditions are not necessarily sufficient to reach the desired temperatures. It has to be considered if a heat up strategy has to be applied for the system start up.

The heat up of the boxes is shown in (Fig. 5.24). The heat exchanger box

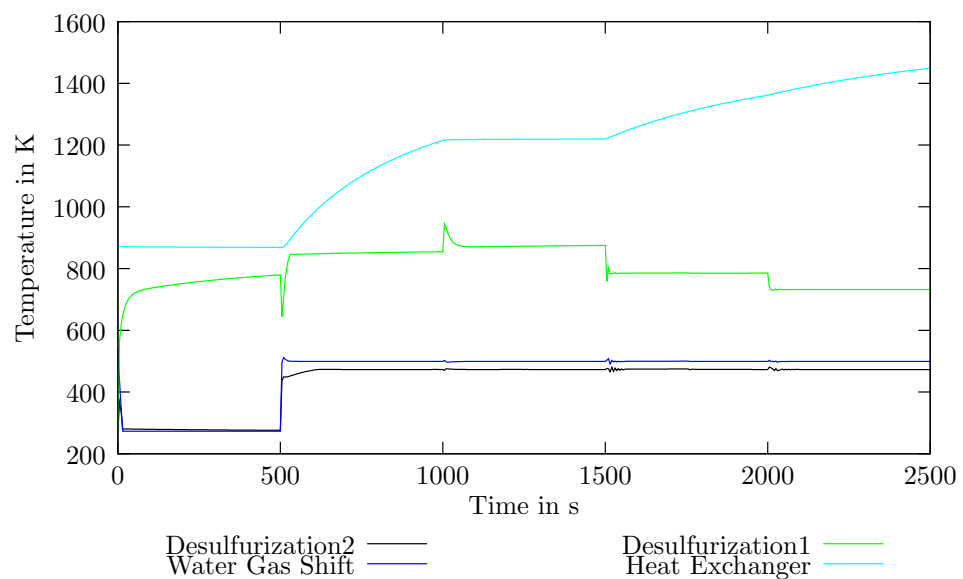


Figure 5.23: Temperature evolution of the gases

shows rapid heat up (also because it has been preheated). It shows the same over/or undershoots for step changes as the gas flows. The other boxes heat up much slower. They do not reach their final temperatures in the period of the experiment.

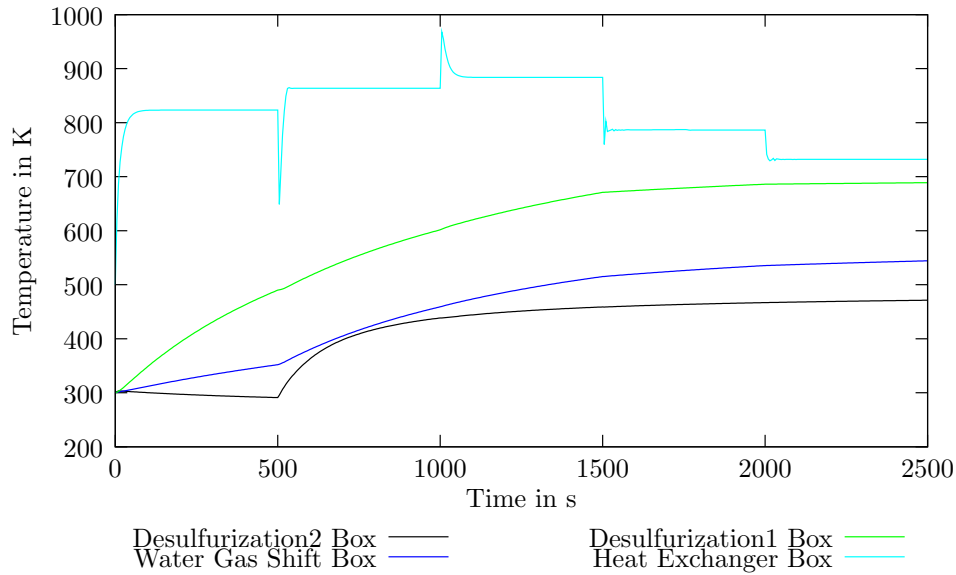


Figure 5.24: Temperature evolution of the surrounding boxes.

5.5 Conclusions and Perspectives of Control Development

In this chapter the control structure for a diesel supplied HTPEMFC system is developed. The control structure with regard to the temperature and the mass flow control for the FCS is developed. After the overall system is introduced using EMR (5.2). The control structure with regard to mass flow control can be derived straight forward by the inversion of the modeling blocks following the control chain (5.3.2). The inversion of the model leads to the control structure. In this case the DC/DC converter constant is changed to adapt the mass flows. For the mass flow control the volumes of all elements of the fuel processor are lumped into one element, the volume of the fuel cell stack is neglected against the volumes inside the fuel processor.

The control structure for the temperature control is evaluated in (5.3.3). The assumption has been made that the cooling is instantaneous. Hence, the temperature control is not time dependent.

The system control is based on a number of hypotheses. The fact that the time dependent behavior of the cooling was neglected might impose differences between the modeled and the real system. It is desirable to refine the modeling and the control approach with this respect. Furthermore, the cathode humidification of the fuel cell stack and the temperature development of the fuel cell stack have not been regarded in this work. The modular approach of EMR gives the

possibility to extend the system model in this respect.

The applied approach for model based control structure design is clear and easy to adapt. It leads rapidly to a control structure without the need to derive the overall system transfer function. The controllers that appear throughout the control structure development can be realized by PI controllers. The application of the control on the model shows good results. The temperature control is applied to every element of the system separately. This approach using only one non-time depending control element shows good results. The desired gas temperature for each element of the fuel processor but the reformer can be reached within less than 20 s.

Chapter 6

Conclusion and Perspectives

The presented work is focused on the development of a model of a diesel fed low temperature fuel cell system that can be used for model based control. Therefore, two aspects are considered in parallel: the technology that is described and the methodology that is used for the description, (*Fig. 6*).

Fuel cell systems (FCS) are considered to be upcoming technology for electricity generation. Fuel cells run on hydrogen that can be produced by conversion of conventional hydrocarbons into a hydrogen rich gas. The use of hydrogen-fueled FCS as auxiliary power in transportation applications is a possible entry market for this technology that utilizes the existing infrastructure for fuel supply. The studied FCS provides 25 kW electric power, and, at the same time, the system waste heat is used for climatization.

Control structure development often requires the transfer function of the system. This can be difficult or even impossible to derive for complex systems. Therefore, control structure development for complex multi-domain systems is often based on empirical observation or experience. It is desirable to find an approach that allows the development of a control structure based on system description. Model based control structure design is an approach that can meet these demands. It is shown that Energetic Macroscopic Representation (EMR) is a methodology that is well adapted to modeling complex multi domain systems like a diesel fed low temperature fuel cell system. The feasibility of EMR for inversion based control structure design is shown for the mass flow and the temperature control of a diesel fed low temperature fuel cell system.

In order for the modeling methodology be capable of modeling complex multi domain systems and to be used for model based control structure design, it has to fulfill certain criteria. To model complex multi domain systems it is advantageous if the system description is graphic to keep an overview about the system.

Furthermore, it is advantageous if the system description is modular in order to be able to start with the modeling of a simplified system and to enlarge it subsequently. The use of an approach based on energy conservation / first law of thermodynamics simplifies the connection between different energetic domains. At the same time the model will be used for inversion based control structure design. Therefore, it has to be causal in order to keep the connections between cause and effect. The modularity helps to divide the complex system into a multitude of blocks that can be inversed element wise.

An introduction of the working principles of the considered fuel cell system is given in chapter (1). It contains the working principle of the fuel cell and an overview of the different fuel cell technologies available. It is introduced how the fuel cell current is derived from the basic chemical equation and the factors that influence the fuel cell voltage. An overview of different goals of modeling and their application is given. It is pointed out that a fuel cell system contains all elements that are needed to operate the fuel cell, including, for example, the fuel processor. The different elements of the fuel processor are presented.

In chapter (2) several modeling methodologies are introduced. It is evaluated to determine if they can be used to model a complex multi-domain system and if they can be used for model based control structure development. They are thus compared to the criteria introduced before. The evaluated modeling methodologies are: Electric Equivalent Model, Bond Graph, Causal Ordering Graph and Energetic Macroscopic Representation. The Energetic Macroscopic Representation (EMR) is identified as the best adapted methodology, because it is an energetic graphic causal modeling approach. The energetic aspect provides the possibility to connect different energetic domains. The graphic aspect helps maintain an overview of a complex structure. And the causal structure means to develop an inversion based control. The EMR is introduced in detail and is adapted to chemical conversion and mass transfer for the use in fuel cell systems. The application of this methodology to a simplified fuel cell system model is published in [58].

In chapter (3) a model of the fuel processor is presented and implemented in Matlab/SimulinkTM, [54]. To obtain a hydrogen rich gas, the supplied hydrocarbon has to be broken up. Subsequently, the gas has to be purified in order to avoid contamination of the fuel cell with sulfur and carbon monoxide. The fuel processor unit incorporates several modules, namely: reformer, heat exchanger, desulfurization, water gas shift, preferential oxidation and condensation. Static conversions are considered along with the time dependency of gas flow and temperature. Some of the modules are cooled externally, and such cooling is considered to be instantaneous. The described fuel processor is based on a multi fuel processor designed by N-Ghy.

In chapter (4) a model of the fuel cell stack is presented. For the modeling in EMR the different layers inside the fuel cell are considered separately with regard to gas flow and electric potential. The model takes into account the gas flows in the different layers, describing membrane humidification along with the voltage supplied by the fuel cell. The model takes into account the influence of the membrane humidity on the stack voltage. It is assumed that the fuel cell temperature is fixed. This can be achieved by an external cooling system.

Among low temperature fuel cells, two technologies are available. The model is first developed for the more common (Polymer Electrolyte Fuel Cell - PEFC), while an emerging technology (High Temperature Proton Exchange Membrane Fuel Cell - HTPEMFC) works at higher temperatures of around 180 °C instead of around 60 °C. The higher temperature shows advantages with regard to system cooling and heat use. Due to simplified cooling, less system volume is expected for a HTPEMFC. Furthermore, the demands of purity for the HTPEMFC are less strict than for the PEFC, leading to simplified fuel processor architecture and a decrease in volume. As for transportation applications in which the system volume is important, the use of a HTPEMFC is promising. Therefore, the models of the fuel processor and the fuel cell stack are also adapted to HTPEMFC technology. With regard to the fuel processor, the modules for the preferential oxidation and condensation are thus removed. With regard to the fuel cell stack, the description of the gas flows is unchanged, but the description of the voltage distribution has been adapted. The influence of carbon monoxide poisoning on the stack voltage is thereby taken into consideration. The demonstrated adaptability of the model underscores the advantage of using a modular approach.

The static behavior of the fuel processor model is validated against values supplied by the system provider N-GHY. The thermal characteristics of the reformer are validated against experimental data. The PEFC model is validated against measurements of a Ballard NexaTM fuel cell system. This validation is done running a Ballard NexaTM fuel cell system on hydrogen and on reformat and shows promising results. The Ballard NexaTM fuel cell system contains a cathodic humidity exchanger, that is not taken into account in the fuel cell model. The fact that the cathodic humidification has not been modeled leads to differences in the measured and modeled values. The model of the HTPEMFC is validated against literature values.

To confirm that the model can be used for model based control development, the control structure with regard to the temperature and the mass flow control for the FCS is developed in chapter (5). It is shown that the control structure of the system can be obtained by block wise inversion of the model. This approach gives the control structure, a choice of controllers, and their parameterization is up to the developer. For the mass flow control the volumes of all elements of the fuel processor are lumped into one element, and the volume of the fuel cell

stack is neglected against the volumes inside the fuel processor. The assumption is made that cooling is instantaneous. Hence, temperature control is not time dependent. Application of control proves that using EMR it is possible to derive a control structure from the model of a complex multi domain system without the need to derive its transfer function.

A methodology that is well adapted to model complex multi domains systems that can be used for model based control structure development is evaluated. Existing EMR methodology is extended from electro-mechanical systems to systems that include thermal aspects, chemical conversion and gas transfers. Therefore, it is necessary to expand the number of exchange parameters from two to three. It is shown that this extension can be made keeping the energetic and causal aspects. This methodology is used to model a diesel fed low temperature fuel cell system. The fuel processor and the fuel cell stack are modeled in detail. The model is used for inversion based control structure design of the gas flow and the system temperature.

It is desirable that the extensions of EMR demonstrated in this work will be used for the model based control structure design of other complex multi domain systems.

With regard to the development of the control of a diesel supplied fuel cell system some improvements can be made. For the mass flow control all volumes of the fuel processor modules are lumped into one single element. This assumption is valid if the gas flow supplied to the fuel cell stack is considered most significant. If the modules of the fuel processor are regarded in more detail, the volumes of the modules have to be considered individually. Furthermore, the fuel cell stack volume is neglected in comparison to the volume of the fuel processor modules. For the moment system cooling is considered to be instantaneous, which leads to a temperature control that is not time dependent. In a further step, the system cooling has to be described in more detail. At the same time the use of the system heat is not taken into consideration. Both aspects are connected and their integration into the model can be seen as one task. The temperature development inside the fuel cell stack is not taken into consideration either. This aspect can be integrated into the description of the fuel cell stack easily as the fuel cell stack is described using three parameters containing temperature. The presented model, which is based on physical description and methodology with its modular and energetic aspects, is a good baseline for those improvements.

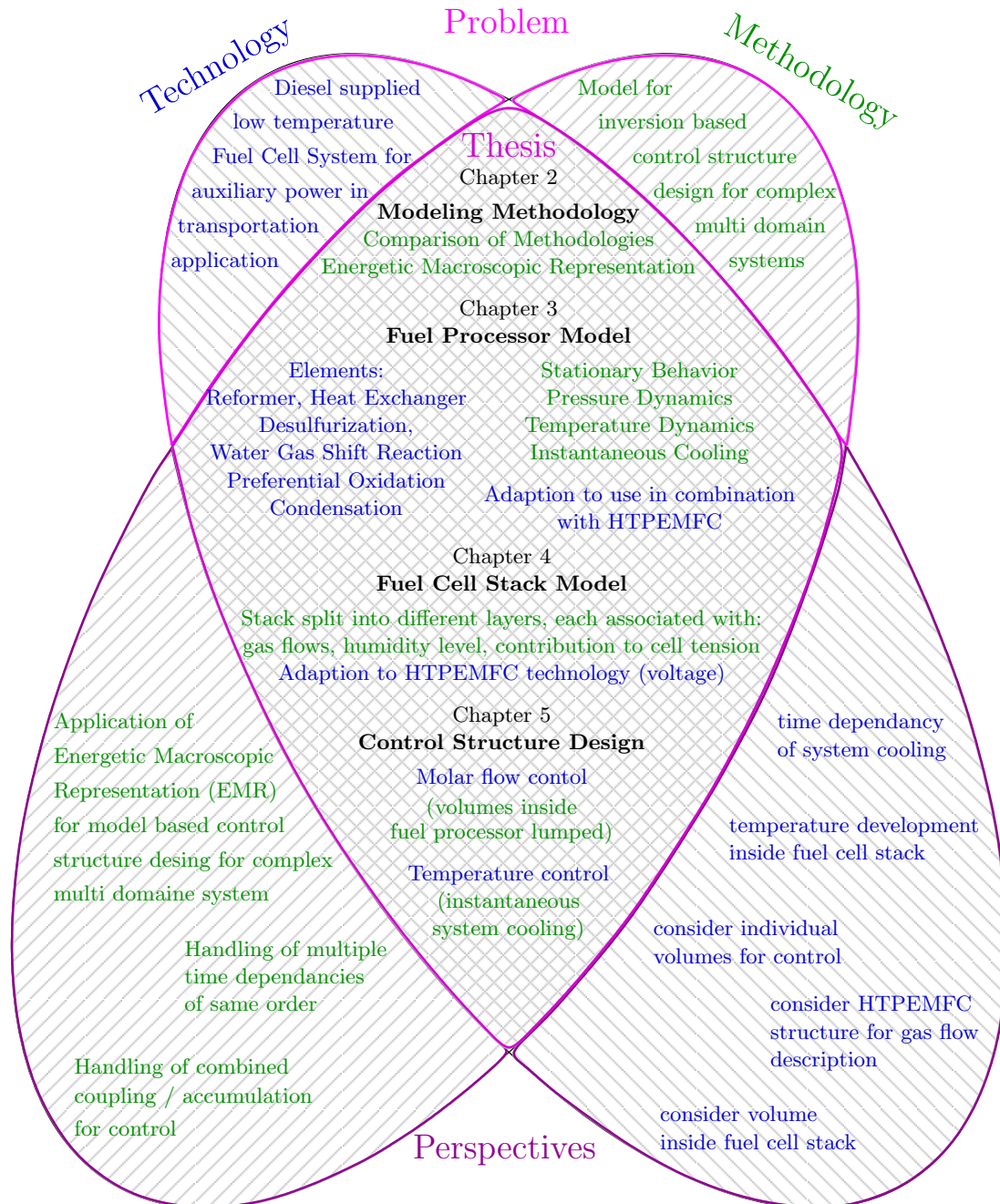


Figure 6.1: Objectives, major work and perspectives

Bibliography

- [1] Bond graph information. www.bondgraph.info.
- [2] *CFC Solutions - Hot Module Fact Sheet*. www.cfc-solutions.com.
- [3] Loremo homepage. <http://evolution.loremo.com>.
- [4] Natural gas vehicle america. www.ngvamerica.org.
- [5] Solid-oxide fuel cell system - for megawatt scale stationary power generation. www.rolls-royce.com/energy/tech/fuelcell.pdf.
- [6] Formalismes graphiques de modélisation et de commande de systèmes électromécaniques. École d'été, July 2005. (in french).
- [7] Biofuels: The promise and the risks world development report 2008: Agriculture for development. <http://econ.worldbank.org>, 2008.
- [8] Monthly oil market report. Organization of the Petroleum Exporting Countries, May 2008. www.opec.org.
- [9] P. A. Aguirre, R. O. Mato, M. C. Mussati, and J. A. Francesconi. Analysis of the energy efficiency of an integrated ethanol processor for pem fuel cell systems. *Journal of Power Sources*, 167:151–161, 2007.
- [10] J. Amphlett, R. F. Mann, B. A. Peppley, P. R. Roberge, A. Rodrigues, and J. Salvador. Simulation of a 250 kw diesel fuel processor/pem fuel cell system. *Journal of Power Sources*, 91:179 – 184, 1999.
- [11] S. J. Andreasen and S. K. Kaer. 400 w high temperature pem fuel cell stack test. *ECS Transaction*, 5:197–207, 2007.
- [12] H.-D. Baehr and S. Kabelac. *Thermodynamik*, volume 13 of ISBN 3-540-32513-1. Springer, 2006. (in german).

- [13] H.-D. Baehr and K. Stephan. *Waerme- und Stoffuebertragung*. Springer, 2006.
- [14] D. Ballerini. *Le plein de biocarburants ? Enjeux et réalités*. IFP Publications, 2007. (in french).
- [15] F. Barbir. *PEM Fuel Cells: Theory and Practice*. Sustainable World Series. Academic Press, June 2005.
- [16] F. Barbir and T. Gomez. Efficiency and economics of proton exchange membrane (pem) fuel cells. *PII*, PII: S0360-3199(96)00030-4:891 – 901, 1996.
- [17] R. Barbir, H. Gorgun, and X. Wang. Relationship between pressure drop and cell resistance as a diagnostic tool for pem fuel cells. *Journal of Power Sources*, 141:96–101, 2005.
- [18] D. M. Bernardi and M. W. Verbrugge. Mathematical model of a gas diffusion electrode bonded on a polymer electrolyte. *AIChE Journal*, 37(8):1151 – 1163, August 1991.
- [19] D. M. Bernardi and M. W. Verbrugge. A mathematical model of the solid-polymer-electrolyte fuel cell. *J. Electrochem. Soc*, 139(9):2477 – 2491, September 1992.
- [20] J. S. Bernitzer, N. Pekula, K. Heller, P. A. Chuang, A. Turhan, M. M. Mech, and K. Ünlü. Study of water distribution and transport in a polymer electrolyte fuel cell using neutron imaging. *Nuclear Instruments and Methods in Physics Research*, 542:134 – 141, 2005.
- [21] B. Blunier. *Modélisation de moto-compresseurs en vue de la gestion de l'air dans les systèmes pile à combustible - simulation et validation expérimentale*. PhD thesis, Université de Technologie de Belfort-Montbéliard, 2007. (in french).
- [22] B. Blunier and A. Miraoui. Modelling of fuel cells using multi-domain vhdl-ams language. *Journal of Power Sources*, 177(2):434–450, 2007.
- [23] B. Bordeau. *L'évolution du parc automobile français entre 1970 et 2010*. PhD thesis, Université de Savoie, 1997. (in french).
- [24] L. Boulon, M.-C. Péra, P. Delarue, A. Bouscayrol, and D. Hissel. Causal fuel cell system mode suitable for transportation simulation applications. In *ASME Conference of fuel cell science and technology*, Brooklyn, USA, 2007.

- [25] L. Boulon, M.-C. Péra, D. Hissel, A. Bouscayrol, and P. Delarue. Energetic macroscopic representation of a fuel cell-supercapacitor system. In *IEEE VPP Conference*, pages 290–297, Arlington, Texas, 2007.
- [26] A. Bouscayrol, B. Davat, B. de Fornel, B. Francois, J. P. Hautier, F. Meibody-Tabar, and M. Pietrzak-David. Multi-converter multi-machine systems: application for electrochemical drivers. *The European Physical Journal - Applied Physics*, 10:131 – 147, 2000.
- [27] A. Bouscayrol, B. Davat, B. de Fornel, B. Francoise, J. P. Hautier, E. Meibody-Tabar, Fand Monmasson, M. Pietrzak-David, H. Razik, E. Se-mail, and M. F. Benkhoris. Control structures for multi-machine multi-converter systems with upstream coupling. *Mathematics and Computers in Simulation*, 63(3-5):261 – 270, November 2003.
- [28] A. Bouscayrol and P. Delarue. Simplifications of the maximum control structure of a wind energy conversion system with an induction genrator. *International Journal of Renewable Energy Engineering*, 4(2):479 – 485, August 2002.
- [29] A. Bouscayrol, P. Delarue, and X. Guillaud. Power strategies for maximum control structure of a wind energy conversion system with a synchronus machine. *Renewable Energy*, 30:2273 – 2288, 2005.
- [30] A. Bouscayrol, P. Delarue, A. Tounzi, X. Guillard, and G. Lancigu. Modelling, control and simulation of an overall wind energy conversion system. *Renewable Energy*, 28:1169 – 1185, 2003.
- [31] A. Bouscayrol, M. Pietrzak David, P. Delarue, R. Pena-Eguiluz, P. E. Vidal, and X. Kestelyn. Weighted control of traction drives with parallel-connected ac machines. *IEEE Transactions on Industrial Electronics*, 53(6):1799–1806, December 2006.
- [32] A. Bouscayrol, R. Schoenfeld, G. Dauphin-Tangy, G.-H. Geitner, X. Guiland, A. Pennamen, and J.-P. Hautier. Different energetic descriptions for electromechanical systems. In *EPE*, Dresden, Germany, September 2005.
- [33] B. B. Bowers, J. L. Zhao, M. Ruffo, R. Khan, D. Dattatraya, N. Dushman, J.-C. Beziat, and F. Boudjemaa. Onboard fuel processor for pem fuel cell vehicles. *Internatioal Journal of Hydrogen Energy*, 32:1437–1442, 2007.
- [34] N. P. Brandon, R. van der Vorst, and C. Handley. Impact of the european union vehicle waste directive on end-of-life options for polymer electrolyte fuel cells. *Journal of Power Sources*, 106:344 – 352, 2002.

- [35] D. Brett, P. Aguiar, N. Brandon, and A. Kucernak. Measurement and mode of carbon monoxide poisoning distribution zithin a polymer electrolyte fuel cell. *International Journal of Hydrogen Energy*, 33:863–871, 2007.
- [36] D. Brunetto, G. Tina, G. Squadrito, and A. Moschetto. Pemfc diagnostics and modelling by electrochemical impedance spectroscopy. *IEEE*, IEEE 2004 0-7803-8271-4104:1045 – 1050, 2004.
- [37] K. Bullis. Gm's new electric vehicle. *Technology Review*, January:2, 2007.
- [38] A. Burcat and B. Ruscic. Third millennium ideal gas and condensed phase thermochemical database for combustion with updates from active thermochemical tables. <http://garfield.chem.elte.hu/Burcat/burcat.html>, September 2005.
- [39] A. Burke. Ultracapacitors: why, how, and where is the technology. *Journal of Power Sources*, 91:37–50, 2000.
- [40] A. Burke. Batteries and ultracapacitors for electric, hybrid, and fuel cell vehicles. *Proceedings of the IEEE*, 95:806–820, 2007.
- [41] D. Candusso, R. Glises, D. Hissel, J. M. Kauffmann, and M.-C. Péra. Piles à combustible pemfc et sofc. description et gestion de système. *Techniques de l'Ingénieur*, 10 2007. BE8595, (in french).
- [42] D. Candusso, R. Glises, D. Hissel, J. M. Kauffmann, and M.-C. Péra. Piles à combustible pemfc et sofc. transferts de chaleur et de masse. *Technique de l'Ingénieur*, 10 2007. BE8596, (in french).
- [43] D. Candusso, L. Valero, and A. Walter. Modelling, control and simulation of a fuel cell based power supply system with energy management. In *IECON 02 [Industrial Electronics Society, IEEE 2002 28th Annual Conference of the]*, volume 2, pages 1294–1299, Sevilla, Spain, Nov 2002.
- [44] M. J. Castaldi and F. Barrai. An investigation into water and thermal balance for a liquid fueled fuel processor. *Catalysis Today*, 129:397–406, 2007.
- [45] S. Caux, J. Lachaize, M. Fadel, P. Shott, and L. Nicod. Modelling and control of a fuel cell system and storage elements in transport applications. *Journal of Process Control*, 15:481 – 491, 2005.
- [46] S. H. Chan, S. K. Goh, and S. P. Jiang. A mathematical model of polymer electrolyte fuel cell with anode co kinetics. *Electrochimica Acta*, 48:1905 – 1919, 2003.

- [47] D. Cheddie and N. Munroe. Review and comparison of approaches to proton exchange membran fuel cell modeling. *Journal of Power Sources*, 147:72–84, 2005.
- [48] D. Cheddie and N. Munroe. Analytical correlation for intermediate temperature pem fuel cells. *Journal of Power Sources*, 160:299–304, 2006.
- [49] D. J. Chmielewski, Y. Hu, and D. Papadias. Autothermal reforming of gasoling for fuel cell applications: Controller design and analysis. *Journal of Power Sources*, 182:298–306, 2008.
- [50] M. Chnani, H. Maker, D. Candusso, M. C. Péra, and D. Hissel. Electrical analogy modelling of pefc system fed by a compressor. In *European Fuel Cell Forum*, Lucerne, Switzerland, 2005.
- [51] D. Chrenko. Characterization of a polymer electrolyte fuel cell system - contribution to the study of fuel cell ageing. Master's thesis, Hamburg University of Applied Science, 2005.
- [52] D. Chrenko and L. Boulon. Energetic macroscopic representation (emr) of a fuel cell system (fcs) for electric vehicles (ev). In A. Bouscayrol, editor, *International Workshop, "Modelling and control for electrical systems"*, Lille, France, 13-14 November 2006 2006.
- [53] D. Chrenko and L. Boulon. Introduction d'une méthodologie de la structure de commande pour des systèmes complexes multi-physiques. In *École d'Énergies*, Fréjus, France, March 2008. (in french).
- [54] D. Chrenko, J. Coulié, M.-C. Péra, and D. Hissel. Static and dynamic modeling of a diesel fuel processing unit for polymer electrolyte fuel cell supply. *Internaltional Journal of Hydrogen Energy*, 2009.
- [55] D. Chrenko, M.-C. Péra, and D. Hissel. Fuel cell system modeling and control with energetic macroscopic representation. In *IEEE ISIE*, Vigo, Spain, 4-7. June 2007.
- [56] D. Chrenko, M.-C. Péra, and D. Hissel. Fuel cell system control structure development: A graphic inversion based approach using energetic macroscopic representation. In *Electrimacs*, Québec, Canada, June 2008.
- [57] D. Chrenko, M.-C. Péra, and D. Hissel. Inversion based control of a diesel fed low temperature fuel cell system. In *EPE-PEMC*, Pozan, Poland, September 2008.

- [58] D. Chrenko, M.-C. Péra, and D. Hissel. Inversion-based control of a pem fuel cell system using energetic macroscopic representation. *ASME Journal of Fuel Cell Science and Technology*, 2008. (in press).
- [59] D. Chrenko, M.-C. Péra, D. Hissel, and M. Geweke. Macroscopic modeling of a pefc system based on equivalent circuits of fuel and oxidant supply. *ASME Journal of Fuel Cell Science and Technology*, 5:011015–1 – 011015–5, 2008.
- [60] G. Dauphin-Tanguy. *Les Bond Graphs*. ISBN 2-7462-0158-5. Hermes Science Publications, 2000. (in french).
- [61] A. Davari, P. A. A. Feliachi, and T. Biswas. Integration of a fuel cell into the power system using an optimal controller based on disturbance accommodation control theory. *Journal of Power Sources*, 128:218–230, 2004.
- [62] D. DiPenta, K. Bencherif, M. Sorine, and Q. Zhang. A reduced fuel cell stack model for control and fault diagnosis. *Asme Journal of Fuel Cell Science and Technology*, 3:p384 – 388, 2006.
- [63] J. Divisek. *Low temperature fuel cells*, chapter 9, pages 99 – 114. Wiley & Sons, 2003.
- [64] F. Druart, P. Moçotéguy, Y. Bultel, S. Besse, and A. Rakotondrainibe. Monodimensional mode and experimental study of the dynamic behavior of proton exhcange membrande fuel cell stack operating in dead-end mode. *Journal of Power Sources*, 167:349 – 357, 2007.
- [65] B. Emonts, J. B. Hansen, S. L. Joergensen, B. Höhle, and R. Peters. Compact methanol reformer test for fuel-cell power light-duty vehicles. *Journal of Power Sources*, 71:288–293, 1998.
- [66] Energy Information Administration. World proved reserves of oil and natural gas, most recent estimates. www.eia.doe.gov/emeu/international/reserves.html, January 2007.
- [67] European Commission Joint Research Center. Status and perspectives of biomass-to-liquid fuels in the european union. EUR 21745 EN, 2005.
- [68] P. Famouri and R. S. Gemmen. Electrochemical circuit model of a pem fuel cell. In *Power Engineering Society General Meeting*, Toronto, Canada, 2003.

- [69] W. Friede. *Modélisation et caractérisation d'une pile á combustible du type PEM*. PhD thesis, Institut National Polytechnique de Lorraine, 2003. (in french).
- [70] E. P. Gatzke and A. T. Stamps. Dynamic modeling of a methanol reformer - pefmfc stack system for analysis and design. *Journal of Power Sources*, 161:356–370, 2006.
- [71] S. Gelfi, A. G. Stefanopoulou, J. T. Pukrushpan, and H. Peng. Dynamics of low-pressure and high-pressure fuel cell air supply systems. *IEEE*, IEEE 2003 0-7803-7896-2:2049 – 2054, June 4-6, 2003 2003. Proceeding of the American Control Conference; Denver, Colorado.
- [72] R. Glises, D. Hissel, F. Harel, and M.-C. Péra. New design of a pem fuel cell air automatic climate control unit. *Journal of Power Sources*, 150:78 – 85, 2005.
- [73] J. Golbert and D. R. Lewin. Model-based control of fuel cells: (1) regulatory control. *Journal of Power Sources*, 135:135–151, 2004.
- [74] J. Golbert and D. R. Lewin. Model-based control of fuel cells: Optimal efficiency. *Journal of Power Sources*, doi:10.1016/j.jpowsour.2007.04.062:12, 2007.
- [75] F. Grasser. *An analytical, control-oriented state space model for a PEM Fuel Cell System*. PhD thesis, École Polytechnique Fédéral de Lausanne - EPFL, 2006.
- [76] F. Grasser and A. C. Rufer. A fully analytical pem fuel cell system model for control application. *IEEE Transactions on Industry Applications*, 43:1499 – 1506, November-December 2007.
- [77] K. Haraldsson and K. Wipke. Evaluating pem fuel cell system models. *Journal of Power Sources*, 126:88 – 97, 2004.
- [78] J. P. Hautier and P. J. Barre. The causal ordering graph - a tool for modelling and control law synthesis. *Studies in Informatics and Control Journal*, 13(4):265–283, december 2004.
- [79] J. P. Hautier and J. Faucher. Le graphe informationnel causal. *Bulletin de l'Union des Physiciens*, 90:167 – 189, 1996.
- [80] R. Hebner, J. Beno, and A. Walls. Flywheel batteries come around again. *IEEE Spectrum*, April:45–51, 2002.

- [81] A. Hernandez, D. Hissel, and R. Outbib. Electric equivalent model for a hydrogen fuel cell (pefc). In CD-ROM, editor, *Electrimacs 2005 Conference*, Hammamet, Tunisia 2005.
- [82] A. Hernandez, D. Hissel, and R. Outbib. Fuel cell fault diagnosis: A stochastic approach. In *IEEE ISIE*, pages 1984–1989, Montréal, Canada, July 2006. IEEE.
- [83] D. Hissel, M.-C. Pera, A. Bouscayrol, and D. Chrenko. Représentation énergétique macroscopique d'une pile à combustible. *Revue internationale de génie électrique.*, 11:603 – 623, 2008. (in french).
- [84] G. e. a. Hoogers. *Fuel Cell Technology Handbook*. CRC Press, 2002.
- [85] Intergovernmental Panel on Climate Change. Climate change 2007: Synthesis report. <http://www.ipcc.ch/>, 2007.
- [86] International Energy Agency. World energy outlook. www.worldenergyoutlook.org.
- [87] J. O. Jensen, Q. Li, C. Pan, A. P. Vestbo, K. Mortensen, H. N. Petersen, C. L. Sorensen, T. N. Clausen, J. Schramm, and N. J. Bjerrum. High temperature pemfc and the possible utilization of the excess heat for fuel processing. *International Journal of Hydrogen Energy*, 32:1567 –1571, 2007.
- [88] D. Karnopp, D. L. Margolis, and R. C. Rosenberg. *System Dynamics: A Unified Approach*. John Wiley & Sons Inc, 1990.
- [89] M. Kaviany and J. Nam. Effective diffusivity and water-saturation distribution in single and two-layer pemfc diffusion medium. *International Journal of Heat and Mass Transfer*, 46:4595 – 611, 2003.
- [90] Kazim. Energy analysis of a pem fuel cell at variable operating conditions. *Energy Conversion and Management*, 45:1949 – 1961, 2004.
- [91] J. M. King and H. R. Kunz. *Phosphoric acid electrolyte fuel cell in Handbook of Fuel Cells*, chapter 16, pages 287 – 300. Wiley, 2003.
- [92] J.-M. Klein, Y. Bultel, S. Gorges, and M. Pons. Modeling of a sofc fuelled by methane: From direct internal reforming to gradual internal reforming. *Chemical Engineering Science*, 62:1636 – 1649, 2007.

- [93] G. Kolb, T. Baier, J. Schürer, D. Tiemann, A. Ziogas, H. Ehwald, and P. Alphose. A micro-structured 5kw complete fuel processor for iso-octane as hydrogen supply system for mobile auxiliary power units. part i. development of autothermal reforming catalyst and reactor. *Chemical Engineering Journal*, 137:653–663, 2008.
- [94] G. Kolb, T. Baier, J. Schürer, D. Tiemann, A. Ziogas, S. Specchia, C. Galletti, G. Germani, and Y. Schuurman. A micro-structured 5kw complete fuel processor for iso-octane as hydrogen supply system for mobile auxiliary power units. part ii - development of water-gas shift and preferential oxidation catalysts reactors and assembly of the fuel processor. *Chemical Engineering Journal*, 138:474–489, 2007.
- [95] A. R. Korsgaard, M. P. Nielsen, and S. K. Kaer. Part one: A novel model of htpem-based micro-combined heat and power fuel cell system. *International Journal of Heat and Mass Transfer*, 33:1909–1920, 2008.
- [96] A. R. Korsgaard, M. P. Nielsen, and S. K. Kaer. Part two: Control of a novel htpem-based micro combined heat and power fuel cell system. *International Journal of Hydrogen Energy*, 33:1921–1931, 2008.
- [97] A. R. Korsgaard, R. Refshauge, M. P. Nielsen, M. Bang, and S. K. Kaer. Experimental characterization and modeling of commercial polybenzimidazole-based mea performance. *Journal of Power Sources*, 162:239–245, 2006.
- [98] J. Larminie and A. Dicks. *Fuel Cell Systems Explained*. John Wiley & Sons, 2003.
- [99] S. Lasseux. A comparative lca of different proton exchange membrane fuel cells (pemfc) and a microturbine for combined production of heat and electricity. In *8th LCA Case Studies Symposium SETAC-Europe*, Brussels, Belgium, 2000.
- [100] F. Laurencelle, R. Chahine, J. Hamelin, K. Agbossou, M. Fournier, T. K. Bose, and A. Laperriere. Characterization of a ballard mk5-e proton exchange membrane fuel cell stack. *Fuel Cells*, 1:66 – 71, 2001.
- [101] A. Leclercq, P. Sicard, A. Bouscayrol, and B. Lemaire-Semail. Control of a tripple drive paper system based on the energetic macroscopic representation. In *IEEE-ISIE*, pages 889 – 893, Ajaccio, Spain, May 2004.

- [102] Z. Lemes, A. Vath, T. Hartkopf, and H. Mäncher. Dynamic fuel cell models and their application in hardware in the loop simulation. *Journal of Power Sources*, 154:386–393, 2006.
- [103] W. Lhomme, R. Trigui, P. Delarue, B. Jeanneret, A. Bouscayrol, and F. Badin. Switched causal model of transmission with clutch in hybrid electric vehicles. *IEEE Transactions on Vehicular Technology*, 57(4):2081–2088, July 2008.
- [104] Q. Li, R. He, A. Bach, J. O. Jensen, and N. J. Bjerrum. Physicochemical properties of phosphoric acid doped polybenzimidazole membrane for fuel cells. *Journal of Membrane Science*, 277:38–45, 2006.
- [105] X. Li, J. J. Baschuk, and A. M. Rowe. Modeling and simulation of pem fuel cells with co poisoning. *Journal of Energy Ressources Technology*, 125:94–100, 2003.
- [106] G. Liu, J. Zhang, W. Yu, and M. Ouyang. Adaptive control of the airflow of a pem fuel cell system. *Journal of Power Sources*, 179:649 – 659, 2008.
- [107] O. Lottin, M. Radulescu, V. Ayel, M. Feidt, B. Antoine, C. Moyne, D. Le Noc, and S. Le Doze. Natural gas electric generator powered by polymer exchange membrane fuel cell: Numerical model and experimental results. *Journal of Energy Conversion and Management*, 49:326 – 335, 2008.
- [108] O. Lottin, M. Radulescu, M. Feidt, C. Lombard, D. Le Noc, and S. Le Doze. Experimental results with a natural gas cogeneration system using a polymer exchange membrane fuel cell. *Journal of Power Sources*, 159:1142 – 1146, 2006.
- [109] R. F. Mann, J. Amphlett, M. Hooper, H. Jensen, B. Peppley, and P. R. Roberge. Development and application of a generalised steady-state electrochemical model for a pem fuel cell. *Journal of Power Sources*, 86:173–180, 2000.
- [110] M. M. Mench, Q. L. Dong, and W. C. Y. In situ water distribution measurements in a polymer electrolyte fuel cell. *Journal of Power Sources*, 124:90 – 98, 2003.
- [111] C. Mengel, M. Konrad, R. Wruck, K. Lucka, and H. Köhne. Diesel steam reforming for pem fuel cells. *Journal of Fuel Cell Science and Technology*, 5(021005):1–5, May 2008.

- [112] A. Miotti, A. Di Domenico, and Y. G. Guezennec. Control-oriented model for an automotive pem fuel cell system with imbedded 1+1d membrane water transport. In IEEE, editor, *Vehicle Power and Propulsion, 2005 IEEE Conference*, pages 611 – 618, Chicago, Illinois, USA, September 2005. IEEE, IEEE.
- [113] A. Narjiss, D. Depernet, F. Gustin, D. Hissel, and A. Berthon. Design and control of a fuel cel dc/dc. In *Power Electronics and Applications, 2007 European Conference on*, Aalborg, Denmark, 2007.
- [114] T. Nguyen and R. White. A water and heat management model for proton-exchange-membrane fuel cells. *Journal of Electrochemical Society*, 140:2178 – 2186, August 1993.
- [115] T. V. Nguyen and D. Natarajan. Three dimensional effects of liquid water flooding in the cathode of a pem fuel cell. *Journal of Power Sources*, 115:66–80, 2003.
- [116] R. O'Hayre, S.-W. Cha, W. Colella, and F. B. Prinz. *Fuel Cell Fundamentals*. Wiley, 2005.
- [117] V. Paladini, T. Donateo, A. de Risi, and D. Laforgia. Control strategy optimization of a fuel-cell electric vehicle. *ASME Journal of Fuel Cell Science and Technology*, 5:021004–1 – 021004–8, 2008.
- [118] H. Paynter. *Analysis and design of engineering systems*. MIT Press, 1961.
- [119] H. Peng, J. T. Pukrushpan, and A. G. Stefanopoulou. Control-oriented modeling and analysis for automotive fuel cell systems. *Journal of Dynamic Systems, Measurement, and Control*, 126:14–25, 2004.
- [120] M.-C. Péra, D. Chrenko, and D. Hissel. De la pile à combustible à son intégration. *3EI : Enseigner l'Électrotechnique et l'Électronique Industrielle*, December 2008. (in press), (in french).
- [121] J. Pukrushpan, A. G. Stefanopoulou, S. Varigonda, J. Eborn, and C. Haugstetter. Control-oriented model of fuel processor for hydrogen generation in fuel cell applications. *Control Engineering Practice*, 14:277 – 293, 2006.
- [122] J. T. Pukrushpan. *Control of Fuel Cell Power Systems*. Springer, 2004.
- [123] A. Rahman, M. Alam, P. Byrne, A. Sahla, R. Thomas, and M. El-Sharkh. A dynamic modell for a stand-alone pem fuel cell power plant for residential application. *Journal of Power Sources*, 0378-7753:doi:10.1016/j.jpowsour.2004.06.037, 2004.

- [124] A. Reiche, K. Foli, O. Gronwald, S. Haufe, S. Kiel, U. Mähr, D. Melzner, F. Walter, and S. Weisshaar. Sartorius ht-pem-fuel cell technology. In *Fuel Cell Seminar*, Honolulu, Hawaii, USA, 2006.
- [125] E. Riensche, J. Meusinger, U. Stimmig, and G. Unverzagt. Optimization of a 200kw sofc cogeneration power plant part ii: variation of the flowsheet. *Journal of Power Sources*, 71:306–314, 1998.
- [126] E. Riensche and G. Simming, Ulrich und Unversagt. Optimization of a 200kw sofc cogeneration power plant part i: Variation of process parameters. *Journal of Power Sources*, 73:251–256, 1998.
- [127] R. Saisset, G. Fontes, C. Turpin, and S. Astier. Bond graph model of a pem fuel cell. *Journal of Power Sources*, 156:100 – 107, 2006.
- [128] E. J. Sandstede, Gand Caafrins, V. S. Begotsky, and K. Wiesner. *History of low temperature fuel cells in Handbook of Fuel Cells*, chapter 12, pages 145 – 218. Wiley & Sons, 2003.
- [129] B. Sauser. Ethanol demand thretens food price. *Technology Review*, February:3, 2007.
- [130] J. Scholta and L. Jörissen. Ht-pemfc - einföhrung und experimentelle erfahrung. In *Riesaer Brennstoffzellenworkshop*, Riesa, Germany, 2007. (in german).
- [131] P. Schott and P. Baurens. Fuel cell operation characterization using simulation. *Journal of Power Sources*, 156:85–91, 2006.
- [132] C. Severin and J. Pischinger, S. und Ogrzewalla. Compact gasoline fuel processor for passenger vehicule apu. *Journal of Power Sources*, 145:675–682, 2005.
- [133] P. Sicard and A. Bouscayrol. Extention of energetic macroscopic representation to time varying systems. In *IEEE ISIE*, pages 1370–1375, Montréal, Quebec, Canada, July 2006.
- [134] M. Siemer. *Lokale Entropieproduktionsraten in der Polymerelektrolyt-Membran-Brennstoffzelle*. PhD thesis, Helmut Schmidt Universität Hamburg, 2007. (in german).
- [135] D. Sopena, A. Melgar, Y. Briceno, R. M. Navarro, M. C. Alvarez-Galvan, and F. Rosa. Diesel fuel processor for hydrogen production for 5 kw fuel cell application. *International Journal of Heat and Mass Transfer*, 32:1429 – 1436, 2007.

- [136] S. Specchia, M. Antonini, G. Saracco, V. Specchia, and A. Cutillo. Diesel fuel processor for pem fuel cells: Two possible alternatives (atr versus sr). *Journal of Power Sources*, 154:379–385, 2006.
- [137] T. E. Springer, T. Rockward, T. A. Zawodzinski, and S. Gottesfeld. Model for polymer electrolyte fuel cell operation on reformat feed. *Journal of The Electrochemical Society*, 148:A11–A23, 2001.
- [138] T. E. Springer, T. A. Zawodzinski, and S. Gottesfeld. Polymer electrolyte fuel cell model. *J. Electrochem. Soc.*, 138(8):2334–2342, August 1991.
- [139] P. Staiti, Z. Poltarzewski, V. Alderucci, G. Maggion, N. Giordano, and F. A. Influence of electrodic properties on water management in a solid electrolyte fuel cell. *Journal of applied Electrochemistry*, 22:663–667, 1992.
- [140] J. Stumper, M. Löhr, and S. Hamada. Diagnostic tools for liquid water in pem fuel cells. In *2001 Fuel Cell Seminar*, number 0378-7753 doi:10/1016/j.powersour.2004.11.036, San Antonio, Texas, USA, 2005.
- [141] K.-W. Suh and A. G. Stefanopoulou. Coordination of converter and fuel cell controllers. In MoP06-2, editor, *Proceeding of the 13th Mediterranean Conference of Control and Automation*, pages 563–568, Cyprus, 2005.
- [142] B. J. Tatarchuk, Y. Lu, and H. Yang. Glass fiber entrapped sorbent for reformates desulfurization for logistic pem fuel cell power systems. *Journal of Power Sources*, 174:302–311, 2007.
- [143] M. Tekin. *Contribution à l'optimisation énergétique d'un système pile à combustible embarqué*. PhD thesis, Université de Franche-Comté, 2004. (in french).
- [144] M. Tekin, D. Hissel, M.-C. Péra, and J.-M. Kauffmann. Energy consumption reduction of a pem fuel cell motor compressor group thanks to efficient control laws. *Journal of Power Sources*, 156:57–63, 2006.
- [145] J. Thoma. Hot fluid convection systems with true and pseudo bondgraphs. *IEEE/CISS*, 1:567–572, 1993.
- [146] J. Thoma and G. Mocellin. *Simulation with Entropy in Engineering Thermodynamics - Understanding Matter and Systems with Bondgraphs*. Springer, 2006.
- [147] P. Thounthong, S. Rael, and B. Davat. Control strategy of fuel cell/supercapacitors hybrid power sources for electric vehicle. *Journal of Power Sources*, 158:806 – 814, 2006.

- [148] V. Treier and V. Palge. Comparison of formulas for calculating water vapour saturation pressure. <http://tehnika.eau.ee/pages/2002/Energy/>.
- [149] C. Turpin. Piles à combustible et composants électrochimiques de stockage: caractérisation, modélisation, et mise en oeuvre dans des systèmes énergétiques. LABORATOIRE PLASMA ET CONVERSION D'ENERGIE UMR5213, 2008. Habilitation degree thesis, (in french).
- [150] U.S. Department of Energy-Office of Fossil Energy, Under Contract No. DE-AM26-99FT40575, editor. *Fuel Cell Handbook (Seventh Edition)*. EG&G Technical Services Inc., November 2004.
- [151] A. Vath, Z. Lemes, H. Maencher, M. Soehn, N. Nicoloso, and T. Hartkopf. Dynamic modelling and hardware-in-the-loop testing of pemfc. *Journal of Power Sources*, 157:816–827, 2006. 0378/7753.
- [152] J.-N. Verhille, A. Bouscayrol, P.-J. Barre, J.-P. Hautier, and E. Semail. The use of energetic macroscopic representation for control of traction systems: application to subway val 206. In *IEEE-VPPC*, Paris, France, 2004.
- [153] M. B. Virji, P. L. Adcock, R. M. Moore, and J. B. Lakeman. Modeling and simulation of an indirect diesel proton exchange membrane fuel cell (pemfc) system for a marine application. *Journal of Fuel Cell Science and Technology*, 4:481–496, 2007.
- [154] B. Wahdame, D. Candusso, and J.-M. Kaufmann. Study of the gas pressures and flow rates influences on a 500w pem fuel cell thanks to experimental design methodology. *Journal of Power Sources*, 156:92–99, 2006.
- [155] A. Weber and J. Newman. Modeling gas-phase transport in polymer-electrolyte fuel cells. Lawrence Berkley National Laboratory, 2006. Paper LBNL 61465.
- [156] W. Wiese, B. Emons, and R. Peters. Methanol steam reforming in a fuel cell drive system. *Journal of Power Sources*, 84:187–193, 1999.
- [157] P. J. H. Wingelaar, J. L. Duarte, and M. A. M. Hendrix. Dynamic characteristics of pem fuel cells. In *PESC*, Aachen, Germany, 2005. IEEE PESC 2005. 0-7803-9033-4/05/20.00.
- [158] P. J. H. Wingelaar, J. L. Duarte, and M. A. M. Hendrix. Dynamic and static simulation tool for pem fuel cells. In IEEE, editor, *IEEE ISIE*, pages 1700–1705, Montréal, Canada, July 2006. IEEE, ISIE. 1-4244-0497-8/06/20.00.

- [159] H. X. Yang, J. K. Feng, J. Sun X, X. P. Ai, and H. X. Cao. Dimethyl methyl phosphates: A new nonflammable electrolyte solvent for lithium-ion batteries. *Journal of Power Sources*, 184:570–573, 2008.
- [160] S. Yu and S. Yuvarajan. A novel circuit model for pem fuel cells. *IEEE*, IEEE 2004 0-7803-8269-2/04/:362 – 366, 2004.
- [161] B. Zhou and A. D. Le. A general model of proton exchange membrane fuel cell. *Journal of Power Sources*, 182:197–222 197–222, 2008.
- [162] W. Zhu, R. Payne, and B. Tararchuk. Critical flow rate of anode fuel exhaust in a pem fuel cell system. *Journal of Power Sources*, 156:512 – 519, 2006.

Appendix A

Parameters and Input Values

Table A.1: Input parameters of the fuel processor unit

Description	Name	Value	Unit
Diesel temperature	T_{Diesel}	313	K
Water temperature	T_{Water}	313	K
Air temperature	T_{Air}	452	K
Pressure at the fuel cell	p_{FC}	$3 \cdot 10^5$	Pa

Table A.2: Parameters to calculate the stationary behavior of the fuel processor unit

Description	Name	Value	Unit
Heat Exchanger and Reformer			
Heat Transfer Coefficient multiplied the Heat Exchange Area	kA	8.5	W K^{-1}
Desulfurization 1			
Selectivity	sel_{D1}	0.975	
Preferential Oxidation			
Selectivity	sel_{PrOx}	0.96	
Condensation			
Selectivity	τ_{cond}	1	
Desulfurization 2			
Selectivity	sel_{D2}	0.909	

Heat capacity vector at 700 °C in $\text{kJ kg}^{-1} \text{K}^{-1}$. Heat capacity vector at 1200 °C in $\text{kJ kg}^{-1} \text{K}^{-1}$.

$$c_{p700} = \begin{bmatrix} 571.87 \\ 29.34 \\ 57.88 \\ 31.13 \\ 40.90 \\ 49.59 \\ 30.72 \\ 37.51 \\ 287.82 \\ 32.99 \end{bmatrix} \quad c_{p1200} = \begin{bmatrix} 740.13 \\ 31.09 \\ 78.38 \\ 34.07 \\ 48.54 \\ 56.13 \\ 33.64 \\ 43.94 \\ 0 \\ 35.57 \end{bmatrix}$$

Table A.3: Parameters to evaluate the dynamic behavior of the fuel processor unit

Description	Name	Value	Unit
Heat Exchanger and Reformer			
Volume	V_{RHex}	$2.5 \cdot 10^{-3}$	m^3
Throttle constant	k_{RHex}	$5.64 \cdot 10^4$	$\text{mol s}^{-1} \text{Pa}^{-1}$
Desulfurization 1			
Volume	V_{Des1}	$0.1 \cdot 10^{-3}$	m^3
Throttle constant	k_{Des1}	$5.65 \cdot 10^4$	$\text{mol s}^{-1} \text{Pa}^{-1}$
Water Gas Shift			
Volume	V_{WGS}	$3 \cdot 10^{-3}$	m^3
Throttle constant	k_{Des1}	$5.65 \cdot 10^4$	$\text{mol s}^{-1} \text{Pa}^{-1}$
Preferential Oxidation			
Volume	V_{PrOx}	$4 \cdot 10^{-3}$	m^3
Throttle constant	k_{PrOx}	$5.48 \cdot 10^4$	$\text{mol s}^{-1} \text{Pa}^{-1}$
Condensation			
Volume	V_{Cond}	$2 \cdot 10^{-3}$	m^3
Throttle constant	k_{Cond}	$5.48 \cdot 10^4$	$\text{mol s}^{-1} \text{Pa}^{-1}$
Desulfurization 2			
Volume	V_{Des2}	$0.1 \cdot 10^{-3}$	m^3
Throttle constant	k_{Des2}	$5.48 \cdot 10^4$	$\text{mol s}^{-1} \text{Pa}^{-1}$

Table A.4: Parameters to evaluate the thermal behavior of the fuel processor unit

Description	Name	Value	Unit
Heat Exchanger and Reformer			
Heat transfer coefficient times surface	kA_{RHex}	2.5	$W K^{-1}$
Mass of the box	m_{RHex}	0.443	kg
Heat Capacity of the box	c_{pRHex}	480	$J kg^{-1} K^{-1}$
Desulfurization 1			
Heat transfer coefficient times surface	kA_{Des1}	2	$W K^{-1}$
Mass of the box	m_{Des1}	2	kg
Heat Capacity of the box	c_{pDes1}	480	$J kg^{-1} K^{-1}$
Water Gas Shift			
Heat transfer coefficient times surface	kA_{WGS}	15	$W K^{-1}$
Mass of the box	m_{WGS}	13.5	kg
Heat Capacity of the box	c_{pWGS}	480	$J kg^{-1} K^{-1}$
Preferential Oxidation			
Heat transfer coefficient times surface	kA_{PrOx}	15	$W K^{-1}$
Mass of the box	m_{PrOx}	13.5	kg
Heat Capacity of the box	c_{pPrOx}	480	$J kg^{-1} K^{-1}$
Condensation			
Heat transfer coefficient times surface	kA_{Cond}	15	$W K^{-1}$
Mass of the box	m_{Cond}	2	kg
Heat Capacity of the box	c_{pCond}	480	$J kg^{-1} K^{-1}$
Desulfurization 2			
Heat transfer coefficient times surface	kA_{Des2}	15	$W K^{-1}$
Mass of the box	m_{Des2}	2	kg
Heat Capacity of the box	c_{pDes2}	480	$J kg^{-1} K^{-1}$

Table A.5: Parameters of Fuel Cell

Name	Sign	Value	Unity
Cathode Gas Diffusion Layer thickness	δ_c	350	μm
Anode Gas Diffusion Layer thickness	δ_a	350	μm
Membrane density	ρ_{dry}	1970	kg m^{-3}
Molar mass of membrane	M_m	1.0	kg mol^{-1}
Active surface	S_{cell}	54	cm^2

Table A.6: Parameters of Diesel, Water and Air Supply

Name	Sign	Value	Unity
Diesel Supply			
Resistance of electric motor	R_d	0.5	Ω
Electric inductance	L_d	$5 \cdot 10^{-3}$	H
Electro-mechanic conversion coefficient	K_{ed}	0.5	N m A^{-1}
Combined friction coefficient of motor and pump	f_d	$3 \cdot 10^{-3}$	N m rad^{-1}
Combined inertia of motor and pump	J_d	$3 \cdot 10^{-3}$	kg m^2
Conversion coefficient of pump	K_{pd}	$1.6 \cdot 10^{-8}$	mol rad^{-1}
Mechanical pump efficiency	η_d	0.7	

Table A.7: Parameters of Diesel, Water and Air Supply

Water Supply			
Resistance of electric motor	R_W	0.5	Ω
Electric inductance	L_W	$5 \cdot 10^{-3}$	H
Electro-mechanic conversion coefficient	$K_{ew} \cdot 0.5$	$N \cdot m \cdot A^{-1}$	
Combined friction coefficient of motor and pump	f_W	$3 \cdot 10^{-3}$	$N \cdot m \cdot rad^{-1}$
Combined inertia of motor and pump	J_W	$3 \cdot 10^{-3}$	$kg \cdot m^2$
Conversion coefficient of pump	K_{pw}	$1.6 \cdot 10^{-8}$	$mol \cdot rad^{-1}$
Mechanical pump efficiency	η_W	0.7	
Air Supply			
Resistance of electric motor	R_a	0.5	Ω
Electric inductance	L_a	$5 \cdot 10^{-3}$	H
Electro-mechanic conversion coefficient	$K_{ea} \cdot 0.5$	$N \cdot m \cdot A^{-1}$	
Combined friction coefficient of motor and pump	f_a	$3 \cdot 10^{-3}$	$N \cdot m \cdot rad^{-1}$
Combined inertia of motor and pump	J_a	$3 \cdot 10^{-3}$	$kg \cdot m^2$
Conversion coefficient of pump	K_{pa}	$1.3 \cdot 10^{-3}$	$mol \cdot rad^{-1}$